NAVAL POSTGRADUATE SCHOOL
Monterey, California

THESIS

G7259

TURBULENCE STRUCTURE RESULTING FROM
INTERACTION BETWEEN AN
EMBEDDED VORTEX AND WALL JET

by

James G. Green

June 1989

Thesis Advisor — Chelakara S. Subramanian
Co-Advisor — Phillip M. Ligrani

Approved for public release; distribution is unlimited.

T24408

nclassified

curity classification of this page

REPORT DOCUMENTATION PAGE

a Report Security Classification Unclassified		1b Restrictive Markings	
a Security Classification Authority		3 Distribution/Availability of Report	
b Declassification Downgrading Schedule		Approved for public release; distribution is unlimited.	
Performing Organization Report Number(s)		5 Monitoring Organization Report Number(s)	
a Name of Performing Organization Naval Postgraduate School	6b Office Symbol *(if applicable)* 69	7a Name of Monitoring Organization Naval Postgraduate School	
c Address *(city, state, and ZIP code)* Monterey, CA 93943-5000		7b Address *(city, state, and ZIP code)* Monterey, CA 93943-5000	
a Name of Funding Sponsoring Organization	8b Office Symbol *(if applicable)*	9 Procurement Instrument Identification Number	
c Address *(city, state, and ZIP code)*		10 Source of Funding Numbers	
		Program Element No / Project No / Task No / Work Unit Accession No	

1 Title *(Include security classification)* TURBULENCE STRUCTURE RESULTING FROM INTERACTION BETWEEN AN EMBEDDED VORTEX AND WALL JET

2 Personal Author(s) James G. Green

3a Type of Report	13b Time Covered	14 Date of Report *(year, month, day)*	15 Page Count
Master's Thesis	From To	June 1989	231

6 Supplementary Notation The views expressed in this thesis are those of the author and do not reflect the official policy or position of the Department of Defense or the U.S. Government.

7 Cosati Codes			18 Subject Terms *(continue on reverse if necessary and identify by block number)*
ield	Group	Subgroup	Embedded vortex, wall jet, turbulence

9 Abstract *(continue on reverse if necessary and identify by block number)*

Interactions of wall jets and vortices embedded in turbulent boundary layers commonly occur near gas turbine blades and ndwalls where film cooling is employed. These interactions frequently result in undesirable heat transfer effects at blade and ndwall surfaces. In this research, a crossed hot-wire probe is used to measure the turbulence structure resulting from this type f interaction.

The vortex is generated using a half-delta-wing vortex generator mounted at 12 degrees with respect to a 10 m/s mean elocity flow over a flat plate. A single injection hole, .95 cm in diameter, inclined 30 degrees to the horizontal, is located nder the vortex downwash, 58 cm downstream from the vortex generator. Baseline measurements were made at one reamwise location downstream of the injection hole for the cases: (1) boundary layer only, (2) boundary layer with vortex, nd (3) boundary layer with wall jet. Measurement of the interaction between the boundary layer, vortex and 2.5 blowing atio wall jet was also made at this location. The 1.5 blowing ratio wall jet interaction was measured at three additional reamwise locations.

Reynolds stress tensor components, vorticity distributions and mean velocities show that the vortex significantly alters the rbulence structure of the 1.5 blowing ratio wall jet at all four streamwise locations. Here the injectant is swept away from ne injection hole by the vortex rotation. The most significant alterations to the turbulence structure occur in the vortex pwash region and beneath the vortex core. The 2.5 blowing ratio jet is much more resistant to disturbance by the vortex.

0 Distribution Availability of Abstract	21 Abstract Security Classification	
☒ unclassified unlimited ☐ same as report ☐ DTIC users	Unclassified	
2a Name of Responsible Individual Phillip M. Ligrani	22b Telephone *(include Area code)* (408) 646-3382	22c Office Symbol 69Li

D FORM 1473,84 MAR 83 APR edition may be used until exhausted
All other editions are obsolete

security classification of this page

Unclassified

Approved for public release; distribution is unlimited.

Turbulence Structure Resulting From Interaction Between an Embedded Vortex and Wall Jet

by

James G. Green
Lieutenant, United States Navy
B.S.C.E., University of Minnesota, 1981

Submitted in partial fulfillment of the
requirements for the degree of

MASTER OF SCIENCE IN MECHANICAL ENGINEERING

from the

NAVAL POSTGRADUATE SCHOOL
June 1989

ABSTRACT

Interactions of wall jets and vortices embedded in turbulent boundary layers commonly occur near gas turbine blades and endwalls where film cooling is employed. These interactions frequently result in undesirable heat transfer effects at blade and endwall surfaces. In this research, a crossed hot-wire probe is used to measure the turbulence structure resulting from this type of interaction.

The vortex is generated using a half-delta-wing vortex generator mounted at 12 degrees with respect to a 10 m/s mean velocity flow over a flat plate. A single injection hole, .95 cm in diameter, inclined 30 degrees to the horizontal, is located under the vortex downwash, 58 cm downstream from the vortex generator. Baseline measurements were made at one streamwise location downstream of the injection hole for the cases: (1) boundary layer only, (2) boundary layer with vortex, and (3) boundary layer with wall jet. Measurement of the interaction between the boundary layer, vortex and 2.5 blowing ratio wall jet was also made at this location. The 1.5 blowing ratio wall jet interaction was measured at three additional streamwise locations.

Reynolds stress tensor components, vorticity distributions and mean velocities show that the vortex significantly alters the turbulence structure of the 1.5 blowing ratio wall jet at all four streamwise locations. Here the injectant is swept away from the injection hole by the vortex rotation. The most significant alterations to the turbulence structure occur in the vortex upwash region and beneath the vortex core. The 2.5 blowing ratio jet is much more resistant to disturbance by the vortex.

TABLE OF CONTENTS

I. INTRODUCTION 1
A. MOTIVATION FOR RESEARCH 1
B. LITERATURE SURVEY 1
C. TURBULENCE TERMINOLOGY 3
1. Instantaneous Velocity 3
2. Reynolds Stress Tensor Components 3
3. Turbulence Intensity 4
4. Diffusive Transport 4
5. Friction velocity, u^+ and y^+ 4
6. Multi-layer Model of Boundary Layer 4
D. DESCRIPTION OF THE PRESENT STUDY 4
E. THESIS OUTLINE 5

II. EXPERIMENTAL APPARATUS 6
A. WIND TUNNEL AND TEST SECTION 6
B. VORTEX GENERATOR 7
C. INJECTION SYSTEM 7

III. HOT-WIRE ANEMOMETER AND DATA ACQUISITION SYSTEMS ... 9
A. PRINCIPLES OF HOT-WIRE ANEMOMETRY 9
B. CROSSED HOT-WIRE PROBES 10
C. CROSSED HOT-WIRE PROBE CALIBRATION 11
1. Velocity Calibration in the uw Plane 12
2. Yaw Calibration 12
3. Velocity Calibration in the uv Plane 13
D. HOT-WIRE ANEMOMETERS 14
E. LOW-SPEED DATA ACQUISITION SYSTEM 14
F. SIGNAL CONDITIONER 14
G. HIGH-SPEED ANALOG-TO-DIGITAL CONVERTER 15
H. PROBE TRAVERSING 16
I. MICROCOMPUTER 16

J. DATA REDUCTION 16
1. Temperature Drift Correction 17
2. Look-up Table 17
3. Calculation of Turbulence Statistics 18

IV. EXPERIMENTAL RESULTS 21
A. CALCULATIONS 21
1. Normalization of Results 21
2. Normalized Secondary Flow Vectors, $\vec{V}$ 21
3. Streamwise Vorticity, ω_x 22
4. Circulation, Γ 22
5. Vortex Core Size 23
B. SURVEY CONDITIONS AND PARAMETERS 24
C. BASELINE DATA 25
1. Boundary Layer 25
2. Boundary Layer / Wall Jet Interaction 25
3. Boundary Layer / Vortex Interaction 26
a. Δ = 0.25 inches 26
b. Δ = 0.10 inches 26
D. BOUNDARY LAYER / VORTEX / WALL JET INTERACTION 27
1. Blowing Ratio = 1.5 27
a. Probe Location B, Δ = 0.25 inches 27
b. Probe Location B, Δ = 0.10 inches 28
c. Streamwise Development 28
2. Blowing Ratio = 2.5 29

V. SUMMARY AND CONCLUSIONS 30

APPENDIX A. SOFTWARE DIRECTORY 32

APPENDIX B. FIGURES 34

LIST OF REFERENCES 209

BIBLIOGRAPHY 212

INITIAL DISTRIBUTION LIST 213

LIST OF TABLES

Table 1. SUMMARY OF SURVEY CONDITIONS AND PARAMETERS 24

LIST OF FIGURES

Figure 1. Flow in gas turbine passages 34
Figure 2. Instantaneous velocity components 35
Figure 3. Multilayer turbulent boundary layer 36
Figure 4. Schematic of wind tunnel 37
Figure 5. Test section schematic 38
Figure 6. Vortex generator 39
Figure 7. Plenum and injection tubes 40
Figure 8. Photograph of plenum and test section 41
Figure 9. Schematic of hot wire and data acquisition systems 42
Figure 10. Block diagram of constant temperature anemometer 43
Figure 11. Effective cooling velocity 44
Figure 12. Effective velocities for crossed wire probe 45
Figure 13. Probe support 46
Figure 14. Velocity calibration plot 47
Figure 15. Wire inclined at $\psi + \delta$ 48
Figure 16. Yaw calibration plot for crossed wire probe 49
Figure 17. Mean velocity profile in turbulent boundary layer measured using various sampling frequencies and sizes 50
Figure 18. Two-axis traversing carriage 51
Figure 19. Fluctuating velocity components in turbulent boundary layer 52
Figure 20. Turbulent shear stress distribution 53
Figure 21. $\bar{u}$ (boundary layer, station B, $\Delta = 0.25$ inches) 54
Figure 22. $\overline{u'^2}$ (boundary layer, station B, $\Delta = 0.25$ inches) 55
Figure 23. $\overline{v'^2}$ (boundary layer, station B, $\Delta = 0.25$ inches) 56
Figure 24. $\overline{w'^2}$ (boundary layer, station B, $\Delta = 0.25$ inches) 57
Figure 25. $\overline{u'v'}$ (boundary layer, station B, $\Delta = 0.25$ inches) 58
Figure 26. $\overline{u'w'}$ (boundary layer, station B, $\Delta = 0.25$ inches) 59
Figure 27. $\overline{u'^3}$ (boundary layer, station B, $\Delta = 0.25$ inches) 60
Figure 28. $\overline{v'^3}$ (boundary layer, station B, $\Delta = 0.25$ inches) 61
Figure 29. $\overline{w'^3}$ (boundary layer, station B, $\Delta = 0.25$ inches) 62
Figure 30. $\overline{u'^2v'}$ (boundary layer, station B, $\Delta = 0.25$ inches) 63

Figure 31. $\overline{u'v'^2}$ (boundary layer, station B, $\Delta = 0.25$ inches) 64
Figure 32. $\overline{u'^2w'}$ (boundary layer, station B, $\Delta = 0.25$ inches) 65
Figure 33. $\overline{u'w'^2}$ (boundary layer, station B, $\Delta = 0.25$ inches) 66
Figure 34. Mean Velocities (boundary layer / wall jet, station B, $\Delta = 0.25$ inches) 67
Figure 35. Streamwise Vorticity ω_x (boundary layer / wall jet, station B, $\Delta = 0.25$ inches) 68
Figure 36. Secondary Flow Vectors (boundary layer / wall jet, station B, $\Delta = 0.25$ inches) 69
Figure 37. $\bar{u}$ (boundary layer / wall jet, station B, $\Delta = 0.25$ inches) 70
Figure 38. $\overline{u'^2}$ (boundary layer / wall jet, station B, $\Delta = 0.25$ inches) 71
Figure 39. $\overline{v'^2}$ (boundary layer / wall jet, station B, $\Delta = 0.25$ inches) 72
Figure 40. $\overline{w'^2}$ (boundary layer / wall jet, station B, $\Delta = 0.25$ inches) 73
Figure 41. $\overline{u'v'}$ (boundary layer / wall jet, station B, $\Delta = 0.25$ inches) 74
Figure 42. $\overline{u'w'}$ (boundary layer / wall jet, station B, $\Delta = 0.25$ inches) 75
Figure 43. $\overline{u'^3}$ (boundary layer / wall jet, station B, $\Delta = 0.25$ inches) 76
Figure 44. $\overline{v'^3}$ (boundary layer / wall jet, station B, $\Delta = 0.25$ inches) 77
Figure 45. $\overline{w'^3}$ (boundary layer / wall jet, station B, $\Delta = 0.25$ inches) 78
Figure 46. $\overline{u'^2v'}$ (boundary layer / wall jet, station B, $\Delta = 0.25$ inches) 79
Figure 47. $\overline{u'v'^2}$ (boundary layer / wall jet, station B, $\Delta = 0.25$ inches) 80
Figure 48. $\overline{u'^2w'}$ (boundary layer / wall jet, station B, $\Delta = 0.25$ inches) 81
Figure 49. $\overline{u'w'^2}$ (boundary layer / wall jet, station B, $\Delta = 0.25$ inches) 82
Figure 50. Mean Velocities (boundary layer / vortex, station B, $\Delta = 0.25$ inches) . . 83
Figure 51. Streamwise Vorticity ω_x (boundary layer / vortex, station B, $\Delta = 0.25$ inches) 84
Figure 52. Secondary Flow Vectors (boundary layer / vortex, station B, $\Delta = 0.25$ inches) 85
Figure 53. $\bar{u}$ (boundary layer / vortex, station B, $\Delta = 0.25$ inches) 86
Figure 54. $\overline{u'^2}$ (boundary layer / vortex, station B, $\Delta = 0.25$ inches) 87
Figure 55. $\overline{v'^2}$ (boundary layer / vortex, station B, $\Delta = 0.25$ inches) 88
Figure 56. $\overline{w'^2}$ (boundary layer / vortex, station B, $\Delta = 0.25$ inches) 89
Figure 57. $\overline{u'v'}$ (boundary layer / vortex, station B, $\Delta = 0.25$ inches) 90
Figure 58. $\overline{u'w'}$ (boundary layer / vortex, station B, $\Delta = 0.25$ inches) 91
Figure 59. $\overline{u'^3}$ (boundary layer / vortex, station B, $\Delta = 0.25$ inches) 92
Figure 60. $\overline{v'^3}$ (boundary layer / vortex, station B, $\Delta = 0.25$ inches) 93
Figure 61. $\overline{w'^3}$ (boundary layer / vortex, station B, $\Delta = 0.25$ inches) 94

Figure 62. $\overline{u'^2v'}$ (boundary layer / vortex, station B, $\Delta = 0.25$ inches) 95
Figure 63. $\overline{u'v'^2}$ (boundary layer / vortex, station B, $\Delta = 0.25$ inches) 96
Figure 64. $\overline{u'^2w'}$ (boundary layer / vortex, station B, $\Delta = 0.25$ inches) 97
Figure 65. $\overline{u'w'^2}$ (boundary layer / vortex, station B, $\Delta = 0.25$ inches) 98
Figure 66. Streamwise Vorticity ω_x (boundary layer / vortex, station B, $\Delta = 0.10$ inches) 99
Figure 67. Secondary Flow Vectors (boundary layer / vortex, station B, $\Delta = 0.10$ inches) 100
Figure 68. $\bar{u}$ (boundary layer / vortex, station B, $\Delta = 0.10$ inches) 101
Figure 69. $\overline{u'^2}$ (boundary layer / vortex, station B, $\Delta = 0.10$ inches) 102
Figure 70. $\overline{v'^2}$ (boundary layer / vortex, station B, $\Delta = 0.10$ inches) 103
Figure 71. $\overline{w'^2}$ (boundary layer / vortex, station B, $\Delta = 0.10$ inches) 104
Figure 72. $\overline{u'v'}$ (boundary layer / vortex, station B, $\Delta = 0.10$ inches) 105
Figure 73. $\overline{u'w'}$ (boundary layer / vortex, station B, $\Delta = 0.10$ inches) 106
Figure 74. $\overline{u'^3}$ (boundary layer / vortex, station B, $\Delta = 0.10$ inches) 107
Figure 75. $\overline{v'^3}$ (boundary layer / vortex, station B, $\Delta = 0.10$ inches) 108
Figure 76. $\overline{w'^3}$ (boundary layer / vortex, station B, $\Delta = 0.10$ inches) 109
Figure 77. $\overline{u'^2v'}$ (boundary layer / vortex, station B, $\Delta = 0.10$ inches) 110
Figure 78. $\overline{u'v'^2}$ (boundary layer / vortex, station B, $\Delta = 0.10$ inches) 111
Figure 79. $\overline{u'^2w'}$ (boundary layer / vortex, station B, $\Delta = 0.10$ inches) 112
Figure 80. $\overline{u'w'^2}$ (boundary layer / vortex, station B, $\Delta = 0.10$ inches) 113
Figure 81. Mean Velocities (boundary layer / vortex / wall jet, station B, $\Delta = 0.25$ inches) 114
Figure 82. Streamwise Vorticity ω_x (boundary layer / vortex / wall jet, station B, $\Delta = 0.25$ inches) 115
Figure 83. Secondary Flow Vectors (boundary layer / vortex / wall jet, station B, $\Delta = 0.25$ inches) 116
Figure 84. $\bar{u}$ (boundary layer / vortex / wall jet, station B, $\Delta = 0.25$ inches) 117
Figure 85. $\overline{u'^2}$ (boundary layer / vortex / wall jet, station B, $\Delta = 0.25$ inches) . . . 118
Figure 86. $\overline{v'^2}$ (boundary layer / vortex / wall jet, station B, $\Delta = 0.25$ inches) . . . 119
Figure 87. $\overline{w'^2}$ (boundary layer / vortex / wall jet, station B, $\Delta = 0.25$ inches) . . 120
Figure 88. $\overline{u'v'}$ (boundary layer / vortex / wall jet, station B, $\Delta = 0.25$ inches) . . 121
Figure 89. $\overline{u'w'}$ (boundary layer / vortex / wall jet, station B, $\Delta = 0.25$ inches) . 122
Figure 90. $\overline{u'^3}$ (boundary layer / vortex / wall jet, station B, $\Delta = 0.25$ inches) . . . 123
Figure 91. $\overline{v'^3}$ (boundary layer / vortex / wall jet, station B, $\Delta = 0.25$ inches) . . . 124

Figure 92. $\overline{w'^3}$ (boundary layer / vortex / wall jet, station B, $\Delta = 0.25$ inches) . . 125
Figure 93. $\overline{u'^2v'}$ (boundary layer / vortex / wall jet, station B, $\Delta = 0.25$ inches) . 126
Figure 94. $\overline{u'v'^2}$ (boundary layer / vortex / wall jet, station B, $\Delta = 0.25$ inches) . 127
Figure 95. $\overline{u'^2w'}$ (boundary layer / vortex / wall jet, station B, $\Delta = 0.25$ inches) . 128
Figure 96. $\overline{u'w'^2}$ (boundary layer / vortex / wall jet, station B, $\Delta = 0.25$ inches) . 129
Figure 97. Streamwise Vorticity ω_x (boundary layer / vortex / wall jet, station B, $\Delta = 0.10$ inches) 130
Figure 98. Secondary Flow Vectors (boundary layer / vortex / wall jet, station B, $\Delta = 0.10$ inches) 131
Figure 99. $\bar{u}$ (boundary layer / vortex / wall jet, station B, $\Delta = 0.10$ inches) 132
Figure 100. $\overline{u'^2}$ (boundary layer / vortex / wall jet, station B, $\Delta = 0.10$ inches) . . 133
Figure 101. $\overline{v'^2}$ (boundary layer / vortex / wall jet, station B, $\Delta = 0.10$ inches) . . 134
Figure 102. $\overline{w'^2}$ (boundary layer / vortex / wall jet, station B, $\Delta = 0.10$ inches) . 135
Figure 103. $\overline{u'v'}$ (boundary layer / vortex / wall jet, station B, $\Delta = 0.10$ inches) . 136
Figure 104. $\overline{u'w'}$ (boundary layer / vortex / wall jet, station B, $\Delta = 0.10$ inches) . 137
Figure 105. $\overline{u'^3}$ (boundary layer / vortex / wall jet, station B, $\Delta = 0.10$ inches) . . 138
Figure 106. $\overline{v'^3}$ (boundary layer / vortex / wall jet, station B, $\Delta = 0.10$ inches) . . 139
Figure 107. $\overline{w'^3}$ (boundary layer / vortex / wall jet, station B, $\Delta = 0.10$ inches) . . 140
Figure 108. $\overline{u'^2v'}$ (boundary layer / vortex / wall jet, station B, $\Delta = 0.10$ inches) . 141
Figure 109. $\overline{u'v'^2}$ (boundary layer / vortex / wall jet, station B, $\Delta = 0.10$ inches) . 142
Figure 110. $\overline{u'^2w'}$ (boundary layer / vortex / wall jet, station B, $\Delta = 0.10$ inches) 143
Figure 111. $\overline{u'w'^2}$ (boundary layer / vortex / wall jet, station B, $\Delta = 0.10$ inches) 144
Figure 112. Mean Velocities (boundary layer / vortex / wall jet, station A′, $\Delta = 0.25$ inches) 145
Figure 113. Mean Velocities (boundary layer / vortex / wall jet, station A″, $\Delta = 0.25$ inches) 146
Figure 114. Mean Velocities (boundary layer / vortex / wall jet, station C, $\Delta = 0.25$ inches) 147
Figure 115. Streamwise Vorticity ω_x (boundary layer / vortex / wall jet, station A′, $\Delta = 0.25$ inches) 148
Figure 116. Streamwise Vorticity ω_x (boundary layer / vortex / wall jet, station A″, $\Delta = 0.25$ inches) 149
Figure 117. Streamwise Vorticity ω_x (boundary layer / vortex / wall jet, station C, $\Delta = 0.25$ inches) 150
Figure 118. Secondary Flow Vectors (boundary layer / vortex / wall jet, station

A′, Δ = 0.25 inches) 151
Figure 119. Secondary Flow Vectors (boundary layer / vortex / wall jet, station A″, Δ = 0.25 inches) 152
Figure 120. Secondary Flow Vectors (boundary layer / vortex / wall jet, station C, Δ = 0.25 inches) 153
Figure 121. $\bar{u}$ (boundary layer / vortex / wall jet, station A′, Δ = 0.25 inches) . . 154
Figure 122. $\bar{u}$ (boundary layer / vortex / wall jet, station A″, Δ = 0.25 inches) . . 155
Figure 123. $\bar{u}$ (boundary layer / vortex / wall jet, station C, Δ = 0.25 inches) . . . 156
Figure 124. $\overline{u'^2}$ (boundary layer / vortex / wall jet, station A′, Δ = 0.25 inches) . 157
Figure 125. $\overline{u'^2}$ (boundary layer / vortex / wall jet, station A″, Δ = 0.25 inches) . 158
Figure 126. $\overline{u'^2}$ (boundary layer / vortex / wall jet, station C, Δ = 0.25 inches) . . 159
Figure 127. $\overline{v'^2}$ (boundary layer / vortex / wall jet, station A′, Δ = 0.25 inches) . 160
Figure 128. $\overline{v'^2}$ (boundary layer / vortex / wall jet, station A″, Δ = 0.25 inches) . 161
Figure 129. $\overline{v'^2}$ (boundary layer / vortex / wall jet, station C, Δ = 0.25 inches) . . 162
Figure 130. $\overline{w'^2}$ (boundary layer / vortex / wall jet, station A′, Δ = 0.25 inches) . 163
Figure 131. $\overline{w'^2}$ (boundary layer / vortex / wall jet, station A″, Δ = 0.25 inches) 164
Figure 132. $\overline{w'^2}$ (boundary layer / vortex / wall jet, station C, Δ = 0.25 inches) . 165
Figure 133. $\overline{u'v'}$ (boundary layer / vortex / wall jet, station A′, Δ = 0.25 inches) 166
Figure 134. $\overline{u'v'}$ (boundary layer / vortex / wall jet, station A″, Δ = 0.25 inches) 167
Figure 135. $\overline{u'v'}$ (boundary layer / vortex / wall jet, station C, Δ = 0.25 inches) . 168
Figure 136. $\overline{u'w'}$ (boundary layer / vortex / wall jet, station A′, Δ = 0.25 inches) 169
Figure 137. $\overline{u'w'}$ (boundary layer / vortex / wall jet, station A″, Δ = 0.25 inches) 170
Figure 138. $\overline{u'w'}$ (boundary layer / vortex / wall jet, station C, Δ = 0.25 inches) 171
Figure 139. $\overline{u'^3}$ (boundary layer / vortex / wall jet, station A′, Δ = 0.25 inches) . 172
Figure 140. $\overline{u'^3}$ (boundary layer / vortex / wall jet, station A″, Δ = 0.25 inches) . 173
Figure 141. $\overline{u'^3}$ (boundary layer / vortex / wall jet, station C, Δ = 0.25 inches) . . 174
Figure 142. $\overline{v'^3}$ (boundary layer / vortex / wall jet, station A′, Δ = 0.25 inches) . 175
Figure 143. $\overline{v'^3}$ (boundary layer / vortex / wall jet, station A″, Δ = 0.25 inches) . 176
Figure 144. $\overline{v'^3}$ (boundary layer / vortex / wall jet, station C, Δ = 0.25 inches) . . 177
Figure 145. $\overline{w'^3}$ (boundary layer / vortex / wall jet, station A′, Δ = 0.25 inches) . 178
Figure 146. $\overline{w'^3}$ (boundary layer / vortex / wall jet, station A″, Δ = 0.25 inches) 179
Figure 147. $\overline{w'^3}$ (boundary layer / vortex / wall jet, station C, Δ = 0.25 inches) 180
Figure 148. $\overline{u'^2v'}$ (boundary layer / vortex / wall jet, station A′, Δ = 0.25 inches) 181
Figure 149. $\overline{u'^2v'}$ (boundary layer / vortex / wall jet, station A″, Δ = 0.25 inches) 182
Figure 150. $\overline{u'^2v'}$ (boundary layer / vortex / wall jet, station C, Δ = 0.25 inches) 183

Figure 151. $\overline{u'v'^2}$ (boundary layer / vortex / wall jet, station A′, $\Delta = 0.25$ inches) 184
Figure 152. $\overline{u'v'^2}$ (boundary layer / vortex / wall jet, station A″, $\Delta = 0.25$ inches) 185
Figure 153. $\overline{u'v'^2}$ (boundary layer / vortex / wall jet, station C, $\Delta = 0.25$ inches) 186
Figure 154. $\overline{u'^2w'}$ (boundary layer / vortex / wall jet, station A′, $\Delta = 0.25$ inches) 187
Figure 155. $\overline{u'^2w'}$ (boundary layer / vortex / wall jet, station A″, $\Delta = 0.25$ inches) 188
Figure 156. $\overline{u'^2w'}$ (boundary layer / vortex / wall jet, station C, $\Delta = 0.25$ inches) 189
Figure 157. $\overline{u'w'^2}$ (boundary layer / vortex / wall jet, station A′, $\Delta = 0.25$ inches) 190
Figure 158. $\overline{u'w'^2}$ (boundary layer / vortex / wall jet, station A″, $\Delta = 0.25$ inches) 191
Figure 159. $\overline{u'w'^2}$ (boundary layer / vortex / wall jet, station C, $\Delta = 0.25$ inches) 192
Figure 160. Mean Velocities (boundary layer / vortex / wall jet, station B, $\Delta = 0.25$ inches, m = 2.5) 193
Figure 161. Streamwise Vorticity ω_x (boundary layer / vortex / wall jet, station B, $\Delta = 0.25$ inches, m = 2.5) 194
Figure 162. Secondary Flow Vectors (boundary layer / vortex / wall jet, station B, $\Delta = 0.25$ inches, m = 2.5) 195
Figure 163. $\overline{u}$ (boundary layer / vortex / wall jet, station B, $\Delta = 0.25$ inches, m = 2.5) 196
Figure 164. $\overline{u'^2}$ (boundary layer / vortex / wall jet, station B, $\Delta = 0.25$ inches, m = 2.5) 197
Figure 165. $\overline{v'^2}$ (boundary layer / vortex / wall jet, station B, $\Delta = 0.25$ inches, m = 2.5) 198
Figure 166. $\overline{w'^2}$ (boundary layer / vortex / wall jet, station B, $\Delta = 0.25$ inches, m = 2.5) 199
Figure 167. $\overline{u'v'}$ (boundary layer / vortex / wall jet, station B, $\Delta = 0.25$ inches, m = 2.5) 200
Figure 168. $\overline{u'w'}$ (boundary layer / vortex / wall jet, station B, $\Delta = 0.25$ inches, m = 2.5) 201
Figure 169. $\overline{u'^3}$ (boundary layer / vortex / wall jet, station B, $\Delta = 0.25$ inches, m = 2.5) 202
Figure 170. $\overline{v'^3}$ (boundary layer / vortex / wall jet, station B, $\Delta = 0.25$ inches, m = 2.5) 203
Figure 171. $\overline{w'^3}$ (boundary layer / vortex / wall jet, station B, $\Delta = 0.25$ inches, m = 2.5) 204
Figure 172. $\overline{u'^2v'}$ (boundary layer / vortex / wall jet, station B, $\Delta = 0.25$ inches, m = 2.5) 205

Figure 173. $\overline{u'v'^2}$ (boundary layer / vortex / wall jet, station B, $\Delta = 0.25$ inches, m = 2.5) 206
Figure 174. $\overline{u'^2w'}$ (boundary layer / vortex / wall jet, station B, $\Delta = 0.25$ inches, m = 2.5) 207
Figure 175. $\overline{u'w'^2}$ (boundary layer / vortex / wall jet, station B, $\Delta = 0.25$ inches, m = 2.5) 208

LIST OF SYMBOLS

SYMBOL	*MEANING*
B,K,n	hot-wire calibration coefficients
C	temperature drift correction factor
C_d	discharge coefficient
d	injection hole diameter
E	anemometer voltage
E_{corr}	anemometer voltage corrected for temperature drift
E_{oc}	no-flow voltage extrapolated from velocity calibration
$E_{o(measured)}$	measured no-flow voltage
m	blowing ratio
OHR	overheat ratio
T	turbulence intensity, temperature
T_∞	freestream temperature
T_{cal}	freestream temperature when hot-wire probe is calibrated
U_{eff}	effective cooling velocity
U_e , U_∞	freestream velocity
U_{inj}	injectant velocity
U,V,W	instantaneous velocities in x,y and z directions respectively
$\overline{u}$, $\overline{v}$, $\overline{w}$	mean velocity components in x,y and z directions respectively
u', v', w'	fluctuating components in x,y and z directions respectively
v^*	friction velocity
$\vec{V}$	secondary flow vector
x	streamwise distance measured from boundary layer trip
x'	streamwise distance measured from downstream edge of injection hole
y	vertical distance
Ycen	vertical location of vortex center
Ycore	average vortex core radius in vertical direction
z	spanwise distance measured from centerline

Zcen	spanwise location of vortex center
Zcore	average vortex core radius in spanwise direction
α	temperature coefficient of resistance
Γ, Cr	circulation
Δ	node spacing
δ	boundary layer thickness, yaw angle
μ	viscosity
ρ_{inj}	injectant density
ρ_{∞}	freestream density
σ	total normal stress
σ'	Reynolds normal stress
τ	total shear stress
τ'	Reynolds shear stress
υ	kinematic viscosity
ψ	effective wire angle
ω_x	streamwise vorticity

ACKNOWLEDGMENTS

I am indebted to my thesis advisors, Professor Phillip Ligrani and Professor Chelakara Subramanian. Professor Ligranni provided encouragement, direction, and solutions to many of the perplexing problems that arose in the course of this research. Professor Subramanian's patience and technical expertise in the laboratory and in the development of required software was crucial to the completion of this work. Thanks also go to the mechanical engineering laboratory and machine shop staff at the Naval Postgraduate School for their skillful assistance. Finally, I would like to thank my wife, Sandy, for her support and encouragement.

I. INTRODUCTION

A. MOTIVATION FOR RESEARCH

Significant secondary flows exist in turbine passages of gas turbine engines. A schematic of these secondary flows is shown in Figure 1, adapted from [Ref. 1: p. 24]. Hot combustion gases initially move in the axial direction as a turbulent boundary layer is formed on the endwall. As the flow approaches the blade, a horseshoe vortex is formed near the endwall and blade leading edge which then splits into a *passage vortex* on the pressure side of the blade, and a *counter vortex* on the suction side of the blade. Because these vortices are *embedded* in the wall bounded boundary layers, they cause significant perturbations to local wall heat transfer and wall shear stress.

One means of protecting the endwall and blade from thermal loading caused from exposure to high gas temperatures (over 1500°F) is film cooling. With film cooling, relatively cool air is injected through rows of holes in blade and endwall surfaces as shown in Figure 1. The problem with this arrangement is that embedded vortices cause significant disturbances to distributions of film injectant. This results in local hot-spots at locations that would otherwise appear to be well protected by film cooling. [Refs. 2, 3 and 4]

The goal of this research effort is to gain understanding of the turbulence structure of turbulent boundary layers with embedded vortex / wall jet interactions. This is a necessary step towards understanding and minimizing the detrimental effects of embedded vortices on distributions of film injectant and on heat transfer rates at turbine passage walls. As the problem is better understood, improved designs will lead to higher turbine inlet temperatures resulting in more efficient engines with improved power-to-weight ratios.

B. LITERATURE SURVEY

To the best knowledge of the author, no turbulence measurements have been made of vortex / wall jet interactions. However, a number of researchers have measured the turbulence structural characteristics of embedded vortices without wall jet interactions. The vortices in these existing studies are generally created with half wing vortex generators positioned at some skew angle to the flow direction. Shabaka, Mehta and Bradshaw [Ref. 5] used this arrangement with the vortex generator located in the wind tunnel settling chamber to study the characteristics of a single vortex embedded in a turbulent

boundary layer. Their work included mean and turbulent fluctuating velocity measurements in various spanwise planes for vortex circulation, Γ, equal to 1.84 U_e mm where U_e is the freestream velocity. Their measurements show that the circulation around the embedded vortex is almost completely conserved. The only reduction is due to the spanwise component of shear stress. The region affected by the vortex grows as it travels downstream, with cross-sectional dimensions which are roughly proportional to the local boundary layer thickness. Eddy viscosity components, deduced from the Reynolds stress components and various triple products, indicate that simple empirical relations used in present day turbulence models are not likely to be accurate. The major conclusion of their work is that the vortex changes the properties of the outer region of the boundary layer.

Eibeck and Eaton [Ref. 6] present heat transfer and fluid dynamic measurements in a turbulent boundary layer with an embedded vortex. Mean velocity profiles in the log-law region are similar to those in two-dimensional turbulent boundary layers. Outer layers are distorted as seen by Shabaka et al [Ref. 5].

Cutler and Bradshaw [Ref. 7] studied the interaction of vortex pairs with the common flow downward in a turbulent boundary layer. Mehta and Bradshaw [Ref. 8] studied a pair of vortices with the common vortex flow upward. These two studies show: (1) dramatic turbulence structure changes that can not be explained using current turbulence models, and (2) the existence of secondary longitudinal vortices having opposite signs (rotation direction) to the principle vortices. The smaller vortices exist to satisfy the condition that spanwise velocity is equal to zero at the wall.

Westphal, Pauley, and Eaton [Ref. 9] made measurements of a single vortex interacting with a turbulent boundary layer. They used vortex generator angles of 12 and 16 degrees and obtained mean and turbulent velocity results similar to Shabaka et al [Ref. 5]. In addition, they observed that the skin friction increased under the vortex downwash and decreased under the vortex upwash. With an adverse pressure gradient, vortex distortion of boundary layer properties is intensified.

The interaction of vortices and jets has been studied by Skow and Peake [Ref. 10], Heffernan [Ref. 11], Schwartz [Ref. 12], Iwanski, et al [Ref. 13], Visser, et al [Ref. 14], Ligrani and Schwartz [Ref. 15], and Ligrani and Williams [Ref. 4]. Most of these studies emphasize vortex control, and none of them present detailed turbulence measurements.

C. TURBULENCE TERMINOLOGY

Some of the terms used to describe turbulence structural characteristics are now described.

1. Instantaneous Velocity

Figure 2 shows an example of the variation of velocity with time in a turbulent flow. At any instant, the velocity U consists of a mean component, $\bar{u}$, and a fluctuating component, u′. Thus, instantaneous velocities in the x, y and z directions, respectively, are given as $U = \bar{u} + u'$, $V = \bar{v} + v'$ and $W = \bar{w} + w'$. By definition, the time average of an instantaneous velocity is equal to the mean velocity component. This means that the time average of the fluctuating component is equal to zero, $\overline{u'} = \overline{v'} = \overline{w'} = 0$.

2. Reynolds Stress Tensor Components

The mean velocity components $\bar{u}$, $\bar{v}$ and $\bar{w}$ in a turbulent flow satisfy the laminar form of the momentum (Navier-Stokes) equations. Fluctuating components u′, v′ and w′ give rise to additional stresses known as apparent, virtual or Reynolds stresses. The components of the Reynolds stress tensor are:

$$\begin{bmatrix} \sigma'_x & \tau'_{xy} & \tau'_{xz} \\ \tau'_{xy} & \sigma'_y & \tau'_{yz} \\ \tau'_{xz} & \tau'_{yz} & \sigma'_x \end{bmatrix} = -\rho \begin{bmatrix} \overline{u'^2} & \overline{u'v'} & \overline{u'w'} \\ \overline{u'v'} & \overline{v'^2} & \overline{v'w'} \\ \overline{u'w'} & \overline{v'w'} & \overline{w'^2} \end{bmatrix}$$

The subscripts x, y and z in the stress terms indicate the plane and the direction in which the stress component acts. For example τ_{xy} denotes the stress acting in the y direction on a plane normal to the x axis. It is important to note that while $\overline{u'} = 0$, the average of u′ squared does not in general equal zero, $\overline{u'^2} \neq 0$. The total stresses are the sums of the viscous stresses and the Reynolds stresses. For example, in a two-dimensional boundary layer,

$$\tau_{xy} = \mu\left(\frac{\partial \bar{u}}{\partial y}\right) - \rho\overline{u'v'}$$

Outside of the viscous sublayer, Reynolds stresses are larger than the viscous stresses.

3. Turbulence Intensity

The turbulence intensity, T, is defined as:

$$T = \frac{\sqrt{\frac{1}{3}\left(\overline{u'^2} + \overline{v'^2} + \overline{w'^2}\right)}}{U_e}$$

where U_e is the freestream velocity. If $\overline{u'^2} = \overline{v'^2} = \overline{w'^2}$, the turbulence is *isotropic* and its intensity is then given by:

$$T = \frac{\sqrt{\overline{u'^2}}}{U_e}$$

4. Diffusive Transport

The terms $\overline{u'^2v'}$, $\overline{u'v'^2}$, $\overline{v'^3}$ and $\overline{w'^2v'}$ represent turbulent diffusive transport in the y direction of $\overline{u'^2}$, $\overline{u'v'}$, $\overline{v'^2}$ and $\overline{w'^2}$ respectively. Because these transport terms are each products of three fluctuating components, they are referred to as *triple products.*

5. Friction velocity, u^+ and y^+

Friction velocity, $v^\times$, is defined as:

$$v^\times = \sqrt{\frac{\tau_o}{\rho}}$$

where τ_o is the total shear stress at the wall and ρ is the fluid density. Using the friction velocity, u^- and y^- are given by $u^- = \frac{\overline{u}}{v^\times}$ and $y^+ = \frac{yv^\times}{\upsilon}$ where υ is kinematic viscosity.

6. Multi-layer Model of Boundary Layer

Turbulent boundary layers may be considered to consist of different layers, each with its own characteristics. The various layers are shown in Figure 3 on a plot of u^- versus y^+ [Ref. 16: p. 35]. The inner layer consists of the viscous sublayer and the log-law region. The remainder of the boundary layer is called the outer layer.

D. DESCRIPTION OF THE PRESENT STUDY

The intent of this study is to obtain turbulence structural information of an embedded vortex influenced by a single wall jet. A freestream velocity of 10 m/s is used and the boundary layer is tripped 1.08 m upstream of the wall jet. A 12 degree vortex generator is positioned 0.487 m downstream from the boundary layer trip and 0.019 m off the tunnel centerline so that the downwash region of the generated vortex is located directly above the wall jet. The jet issues from a 0.952 cm diameter hole located at the centerline of the tunnel and inclined at 30 degrees with respect to the horizontal. The

ratio of boundary layer displacement thickness to injection hole diameter δ_1/d is equal to 0.38 at the injection site. Blowing ratios of 1.5 and 2.5 are used (blowing ratio m, is defined as the ratio of injectant mass flux to freestream mass flux).

A crossed hot-wire probe is used to measure mean and instantaneous velocity components in spanwise planes at 4 different streamwise locations. These locations correspond to x'/d values of 5.9, 19.2, 30.1 and 70.3 (x′ is the distance from the downstream edge of the injection hole). Data is presented for m = 1.5 at all four locations and at $x'/d = 19.2$ for m = 2.5. Baseline measurements consist of turbulence surveys for the following three conditions at $x'/d = 19.2$: (1) boundary layer with no vortex, no injection (2) boundary layer with 12 degree vortex generator installed, no injection (3) boundary layer with injection (m = 1.5), no vortex. Contour plots of streamwise mean velocity, five of the six Reynolds stress tenser components, turbulence triple products and streamwise vorticity are given for each measurement location and flow condition in addition to cross-flow velocity vector plots.

E. THESIS OUTLINE

The material in this thesis is organized as follows. Chapter II describes the wind tunnel, injection system and vortex generator. The details of the hot-wire anemometer, data acquisition, computer and probe traversing systems are discussed in Chapter III. Experimental results are presented in Chapter IV and conclusions are summarized in Chapter V. Descriptions of the software developed for this research are provided in Appendix A. Appendix B contains all the figures and plots referred to in the text.

II. EXPERIMENTAL APPARATUS

A. WIND TUNNEL AND TEST SECTION

The experiments were performed in the open circuit, subsonic wind tunnel shown schematically in Figure 4. The wind tunnel was manufactured by Aerolab and is located in the laboratories of the Mechanical Engineering Department at the Naval Postgraduate School. At the tunnel inlet, air from inside the room passes through a cloth filter and enters a centrifugal blower at the upstream end of the tunnel. The blower discharges into a diffuser section containing a dust filter pack and four baffle vanes which reduce noise and minimize the likelihood of flow separations. A 1.6 mm clearance between the blower outlet and the diffuser inlet isolates the wind tunnel test section from blower vibration. From the diffuser, the flow passes through a header containing a honeycomb and three anti-turbulence screens. A 2-dimensional 16:1 contraction ratio nozzle leads from the header to the test section. The test section is a rectangular duct 3.05 m long and 0.61 m wide. The top wall (ceiling) is a continuous panel fabricated from 4.76 mm thick LEXAN sheet. The height of the ceiling panel can be adjusted along the length of the test section in order to control the streamwise pressure gradient. Adjustments are made in order to maintain a zero pressure gradient (to within .018 cm of water with no vortex or injection). For these experiments, the nominal height of the ceiling panel at the nozzle exit is 23 cm. Air speed through the test section is adjustable from 5 to 40 m/s. The freestream turbulence intensity is about 0.10 percent for freestream velocities of 20 to 30 m/s. The freestream velocity used here is 10 m/s and the freestream turbulence intensity is 0.16 to 0.20 percent. The flow is tripped at the entrance to the test section with a 1.5 mm high tape strip. A schematic of the test section is shown in Figure 5.

The coordinate system origin is located on the lower wall of the test section at the intersection of the trip and the spanwise centerline. The positive x direction is measured downstream from the trip. The positive y direction is measured upward from the bottom wall and the positive z direction is measured to the right of the longitudinal centerline when looking downstream. The leading edge of the vortex generator delta wing is positioned 48.7 cm downstream from the trip and the downstream edges of the injection nozzles are located 108 cm from the trip. Also indicated in Figure 5 are the four streamwise locations (denoted A′, A″, B and C) where the hot-wire probe is positioned

for data collection. To designate the distance from the downstream edge of the injection holes, the symbol x′ is used. A total pressure probe is used to measure freestream velocity and is positioned 95 cm downstream from the trip and 20 cm off the longitudinal centerline (in the positive z direction). In this location, the wake of the Kiel probe is well clear of the generated vortex. A thermocouple is located at x = 274 cm for free stream temperature measurement. Further information concerning the wind tunnel design and qualification testing may be found in [Ref. 17: pp. 38-40].

B. VORTEX GENERATOR

The vortex generator with dimensions as shown in Figure 6 is used to generate a single longitudinal vortex. The vortex generator, manufactured by attaching a stainless steel wing at a 12 degree angle with respect to the streamwise direction to a thin LEXAN base plate, is positioned so that the downwash portion of the generated vortex is located above the center injection hole. The generator remains in this position until vortex data runs are completed. The location and orientation of the vortex generator is shown in Figure 6. The same vortex generator and location is used by Craig [Ref. 18] in the investigation of the effects of vortex / wall jet interactions on heat transfer.

C. INJECTION SYSTEM

Air for the injection system is supplied by a two stage, 150 PSIG Ingersol-Rand air compressor. From the compressor, the air flows through a globe valve used for throttling, a moisture separator, and a rotometer (Fisher and Porter, 19.8 SCFM full scale) before entering a diffuser and the plenum chamber shown in Figure 7.

The plenum chamber is constructed of 0.7 cm thick plexiglass with outside dimensions of 30.5 x 50.8 x 45.7 cm. Three baffle plates are positioned horizontally in the plenum to provide a passage for heating the injectant and to create uniform flow at the top of the chamber where the air enters the injection tubes. The injection air is not heated in this experiment. The thirteen injection nozzles have inside diameters of 0.952 cm and are aligned in the spanwise direction with a three diameter spacing between centers. The middle nozzle is centered in the spanwise direction on the test section surface. The nozzles are positioned so that they discharge in the downstream direction at a 30 degree angle relative to the horizontal test section floor.

In the present study, the interaction of an embedded vortex with injectant from a single film-cooling hole is of interest. Injectant from the centerline injection tube is used for this purpose. Thus, all other tube exits are sealed with tape except for the two on the ends of the row. These two are used in conjunction with the centerline tube to

provide injectant at controlled and measurable flow rates. Injectant from the two end tubes does not interact with the generated vortex. Figure 8 shows the plenum installed under the test section. The vortex generator and injection nozzles are also visible in this photograph.

Static pressure taps in the plenum and test section side wall allow measurement of the pressure drop between the injection plenum and the static freestream. Thermocouples located in the plenum and test section are used to measure temperatures for determination of freestream and injection densities.

The discharge coefficient, C_d, and the blowing ratio, m, are determined for each experimental run. The discharge coefficient is defined as the ratio of the actual injection mass flux to the ideal (isentropic) injection mass flux.

$$C_d = \frac{\rho_{inj} U_{inj}}{(\rho_{inj} U_{inj})_{ideal}} \qquad \{1\}$$

Discharge coefficient magnitudes are used to determine proper performance of the injection system, particularly whether or not leaks are present.

The blowing ratio is defined as the injection mass flux divided by the free stream mass flux.

$$m = \frac{\rho_{inj} U_{inj}}{\rho_\infty U_\infty} \qquad \{2\}$$

In these experiments, blowing ratios of 1.5 and 2.5 were used. Details concerning measurement and calculation of the injection parameters C_d and m are contained in [Ref. 17 : pp. 23-26].

III. HOT-WIRE ANEMOMETER AND DATA ACQUISITION SYSTEMS

A schematic of the hot-wire anemometer and data acquisition systems is shown in Figure 9. A brief description of each of the major components and their operating principles follows.

A. PRINCIPLES OF HOT-WIRE ANEMOMETRY

The most common instrument used for measuring instantaneous velocities in turbulent flows is the hot-wire anemometer. The basic theory of operation is quite straightforward. A hot-wire anemometry system consists of one or more thin sensor wires connected to supports, each wire forming a leg of a Wheatstone bridge, as shown in Figure 10, adapted from [Ref. 19: p. 3]. In a constant temperature hot-wire system (used in these experiments) the bridge is balanced before the probe is exposed to the flow by means of a variable resistor. This resistance required to balance the bridge is called the "cold wire" resistance. The variable resistance is then increased to an arbitrary value, usually from 1.2 to 1.8 times the "cold wire" resistance (the value from 1.2 to 1.8 is called the overheat ratio). To operate the system, a small current (60mA) is passed through the circuit causing resistive heating and a temperature increase in the wire. The resistance of the wire increases until the bridge is rebalanced. The resistance is related to temperature by:

$$R = R_o(1 + \alpha(T - T_o)) \qquad \{3\}$$

where R is the resistance at temperature T, R_o is the resistance at reference temperature T_o and α is the temperature coefficient of resistance.

When the probe is exposed to a flow, convective cooling of the wire occurs and the wire resistance will decrease causing a bridge unbalance. A feedback loop is used to detect this unbalance and the current flow in the circuit is increased by a feedback amplifier, rebalancing the bridge. Since the feedback amplifier responds very quickly, the wire temperature and resistance remain virtually constant and flow velocity is measured as a function of bridge voltage. This bridge voltage is directly proportional to the current.

The most widely accepted relationship between bridge voltage and effective cooling velocity is given by:

$$U_{eff} = K(E^2 - E_{oc}^2)^{\frac{1}{n}} \quad \{4\}$$

where E is the bridge voltage at effective cooling velocity U_{eff}, and E_{oc} is the bridge voltage extrapolated from forced convection calibration to $U_{eff} = 0$ (no-flow voltage). K and n are empirical constants found by calibration. Usually, n is taken to be equal to 0.45 based on Collis and Williams heat transfer data [Ref. 20]. The effective cooling velocity is defined as the component of the velocity vector that is normal to the wire. When the wire is inclined at an angle ψ to the flow direction as shown in Figure 11, the effective cooling velocity, U_{eff} is defined as:

$$U_{eff} = U \cos \psi \quad \{5\}$$

Substituting this expression into Equation {4} gives:

$$U_{eff} = U \cos \psi = K(E^2 - E_{oc}^2)^{\frac{1}{n}} \quad \{6\}$$

where K, E_{oc}, n and ψ are constants for the wire in a specific orientation with respect to the flow.

B. CROSSED HOT-WIRE PROBES

Crossed hot-wire probes consist of two wires, one wire inclined at $\psi \approx 45$ degrees and the other wire inclined at $\psi \approx -45$ degrees as shown in Figure 12, where ψ is the wire angle in the plane of the wires measured from the direction of the probe stem. For a crossed wire probe exposed to instantaneous velocities U and V, as shown in Figure 12, the effective velocities for each wire are:

$$U_{eff_1} = U \cos \psi_1 + V \sin \psi_1 = K_1(E_1^2 - E_{oc_1}^2)^{\frac{1}{n_1}} \quad \{7\}$$

$$U_{eff_2} = U \cos \psi_2 - V \sin \psi_2 = K_2(E_2^2 - E_{oc_2}^2)^{\frac{1}{n_2}} \quad \{8\}$$

If the constants K, E_{oc}, ψ and n are known for each wire and the bridge voltages E are measured on each wire, these two equations can be solved to find the two unknowns, namely U and V, the instantaneous velocities in the x and y directions. If the probe is

rotated 90 degrees, two equations in U and W will result so all three velocity components can be calculated. From these instantaneous velocity components, statistical methods are used to separate the mean and fluctuating components (see section III. J. 3).

DANTEC type 55P51 crossed wire probes are used in these experiments. The sensors are 90% Platinum - 10% Rhodium with 5 μm diameters. The two wires are mounted perpendicular to each other at approximately $\pm$ 45 degrees with respect to the supports. The two planes of the wires and their supports are separated by about 1mm. The active length of each wire is approximately 1mm. The "cold" resistance of each wire is about 3.5 ohms and an overheat ratio of 1.8 is used in all experiments. According to the manufacturer, the temperature coefficient of resistance α is 0.0036 ohms/°C. The probe is mounted using a DANTEC probe holder attached to a support manufactured in the Naval Postgraduate School mechanical engineering shop. The support, shown in Figure 13, has a notched indexing mechanism that allows the probe to be rotated in 45 degree increments. This provides a means to reorient the probe and change from the uv to the uw measurement planes. In addition, the entire probe support may be rotated about the y axis ("yawed") for calibration purposes, as discussed in the next section.

C. CROSSED HOT-WIRE PROBE CALIBRATION

As mentioned earlier, K, E_{oc}, n and ψ must be known for each wire before Equations {7} and {8} can be used. These are determined by calibration, and calibrations are made before each experiment for two reasons. First, the effective wire angles change slightly each time the probe is moved from one streamwise location to another, and each time the probe is rotated from the uv measurement plane to the uw measurement plane. Secondly, wire resistance changes slightly as the wires are used. Over a 3 month period, over 400 hours of measurements were obtained, during which time, the cold wire resistances increased from 3.5 to 4.2 ohms.

Before each calibration, the electronics are allowed to warm up to steady state condition. The resistance for zero flow velocity is then checked, and the overheat ratio is applied. Calibration is accomplished using the program HWCAL, (see Appendix B), run on the Hewlett Packard 9836S computer. This program is based on one described by Westphal and Mehta [Ref. 21].

The calibration is a three step process consisting of: velocity calibration in the uw plane, yaw calibration in the uw plane, and velocity calibration in the uv plane (this step is required only for uv plane measurements). A brief description of each step follows.

1. Velocity Calibration in the uw Plane

Velocity calibration involves placing the probe at a fixed orientation to a steady flow of known velocity U, recording the measured voltage E, and then repeating this procedure for a number of known flow velocities. The calibration is done outside the turbulent boundary layer where turbulence intensity is lowest.

By rearranging Equation {6} to the form:

$$U^n\left(\frac{\cos\psi}{K}\right)^n = E^2 - E_{oc}^2 \qquad \{9\}$$

and defining a coefficient B using:

$$B = \left(\frac{\cos\psi}{K}\right)^n \qquad \{10\}$$

a simple linear relationship between E^2 and U^n is obtained which is given by:

$$E^2 = E_{oc}^2 + BU^n \qquad \{11\}$$

By varying the flow velocity U, and measuring the corresponding bridge voltages, a least-squares fit is be used to find B and E_{oc}^2 with n specified. For calibrations with flow velocities between 4 m/s and 30 m/s, a good fit is obtained with n = 0.45. An example of an E^2 versus U^n data set for one wire of a crossed wire probe is shown in Figure 14. From the plot, values of 8.4 and 4.0 are obtained for coefficients E_{oc}^2 and B.

2. Yaw Calibration

If the effective wire angle ψ, is known, the coefficient K, in Equation {6} can be calculated. To obtain the effective wire angle, a yaw calibration is performed. This procedure involves "yawing" the probe through a series of known angles δ with the probe exposed to a steady flow. The yaw angle of the probe is changed by rotating the probe about the support stem. From Figure 7, the total angle of inclination is $\psi_{total} = \psi + \delta$ with the wire yawed at an angle δ. At yaw angle δ, Equation {6} is:

$$U\cos(\psi + \delta) = K(E_\delta^2 - E_{oc}^2)^{\frac{1}{n}} \qquad \{12\}$$

where E_δ is the bridge voltage at yaw angle δ. From Equation {6} with zero yaw angle:

$$K = \frac{U\cos\psi}{(E^2 - E_{oc}^2)^{\frac{1}{n}}} \qquad \{13\}$$

where E = bridge voltage when yaw angle is equal to zero. Replacing K in Equation {12} with Equation {13} gives:

$$U\cos(\psi+\delta)=\left(\frac{U\cos\psi}{(E^2-E_{oc}^2)^{\frac{1}{n}}}\right)(E_\delta^2-E_{oc}^2)^{\frac{1}{n}} \qquad \{14\}$$

or, after rearranging and simplifying:

$$\tan\psi=\left(\cos\delta-\left(\frac{E_\delta^2-E_{oc}^2}{E^2-E_{oc}^2}\right)^{\frac{1}{n}}\right)\frac{1}{\sin\delta} \qquad \{15\}$$

Equation {15} is used to determine ψ. One way this can be done is by plotting $\cos\delta-\left(\frac{E_\delta^2-E_{oc}^2}{E^2-E_{oc}^2}\right)^{\frac{1}{n}}$ versus (sin δ) for each wire. The effective wire angle, ψ can then be determined from the plot. Figure 16 shows a yaw calibration plot for a cross wire probe similar to the one used in these experiments. Here, effective wire angles ψ_1 and ψ_2 are +45 and -46 degrees, respectively.

In HWCAL, effective wire angles are determined directly from Equation {15} after the probe is moved through six different values of δ, (δ = -15, -10, -5, 5, 10 and 15 degrees). The final ψ for each wire is then the average of the six ψ's calculated at the six different yaw angles. In the present study, the probe is yawed with wires in the uw plane by rotating the probe support and measuring δ with an attached protractor.

With ψ, B and n known for each wire, K is then calculated using Equation {10}. The probe is now fully calibrated for measurements in the uw plane.

3. Velocity Calibration in the uv Plane

Measurements in the uv plane are made with the probe rotated 90 degrees with respect to the uw plane. After rotation, effective wire angles change slightly if the probe support is not perfectly square, and aligned with respect to the flow direction. In order to find the effective wire angles in the uv plane, the velocity calibration is repeated. Because the coefficients E_{oc}^2, n, and K do not depend on the wire angle, a least squares fit is used to find B in Equation {11}. With B, n and K known, the effective wire angles in the uv plane are calculated using Equation {10}.

With all of these steps completed, the crossed-wire probe is fully calibrated for measurements in the uv plane. The program HWCAL produces a hard copy summary of calibration results and also writes the calibration constants to a data file which is read by the data acquisition programs HOTWIREUV or HOTWIREUW.

D. HOT-WIRE ANEMOMETERS

Two DANTEC 55M constant temperature bridges / amplifiers are used to operate the hot-wires. The hot-wires are connected to the bridges using 5 meter BNC cables. Each anemometer has a built-in 1 kHz square wave generator used to provide a test signal so that the frequency response of each circuit can be optimized. Optimum response is obtained by adjusting the bridge gain, high pass (HP) filter and cable compensation settings. Bridge gains of 3 and HP filter settings of 2 give the best results. Typically, the "-3 dB" point (this is the frequency at which the mean-square response of the anemometer has fallen to half its nominal value) is about 20kHz on each channel.

Each anemometer has two BNC cable connectors for analog signal output. One signal from each wire is connected to the signal conditioner input terminals and then to the analog-to-digital converter for eventual determination of turbulence quantities. The other two anemometer outputs are used for probe calibration and are connected to the low-speed data acquisition system.

E. LOW-SPEED DATA ACQUISITION SYSTEM

A Hewlett-Packard 3497A control unit is used for low-speed data acquisition and analog-to-digital conversion. The low-speed data acquisition system is used to obtain readings of the relatively constant analog outputs from the freesteam velocity measuring device (Kiel probe and electronic manometer), freestream and injection thermocouples, and hot-wire anemometers during probe calibration. Typically, about 50 samples of each input are taken with a sampling frequency of 5 Hz. Temperature and pressure data are read by the low-speed data acquisition system during probe calibration and as turbulence measurements are made. The low-speed data acquisition system is used to acquire anemometer voltage signals only during probe calibration.

F. SIGNAL CONDITIONER

A DANTEC model 56N20, two-channel signal conditioner is used to low pass filter and amplify the anemometer output signals as turbulence measurements are made.

The HP filters on the signal conditioner are set to the DC mode. Low pass filters with 10 kHz cut-off frequencies are used to remove spurious electronic noise and to

prevent digital aliasing. A gain of 2 (with 0 offset voltage) is also applied to each circuit, to optimize use of the voltage range (±10 Volts) of the analog-to-digital converter. The exact gains and offsets for each circuit are measured and recorded before each experiment. The offsets are found by shorting the signal conditioner inputs and recording the outputs from the analog-to-digital converter. The system gains are found by inputting a 1.5 kHz sinusoidal signal of known RMS voltage and comparing this value to the analog-to-digital converter outputs. Measured gains and offsets have typical values of 1.925 and 0.0005 Volts, respectively. These calculations are performed by the computer system as one of the preliminary steps in the data acquisition programs HOTWIREUV or HOTWIREUW. During measurements, signal conditioner outputs are also monitored using an oscilloscope connected in parallel with the analog-to-digital converter.

G. HIGH-SPEED ANALOG-TO-DIGITAL CONVERTER

Analog signals from the signal conditioners are digitized so that signals can be read, processed and stored by the digital microcomputer. A Hewlett-Packard 6944A Series 200 Multiprogrammer with a buffered 69759A A/D card is used. The buffer feature allows digitized data to be stored in the multiprogrammer while the computer is performing other tasks and is unavailable to read data. When the computer is free, a portion of the buffer contents can be read, freeing up memory space in the buffer. This allows continuous data acquisition as long as the rate at which data is read by the computer is greater than the rate that data is written to the buffer.

The sampling rate and the number of samples collected at each data point are specified so that accurate time-averaged velocity values are obtained. Figure 17 shows a portion of the mean velocity profile in the turbulent boundary layer near a flat plate measured with different combinations of sampling frequency and sample size. From this experiment, a sampling frequency of 5,000 Hz per channel and a sample size of 20,000 samples per channel was selected. This combination results in 4 seconds of real sample time per channel at each data point. With a flow velocity of 10 m/s and a boundary layer thickness of 2 cm, the typical time-scale of large scale eddies (which affect boundary layer mean velocities) is given by $\delta/U = 0.02/10 = 0.002$ seconds. The ratio of real sampling time to eddy time-scale is then $4/0.002 = 2000$. The accuracy of the time-average of mean velocities increases as this ratio increases. Decreasing the sampling frequency or increasing the number of samples results in an increase of this ratio. Unfortunately, increasing sample size dramatically increases computer run time and

lowering the sampling frequency could result in less resolution of small time-scale turbulence features. The chosen parameters represent a practical compromise.

The high speed analog-to digital converter card reads analog inputs and converts them to 12-bit binary numbers. The card is configured to measure analog inputs ranging from -10.240 Volts to +10.235 Volts. A -10.240 Volt input is assigned the binary value -2047, zero voltage input is assigned the binary value 0, and a 10.235 Volt input is assigned the binary value +2048. The 20.475 Volt input range is thus divided into 4096 increments of .005 Volt size.

H. PROBE TRAVERSING

For all surveys except two, the hotwire probe is traversed through a 3.0 x 4.5 inch spanwise normal (yz) plane divided into 228 nodes spaced 0.25 inches apart. For two other more detailed surveys, a 1.5 x 2.0 inch plane is divided into about 300 nodes spaced 0.1 inches apart. During a survey, the probe is automatically moved from one node to the next using the 2-axis traversing device shown in Figure 18. The probe support stem is secured to a traveling block which is moved in the y and z directions by two lead screws, each with 20 threads-per-inch pitch. The lead screws are rotated using D.C. stepping motors (SLO-SYN M092-FD310) which are controlled by a MODULYNX MITAS controller (type PMS085-C2AR) and driven by a MODULYNX MITAS drive (type PMS085-D050). The motor controller is operated in the remote mode, as it is linked to the microcomputer by means of a Datacomm interface card and cable. This allows probe traversing commands to be included in the data acquisition software HOTWIREUV or HOTWIREUW.

I. MICROCOMPUTER

The workhorse of the system is a Hewlett-Packard model 9836S Series 300 computer. The computer is equipped with interface cards that link it to the high-speed analog-to-digital converter, low-speed data acquisition system, and the motor controller. The computer is also equipped with a 3.5″ disk drive, a 10 Mbyte hard disk, a printer and a plotter.

J. DATA REDUCTION

As mentioned earlier, 20,000 samples per channel are collected at each node. With 2 channels and 228 nodes, over 9.1 million samples are collected per survey. The reduction of this data is done on line, by the microcomputer as the data is collected. The reduction of data includes the following three steps:

1. Temperature Drift Correction

A 228 node turbulence survey requires about 18 hours to complete. It is not realistic to assume that the freestream air temperature remains constant during this time period. Because the calibration constants E_{oc}^2 and K from the velocity calibration are dependent on the "cold wire resistance" at the freestream air temperature during calibration, a change in freestream temperature from this value causes a change to the hotwire calibration.. To correct for such variations resulting from drift of the freestream temperature, the measured bridge voltage, $E_{measured}$, is corrected using:

$$E_{corr} = E_{measured}(1 + C) \qquad \{16\}$$

where: E_{corr} = corrected voltage, $E_{measured}$ = measured voltage, and C = temperature correction factor given by:

$$C = \frac{\alpha}{2(OHR - 1)}(T_\infty - T_{cal}) \qquad \{17\}$$

where: α = temperature coefficient of resistance, OHR = overheat ratio, T_∞ = freestream temperature, and T_{cal} = freestream temperature at time of calibration.

2. Look-up Table

The use of Equations {7} and {8} to calculate effective velocities from bridge voltages for each of the 9.1 million measurements per survey is extremely time consuming. This is because these calculations involve exponential functions which are relatively time consuming compared to addition and multiplication. To minimize the time used for on-line data processing, a look-up table is used instead. The look-up table contains one effective velocity for each of the 4096 binary values assigned to voltages by the high-speed analog-to digital converter. This means that Equations {7} and {8} are each used only 4096 times to calculate effective velocities from voltages rather than 9.1 million times, which represents a huge savings in computer run time. Because appropriate calibration coefficients and system gains are used in the determination of look-up table values, they are automatically accounted for as effective velocities are determined. When the table is used, the computer simply reads a binary value from the high-speed analog-to-digital converter, finds this value in the look-up table and reads the corresponding effective velocity. The look-up table contains two effective velocity arrays, one for each of the crossed wires.

With the effective velocities known for each wire, the instantaneous velocities U and V, or U and W, can be calculated from Equations {7} and {8}. Instantaneous velocities must still be calculated 9.1 million times per survey but this calculation is much faster than the effective velocity calculation because no exponential functions are involved.

3. Calculation of Turbulence Statistics

The collection of 20,000 samples per wire at each node is done in ten loops, each containing 2,000 samples. This is done because computer memory limits the array size to 2,000 elements. Turbulence statistics are calculated and averaged for each loop; the averages from the ten loops are then averaged.

With this procedure, turbulence statistics (in the uv plane) are calculated as follows:

$$
\begin{aligned}
&\bar{u} = S_u \\
&\bar{v} = S_v \\
&\overline{u'^2} = S_{uu} - S_u S_u \\
&\overline{v'^2} = S_{vv} - S_v S_v \\
&\overline{u'v'} = S_{\overline{u'v'}} - S_u S_v \\
&\overline{(u')^2 v'} = S_{uuv} - S_v\left(S_u S_u - (u')^2\right) - 2S_u\overline{u'v'} \\
&\overline{u'(v')^2} = S_{uvv} - S_u\left(S_v S_v - (v')^2\right) - 2S_v\overline{u'v'} \\
&\overline{u'^3} = S_{uuu} - S_u\left(S_u S_u + 3(u')^2\right) \\
&\overline{v'^3} = S_{vvv} - S_v\left(S_v S_v + 3(v')^2\right)
\end{aligned}
\qquad \{18\}
$$

where:

$$S_u = \frac{1}{20{,}000} \sum_{loop=1}^{10} \sum_{sample=1}^{2{,}000} U$$

$$S_v = \frac{1}{20{,}000} \sum_{loop=1}^{10} \sum_{sample=1}^{2{,}000} V$$

$$S_{uu} = \frac{1}{20{,}000} \sum_{loop=1}^{10} \sum_{sample=1}^{2{,}000} UU$$

$$S_{vv} = \frac{1}{20{,}000} \sum_{loop=1}^{10} \sum_{sample=1}^{2{,}000} VV$$

$$S_{\overline{u'v'}} = \frac{1}{20{,}000} \sum_{loop=1}^{10} \sum_{sample=1}^{2{,}000} UV \qquad \{19\}$$

$$S_{uuv} = \frac{1}{20{,}000} \sum_{loop=1}^{10} \sum_{sample=1}^{2{,}000} UUV$$

$$S_{uvv} = \frac{1}{20{,}000} \sum_{loop=1}^{10} \sum_{sample=1}^{2{,}000} UVV$$

$$S_{uuu} = \frac{1}{20{,}000} \sum_{loop=1}^{10} \sum_{sample=1}^{2{,}000} UUU$$

$$S_{vvv} = \frac{1}{20{,}000} \sum_{loop=1}^{10} \sum_{sample=1}^{2{,}000} VVV$$

In these equations, U and V are instantaneous velocities.

For the uw measurement plane, turbulence statistics are calculated using the following equations:

$$\begin{aligned}
&\overline{u} = S_u \\
&\overline{w} = S_w \\
&\overline{u'^2} = S_{uu} - S_u S_u \\
&\overline{w'^2} = S_{ww} - S_w S_w \\
&\overline{u'w'} = S_{\overline{u'w'}} - S_u S_w \\
&\overline{(u')^2 w'} = S_{uuw} - S_w\left(S_u S_u - (u')^2\right) - 2S_u\overline{u'w'} \\
&\overline{u'(w')^2} = S_{uww} - S_u\left(S_w S_w - (w')^2\right) - 2S_w\overline{u'w'} \\
&\overline{u'^3} = S_{uuu} - S_u\left(S_u S_u + 3(u')^2\right) \\
&\overline{w'^3} = S_{www} - S_w\left(S_w S_w + 3(w')^2\right)
\end{aligned} \qquad \{20\}$$

where:

$$S_u = \frac{1}{20{,}000} \sum_{loop=1}^{10} \sum_{sample=1}^{2{,}000} U$$

$$S_w = \frac{1}{20{,}000} \sum_{loop=1}^{10} \sum_{sample=1}^{2{,}000} W$$

$$S_{uu} = \frac{1}{20{,}000} \sum_{loop=1}^{10} \sum_{sample=1}^{2{,}000} UU$$

$$S_{ww} = \frac{1}{20{,}000} \sum_{loop=1}^{10} \sum_{sample=1}^{2{,}000} WW$$

$$S_{\overline{u'w'}} = \frac{1}{20{,}000} \sum_{loop=1}^{10} \sum_{sample=1}^{2{,}000} UW \qquad \{21\}$$

$$S_{uuw} = \frac{1}{20{,}000} \sum_{loop=1}^{10} \sum_{sample=1}^{2{,}000} UUW$$

$$S_{uww} = \frac{1}{20{,}000} \sum_{loop=1}^{10} \sum_{sample=1}^{2{,}000} UWW$$

$$S_{uuu} = \frac{1}{20{,}000} \sum_{loop=1}^{10} \sum_{sample=1}^{2{,}000} UUU$$

$$S_{www} = \frac{1}{20{,}000} \sum_{loop=1}^{10} \sum_{sample=1}^{2{,}000} WWW$$

U and W are instantaneous velocities.

IV. EXPERIMENTAL RESULTS

A. CALCULATIONS

All results are presented in graphical form. A directory of the software used to make all calculations and to plot the results is included in Appendix B. A summary of the important calculations is presented here.

1. Normalization of Results

Average velocities, Reynolds stress tensor components, and triple products are normalized with respect to the freestream velocity. The plotted quantities are then $\bar{u}/U_e$, $\overline{v'^2}/U_e^2$, $\overline{u'^2w'}/U_e^3$ etc., where U_e is the freestream velocity at the top of each column of nodes in the survey. For example, in a survey with 0.25 inch node spacing, the nodes are arranged in 19 columns with 12 nodes in each column. The top node of each column is well outside of the boundary layer so the measured $\bar{u}$ is equal to the freestream velocity, $\bar{u} = U_\infty = U_e$. A different normalizing velocity, U_e, is used for each column to correct for any small change or drift of the freestream velocity during the survey. Typically, the freestream velocity decreases about two percent in the 18 hours required to complete a 228 node survey. By measuring the freestream at the top of each column of nodes and using these 19 velocities for normalization, the normalized results result reflect a freestream velocity that is constant to within 0.1 percent.

2. Normalized Secondary Flow Vectors, $\vec{V}$

The vector sum of the normalized vertical and spanwise mean velocities, $\bar{v}/U_e$ and $\bar{w}/U_e$, is calculated and plotted at each node. The magnitude of the vector is:

$$|\vec{V}| = \sqrt{\left(\frac{\bar{v}}{U_e}\right)^2 + \left(\frac{\bar{w}}{U_e}\right)^2} \qquad \{22\}$$

The direction of the vector, measured counter-clockwise from the positive z-axis is:

$$\begin{aligned} \angle\vec{V} &= \tan^{-1}\left(\frac{\bar{v}}{\bar{w}}\right) \quad \text{if } \bar{w} > 0 \\ \angle\vec{V} &= 180 + \tan^{-1}\left(\frac{\bar{v}}{\bar{w}}\right) \quad \text{if } \bar{w} < 0 \end{aligned} \qquad \{23\}$$

3. Streamwise Vorticity, ω_x

The streamwise component of vorticity, ω_x, is defined as:

$$\omega_x = \frac{\partial \overline{w}}{\partial y} - \frac{\partial \overline{v}}{\partial z} \qquad \{24\}$$

ω_x is estimated at each node using the central-finite-difference equation:

$$\omega_x(y,z) = \frac{\overline{w}(y+\Delta,\ z) - \overline{w}(y-\Delta,\ z)}{2\Delta} - \frac{\overline{v}(y,\ z+\Delta) - \overline{v}(y,\ z-\Delta)}{2\Delta} \qquad \{25\}$$

where Δ is the node spacing. A uniform grid is used so $\Delta_y = \Delta_z = \Delta$. The vorticity calculated with Equation {25} is dependent on node spacing. The maximum vorticity calculated using 0.1 inch node spacing is almost twice that calculated using 0.25 inch spacing for identical flow conditions. Part of this discrepancy is believed to be due to spatial resolution errors of the hot-wire probe in regions where severe velocity gradients occur, i.e., near the vortex center. Because ω_x depends so strongly on node spacing, quantitative comparisons of vorticity can only be made between measurements made with equal node spacing.

Two node spacings are used in this study. The majority of the measurements are made with 0.25 inch spacing. However, surveys for two flow conditions are made with 0.10 inch spacing. The maximum vorticity for each experiment, and the y, z coordinates of the node with maximum vorticity are denoted as Wxmax, Ycen, and Zcen respectively on the vorticity plots.

4. Circulation, Γ

Circulation, Γ, is defined as the line integral around a closed curve, C, of the velocity component, V_t, tangent to the curve:

$$\Gamma = \oint_C V_t \, dl \qquad \{26\}$$

where dl is an elemental arc length along curve C. By Stokes' theorem, this line integral, when evaluated around a closed curve in the y-z plane, is equal to the streamwise vorticity integrated over the area enclosed by the curve:

$$\Gamma = \oint_C V_t \, dl = \int_A \omega_x \, dA \qquad \{27\}$$

Here, A is the area enclosed by the curve C, and dA is an elemental area.

Circulation is estimated using a method proposed by Schwartz [Ref. 12: pp. 17-18]. In this method, the circulation is calculated by multiplying the vorticity at each node by the area enclosing the node, and then summing this product, ($\omega_x\Delta^2$), over all nodes where the vorticity exceeds some arbitrary *threshold* level. The threshold level chosen here is ten percent of the maximum vorticity measured at probe location B with no injection. This maximum vorticity, measured with 0.25 inch grid size, is 569.9 s^{-1} giving a threshold level of 56.99 s^{-1}. Circulation is not calculated for 0.10 inch node spacing surveys because the measurement grid is not large enough to include all nodes where the vorticity is above the threshold level. The threshold level provides a means of *filtering* small values of spurious vorticity "noise" from the integration. Circulation is denoted as Cr on the vorticity plots.

A non-dimensional parameter relating circulation, Γ, to injectant (cooling) jet velocity, U_c, is given by:

$$ND\Gamma_2 = \frac{\Gamma}{U_c d} \qquad \{28\}$$

where d is the injection hole diameter [Ref. 12: p. 18]. This parameter is calculated and listed on vorticity plots where injection is used.

5. Vortex Core Size

The average vortex core radii in the y and z directions, Ycore and Zcore, are estimated using two approaches. In the first method, proposed by Schwartz [Ref. 12: p. 19], all vorticity is assumed to be contained within the vortex core and the core boundary is assumed to be located where secondary velocity vectors reach local maxima. Ycore is estimated by measuring, in the +y and -y directions, the distances from the node of maximum vorticity (core center) to nodes where secondary velocities are maximum (core edges). The average of these two distances gives Ycore. Zcore is estimated by measuring in the +z and -z directions. The disadvantage of this method is that the core edge location is estimated to the nearest node, so the core dimensions are estimated to an accuracy of only $\pm\Delta$.

A second method is proposed by Craig [Ref. 18: pp. 23-25] and is based on a method described by Westphal et al [Ref. 9: p. 7]. In this method, the core is assumed to extend from the node of maximum vorticity to a boundary where the vorticity is 40 percent of the maximum. This 40 percent value is chosen since Craig's data shows this to approximately correspond to locations where secondary flow vectors are maximum. This method is advantageous because the location of the core boundary is not

"rounded-off" to the nearest node. If core boundaries are located between nodes, linear interpolation is used to find the core dimensions. Ycore and Zcore are calculated using both methods and are listed on the vorticity plots.

B. SURVEY CONDITIONS AND PARAMETERS

The conditions and parameters for each survey are shown in Table 1. Discussion of results proceeds in the same order as surveys are listed in Table 1.

Table 1. SUMMARY OF SURVEY CONDITIONS AND PARAMETERS

Run Number (Date/Time)	Probe Location	Probe Orientation	Node Spacing (in)	Blowing Ratio, m	Vortex Generator
31689.1412	B	uv	0.25	0	NO
31789.1222	B	uw	0.25	0	NO
31889.1131	B	uv	0.25	1.5	NO
31989.1131	B	uw	0.25	1.5	NO
21489.2041	B	uv	0.25	0	YES
21589.2146	B	uw	0.25	0	YES
30389.1945	B	uv	0.10	0	YES
30589.0045	B	uw	0.10	0	YES
22289.1659	B	uv	0.25	1.5	YES
22789.1223	B	uw	0.25	1.5	YES
30689.1355	B	uv	0.10	1.5	YES
30789.2005	B	uw	0.10	1.5	YES
31189.1531	A′	uv	0.25	1.5	YES
31289.1422	A′	uw	0.25	1.5	YES
31389.1941	A″	uv	0.25	1.5	YES
31489.1701	A″	uw	0.25	1.5	YES
30989.1655	C	uv	0.25	1.5	YES
31089.1529	C	uw	0.25	1.5	YES
21889.1108	B	uv	0.25	2.5	YES
21989.1355	B	uw	0.25	2.5	YES

Notes:
1. *Freestream velocity = 10.0 m/s*
2. *Probe locations.... A′: x′/d = 5.9, A″: x′/d = 19.2, B: x′/d = 30.1, C: x′/d = 70.3*
3. *12 degree vortex generator positioned with leading edge at: x = 48.7cm, z = 1.9cm*

C. BASELINE DATA

1. Boundary Layer

Measurements (made with 0.25 inch grid size) of the turbulent boundary layer at probe location B with no injection and no vortex generator are plotted in Figures 19-33.

Figure 19 shows the fluctuating velocity distributions plotted with data from Klebanoff [Ref. 22: p. 34]. The data show very good agreement, particularly in the v' and w' profiles. The measured streamwise fluctuating velocity component, u', was five to ten percent higher than found by Klebanoff. Other researchers, including Orlando et al [Ref. 23: p. 84] and Wang et al [Ref. 24: p. 8] have also measured higher values of u' in the outer region of the boundary layer and have attributed this difference to a higher freestream turbulence intensity than was present in Klebanoff's work. The freestream turbulence intensity in the present study is roughly ten times that in Klebanoff's study.

Figure 20 shows the turbulent shear stress distribution in the boundary layer. These results are also plotted with data from Klebanoff [Ref. 22: p. 35]. Excellent agreement is seen in this data.

The mean velocity, fluctuating velocity and τ'_{xy} contours, Figures 21-25, show the boundary layer to be spanwise uniform except for a small perturbation appearing at the location of the injection hole (z = 0). The perturbation may be caused by the tape strip covering the hole during this baseline survey. Whatever the cause, the perturbation is insignificant compared to the effects of the injectant air flow during vortex / wall jet interaction measurements. The τ'_{xz} and triple product contours in Figures 26-33 are not informative because these quantities are relatively constant over large areas of the plots. Consequently, scattered contour levels with very narrow ranges are present which can not be plotted accurately with the contouring software.

2. Boundary Layer / Wall Jet Interaction

Figures 34-49 show the effects of injection (m = 1.5) on the boundary layer structure at probe location B. The jet displaces the boundary layer away from the wall creating a dome-shaped $\bar{u}$ deficit centered at the location of the jet axis (z = 0). Two relatively weak vortices with opposing rotations form on opposite sides of the jet. The vortex on the -z side rotates in the counter-clockwise direction, the vortex on the +z side rotates in the clockwise direction. In the counterclockwise vortex, the spanwise shear, $\overline{u'w'}$, shows large positive values and the triple products $\overline{w'^3}$ and $\overline{u'^2w'}$ show large negative

values. In the clockwise vortex, the spanwise shear is negative and these two triple products have positive values. Common to both vortices is a region of large positive $\overline{u'^3}$. Between the vortices, at z = 0, a region of large negative $\overline{u'^3}$ exists near the wall. A dome-shaped region of large positive $\overline{v'^3}$ projects outside the boundary layer at z = 0. A similarly shaped structure is seen in the $\overline{u'^2v'}$, $\overline{u'v'^2}$ and $\overline{u'w'^2}$ contours. The boundary layer away from the jet in the -z direction shows little or no distortion due to the presence of the jet.

3. Boundary Layer / Vortex Interaction

With the vortex generator installed as described in Chapter II, measurements were made at probe location B using two node spacings, Δ = 0.25 inches and Δ = 0.10 inches.

a. Δ = 0.25 inches

Figures 50-65 show the turbulence structure resulting from the interaction of the boundary layer and the generated vortex. The vortex center, located at z = -3.18 cm, y = 2.46 cm, is surrounded by a region of relatively low streamwise velocity. The vortex downwash forces freestream flow towards the wall resulting in a very thin boundary layer at $-3 < z < 0$. The reverse effect is seen at $-7 < z < -3$ where the slower moving fluid is convected away from the wall by the vortex upwash, creating a thick boundary layer. The streamwise vorticity, ω_x, calculated with $\Delta = 0.25$ inches is equal to 569.99 s^{-1}. This is the vorticity upon which the threshold level is based (for calculation of circulation). The vortex core is essentially circular with an average radius of 0.71 cm. Large gradients in the normal Reynolds stress components $\overline{u'^2}$, $\overline{v'^2}$ and $\overline{w'^2}$, exist in the vortex core. These stresses are large at the vortex center and in the downwash region near the wall. Regions of positive Reynolds shear stress, $\overline{u'v'}$ and $\overline{u'w'}$, exist near the vortex core. Steep, decreasing gradients of these shear stresses are seen at $z \approx -6$. Large triple product gradients exist near the wall in the downwash region of the vortex. Similar trends are described by Shabaka, Mehta and Bradshaw [Ref. 5] except near the vortex core where large normal Reynolds stress gradients were not found as described here.

b. Δ = 0.10 inches

To resolve the structure of the boundary layer / vortex interaction into greater detail, the experiment was repeated using node spacing of 0.10 inches. The location of the grid was chosen to include the regions where the most significant turbulence structure changes were expected to occur (the vortex upwash region and the near-wall region between the injection hole and the upwash). The results are shown in

Figures 66-80. Compared to the $\Delta = 0.25$ inch results, these results are smoother with more coherent contours. Comparison of $\Delta = 0.25$ and $\Delta = 0.10$ plots show excellent qualitative and quantitative agreement. The most dramatic feature in the more detailed plots is the structure of the vortex center where local maxima and local minima of the diffusive transport quantities $\overline{v'^3}$, $\overline{w'^3}$, $\overline{u'^2v'}$, $\overline{u'v'^2}$ and $\overline{u'^2w'}$ exist. These result in severe triple product gradients in the vortex core. Also visible in the detailed vorticity plot are scattered regions of negative vorticity near the wall.

D. BOUNDARY LAYER / VORTEX / WALL JET INTERACTION

The interaction of the boundary layer, vortex and wall jet is examined in the following manner. First, the structure is measured at probe location B using a blowing ratio of m = 1.5. This is the same blowing ratio and probe location used in the baseline measurements. Next, streamwise development with the same blowing ratio is examined. Data obtained at probe locations A′, A″ and C are presented in addition to the data at location B. Finally, data obtained at probe location B using a blowing ratio of m = 2.5 is presented to show the effect of increasing blowing ratio.

1. Blowing Ratio = 1.5

a. Probe Location B, Δ = 0.25 inches

Figures 81-96 show the interaction of the boundary layer, vortex and wall jet measured at probe location B with $\Delta = 0.25$. The mean velocities are dominated by the vortex. The high velocity injectant has been swept in the -z direction by the vortex as is evident by the region of high $\bar{u}$ and the upward rotation of the secondary flow vectors at $z \approx -4$ Because the wall jet is located under the vortex downwash, the vortex rotation is opposed and the maximum vorticity is decreased. In addition, the vortex center is forced away from the wall jet. The vortex center is been displaced 0.64 cm in the +y direction and 0.63 cm in the -z direction. The vortex core size is unchanged. Near the wall at $z \approx -4.5$, a weak vortex with rotation opposite to that of the main vortex exists.

The spatial extents of the high normal Reynolds stress regions near the vortex center are increased because of the wall jet. The dome-shaped region of low streamwise turbulent shear stress $\overline{u'v'}$, most evident for wall jet data / boundary layer data with no vortex, has decreased in size and has moved in the -z direction to z = -3.5. A region of negative spanwise shear, $\overline{u'w'}$, which becomes less negative as y increases, is present near the wall at z = -2.5. The direction and shape of the gradient is similar to

the $\overline{u'w'}$ gradient observed on the +z side of the wall jet in the boundary layer / wall jet baseline data.

The effect of the wall jet on turbulent transport is largest near the wall at $-5 < z < -1$. Here, spanwise uniform distributions with no wall jet are disturbed with the addition of the jet.

b. Probe Location B, Δ = 0.10 inches

Results of the more detailed survey at probe location B with boundary layer / vortex / wall jet interaction are shown in Figures 97-111.

Existence of a secondary vortex with rotation opposite to the main vortex is clearly seen in Figures 97 and 98. A region of negative vorticity centered at z = -4.0, y = 0 is much larger and more organized than the scattered negative vorticity regions observed in the previous case (boundary layer and vortex with no wall jet). This region of negative vorticity coincides with high $\bar{u}$.

In the boundary layer / vortex / wall jet flow, a dome-shaped region of increased $\overline{u'^2}$ exists near the wall for $-4 < z < -2.5$. Similar distributions are seen in the turbulent shear stresses $\overline{u'v'}$ and $\overline{u'w'}$. The reduced node spacing also reveals severe gradients of $\overline{u'v'}$ in or near the vortex core. This streamwise component of turbulent shear stress also changes from a large positive value to a large negative value near the vortex center.

The effect of the wall jet on near-wall turbulent transport distributions is clearly visible. With the wall jet, a region of large positive $\overline{u'^3}$ is present near the wall where large negative regions of $\overline{u'^3}$ exist without the wall jet. Similar structural changes are observed for the $\overline{u'^2v'}$, $\overline{u'^2w'}$ and $\overline{u'w'^2}$ distributions.

c. Streamwise Development

In order to study the streamwise development of the boundary layer / vortex / wall jet interaction, results are given for probe locations A′, A″ and C. Plots of the velocity, vorticity, Reynolds stress components and triple products are arranged in streamwise order in Figures 112-159.

At probe location A′ (5.6 cm downstream from the injection hole), the effect of the wall jet is very conspicuous. In Figure 118, the secondary flow vectors show a strong $\bar{v}$ component at z = -0.5. As the flow moves downstream, this $\bar{v}$ component diminishes. At probe location C (175 cm downstream from the injection hole), no wall jet effect is evident in the secondary flow vectors (Figure 120). Spanwise and vertical movement of the vortex center is evident in Figures 115-117. The vortex center moves 1.91 cm in the -z direction and 0.64 cm in the +y direction as the vortex travels down

stream from location A′ to location C. As expected, the maximum vorticity decreases and the size of the vortex core increases as vorticity is diffused. Regions of negative vorticity near the wall are visible at locations A′ and A″. This is consistent with the structure observed in the boundary layer / wall jet baseline measurements which indicate the presence of a horseshoe vortex near the injection hole as slower moving boundary layer fluid "wraps" around injectant. The region of negative vorticity moves in the -z direction as the flow progresses downstream to become almost totally dissipated at probe location C.

Mean streamwise velocity contours in Figures 121-123, show that high velocity injectant fluid is swept in the -z direction by the vortex. Figure 121 further suggests that two regions of high $\bar{u}$ fluid are created by the wall jet. As these two regions are swept along by the vortex, they eventually merge (see Figure 84), and streamwise velocity magnitudes decrease. By the time the flow reaches location C, little evidence of the wall jet is seen in the $\bar{u}$ contours. Similar convection and diffusion phenomena are also evident in the streamwise development of all Reynolds stress components and triple products.

2. Blowing Ratio = 2.5

Results in Figures 160 to 175 are for a blowing ratio of 2.5 at probe location B. In this case the effect of the wall jet is significantly greater than when m = 1.5. For m = 2.5, high $\bar{u}$ injectant has not been swept away by the vortex. A large region of high streamwise velocity remains at z = -1, very near the spanwise location of the injection hole. The maximum vorticity is reduced from 410 s^{-1} to 167 s^{-1}. The vortex core is enlarged and is elliptical rather than circular in shape. Distortion of the vortex core is also evident from the secondary flow vectors.

The Reynolds stress component distributions are all altered significantly by the m = 2.5 jet. In general, the stress distributions are "flatter" and "wider"than when m = 0 or when m = 1.5, and the circular shape of the turbulence structure is now elliptical in shape. The same change is also evident in regard to triple product contours. In addition, the structure of the vortex core is altered. Gradients between large negative and large positive values of $\overline{v'^3}$, $\overline{w'^3}$, $\overline{u'^2v'}$ and $\overline{u'^2w'}$, evident when m = 0 and m = 1.5, are not present in the vortex core when m = 2.5.

V. SUMMARY AND CONCLUSIONS

The turbulence structure resulting from the interaction of an embedded vortex and a single wall jet located under the downwash of the vortex was investigated. The vortex was generated using a 12 degree delta wing mounted on the test section floor. Blowing ratios of 1.5 and 2.5 were used with a freestream velocity of 10 m/s and zero pressure gradient. Baseline measurements were made for three situations: (1) boundary layer only, (2) boundary layer / wall jet, (3) boundary layer / vortex. Additional hot-wire anemometer measurements were made at four streamwise locations. The major conclusion of the investigation is that in the boundary layer, the vortex significantly alters the turbulence structure of the wall jet and vice versa. The injectant is distorted and convected away from the injection hole by vortex secondary flows. In general, this spanwise convection and streamwise diffusion phenomena are observed in all Reynolds stress tensor and turbulent diffusion components. Specific results and conclusions follow.

- Reynolds stress tensor components measured in the turbulent boundary layer (with no vortex or wall jet) show excellent agreement with results found in the literature [Refs. 22, 23 and 24]. This agreement is crucial in that it provides a basis for confidence in the results obtained from subsequent measurements.
- Results of the boundary layer / wall jet baseline measurements show that two regions of vorticity with opposing rotations exist at opposite spanwise sides of the wall jet. This is believed to be due to the formation of a horseshoe vortex near the injection hole as the slower moving boundary layer fluid is forced to the sides of the jet. The turbulent spanwise shear, $u'w'$, and the triple products w'^3 and u'^2w' are opposite in sign in the two regions of opposing vorticity. The boundary layer above the injection hole is displaced away from the wall creating a dome-shaped deficit streamwise velocity region.
- Interaction of the boundary layer and vortex results in a decrease of boundary layer thickness in the vortex downwash and an increase of boundary layer thickness in the upwash region. Severe gradients of Reynolds shear stress, $u'v'$ and $u'w'$, exist in the vortex upwash. Large gradients of Reynolds normal stress components, u'^2, v'^2 and w'^2, were found near the vortex core. Local maxima and minima of diffusive transport exist near the vortex core resulting in very severe gradients of these quantities.
- In the interaction of the boundary layer, vortex and wall jet, the vortex has the most influence on the turbulence structure. As expected, if the blowing ratio is increased, the effect of the wall jet becomes larger.
- When m = 1.5, the injectant is swept towards the upwash region of the vortex. Wall jet stress and diffusive transport distributions are moved away from the injection hole and are redistributed near the wall under the vortex core. A region of negative vorticity is also observed at this position.

- Streamwise development measurements suggest that as the injectant leaves the injection hole, two regions of high $\bar{u}$ fluid are formed. These regions are first swept towards the vortex core. Eventually, they merge and diffuse as the flow moves downstream.
- When m= 2.5, the wall jet is not as easily distorted as when m= 1.5. In spanwise normal planes, the overall turbulence structure is elliptical rather than circular. The structure of the vortex core is altered as evidenced by gradients of $\overline{v'^3}$, $\overline{w'^3}$, $\overline{u'^2v'}$, and $\overline{u'^2w'}$ which are much smaller than when m= 0 or m= 1.5.

As Theodore von Kármán once said, "People working on turbulence shall never run out of work." Much work remains to be done towards understanding the complex turbulent structure described in this thesis. Work currently ongoing at the Naval Postgraduate School under the direction of Professors Ligrani and Subramanian includes the study of the streamwise development of a wall jet / boundary layer interaction, measurement of the $\overline{v'w'}$ Reynolds stress component int the boundary layer / vortex / wall jet interaction, and measurement of the turbulence structure resulting from a wall jet located under the vortex upwash.

APPENDIX A. SOFTWARE DIRECTORY

Calibration, data acquisition and plotting programs are written in the HP-BASIC language. Program names and descriptions are provided here.

Program name	*Description*
AVG	Reads from uv and uw data files and normalizes $\overline{u}$, $\overline{u'^2}$ and $\overline{u'^3}$at each node with respect to &ubar, $\overline{u}^2$ or $\overline{u}^3$ measured at the top of each column of nodes. Averages normalized quantities from uv and uw data files. Results are plotted in contour format.
HOTWIREUV	Data acquisition program for measurements in the uv plane. Measures actual system gain and offset, then constructs look-up table using probe calibration constants read from file Cal#UV. The program includes commands to automatically move the probe through the desired number of nodes at the desired node spacing. Calculates $\overline{u}$, u'^2, v'^2, u'^3, v'^3, u'^2v' and $u'v'^2$ at each node. The results are written to a data file named by the user. This file is referred to as the *uv data file.*
HOTWIREUW	Data acquisition program for measurements in the uw plane. Reads probe calibration constants from file Cal#UW and writes results to the *uw data file.*
HWCAL	Performs velocity and yaw calibration for crossed wire probe. Calibration constants for measurements in uv and uw planes are written to files Cal#UV and Cal#UW respectively. In these file names, # is an integer automatically assigned to index the calibration files. Each time the probe is calibrated, # is incremented. This allows a complete history of probe calibration to be retained on a floppy disk.
SETCOND	Calculates blowing ratio, discharge coefficient and freestream velocity before each experiment. User must input total freestream pressure, pressure drop across injection holes, number of injection holes in use, and injectant flow rate.
HWVECTOR	Reads from uv and uw data files, calculates magnitude and direction of secondary flow vectors. Vector magnitudes are normalized with respect to $\overline{u}$ measured at the top of each column of nodes. The normalized secondary flow vectors are plotted at each node.
VORTY	Reads from uv and uw data files, calculates streamwise vorticity at each node. Circulation, based on a vorticity threshold of 56.99 s^{-1} (40% of maximum vorticity measured at probe location B with a 12 degree vortex generator and no injection). Two methods are used to estimate vortex core radii, Ycore and Zcore. In the first method, secondary flow vector magnitude is used to locate the core boundary, in the second method, vorticity magnitude is used. The

location of the vortex center is also calculated. Results are presented in contour plot format.

2UV Reads data from uv data file and plots contours of $\overline{v'^2}$ and $\overline{u'v'}$ normalized with respect to $\overline{u}^2$ measured at the top of each column of nodes.

2UW Reads data from uw data file and plots contours of $\overline{w'^2}$ and $\overline{u'w'}$ normalized with respect to $\overline{u}^2$ measured at the top of each column of nodes.

3UV Reads from uv data file and plots contours of $\overline{v'^3}$, $\overline{u'^2v'}$ and $\overline{u'v'^2}$ normalized with respect to $\overline{u}^3$ measured at the top of each column of nodes.

3UW Reads from uw data file and plots contours of $\overline{w'^3}$, $\overline{u'^2w'}$ and $\overline{u'w'^2}$ normalized with respect to $\overline{u}^3$ measured at the top of each column of nodes.

APPENDIX B. FIGURES

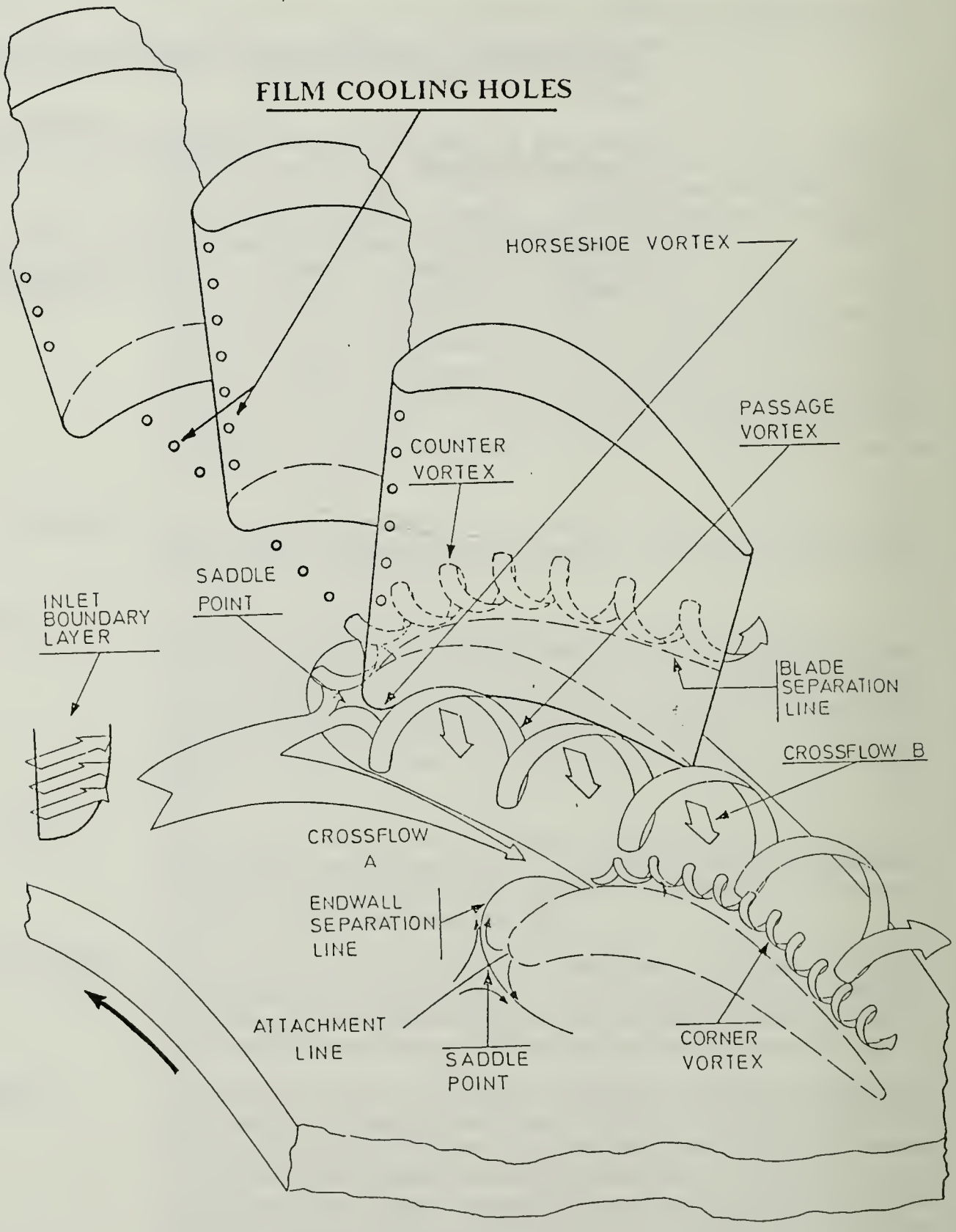

Figure 1. Flow in gas turbine passages

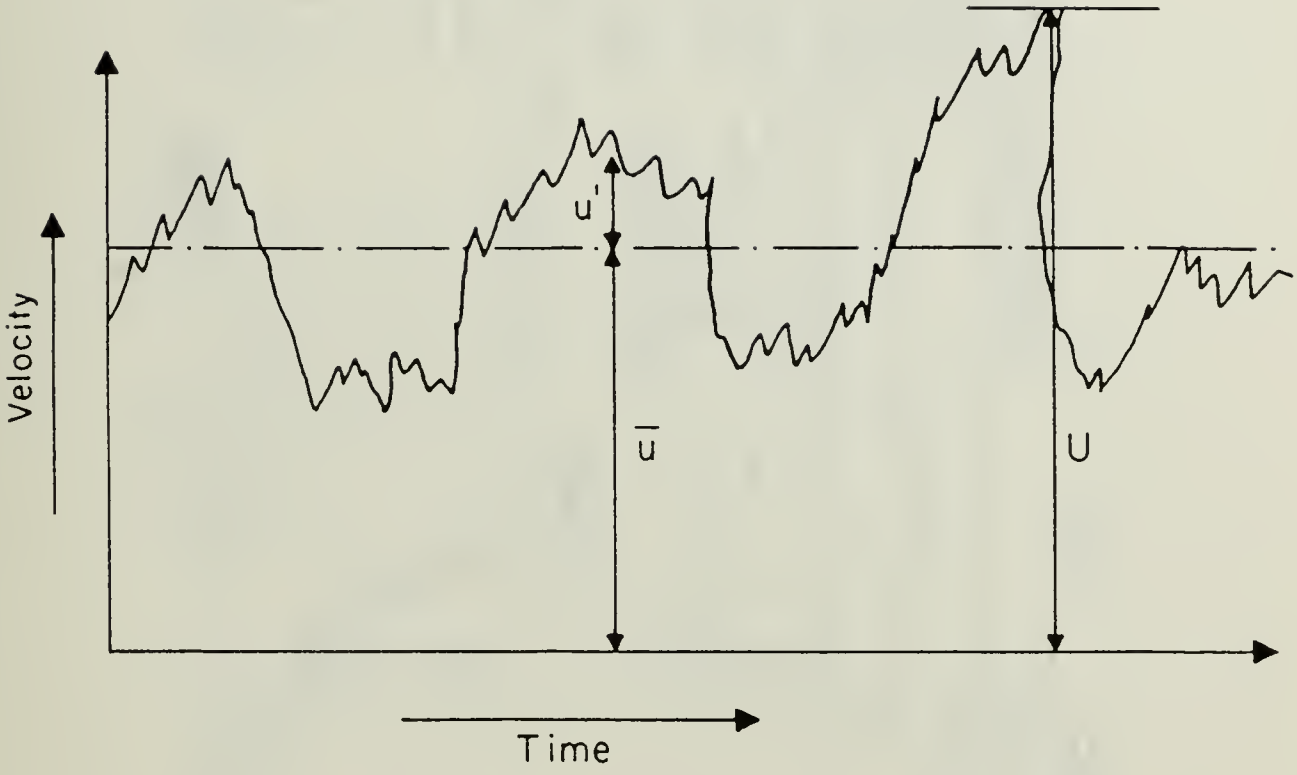

Figure 2. Instantaneous velocity components

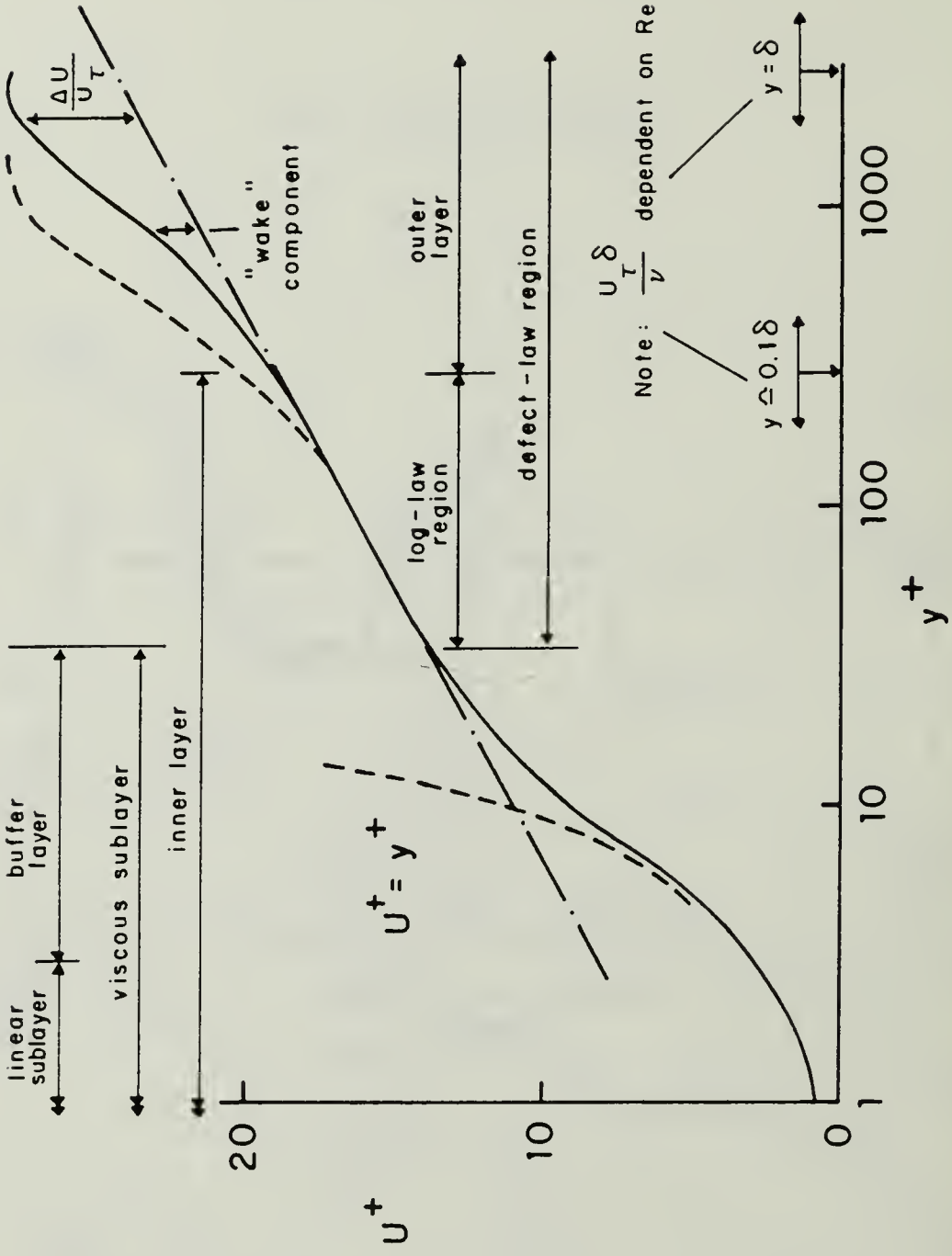

Figure 3. Multilayer turbulent boundary layer

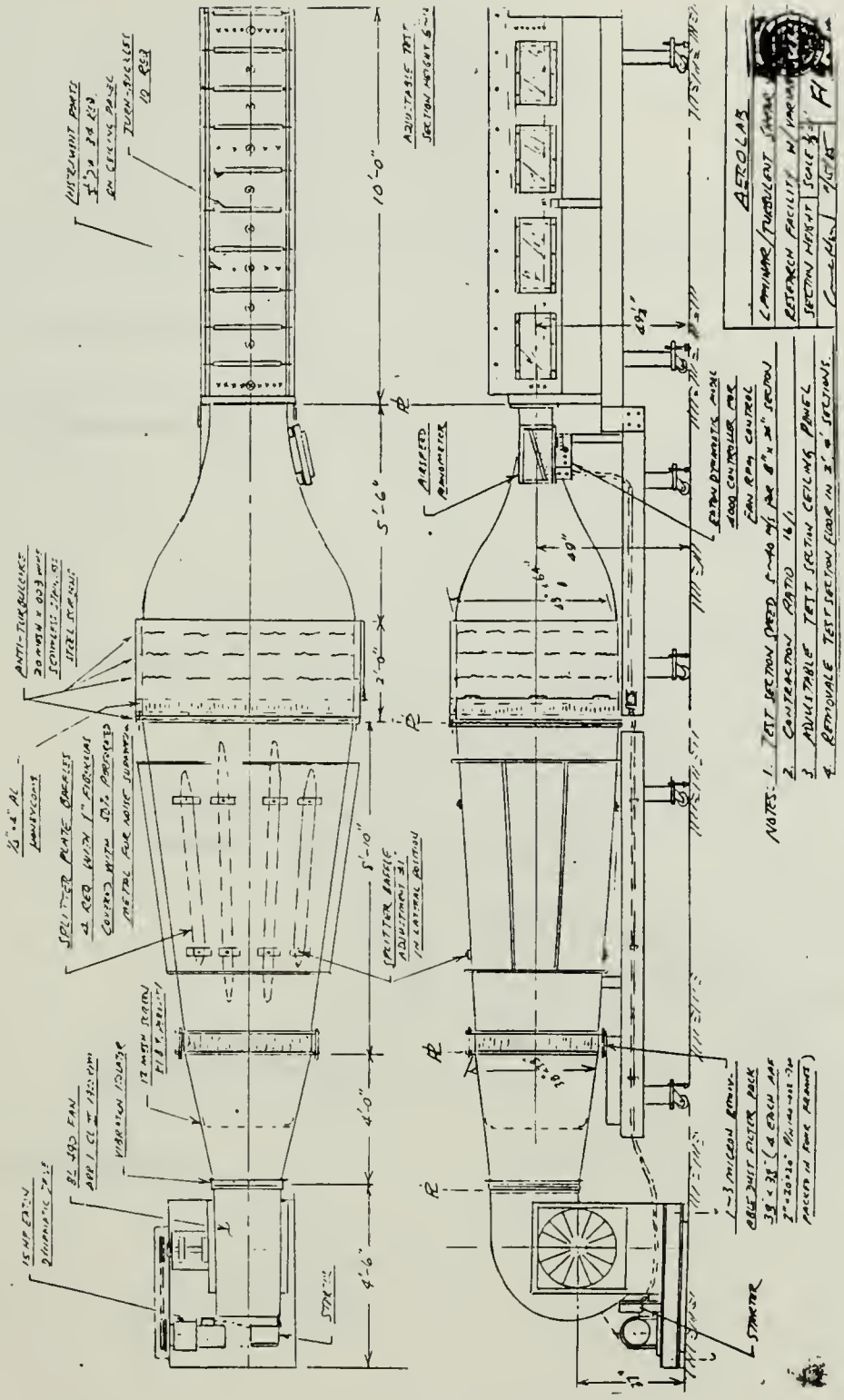

Figure 4. Schematic of wind tunnel

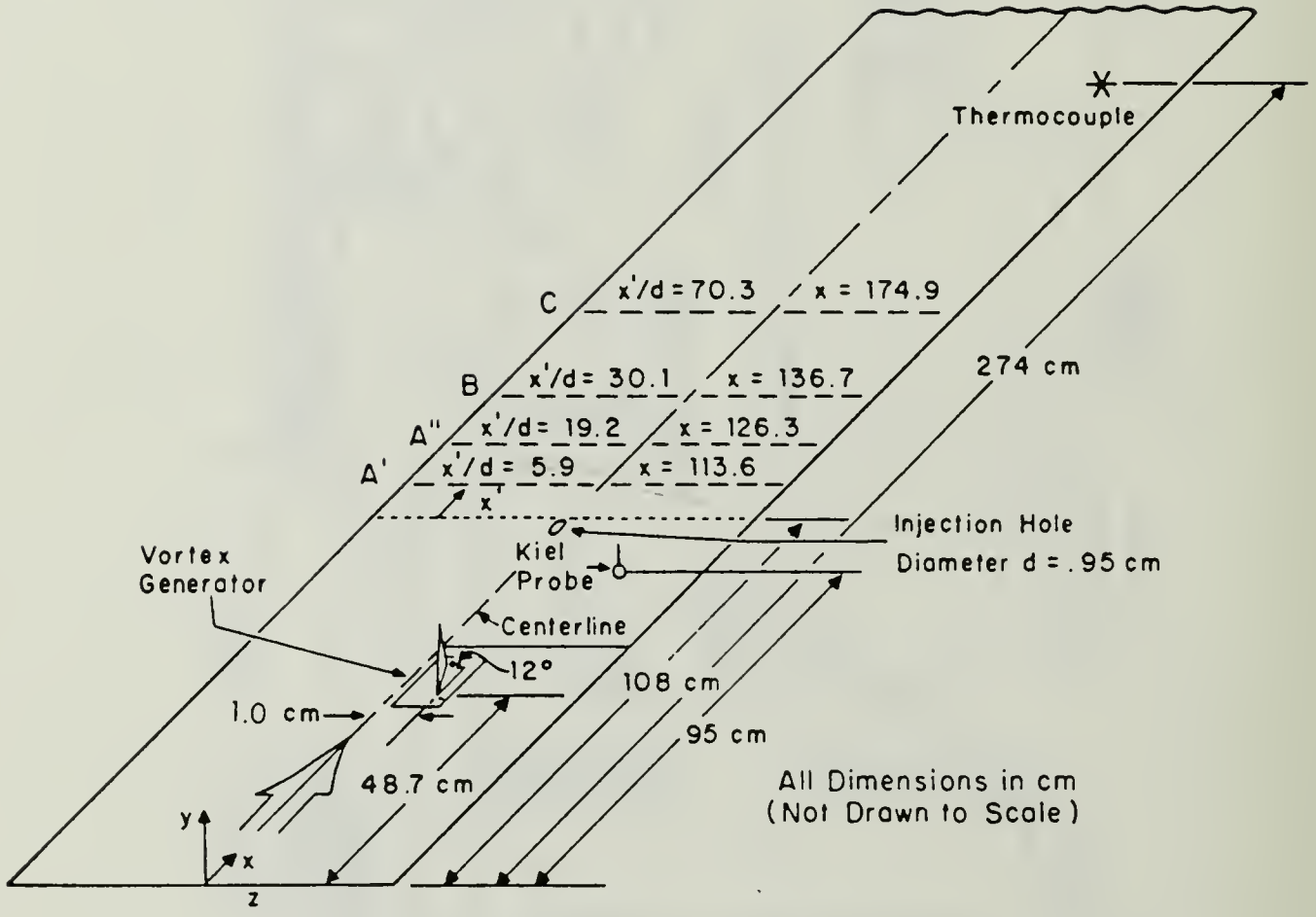

Figure 5. Test section schematic

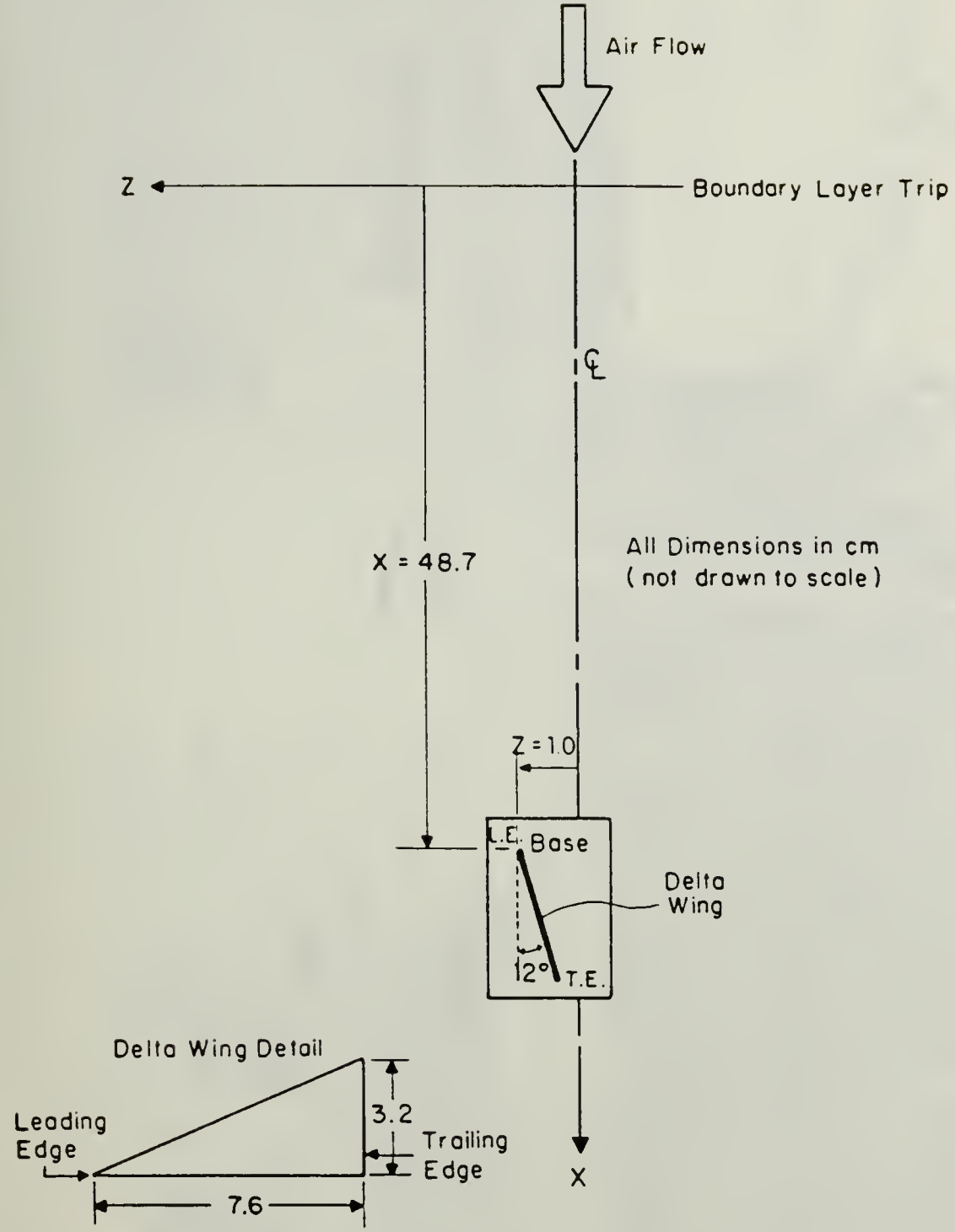

Figure 6. Vortex generator

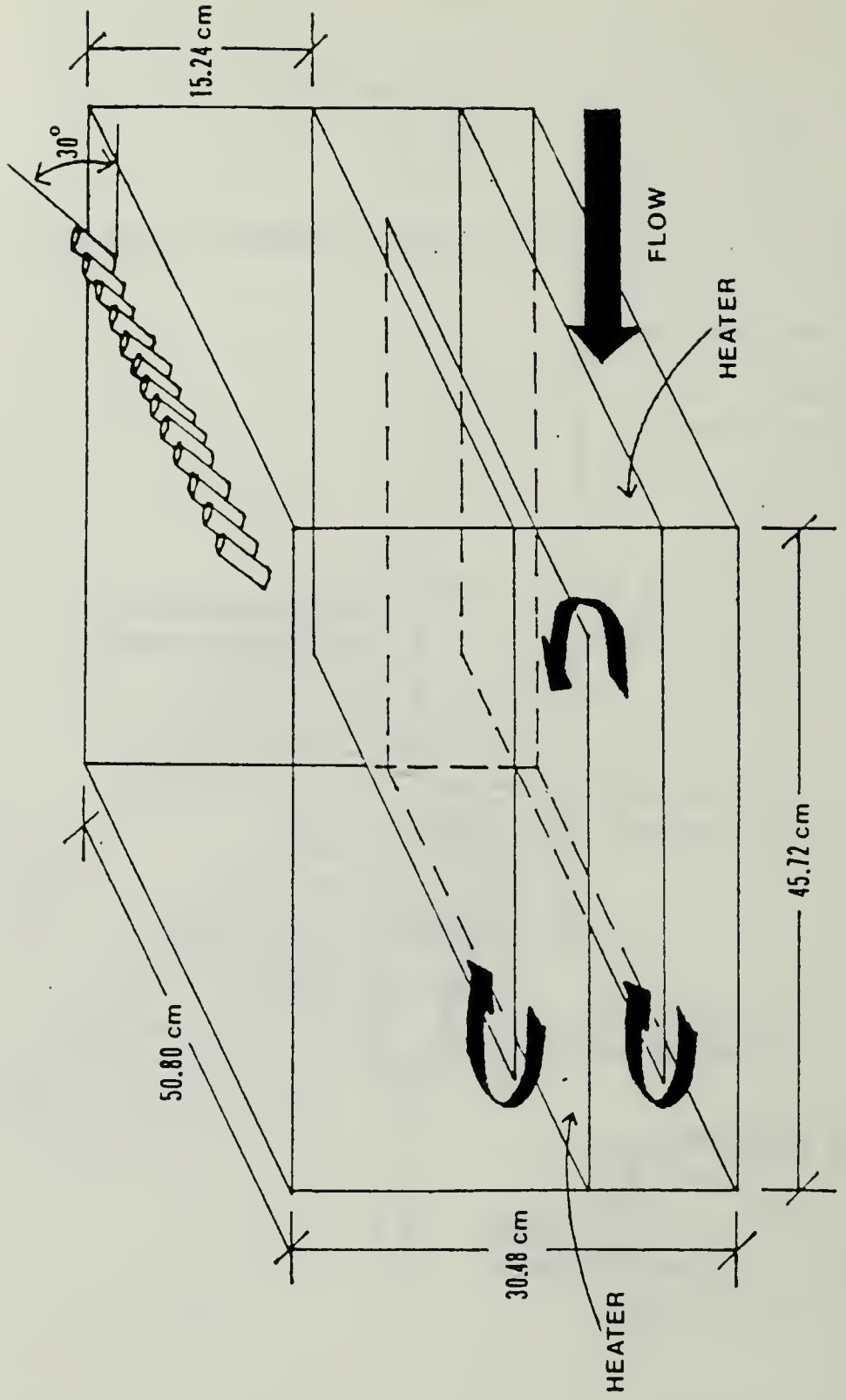

Figure 7. Plenum and injection tubes

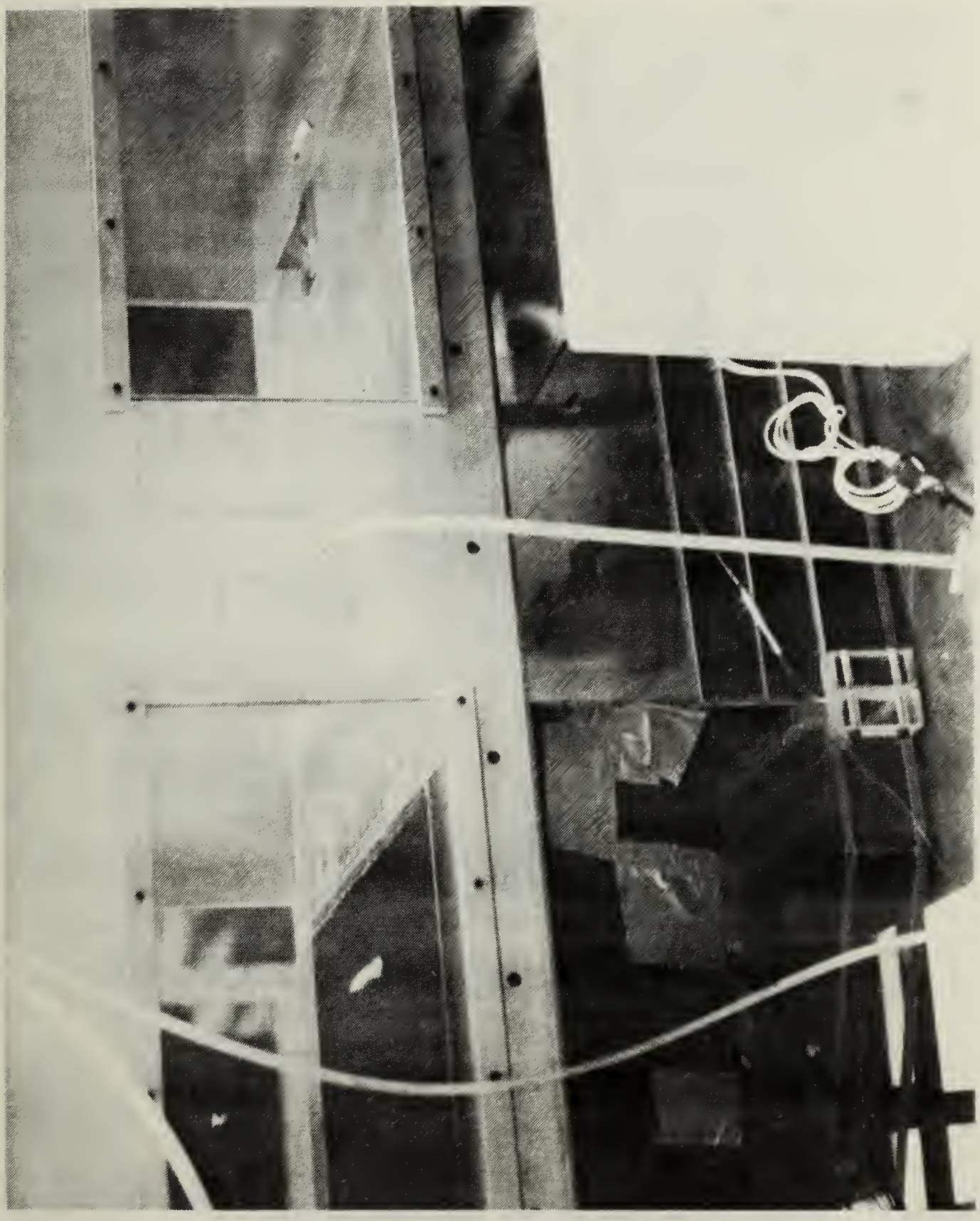

Figure 8. Photograph of plenum and test section

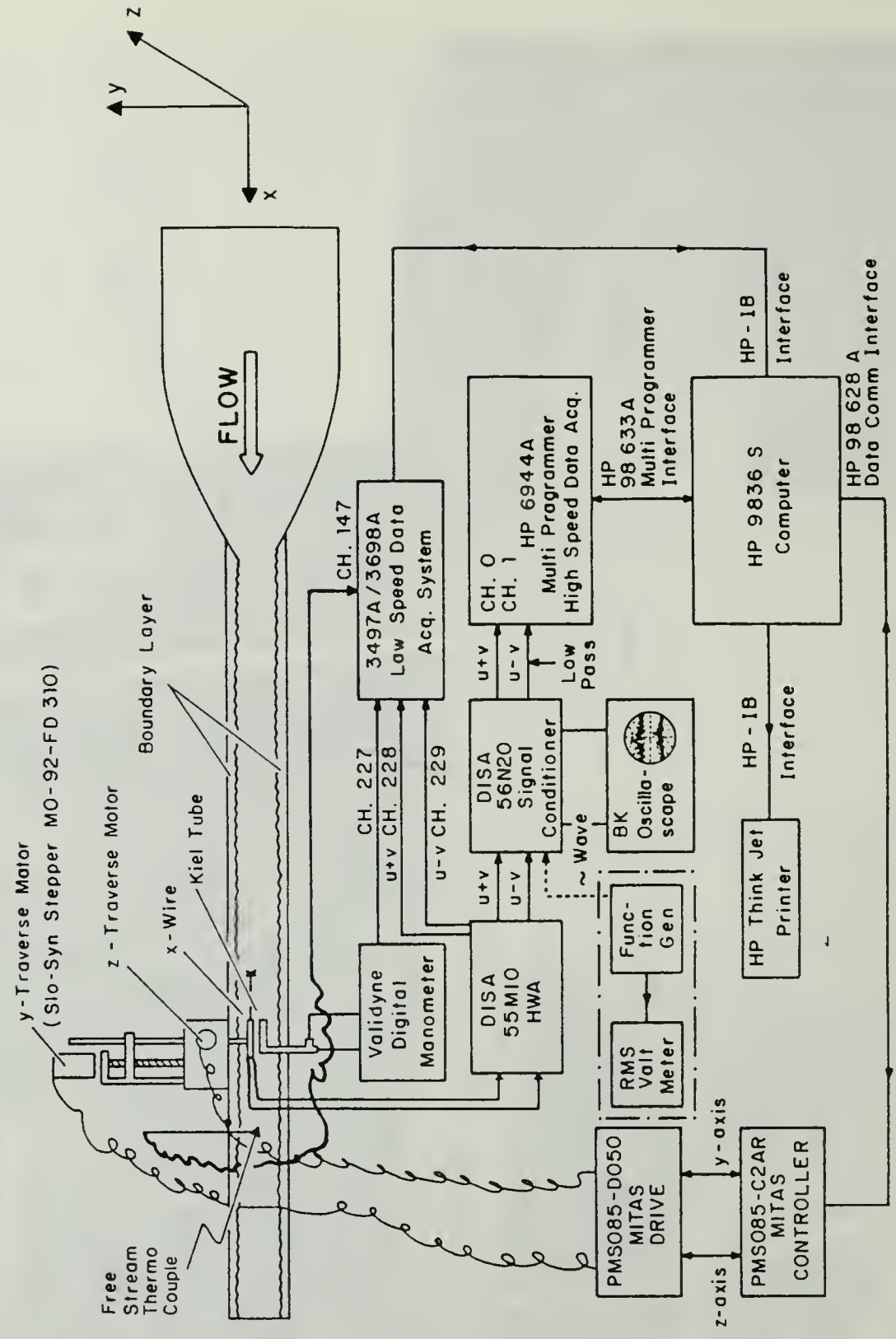

Figure 9. Schematic of hot wire and data acquisition systems

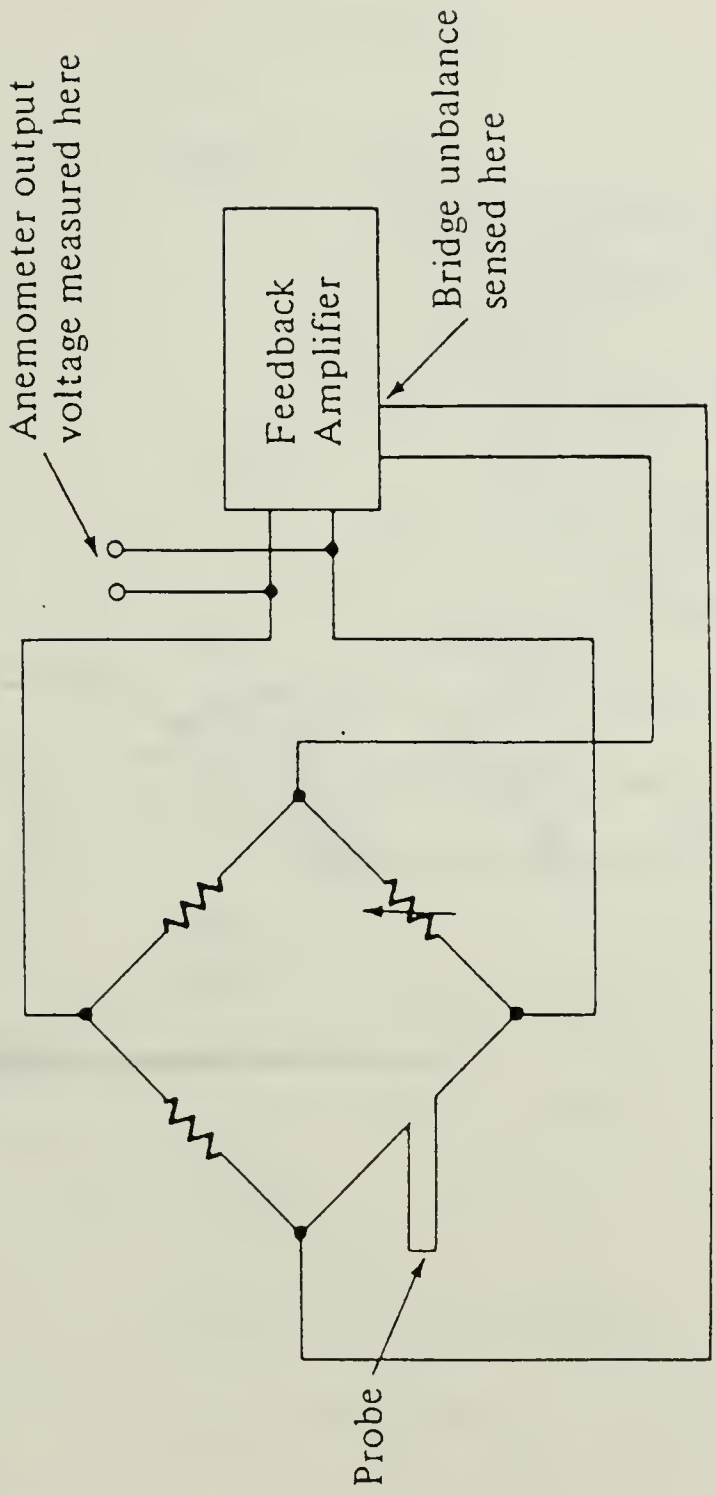

Figure 10. Block diagram of constant temperature anemometer

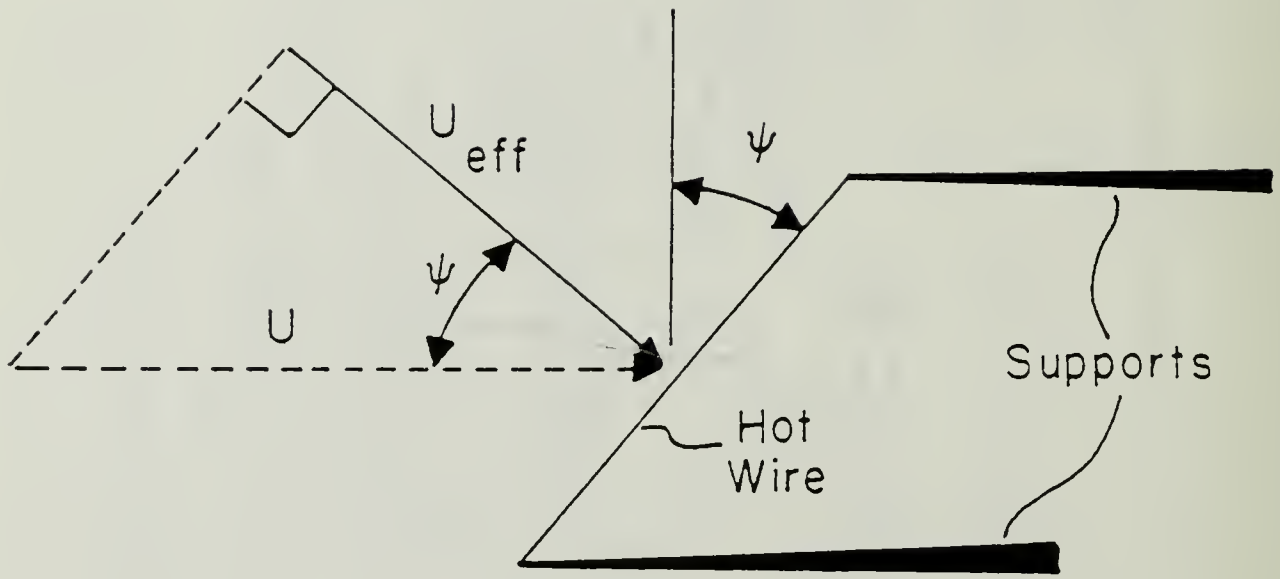

Figure 11. Effective cooling velocity

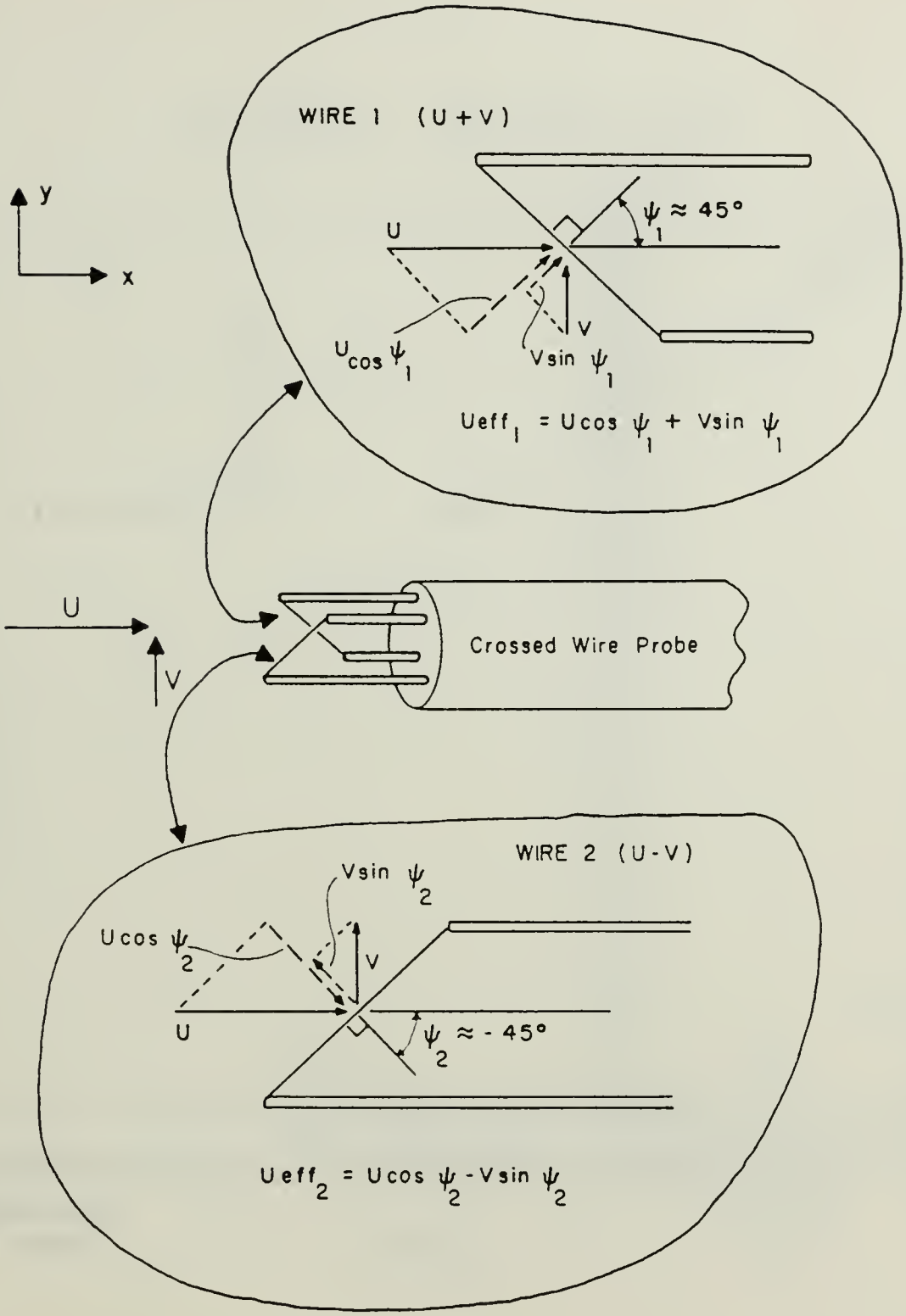

Figure 12. Effective velocities for crossed wire probe

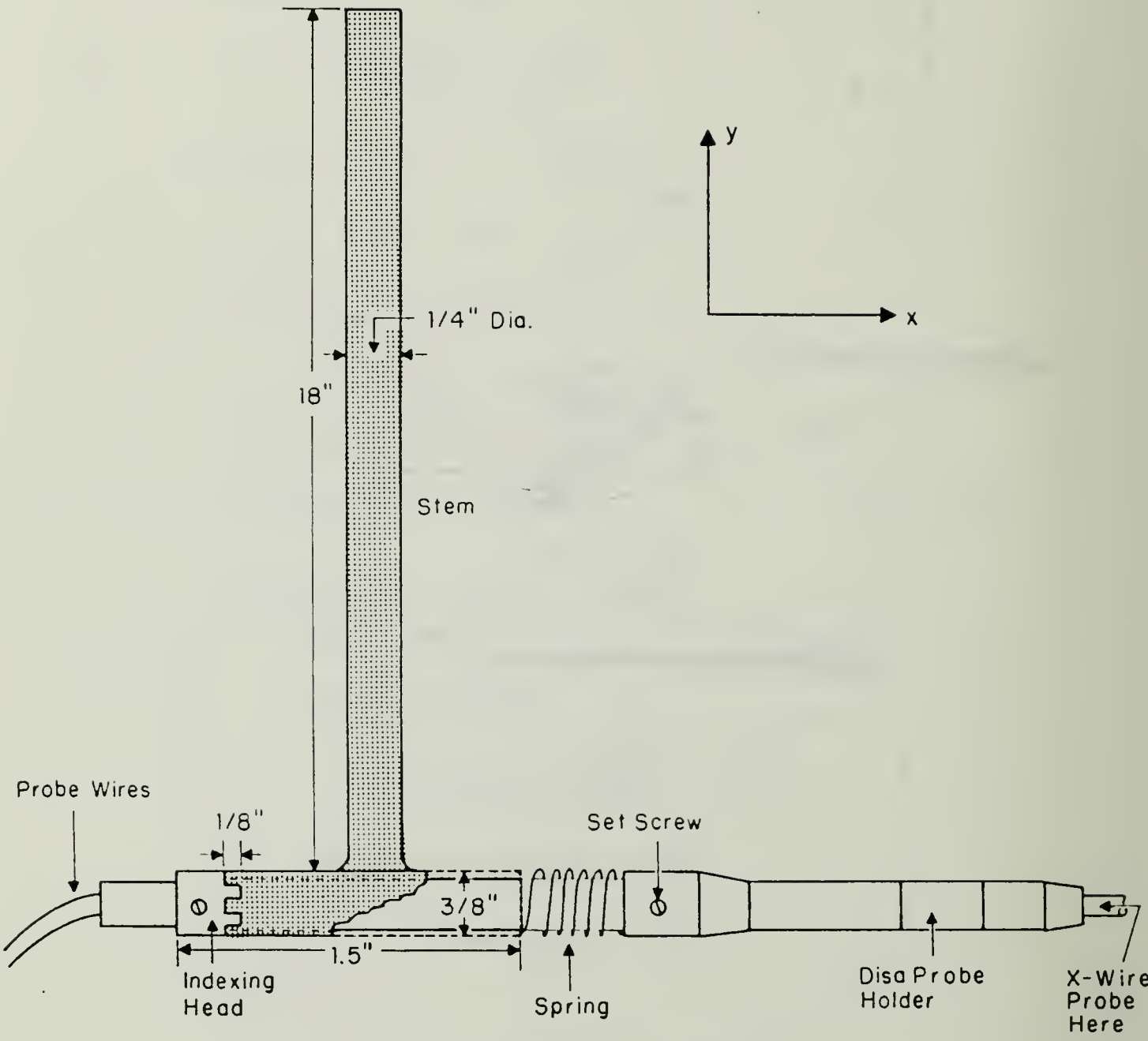

Figure 13. Probe support

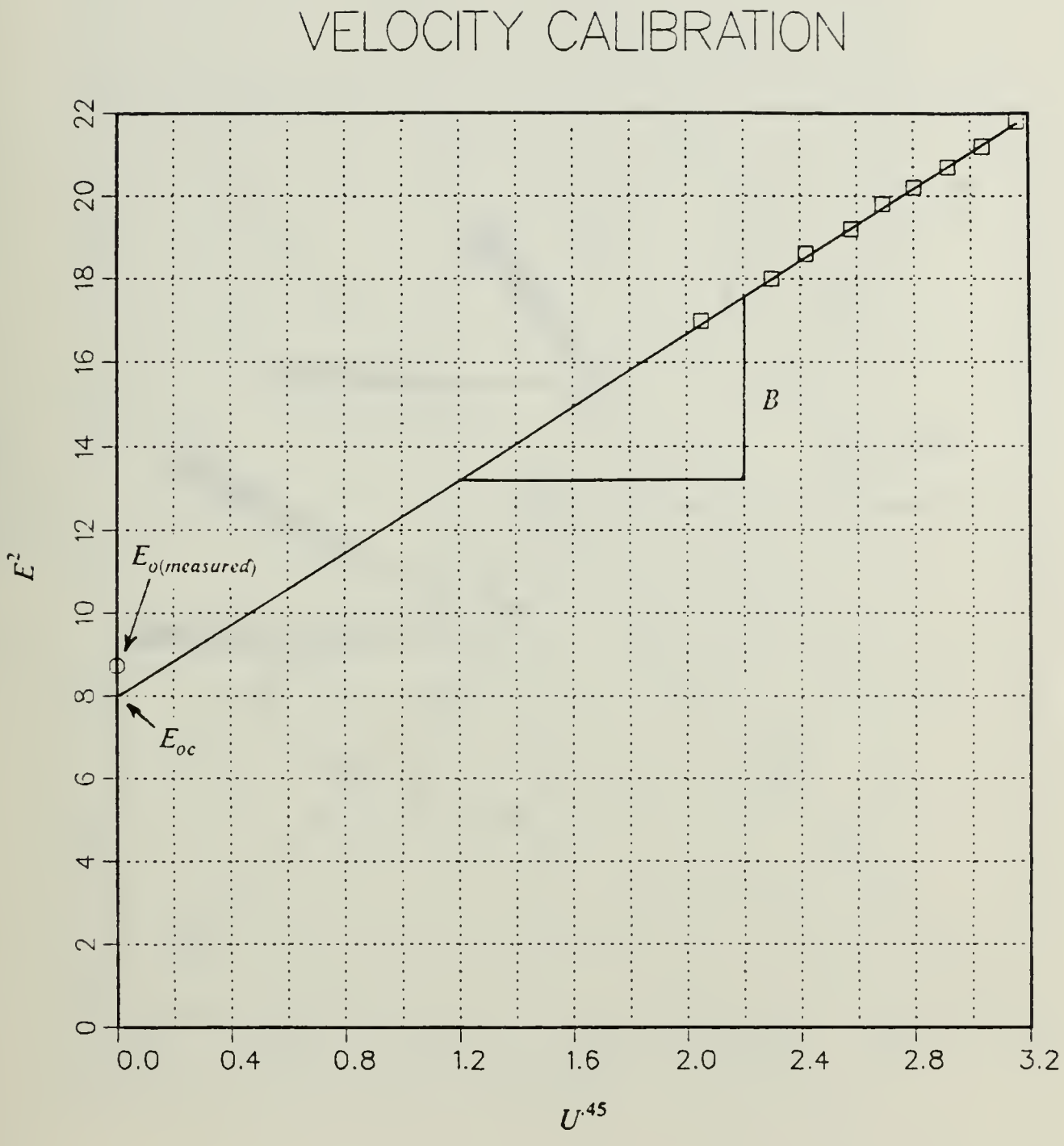

Figure 14. Velocity calibration plot

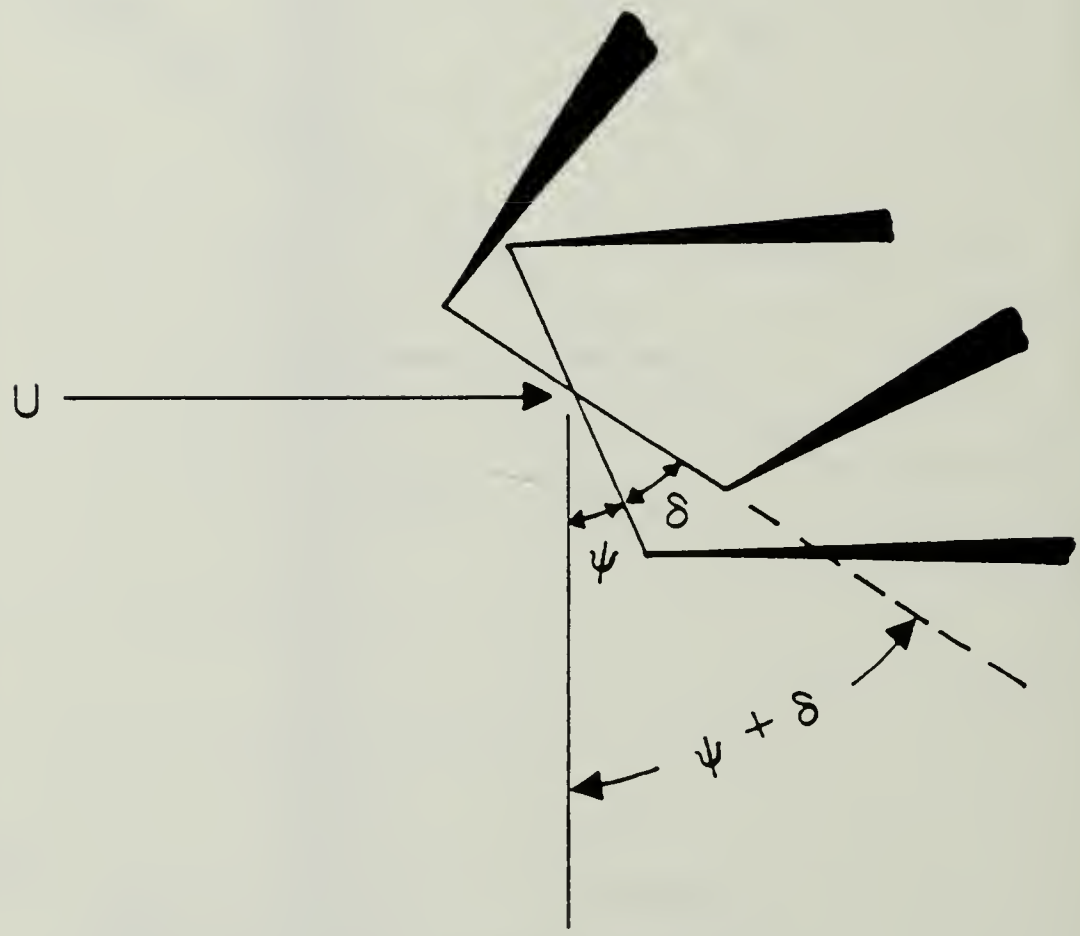

Figure 15. Wire inclined at $\psi + \delta$

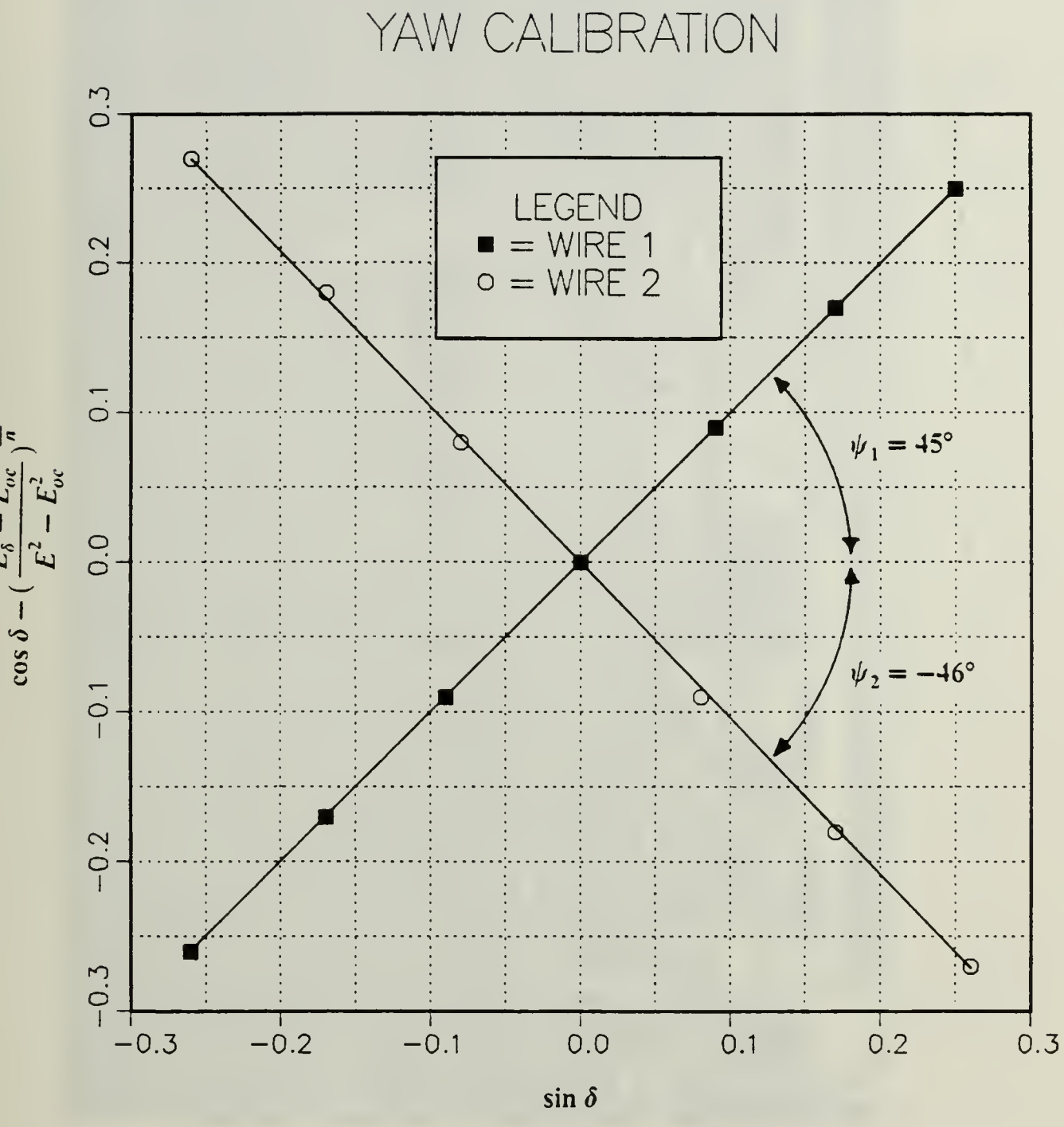

Figure 16. Yaw calibration plot for crossed wire probe

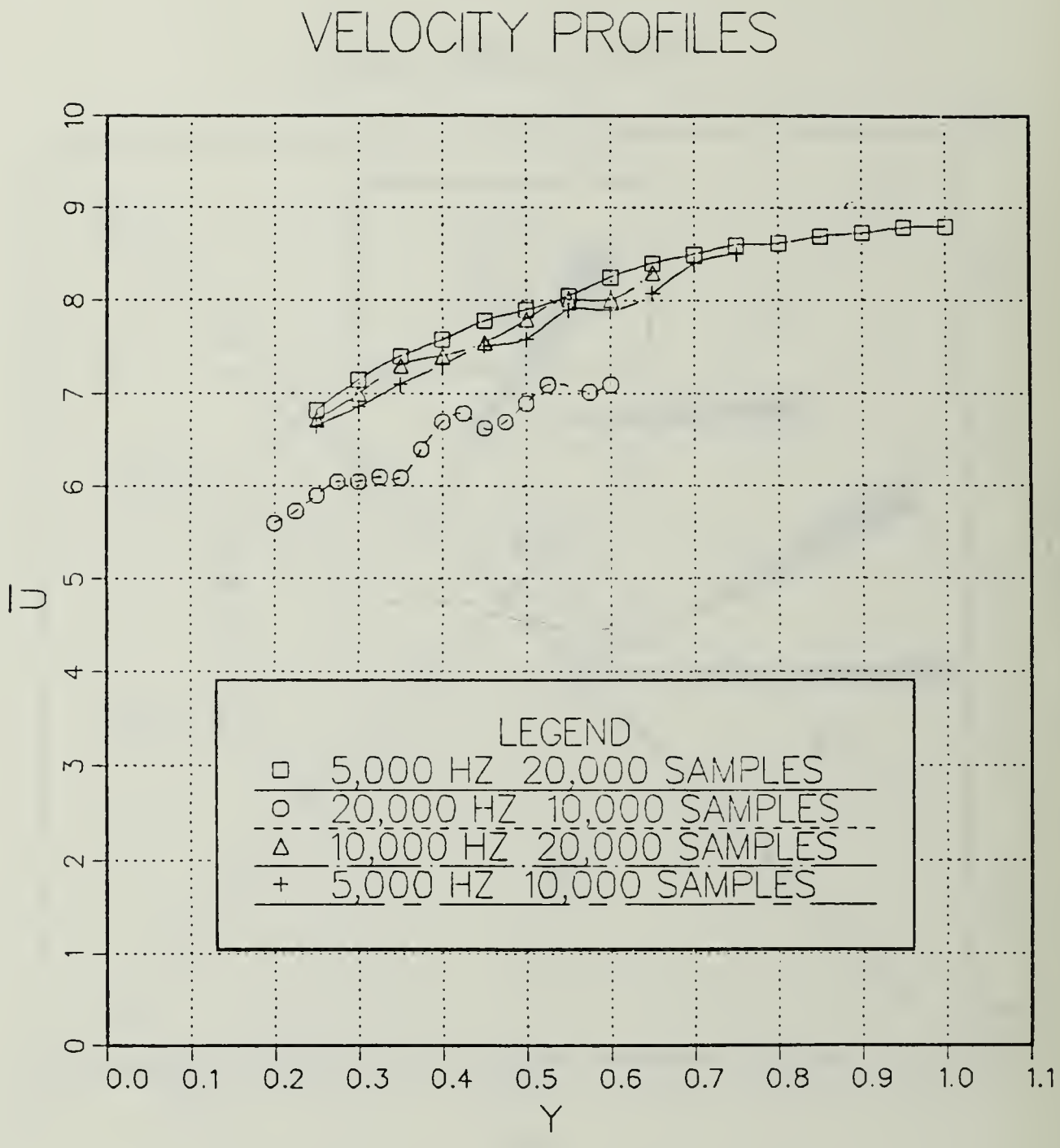

Figure 17. **Mean velocity profile in turbulent boundary layer measured using various sampling frequencies and sizes**

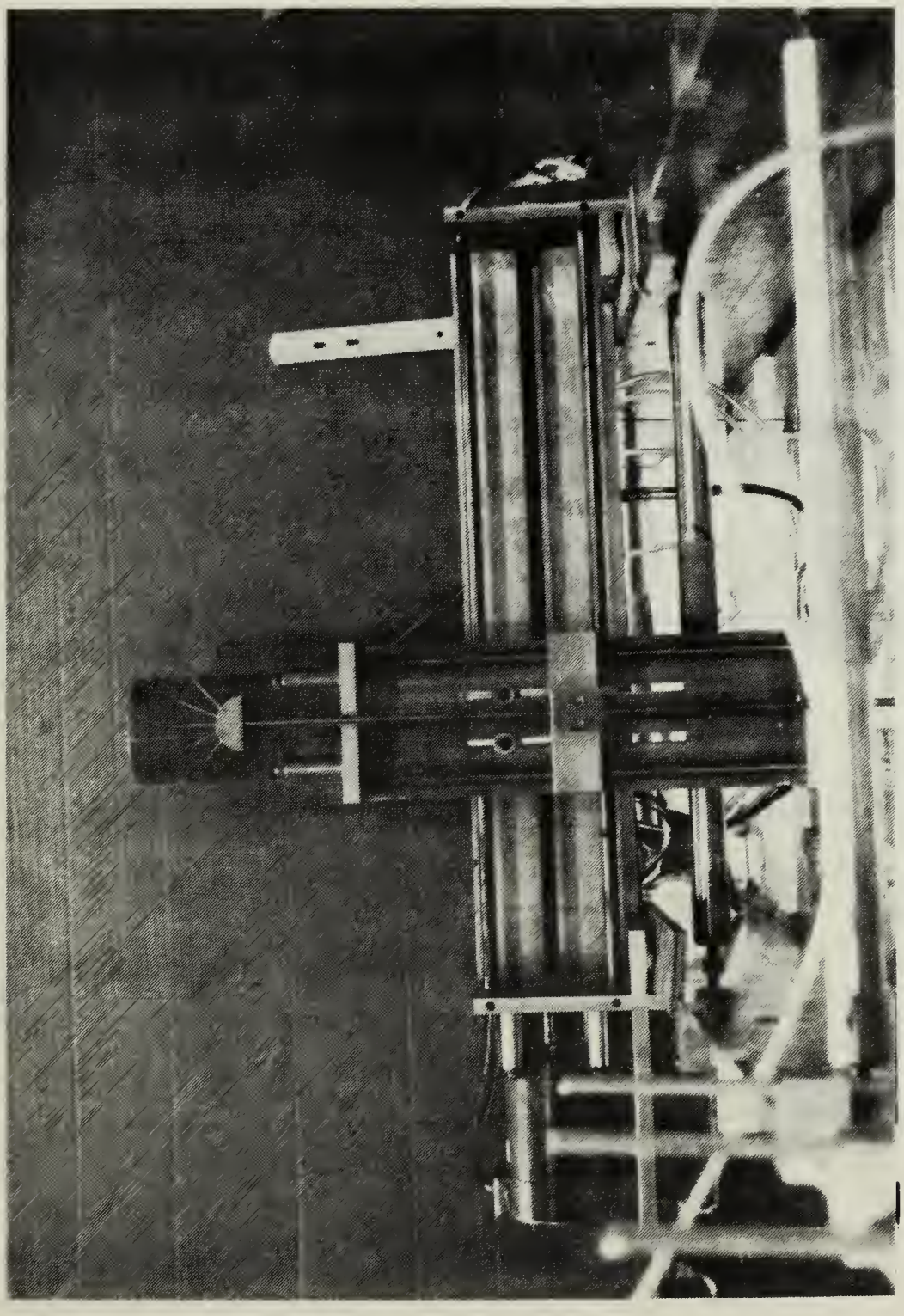

Figure 18. Two-axis traversing carriage

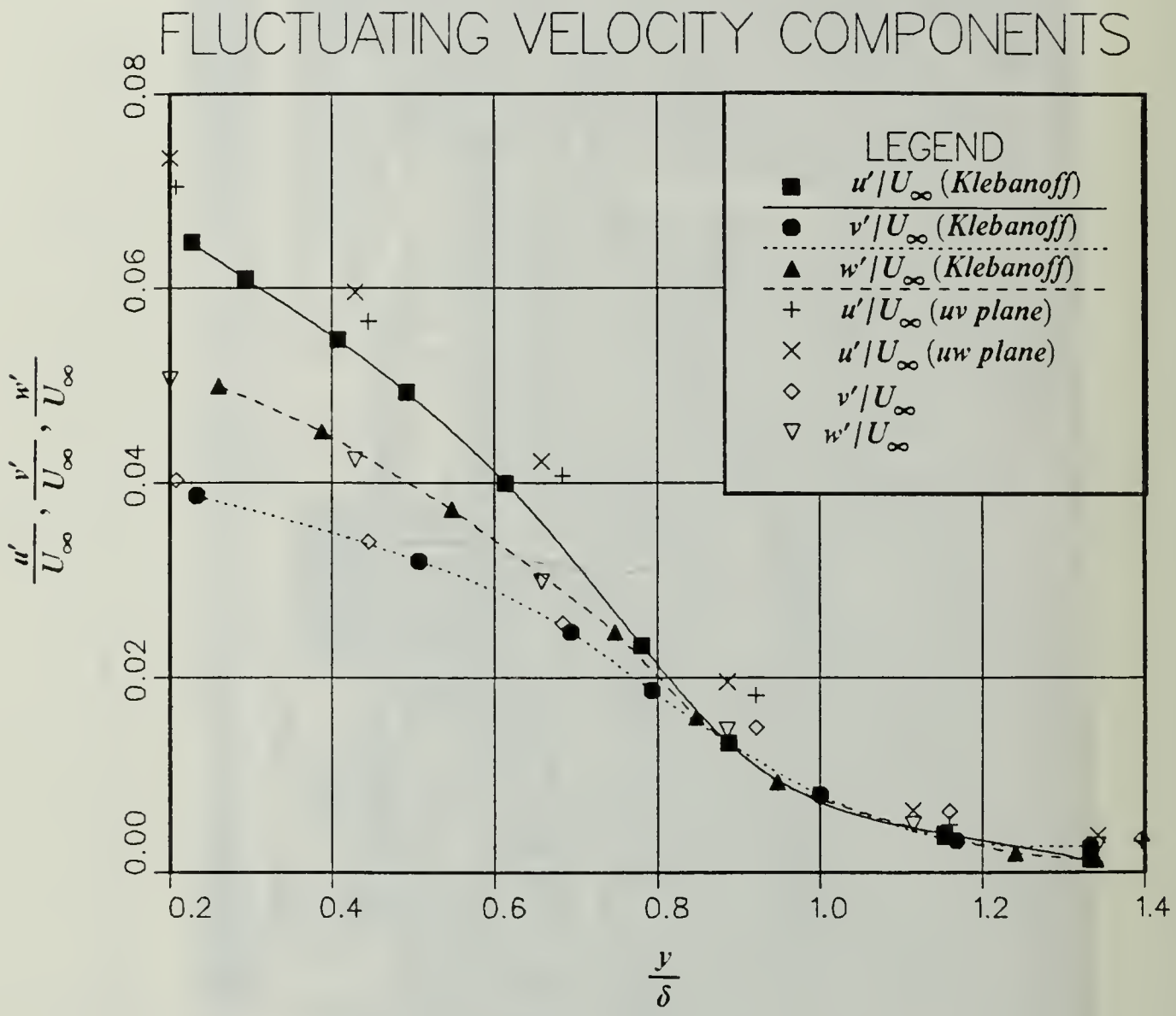

Figure 19. Fluctuating velocity components in turbulent boundary layer

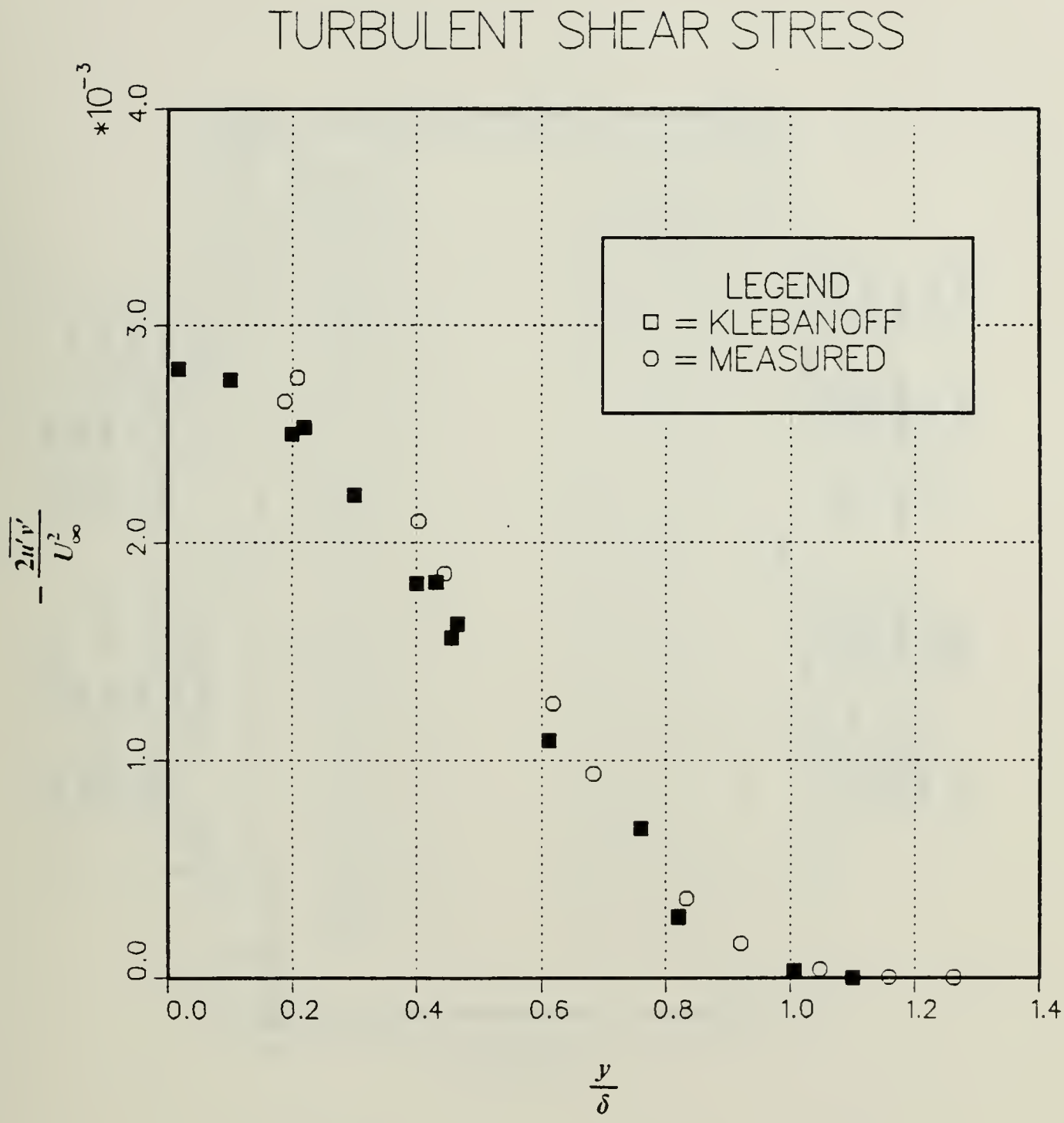

Figure 20. Turbulent shear stress distribution

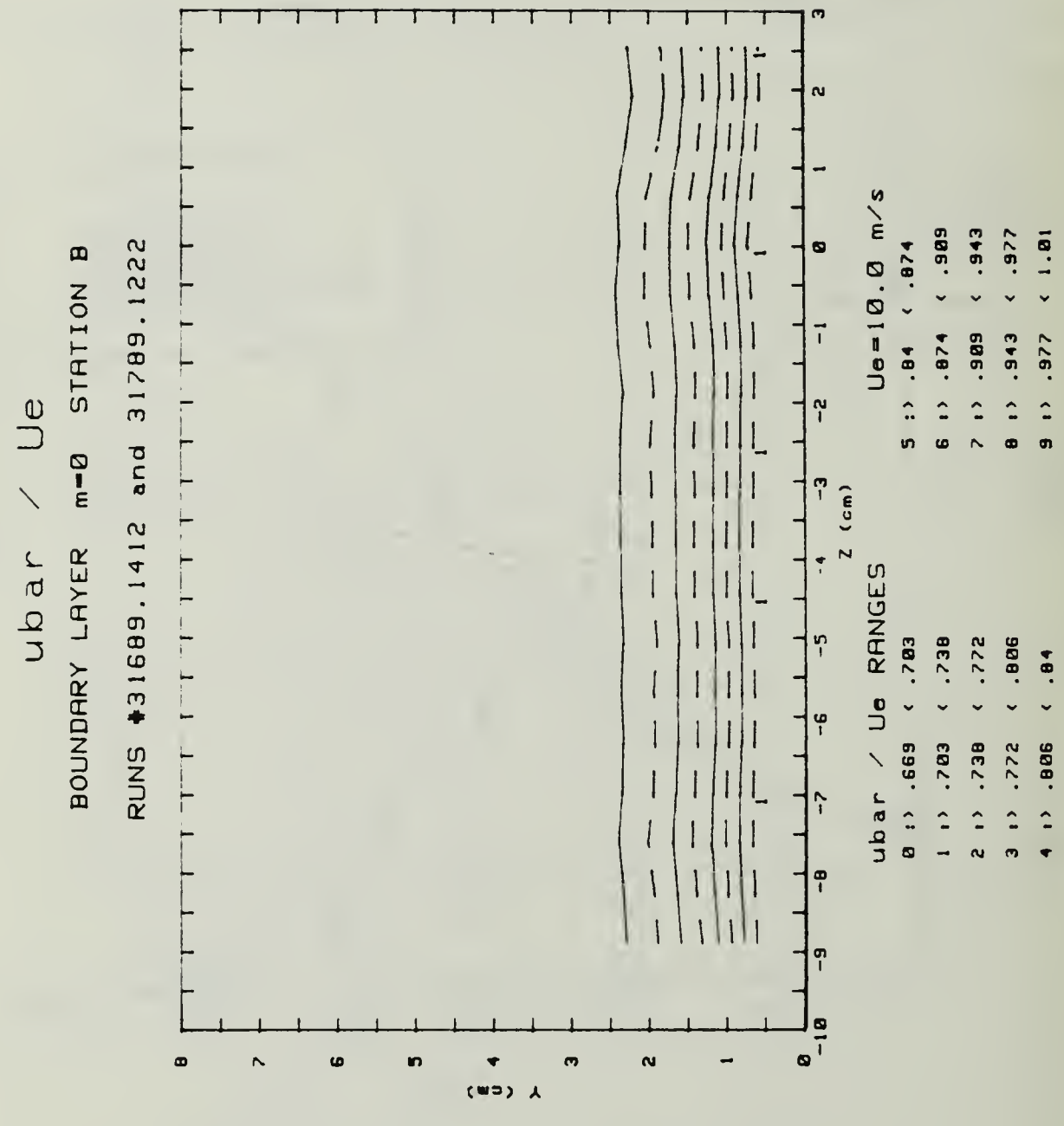

Figure 21. $\bar{u}$ (boundary layer, station B, $\Delta = 0.25$ inches)

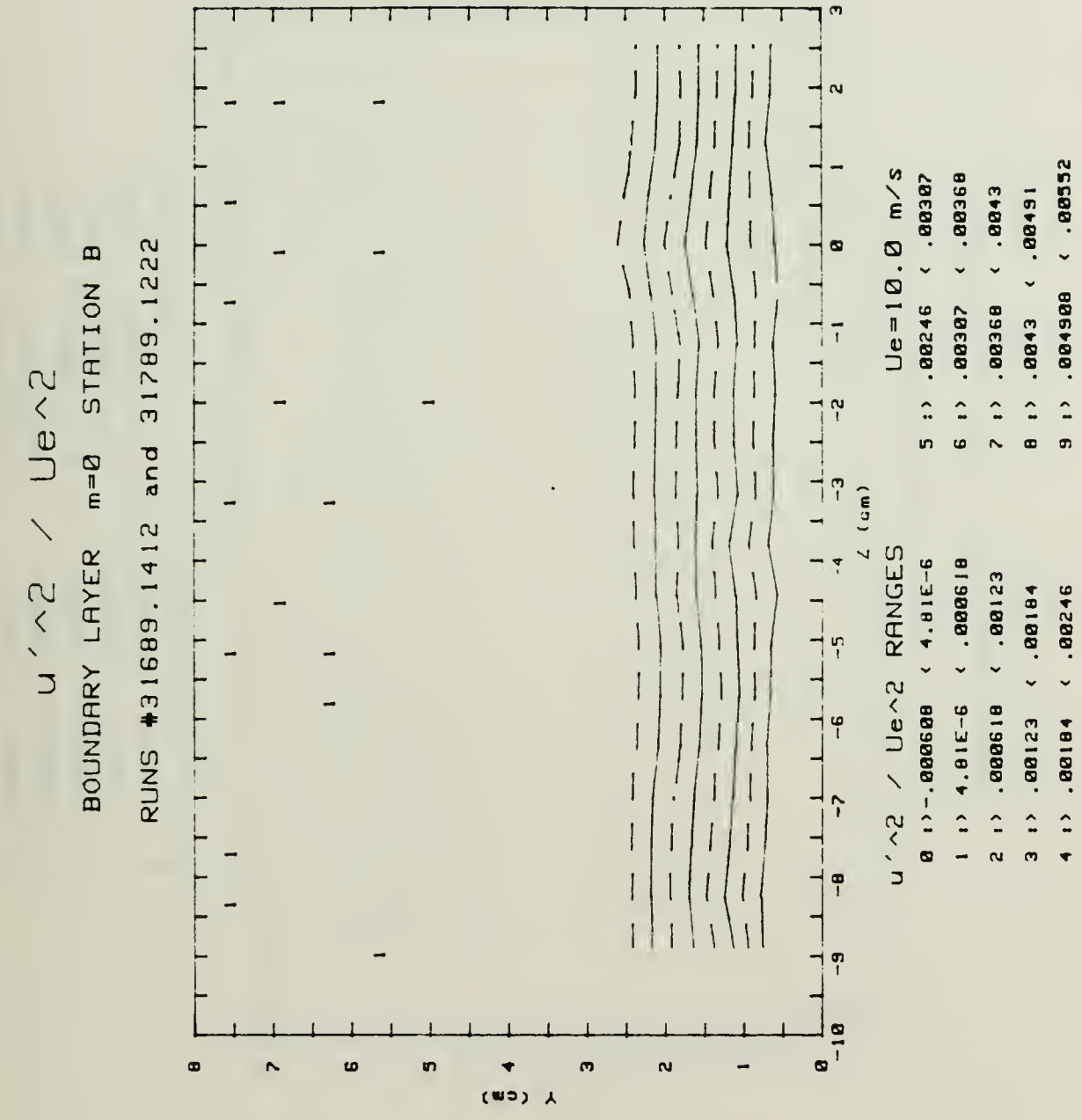

Figure 22. $\overline{u'^2}$ (boundary layer, station B, $\Delta = 0.25$ inches)

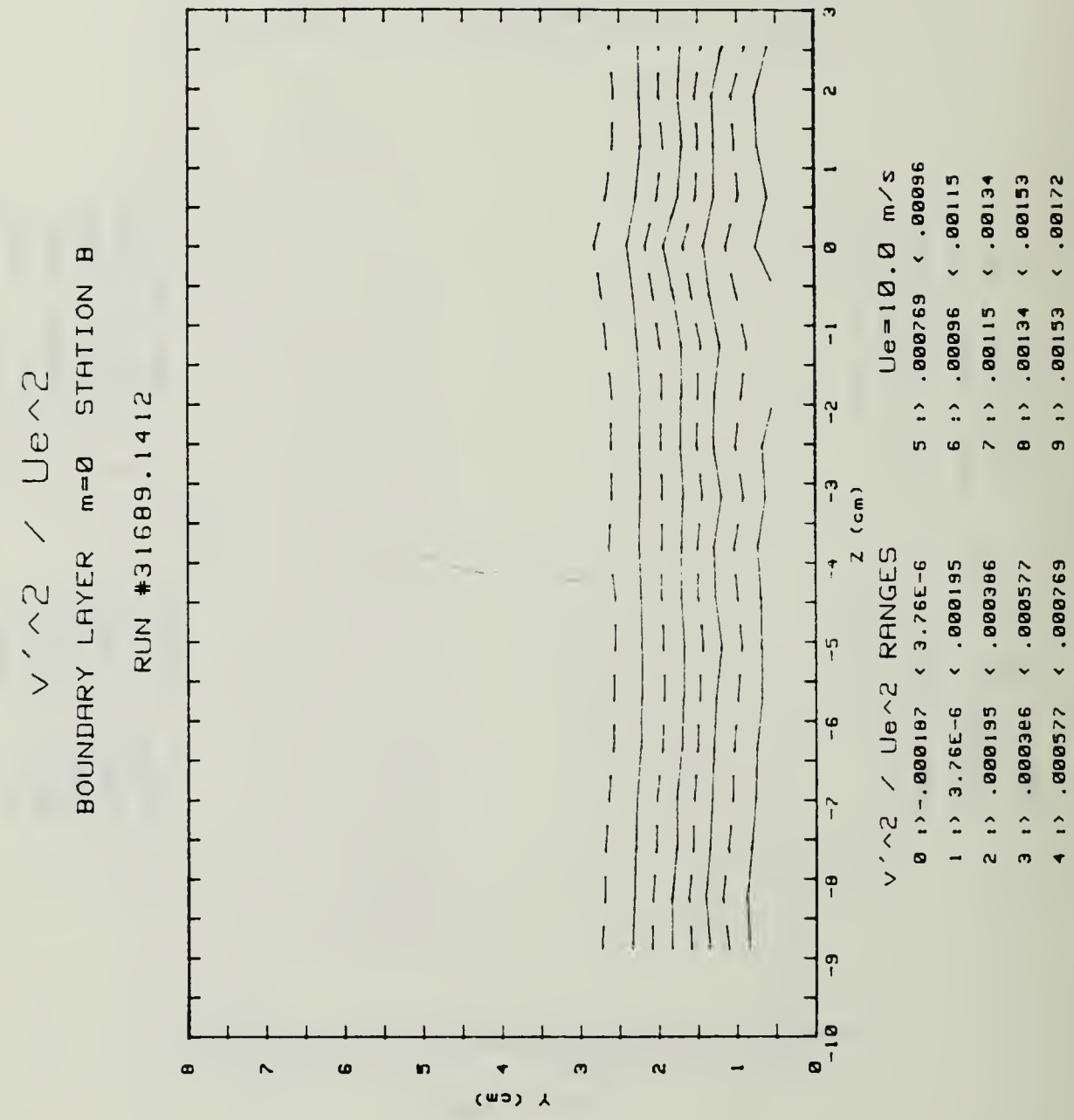

Figure 23. $\overline{v'^2}$ (boundary layer, station B, $\Delta = 0.25$ inches)

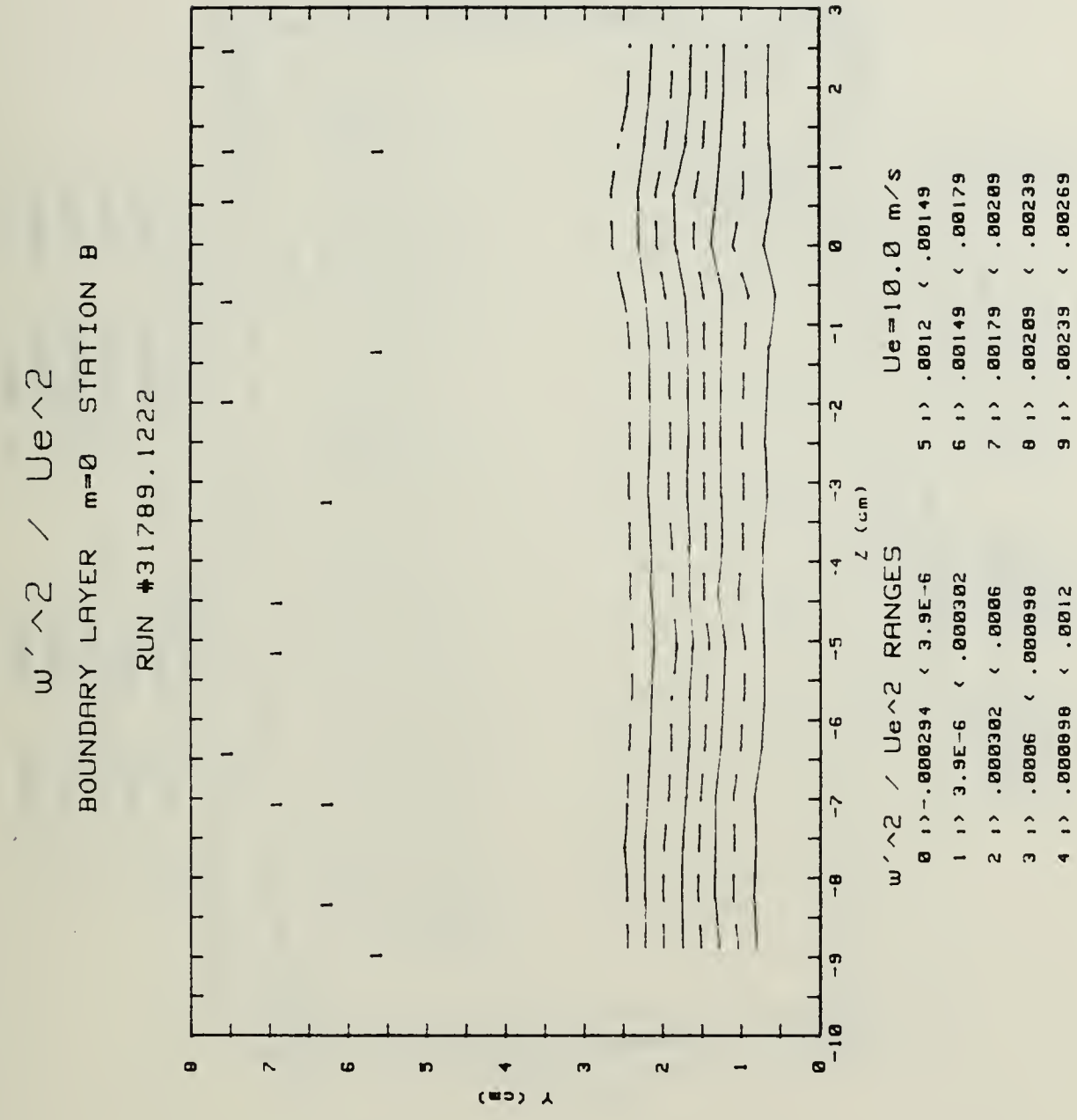

Figure 24. $\overline{w'^2}$ (boundary layer, station B, $\Delta = 0.25$ inches)

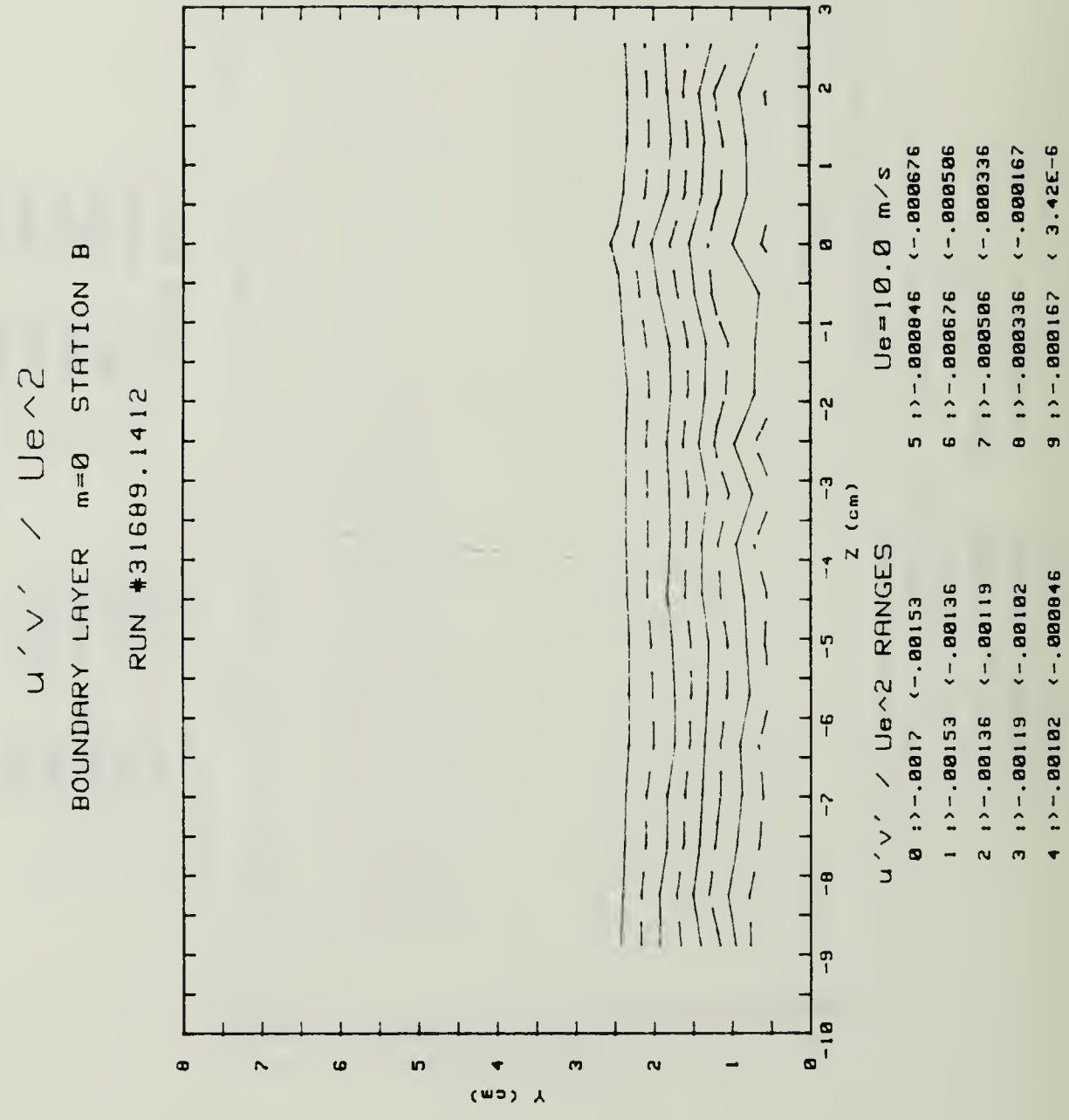

Figure 25. $\overline{u'v'}$ (boundary layer, station B, $\Delta = 0.25$ inches)

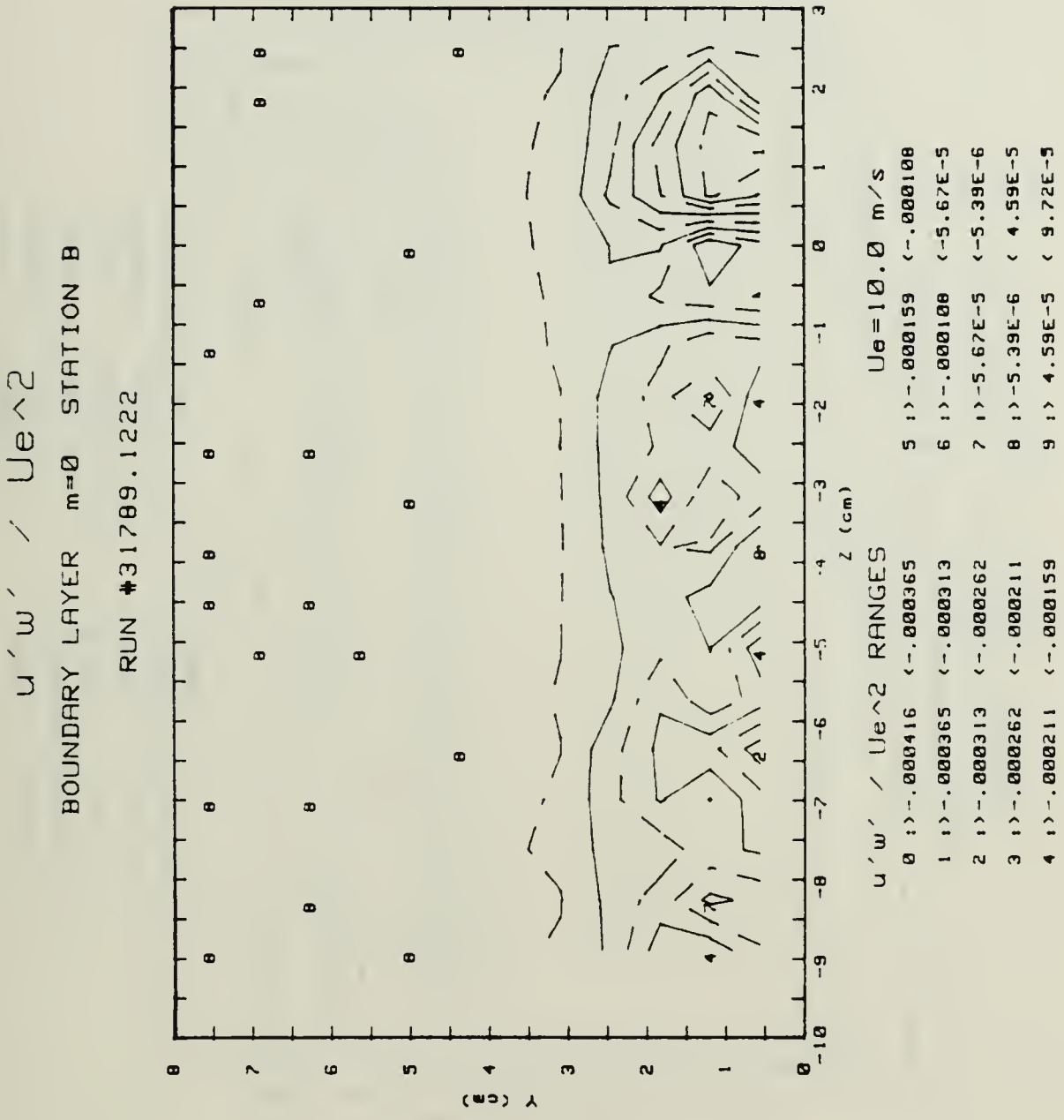

Figure 26. $\overline{u'w'}$ (boundary layer, station B, $\Delta = 0.25$ inches)

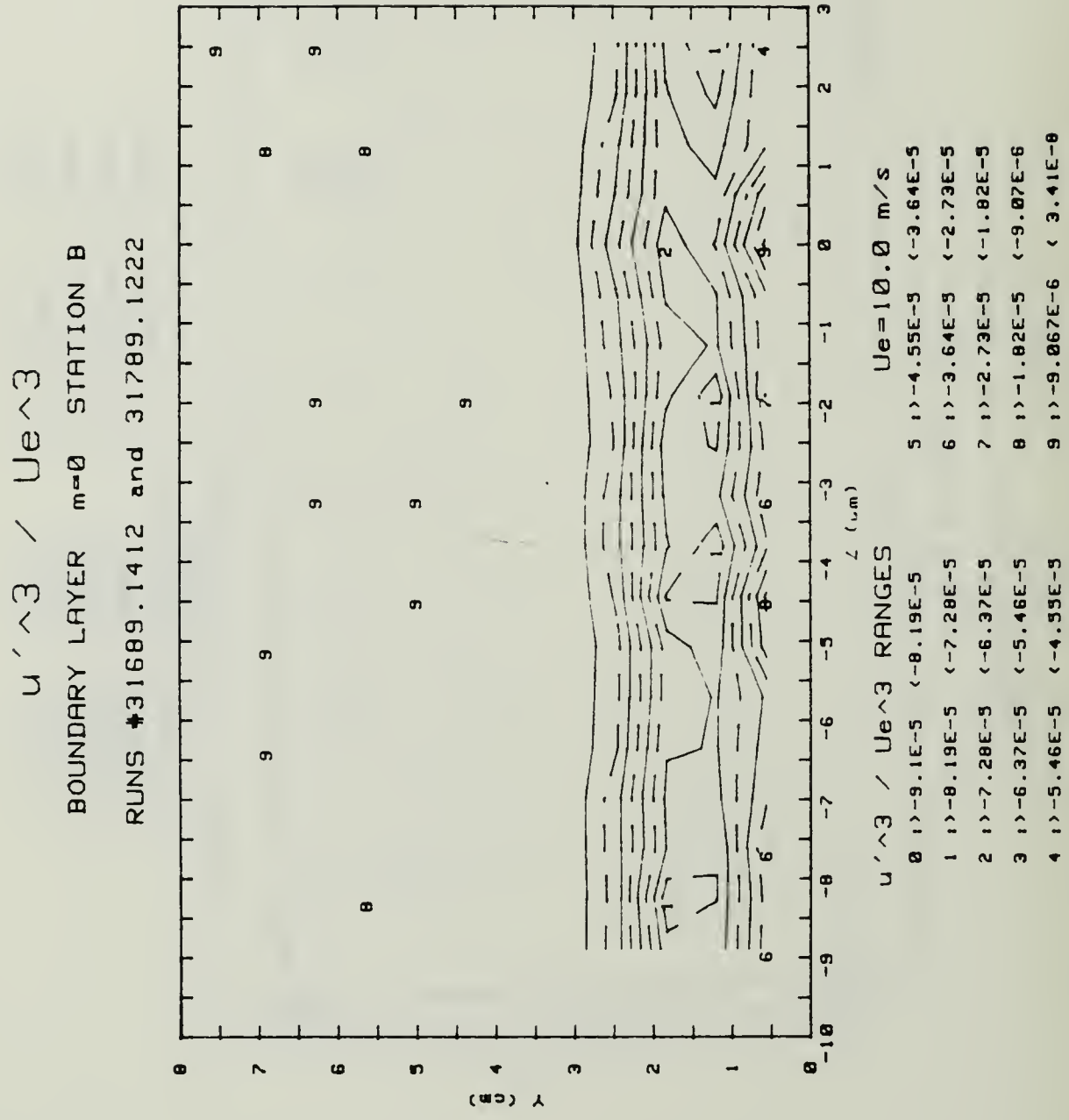

Figure 27. $\overline{u'^3}$ (boundary layer, station B, $\Delta = 0.25$ inches)

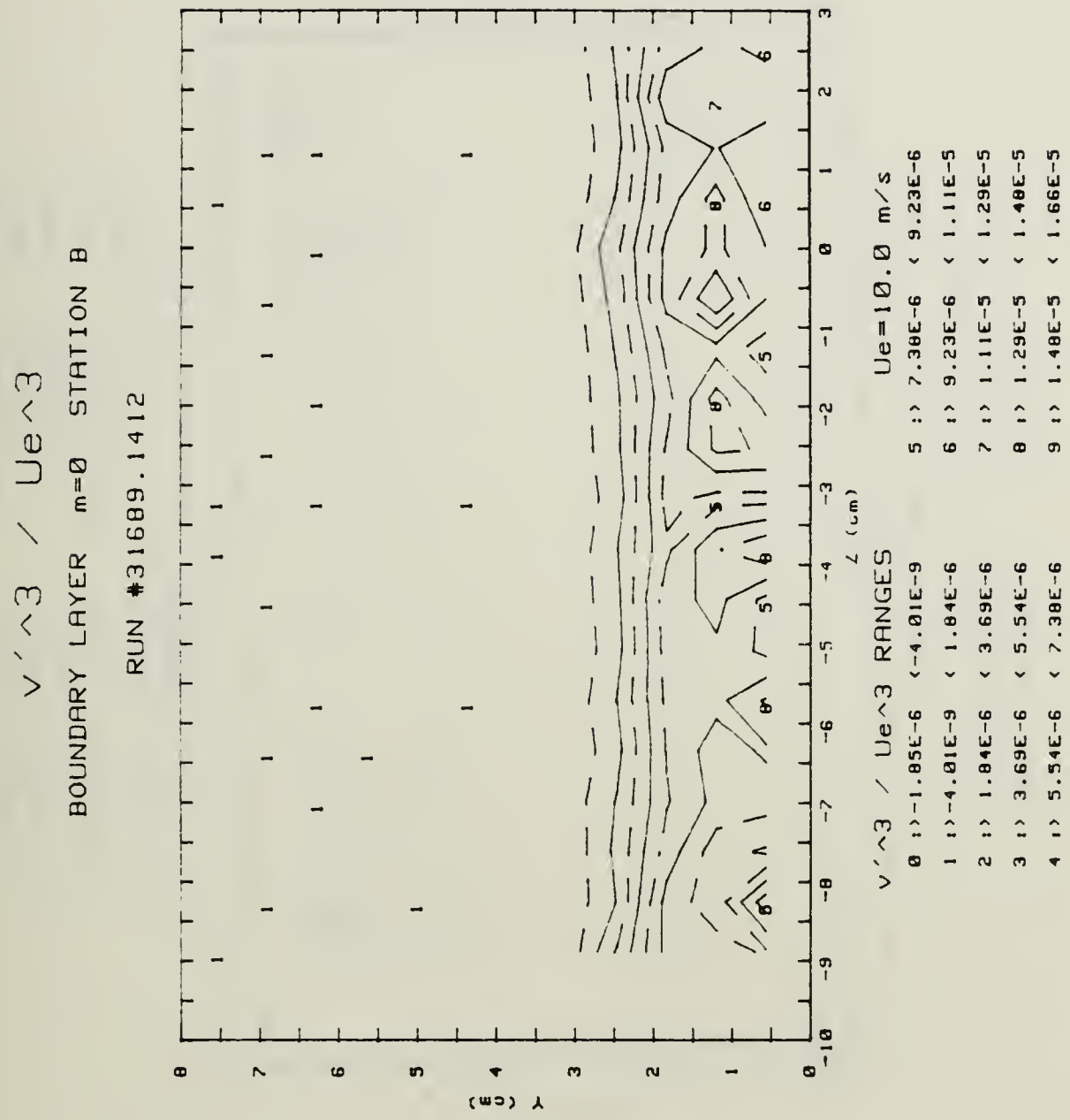

Figure 28. $\overline{v'^3}$ (boundary layer, station B, $\Delta = 0.25$ inches)

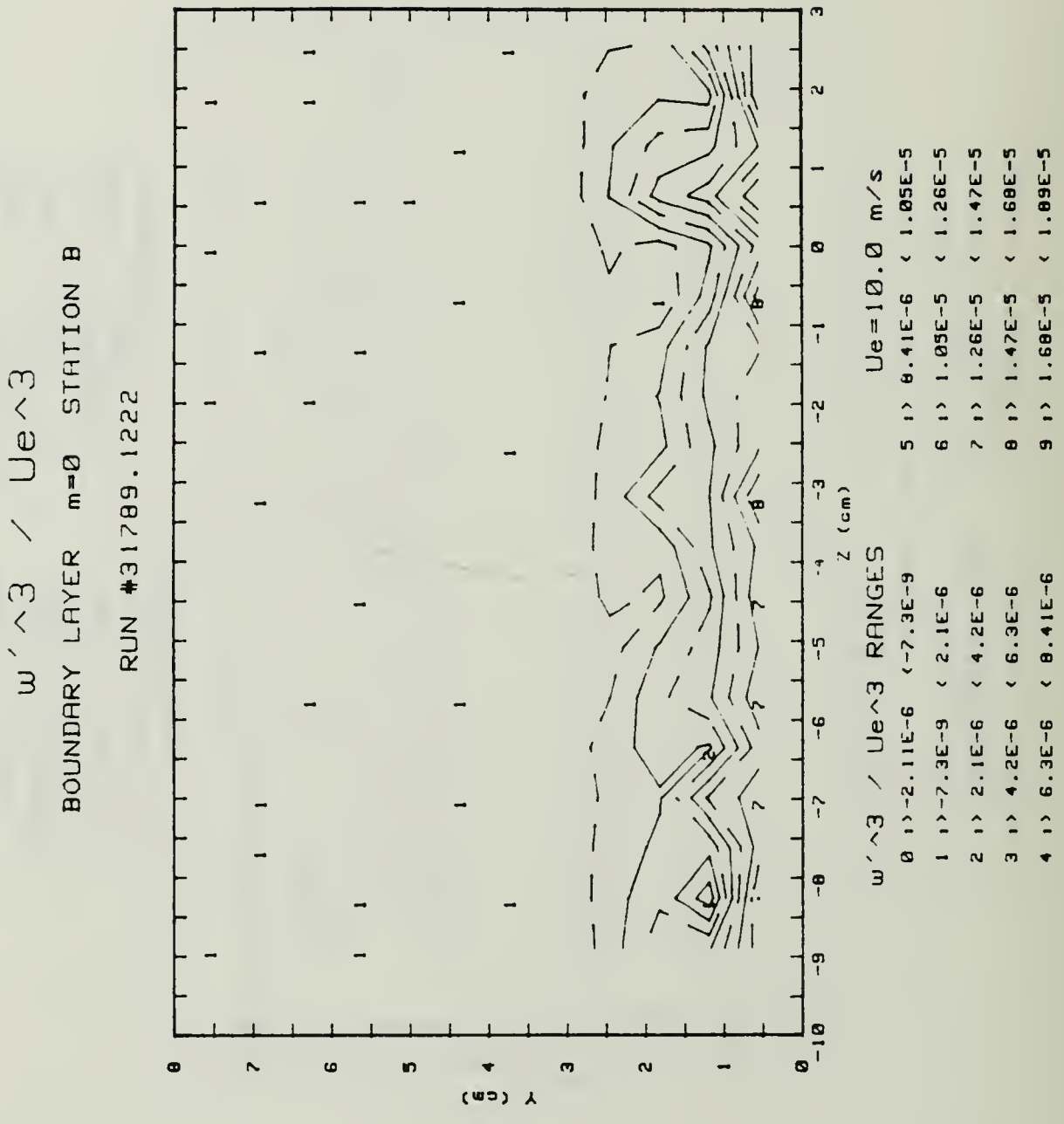

Figure 29. $\overline{w'^3}$ (boundary layer, station B, $\Delta = 0.25$ inches)

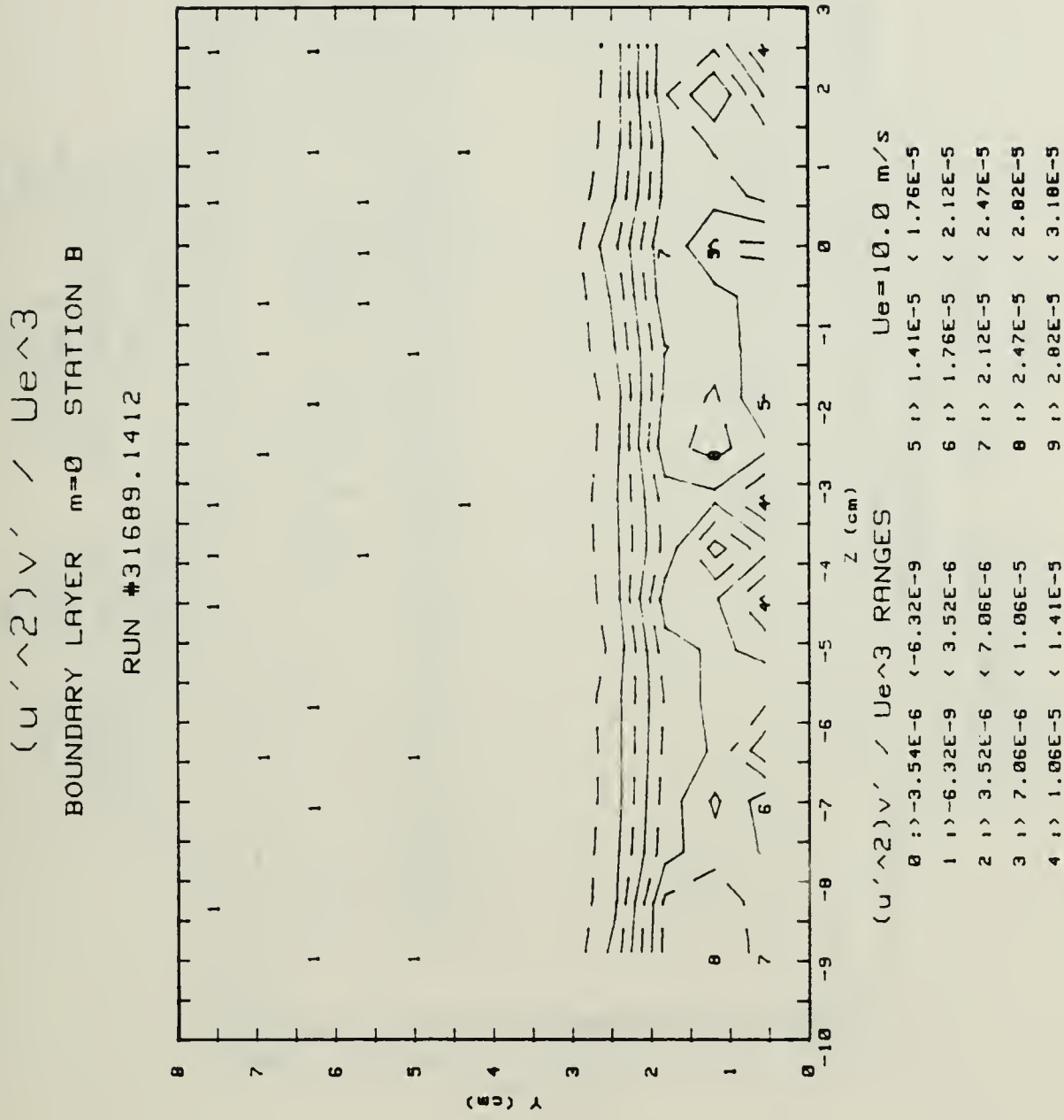

Figure 30. $\overline{u'^2v'}$ (boundary layer, station B, $\Delta = 0.25$ inches)

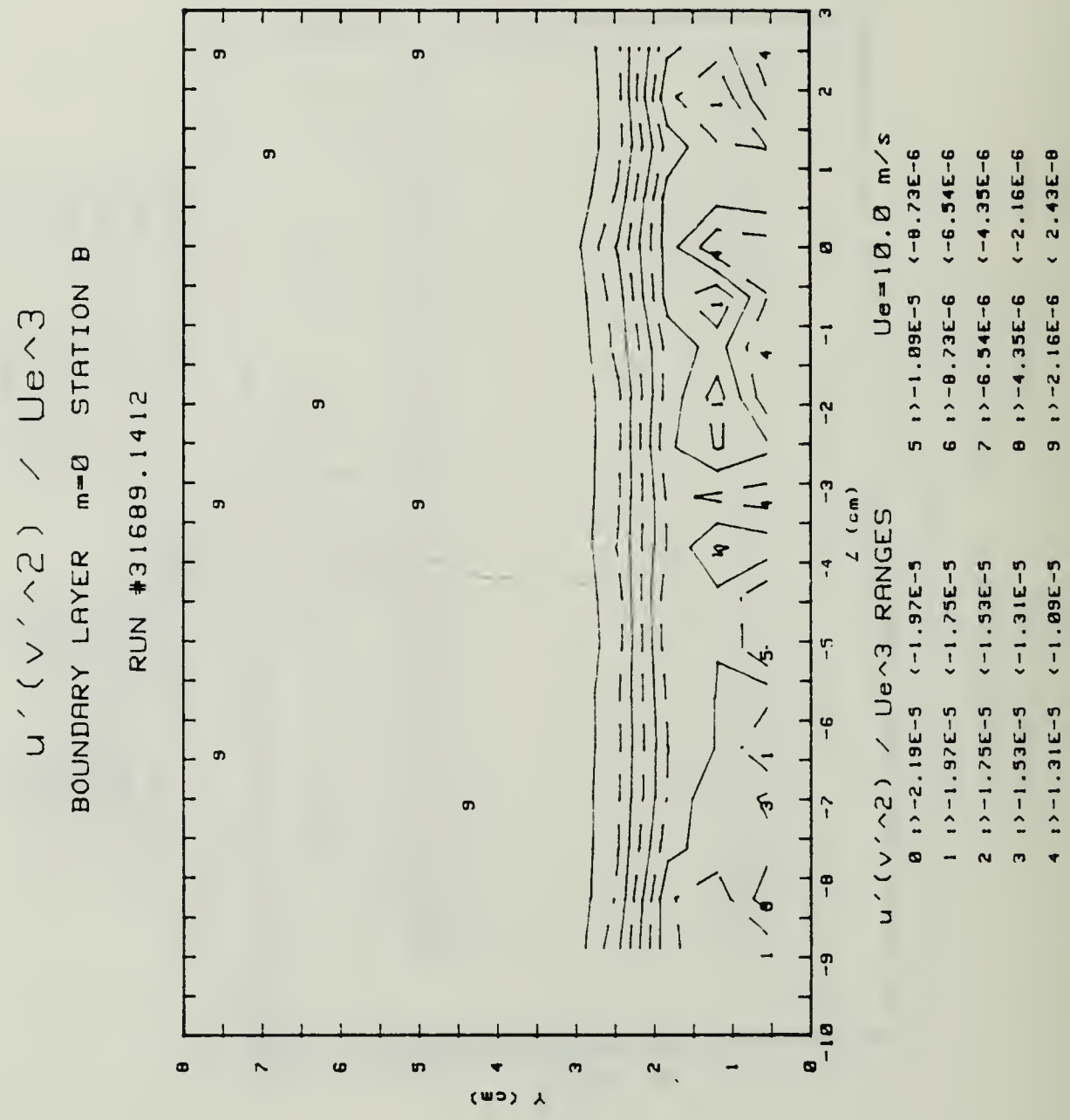

Figure 31. $\overline{u'v'^2}$ (boundary layer, station B, $\Delta = 0.25$ inches)

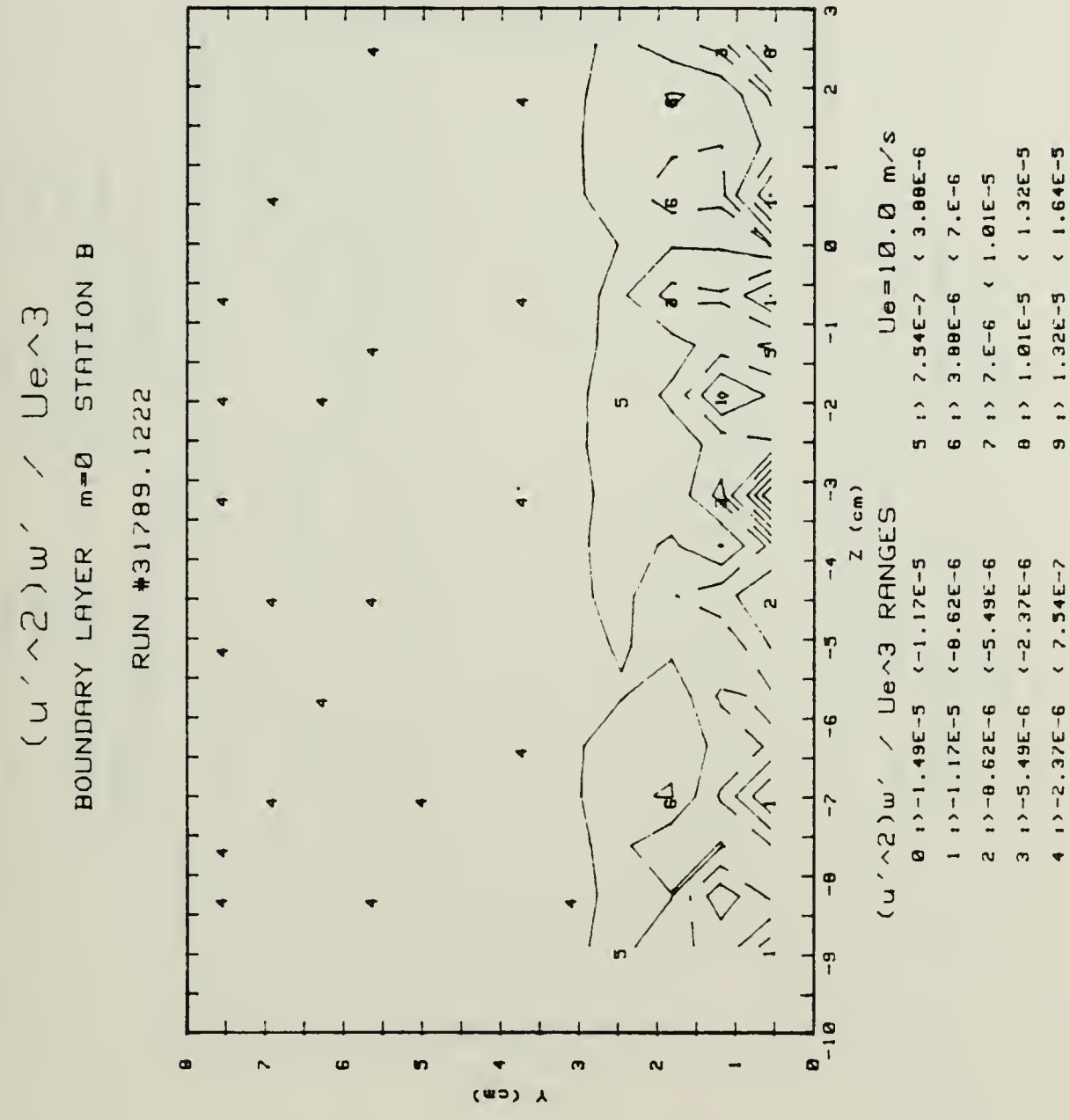

Figure 32. $\overline{u'^2w'}$ (boundary layer, station B, $\Delta = 0.25$ inches)

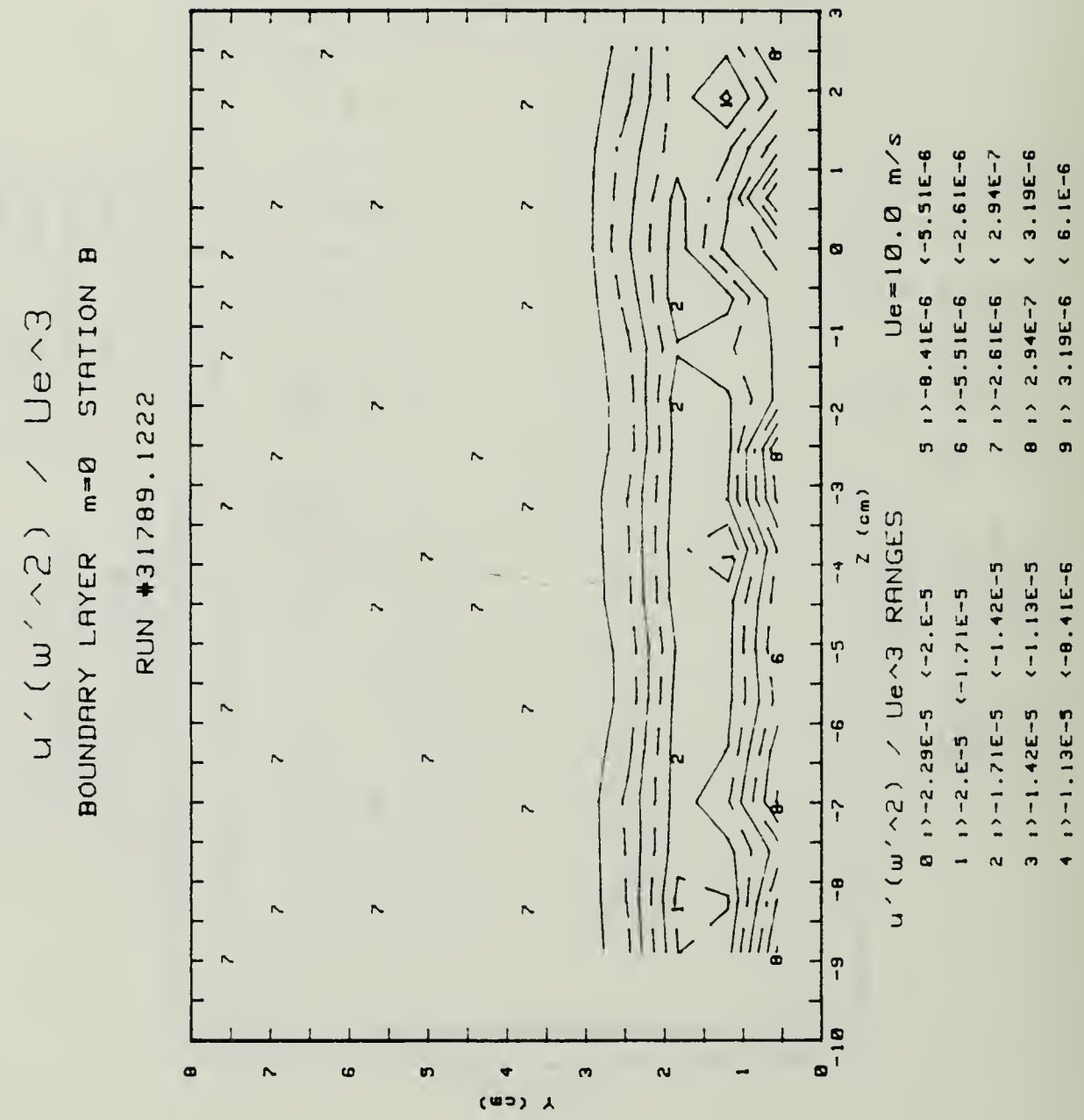

Figure 33. $\overline{u'w'^2}$ (boundary layer, station B, $\Delta = 0.25$ inches)

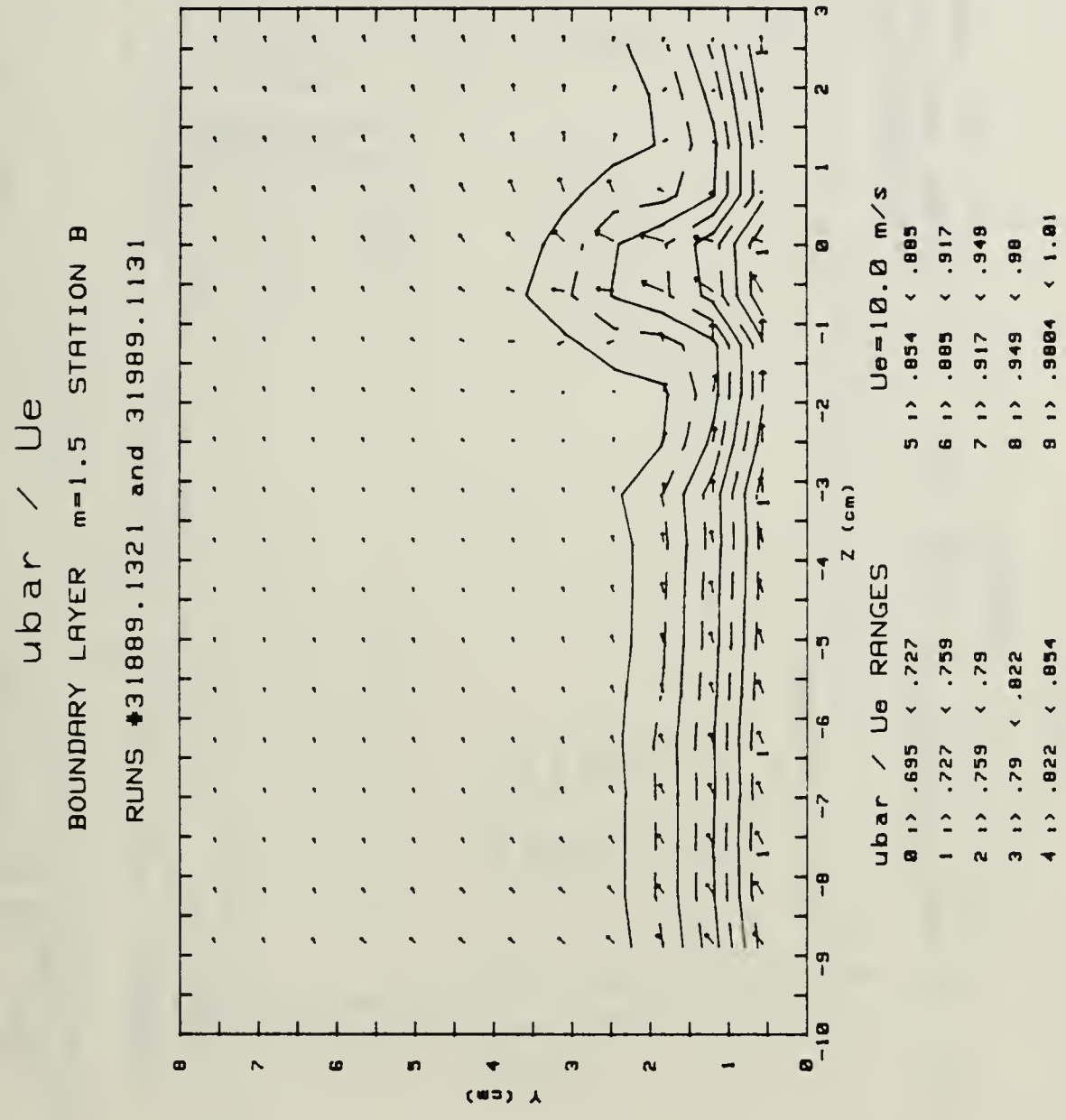

Figure 34. Mean Velocities (boundary layer / wall jet, station B, Δ = 0.25 inches)

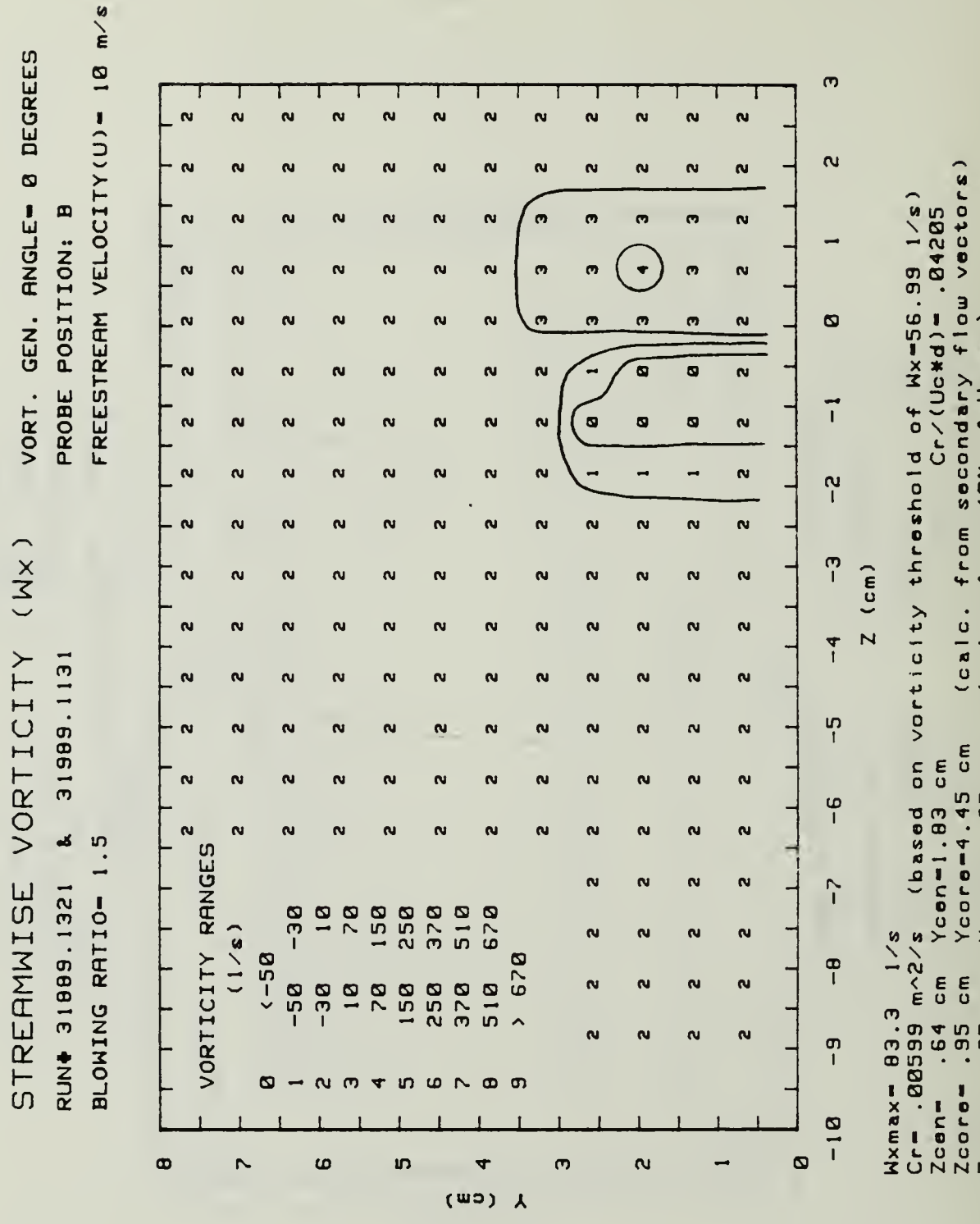

Figure 35. Streamwise Vorticity ω_x (boundary layer / wall jet, station B, $\Delta = 0.25$ inches)

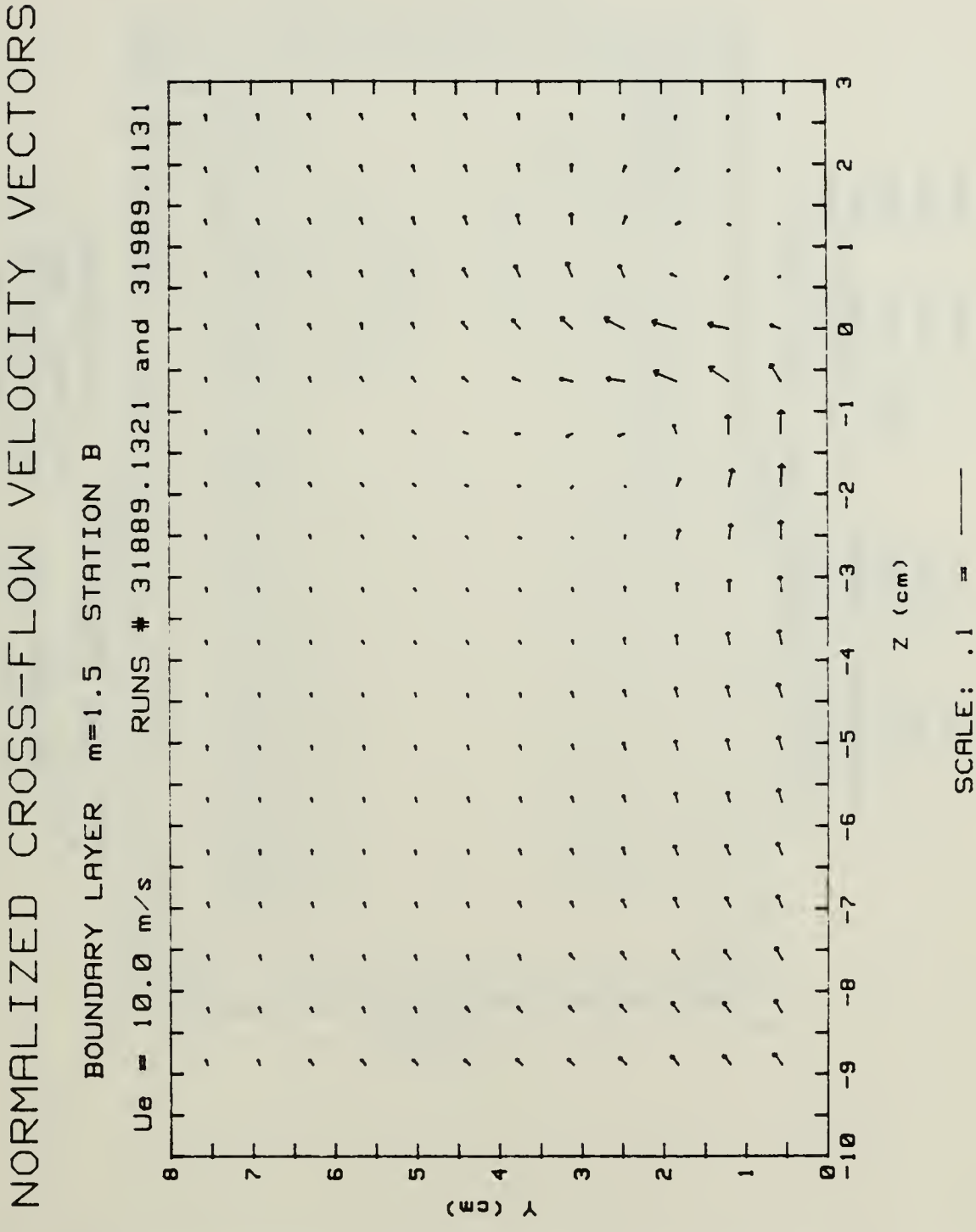
NORMALIZED CROSS-FLOW VELOCITY VECTORS
BOUNDARY LAYER m=1.5 STATION B
Ue = 10.0 m/s RUNS # 31889.1321 and 31989.1131
Y (cm)
Z (cm)
SCALE: .1 =

Figure 36. Secondary Flow Vectors (boundary layer / wall jet, station B, $\Delta = 0.25$ inches)

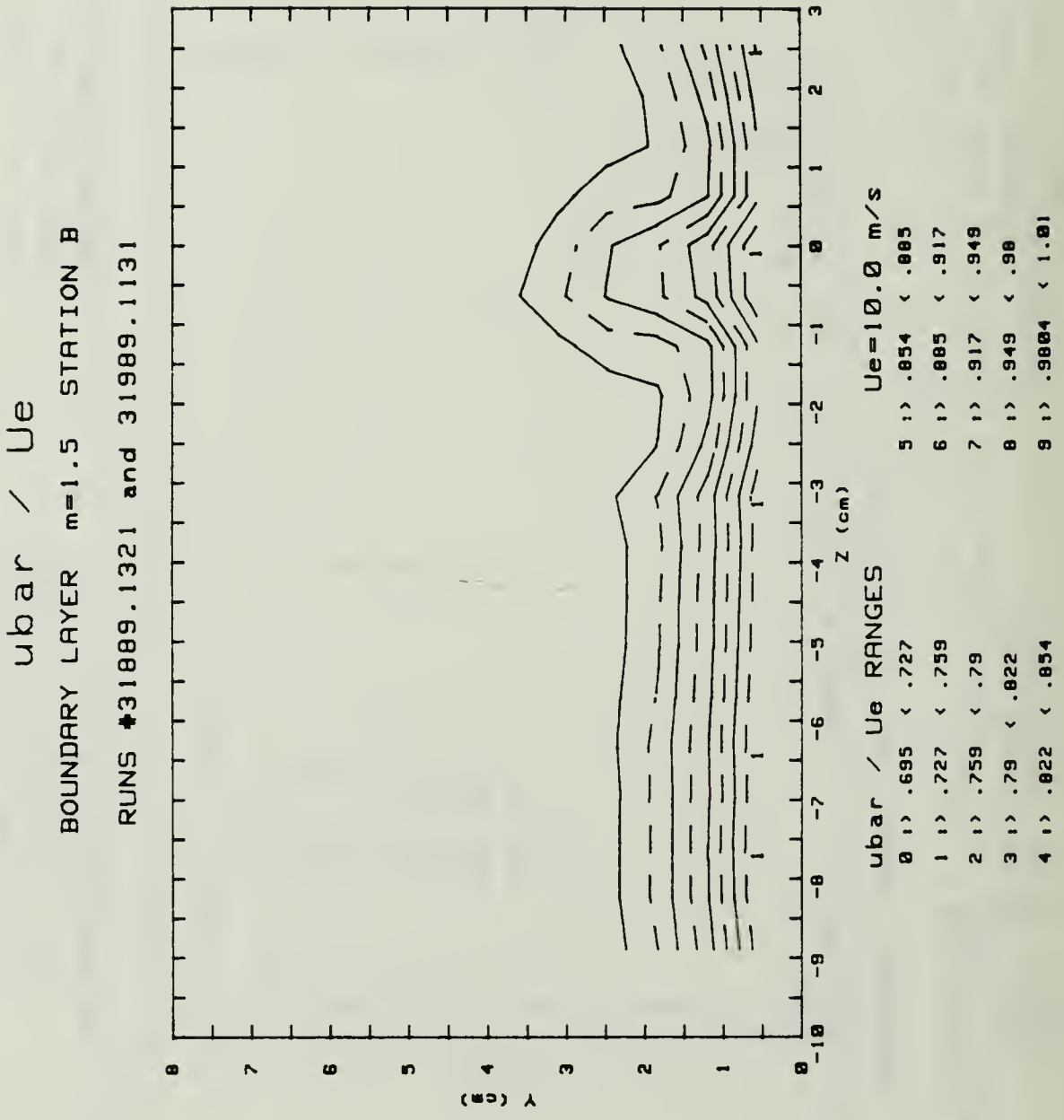

Figure 37. $\bar{u}$ (boundary layer / wall jet, station B, $\Delta = 0.25$ inches)

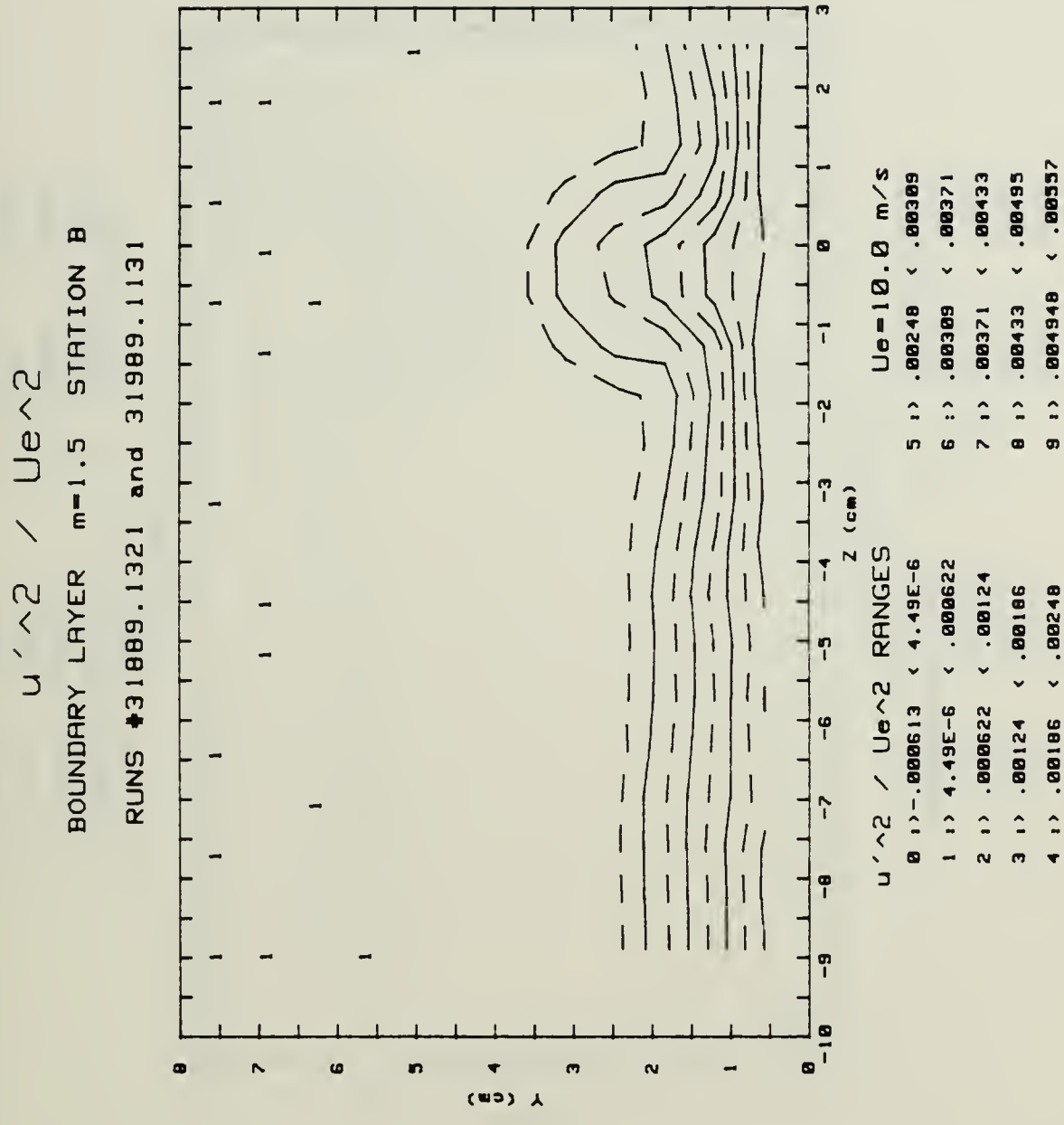

Figure 38. $\overline{u'^2}$ (boundary layer / wall jet, station B, $\Delta = 0.25$ inches)

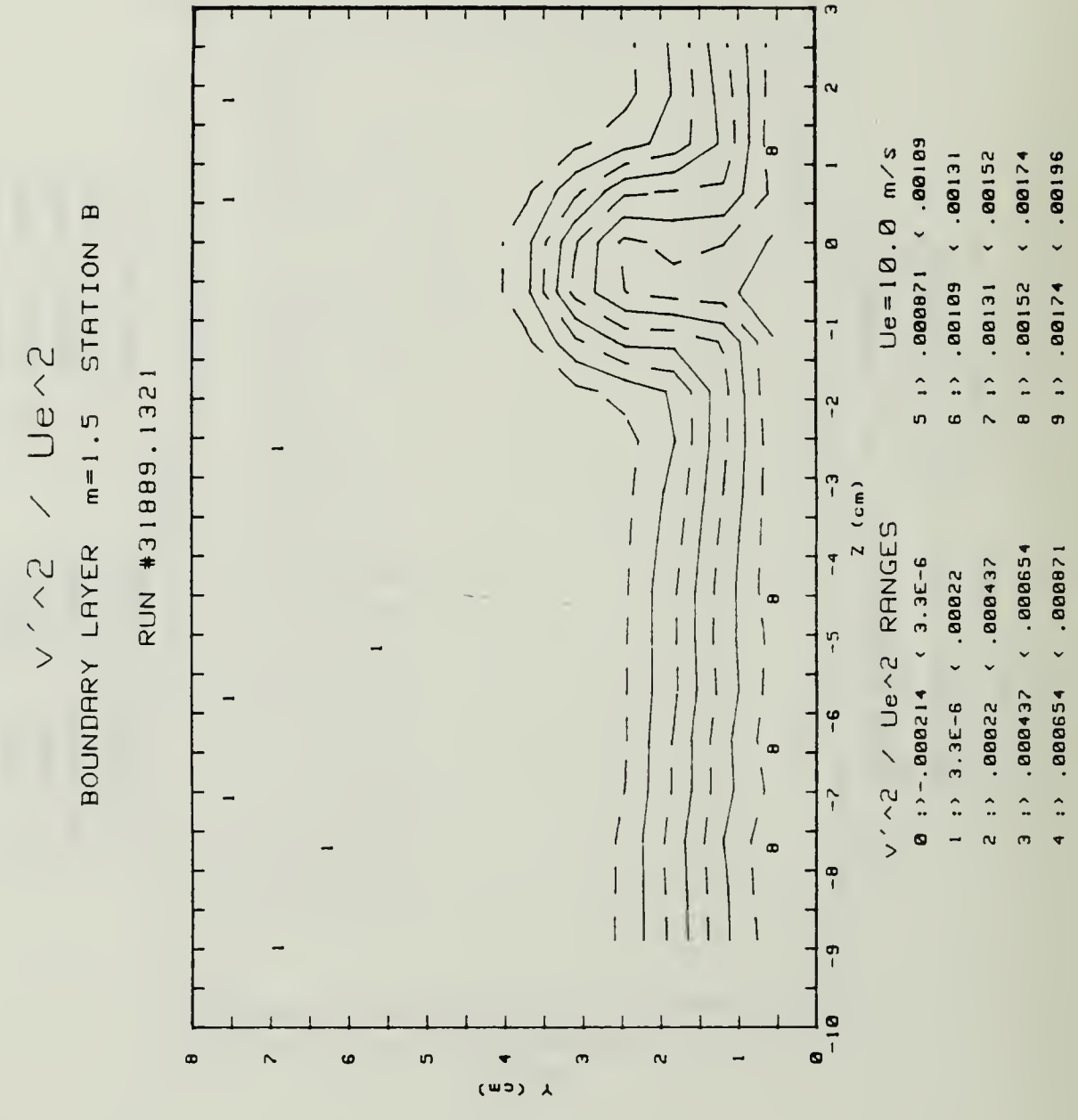

Figure 39. $\overline{v'^2}$ (boundary layer / wall jet, station B, $\Delta = 0.25$ inches)

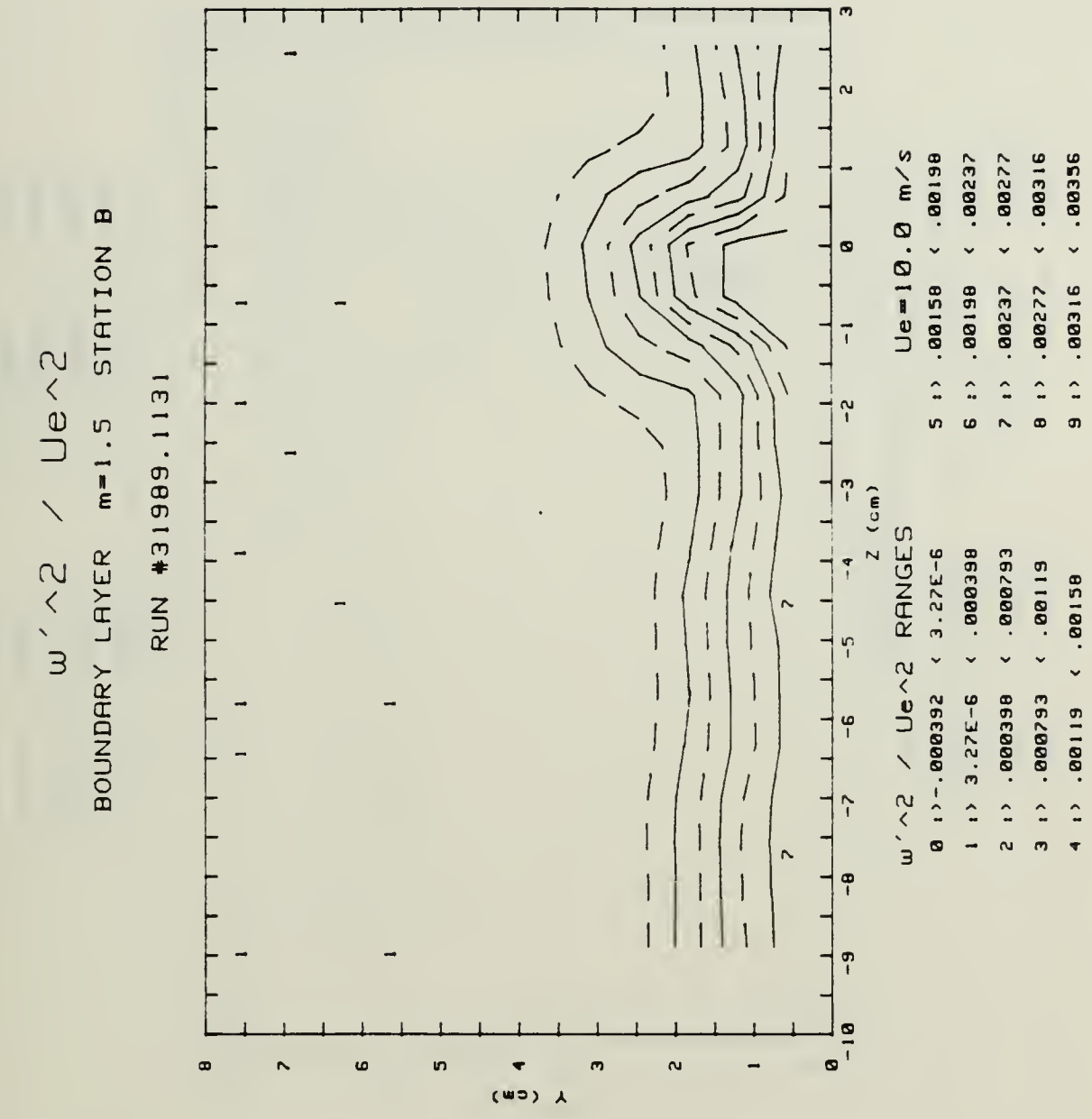

Figure 40. $\overline{w'^2}$ (boundary layer / wall jet, station B, $\Delta = 0.25$ inches)

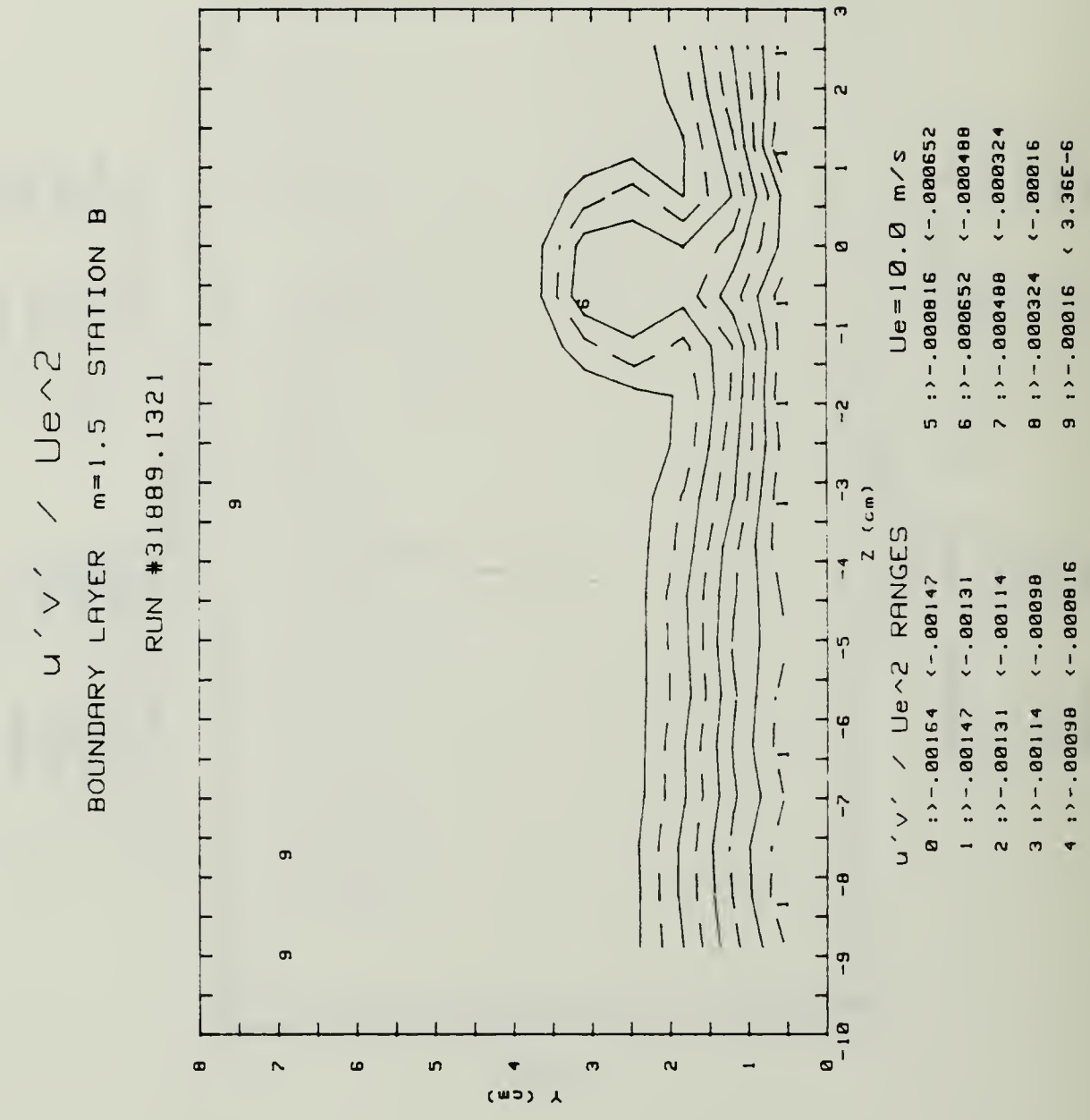

Figure 41. $\overline{u'v'}$ (boundary layer / wall jet, station B, $\Delta = 0.25$ inches)

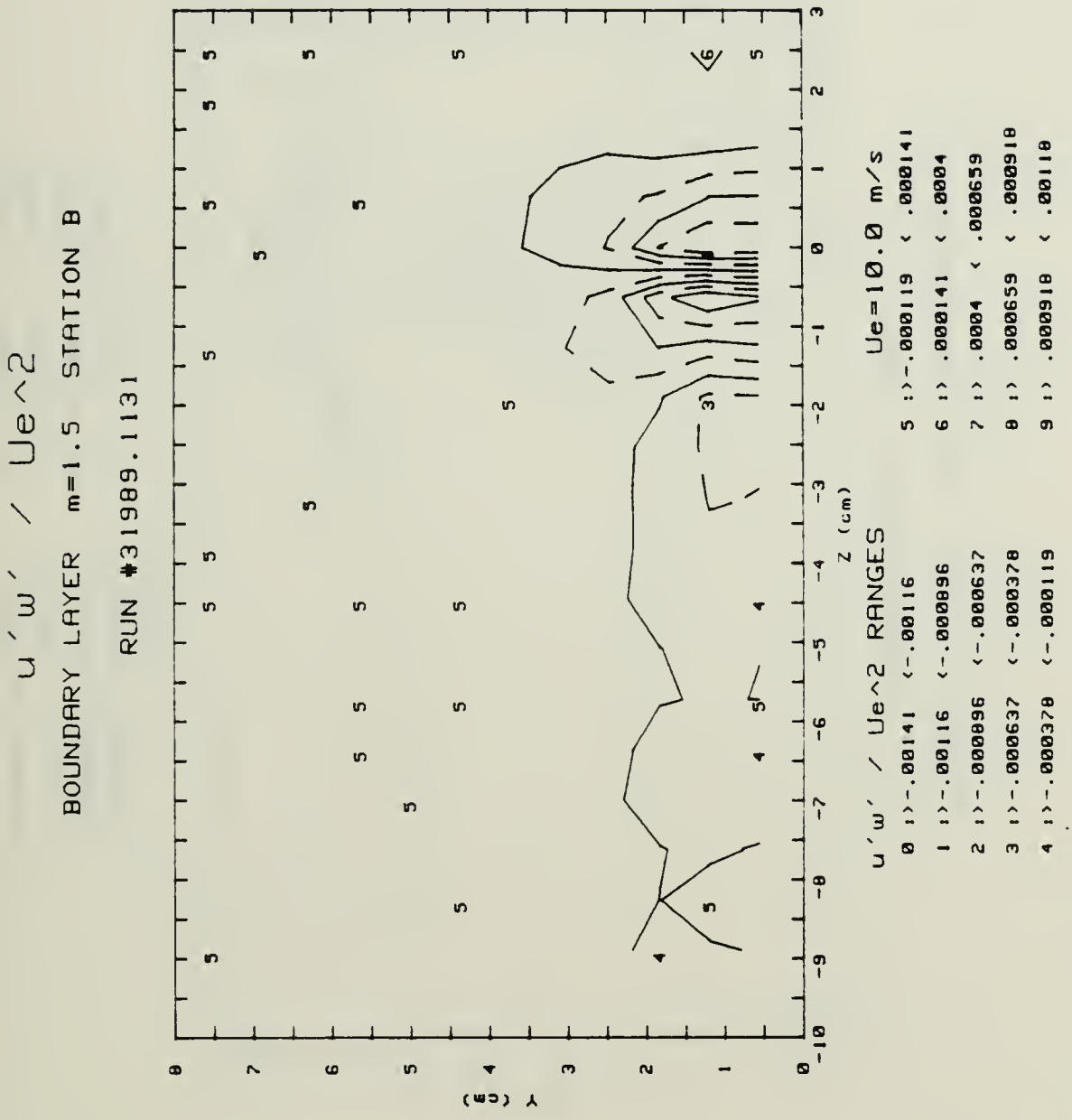

Figure 42. $\overline{u'w'}$ (boundary layer / wall jet, station B, $\Delta = 0.25$ inches)

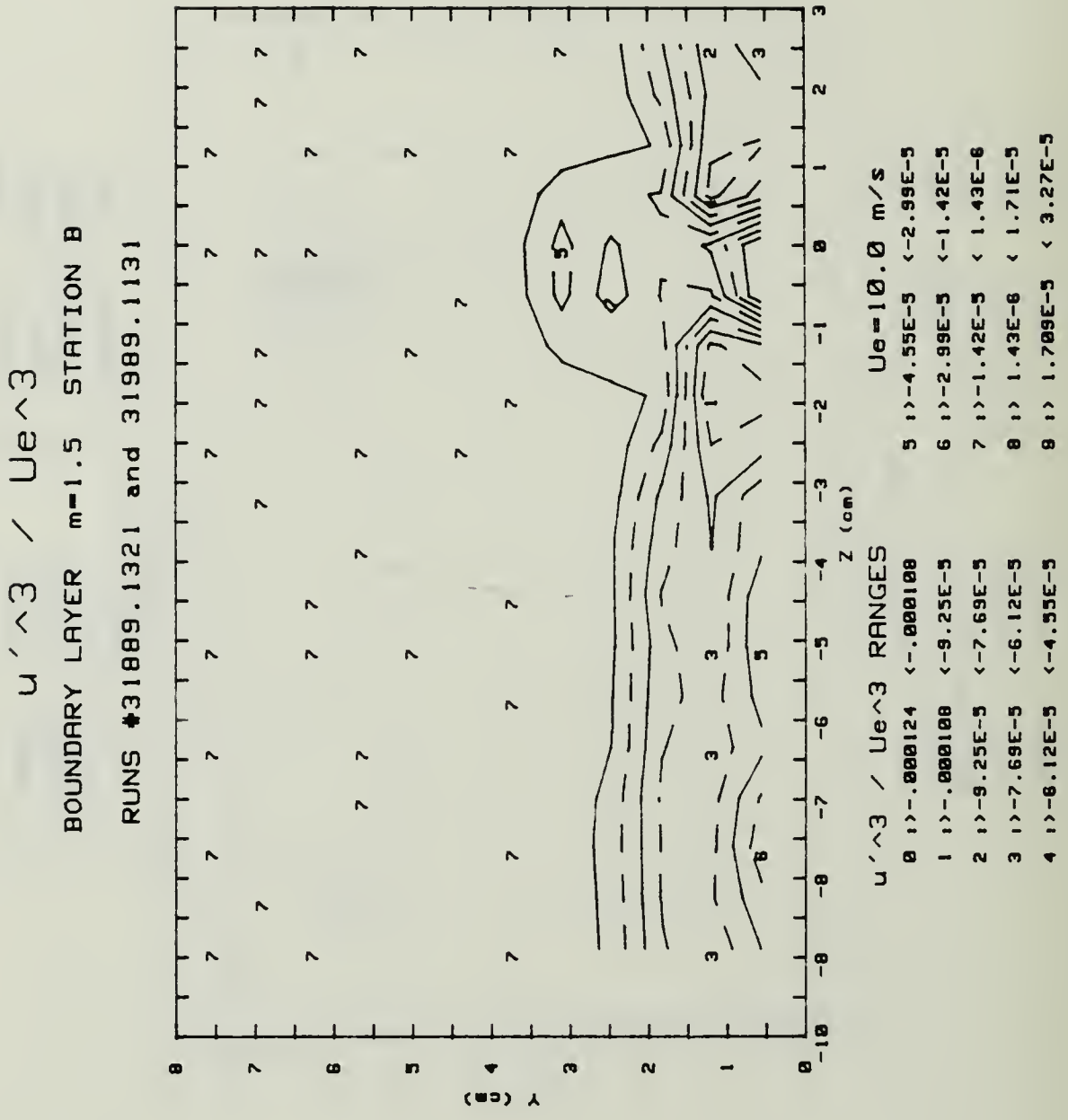

Figure 43. $\overline{u'^3}$ (boundary layer / wall jet, station B, $\Delta = 0.25$ inches)

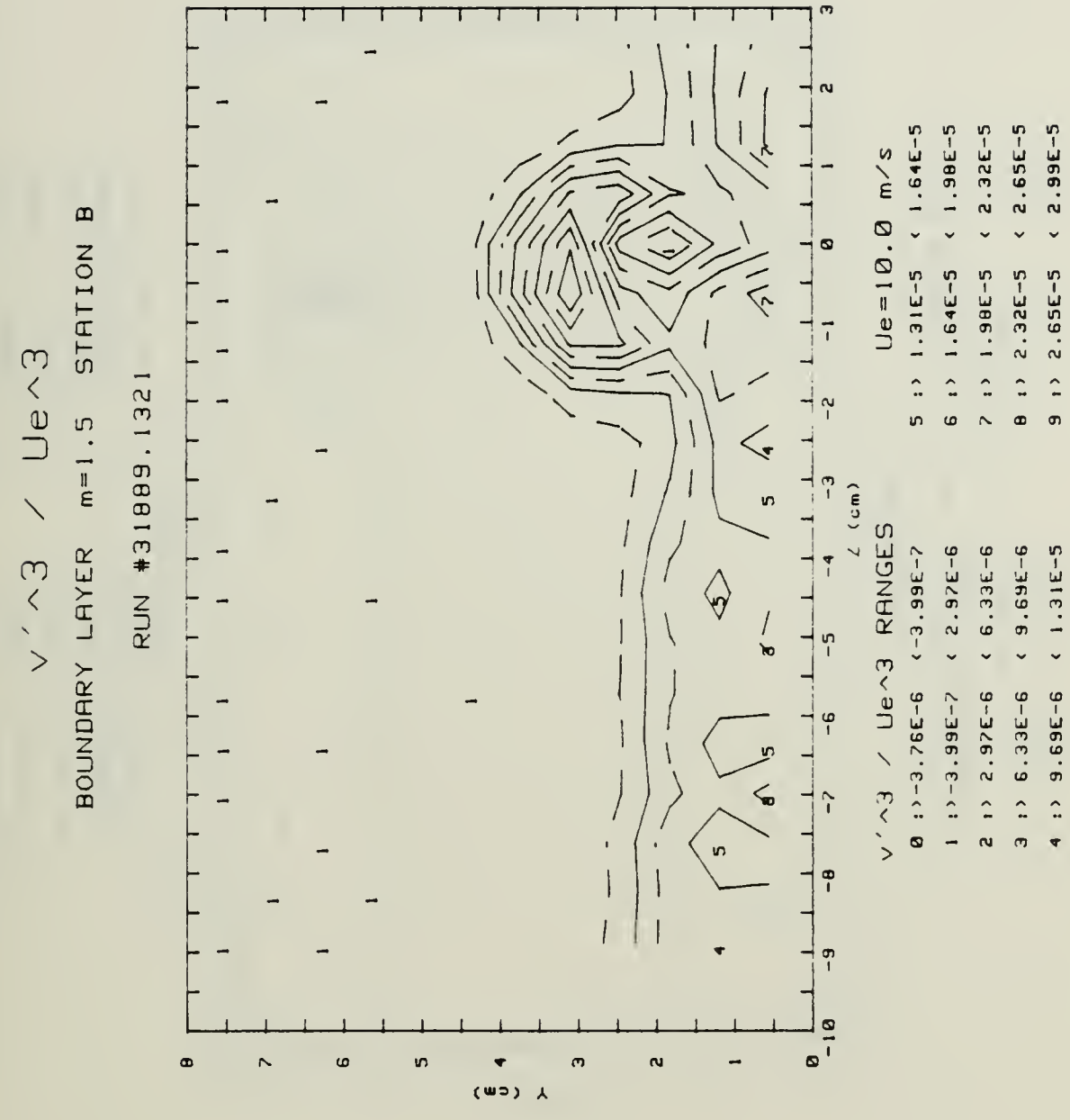

Figure 44. $\overline{v'^3}$ (boundary layer / wall jet, station B, $\Delta = 0.25$ inches)

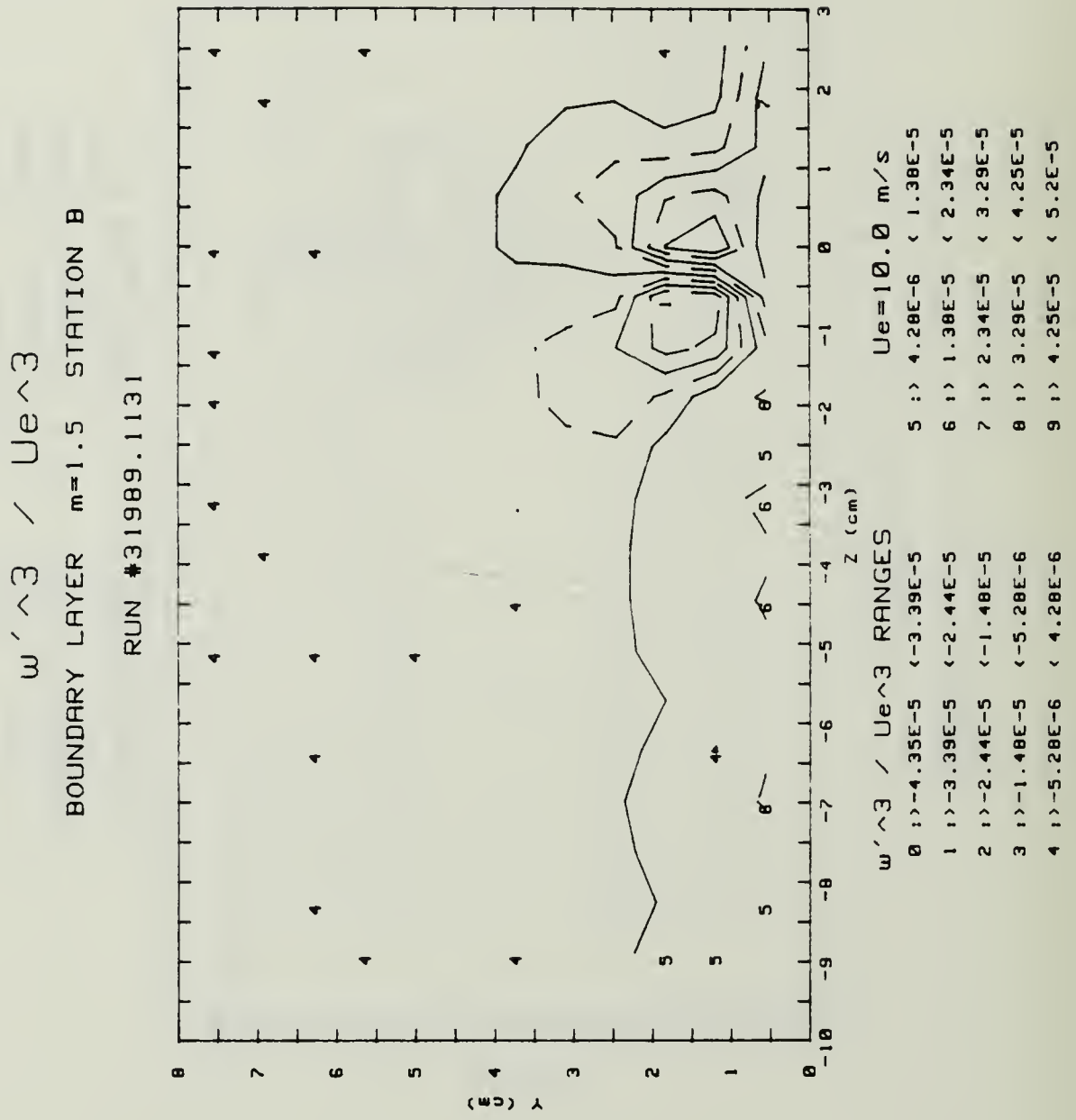

Figure 45. $\overline{w'^3}$ (boundary layer / wall jet, station B, $\Delta = 0.25$ inches)

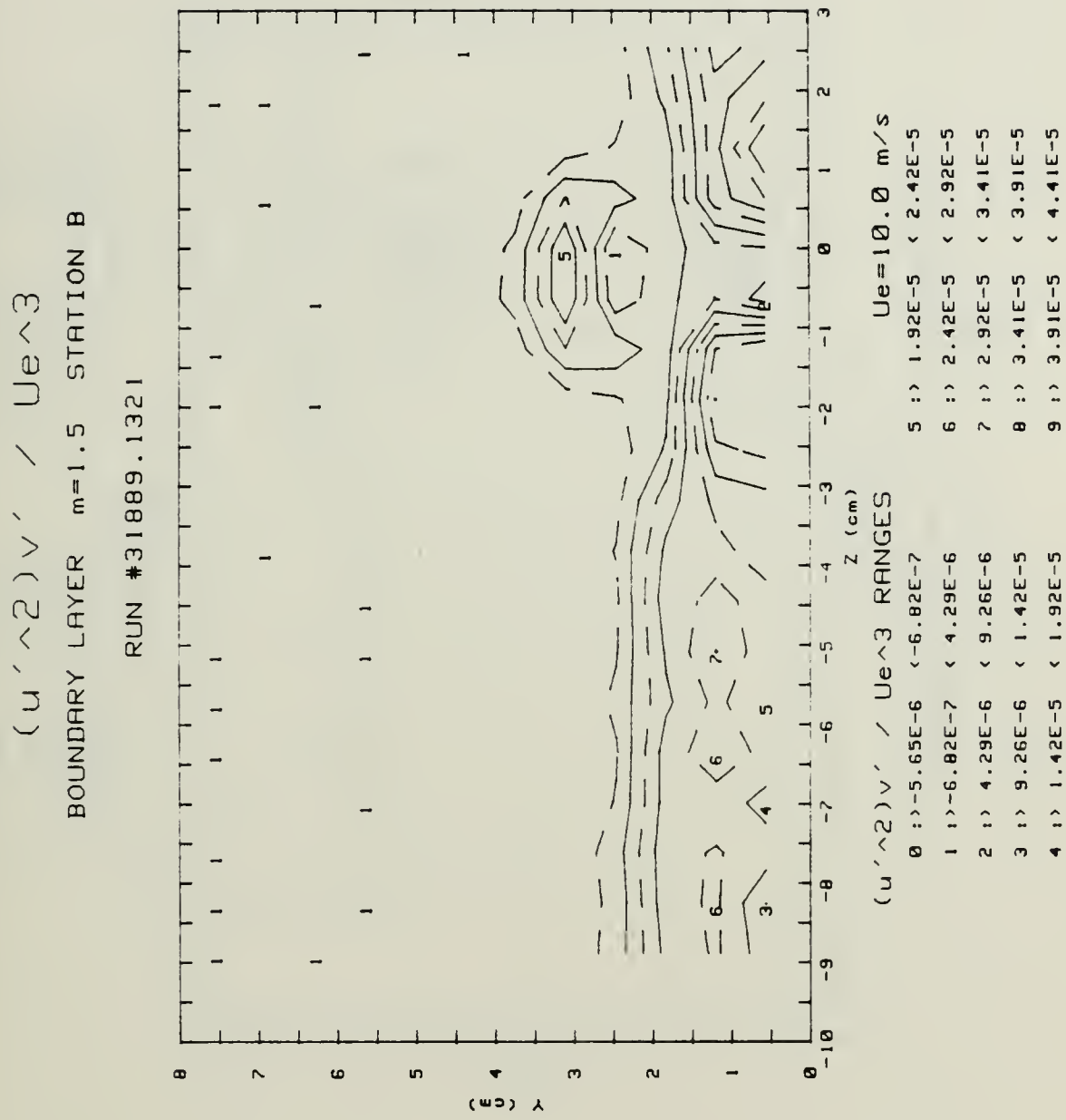

Figure 46. $\overline{u'^2v'}$ (boundary layer / wall jet, station B, $\Delta = 0.25$ inches)

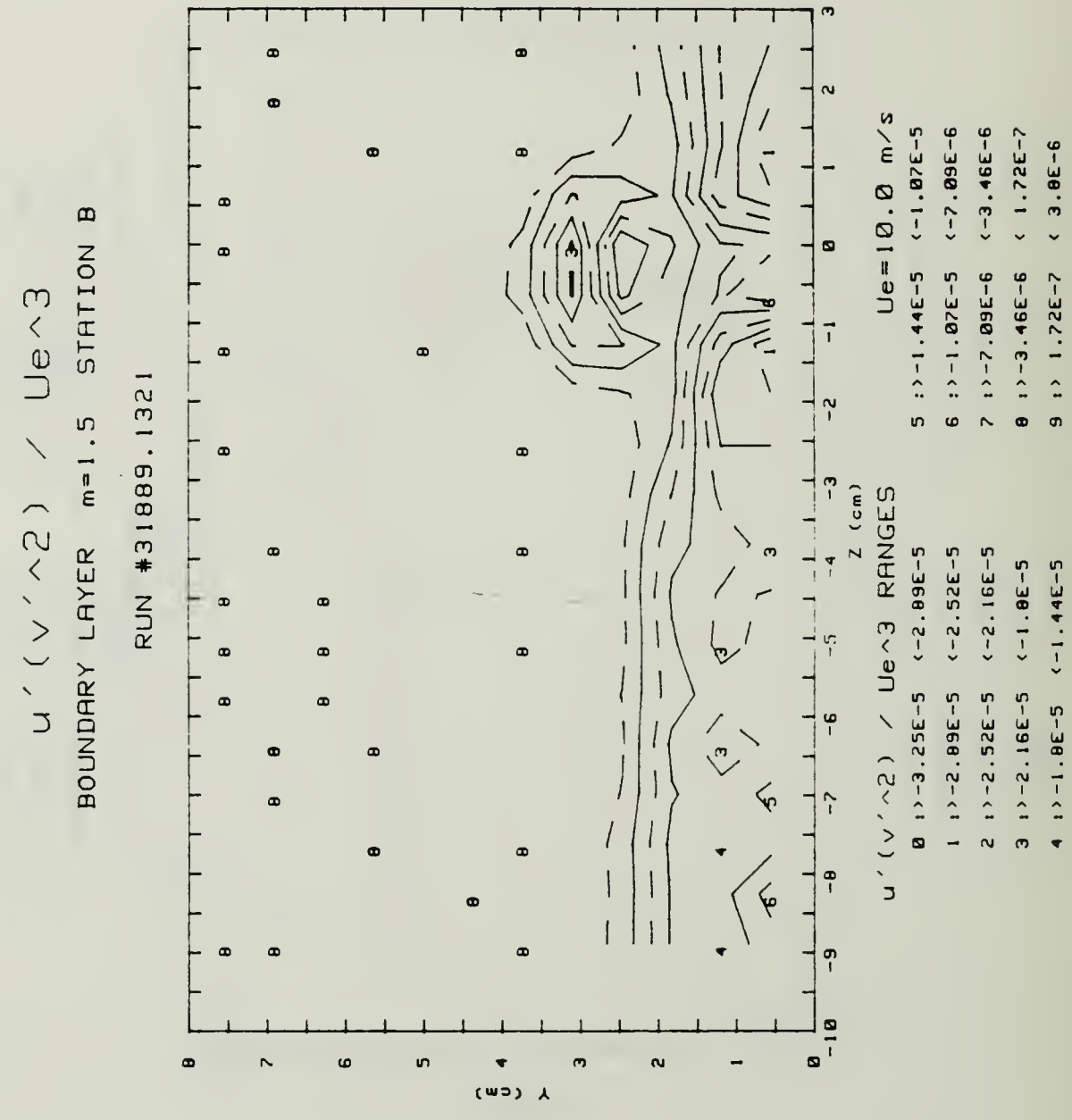

Figure 47. $\overline{u'v'^2}$ (boundary layer / wall jet, station B, $\Delta = 0.25$ inches)

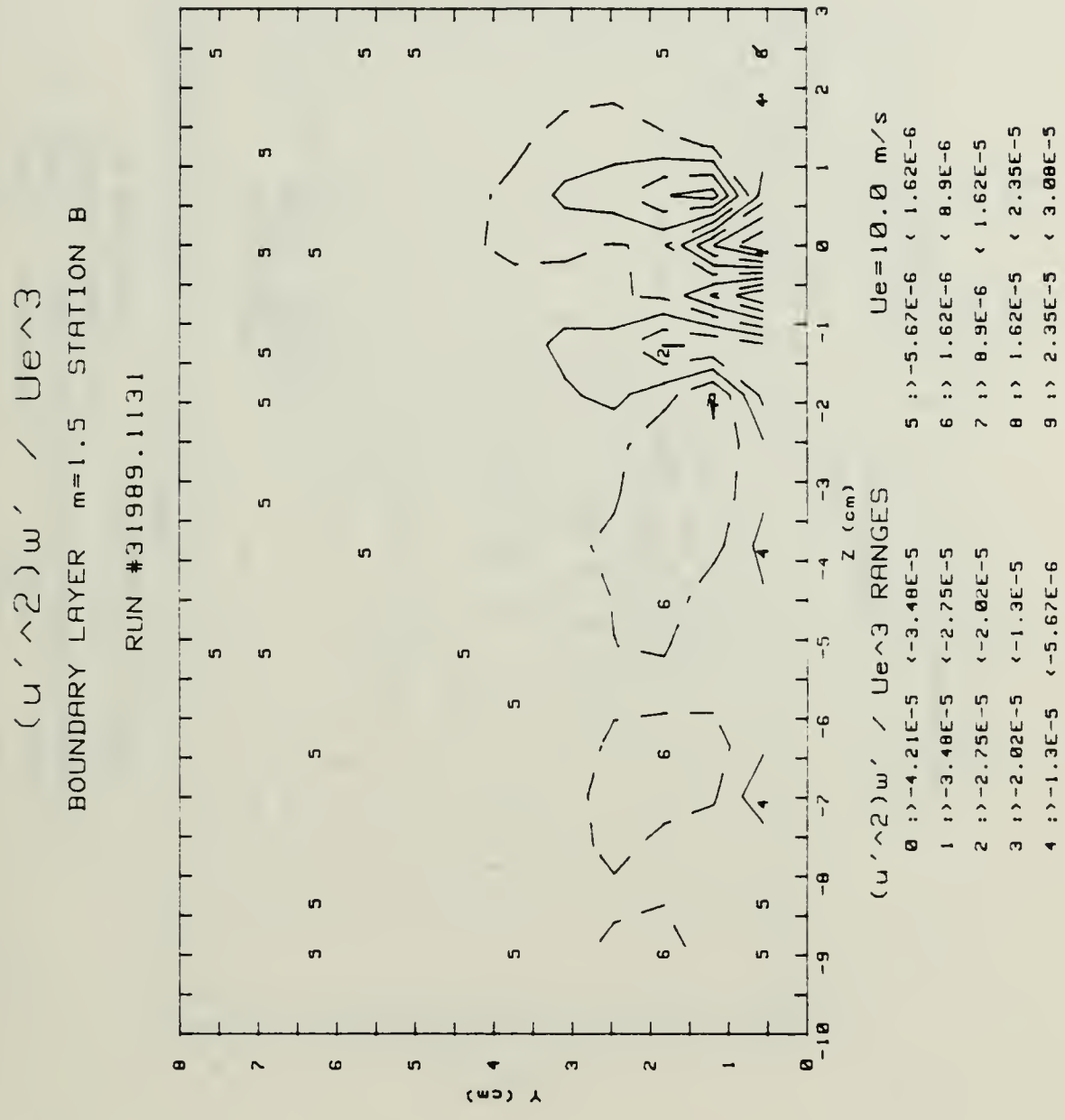

Figure 48. $\overline{u'^2w'}$ **(boundary layer / wall jet, station B, Δ = 0.25 inches)**

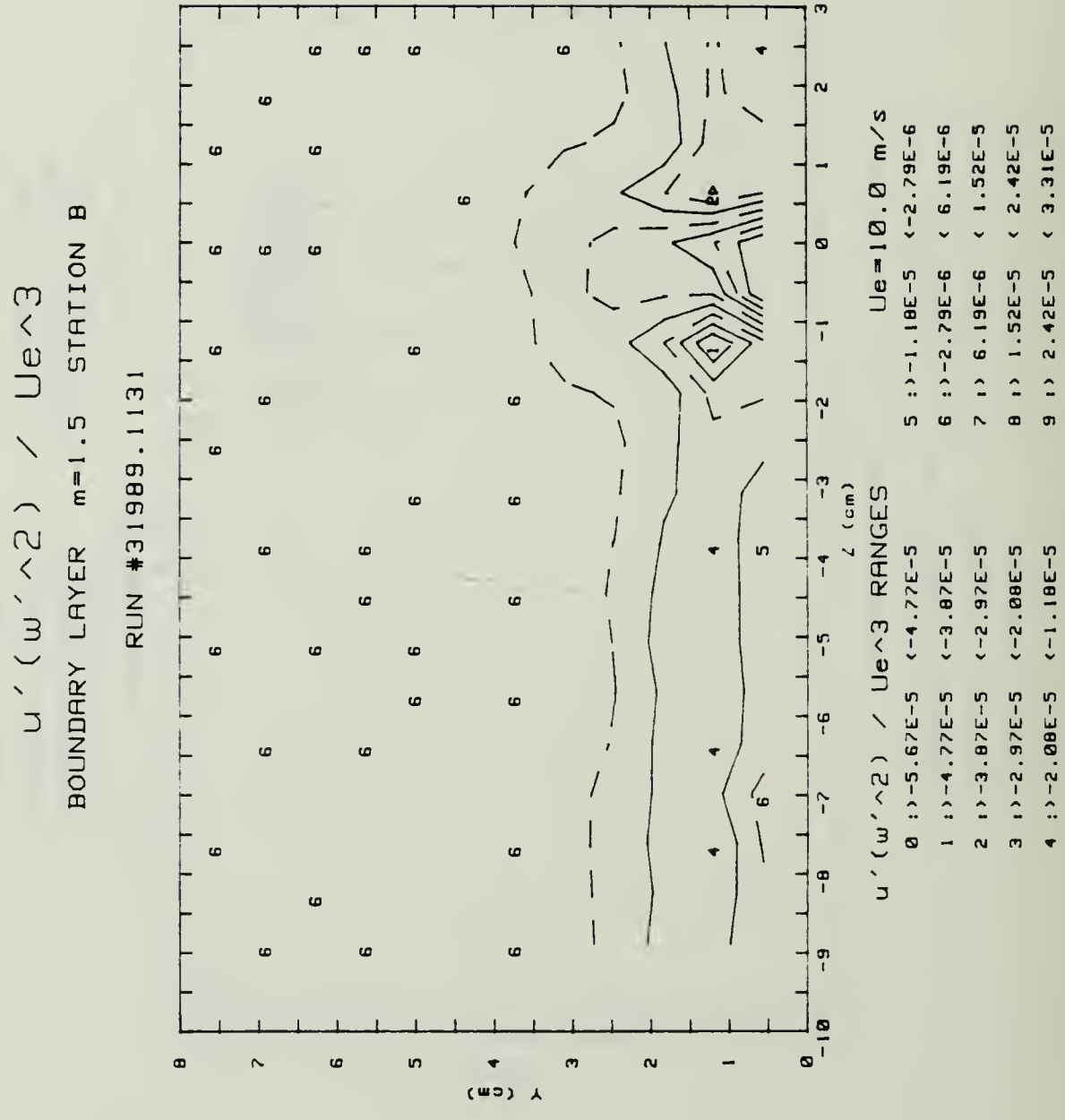

Figure 49. $\overline{u'w'^2}$ (boundary layer / wall jet, station B, $\Delta = 0.25$ inches)

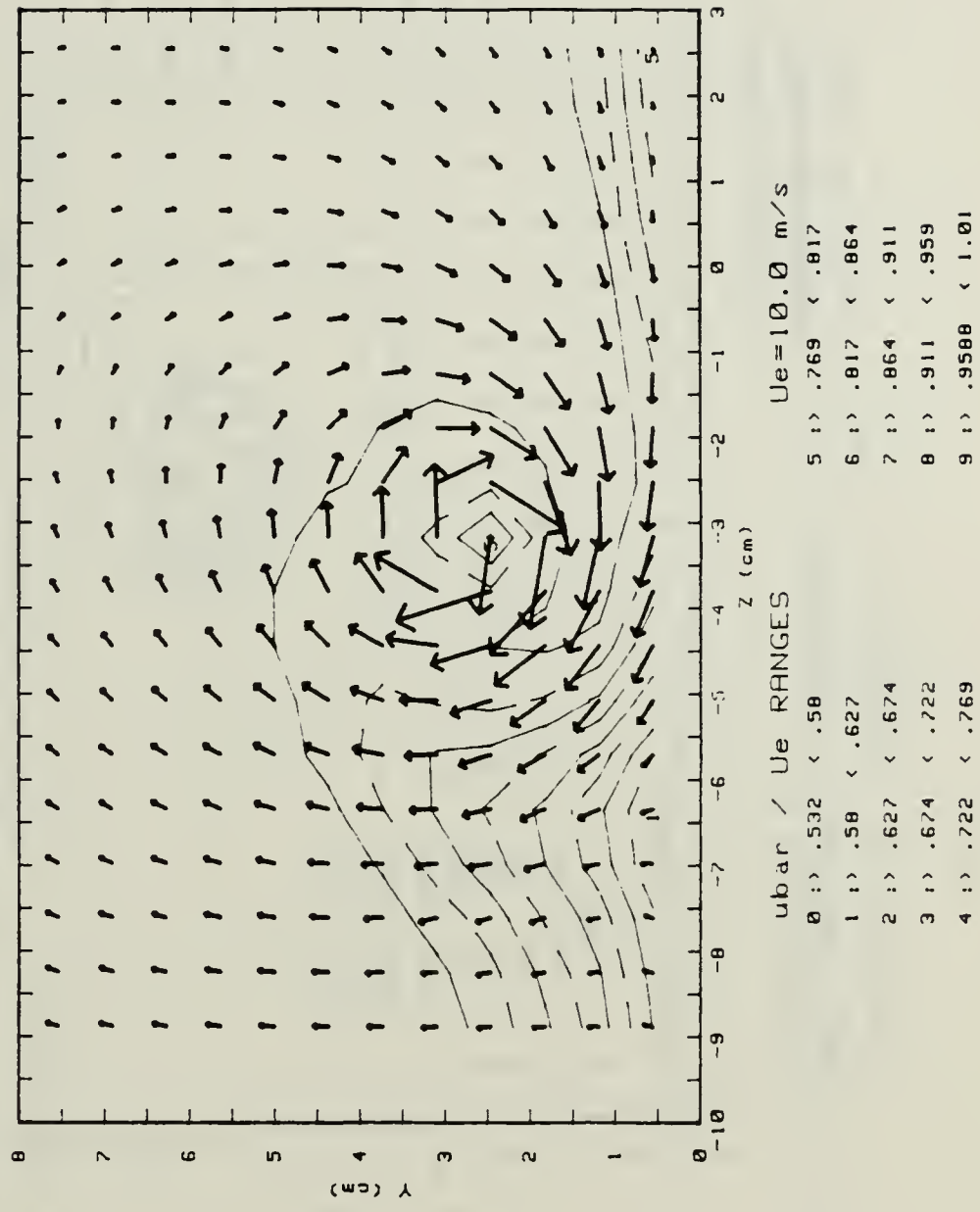

Figure 50. Mean Velocities (boundary layer / vortex, station B, $\Delta = 0.25$ inches)

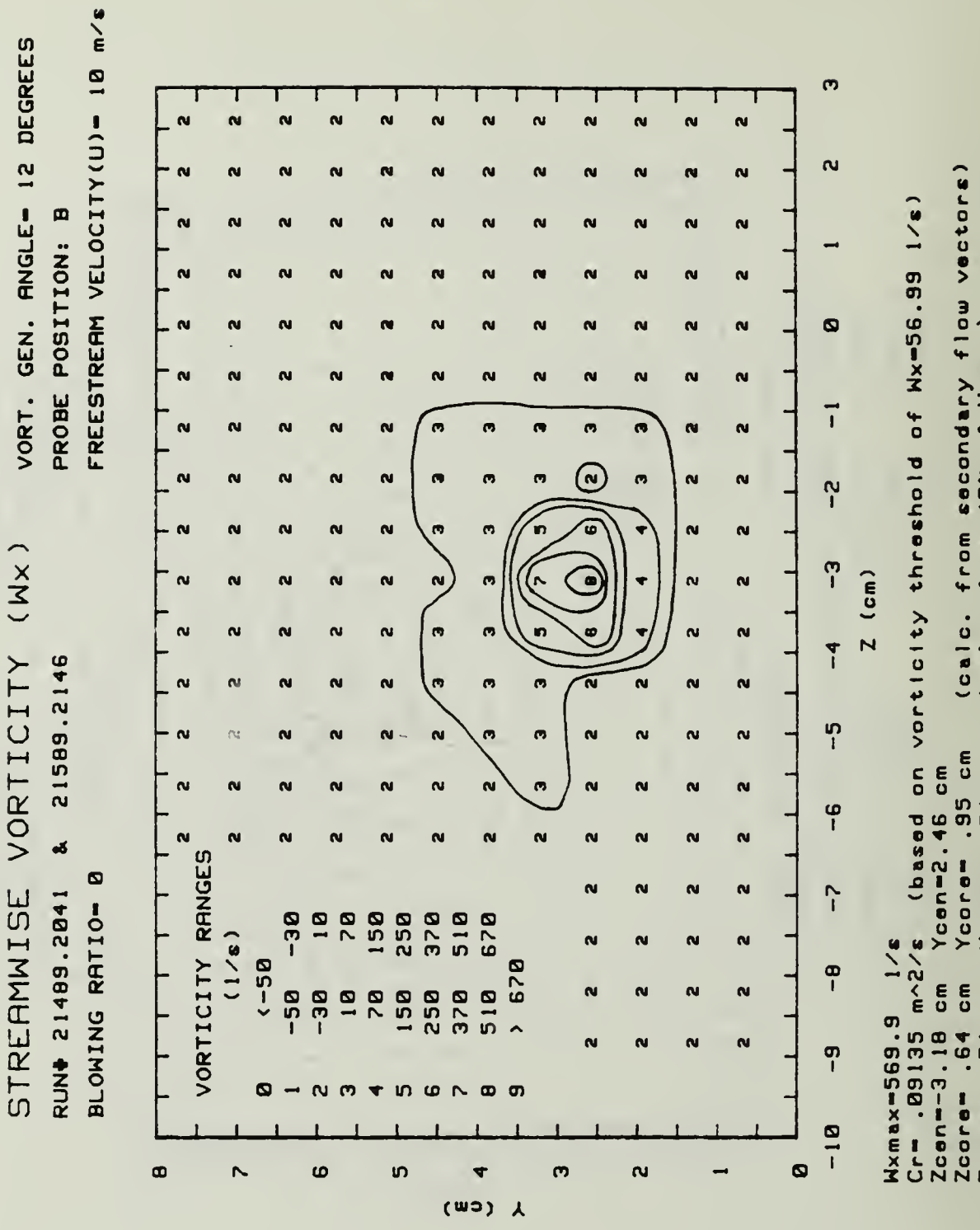

Figure 51. Streamwise Vorticity ω_x (boundary layer / vortex, station B, $\Delta = 0.25$ inches)

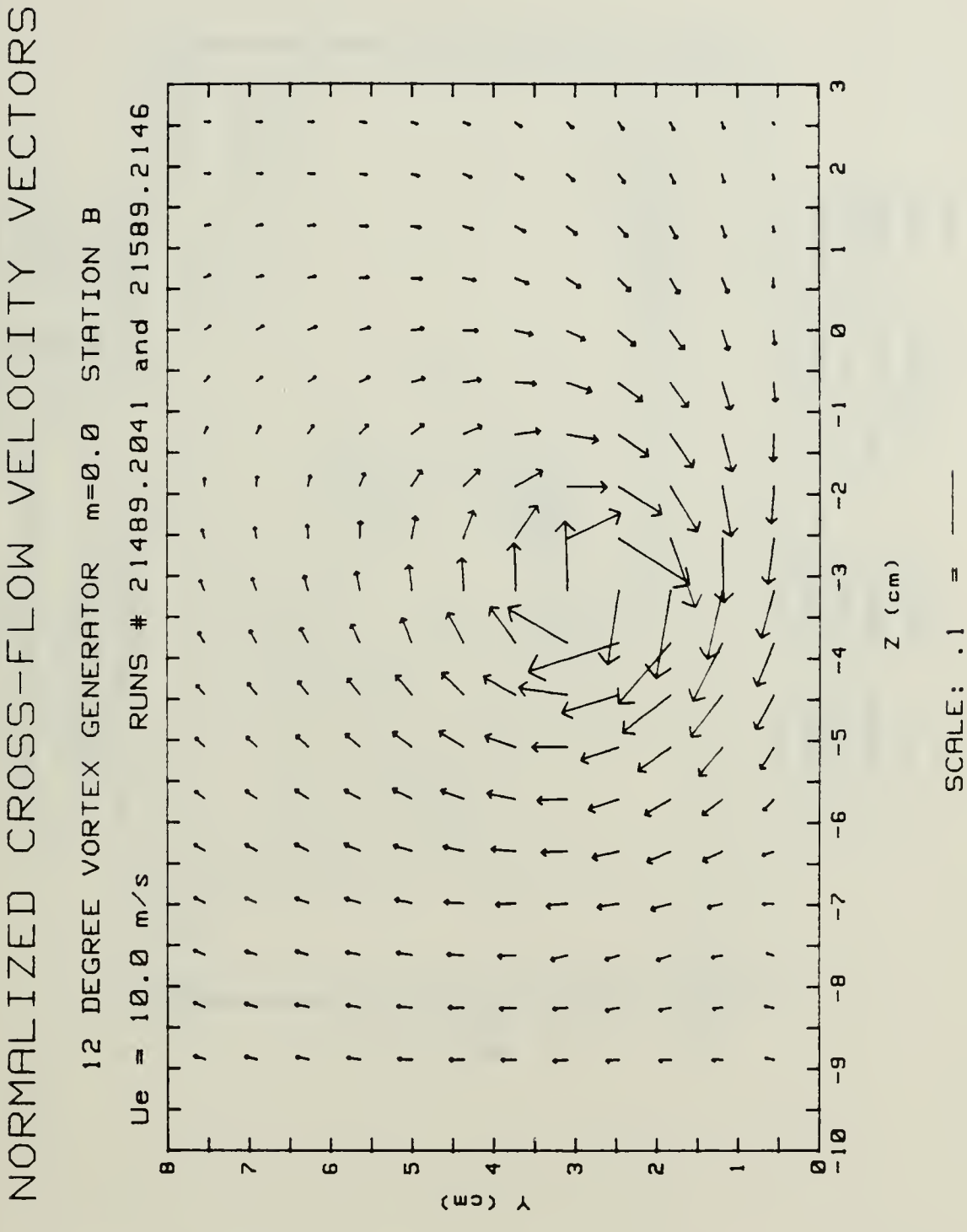
NORMALIZED CROSS-FLOW VELOCITY VECTORS
12 DEGREE VORTEX GENERATOR m=0.0 STATION B
Ue = 10.0 m/s RUNS # 21489.2041 and 21589.2146
Y (cm)
Z (cm)
SCALE: .1 = ——

Figure 52. Secondary Flow Vectors (boundary layer / vortex, station B, $\Delta = 0.25$ inches)

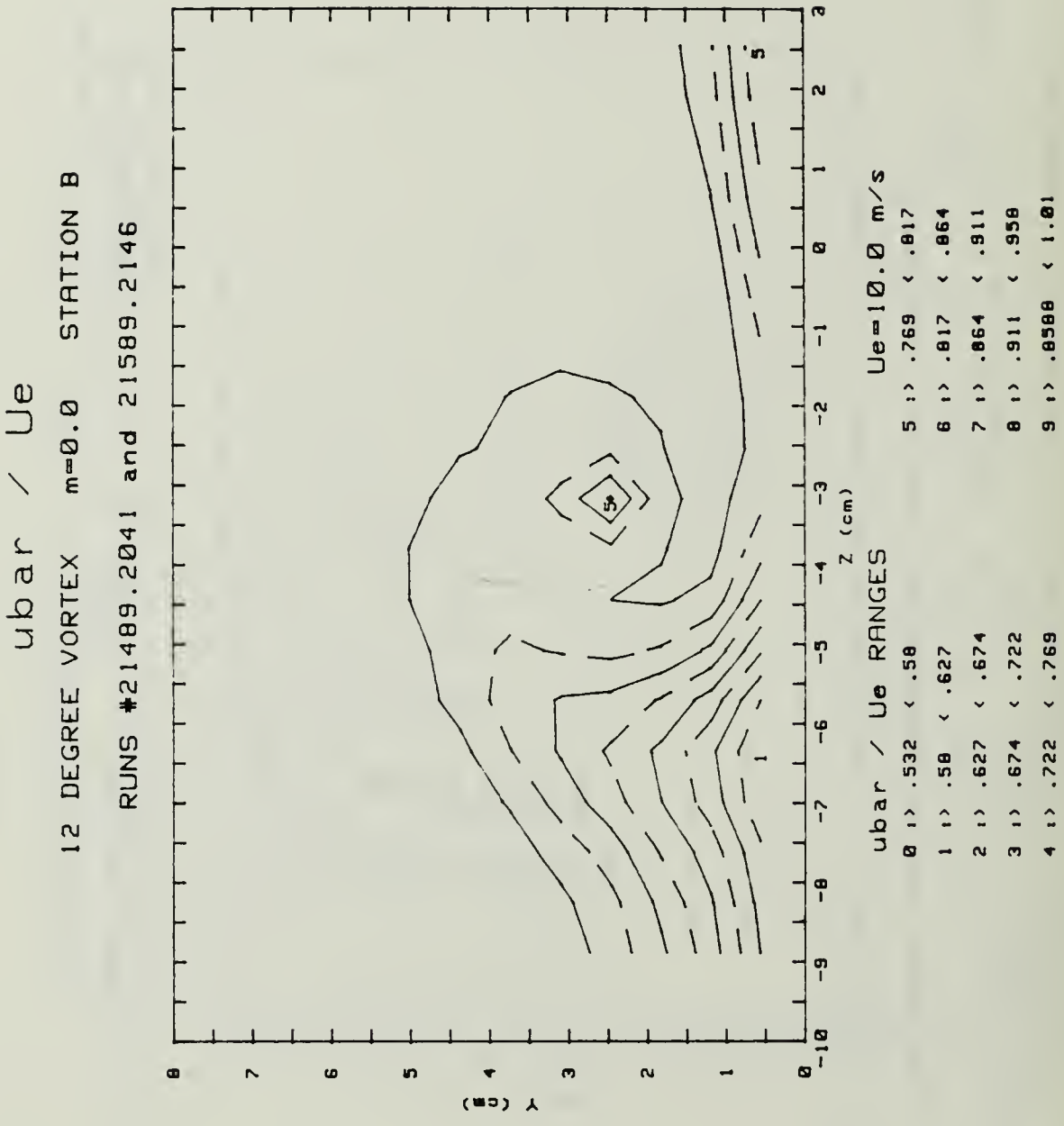

Figure 53. $\bar{u}$ (boundary layer / vortex, station B, $\Delta = 0.25$ inche s)

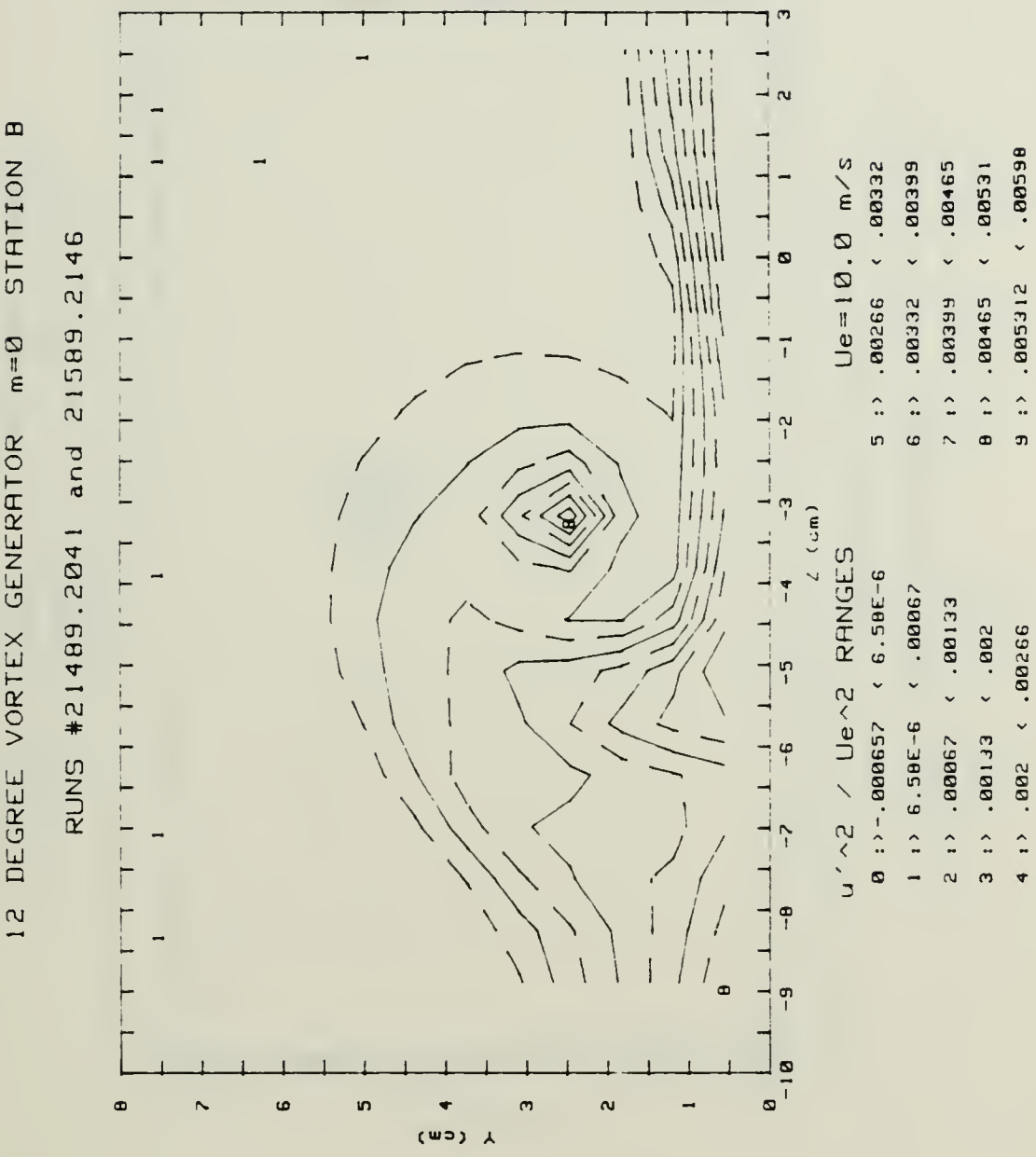

Figure 54. $\overline{u'^2}$ **(boundary layer / vortex, station B, Δ = 0.25 inches)**

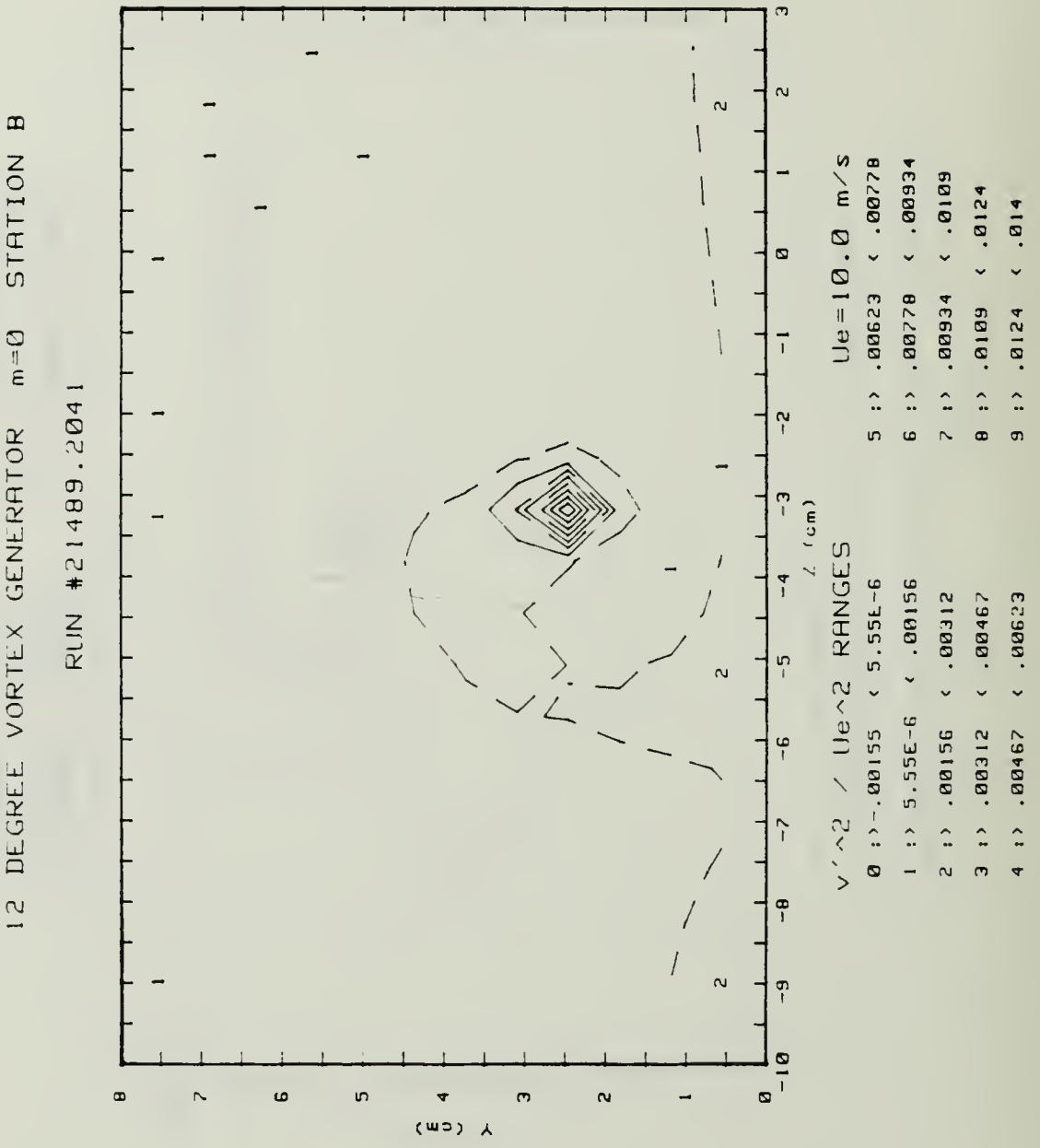

Figure 55. $\overline{v'^2}$ (boundary layer / vortex, station B, $\Delta = 0.25$ inches)

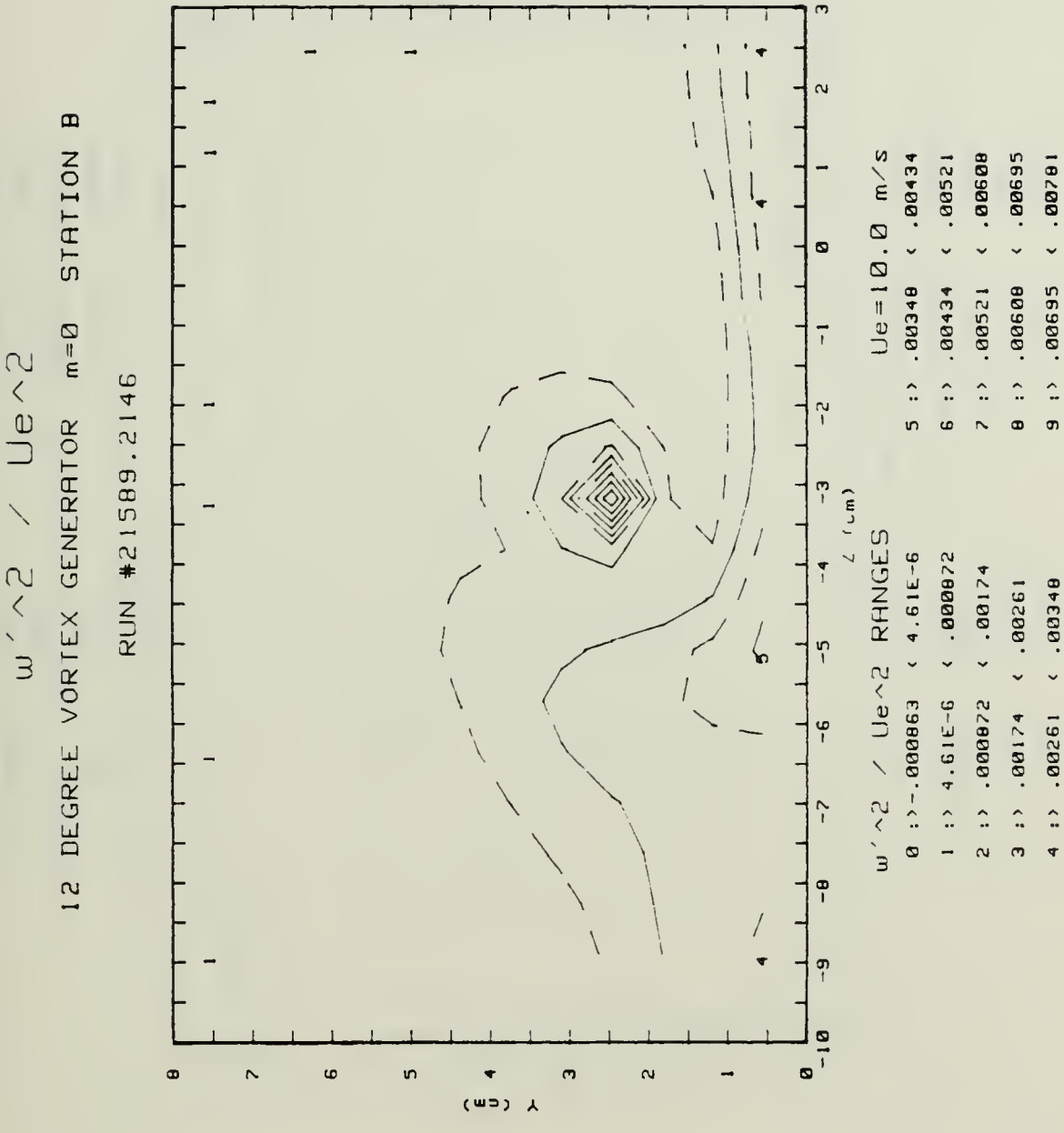

Figure 56. $\overline{w'^2}$ **(boundary layer / vortex, station B, Δ = 0.25 inches)**

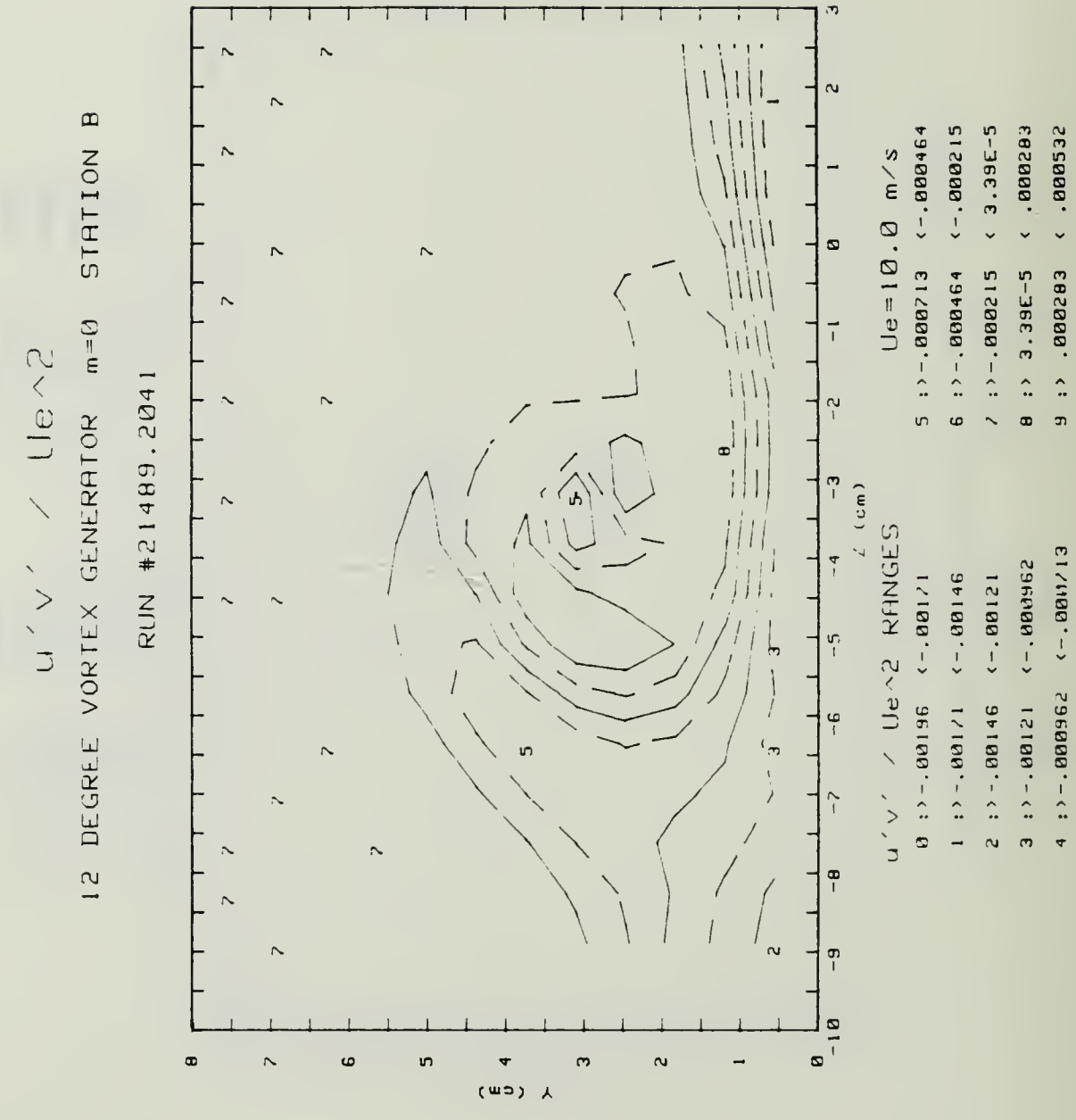

Figure 57. $\overline{u'v'}$ (boundary layer / vortex, station B, $\Delta = 0.25$ inches)

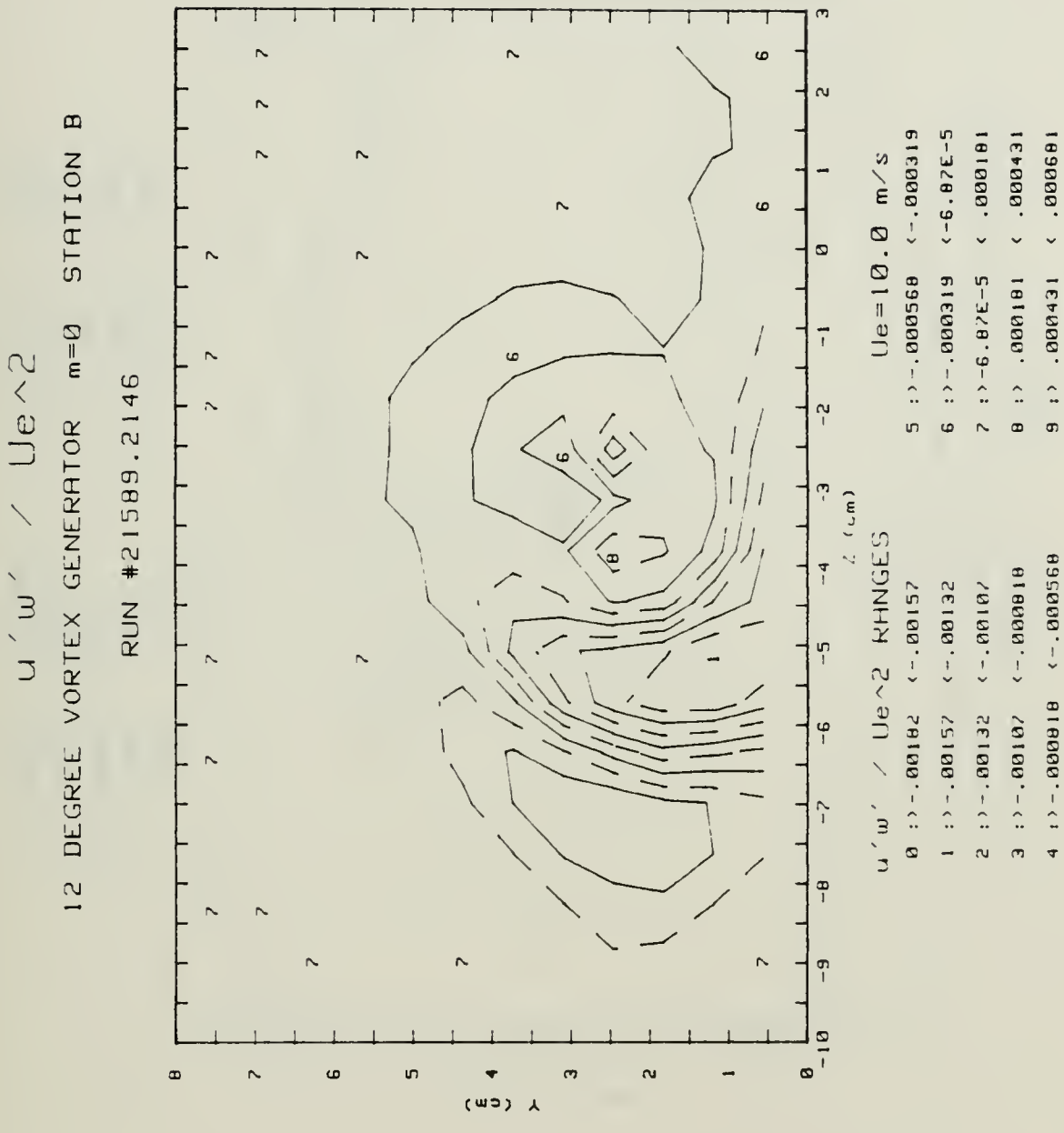

Figure 58. $\overline{u'w'}$ (boundary layer / vortex, station B, $\Delta = 0.25$ inches)

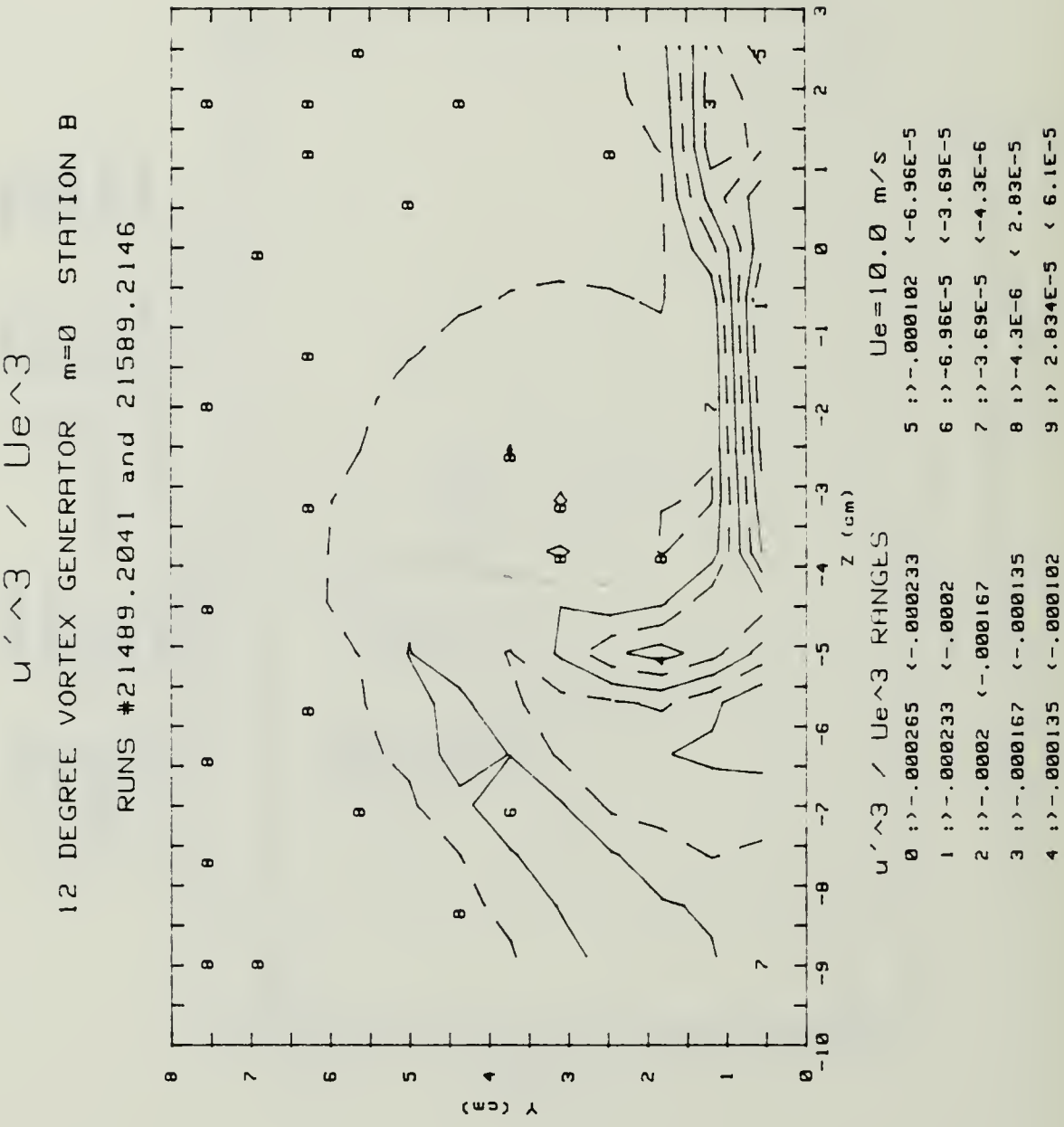

Figure 59. $\overline{u'^3}$ (boundary layer / vortex, station B, $\Delta = 0.25$ inches)

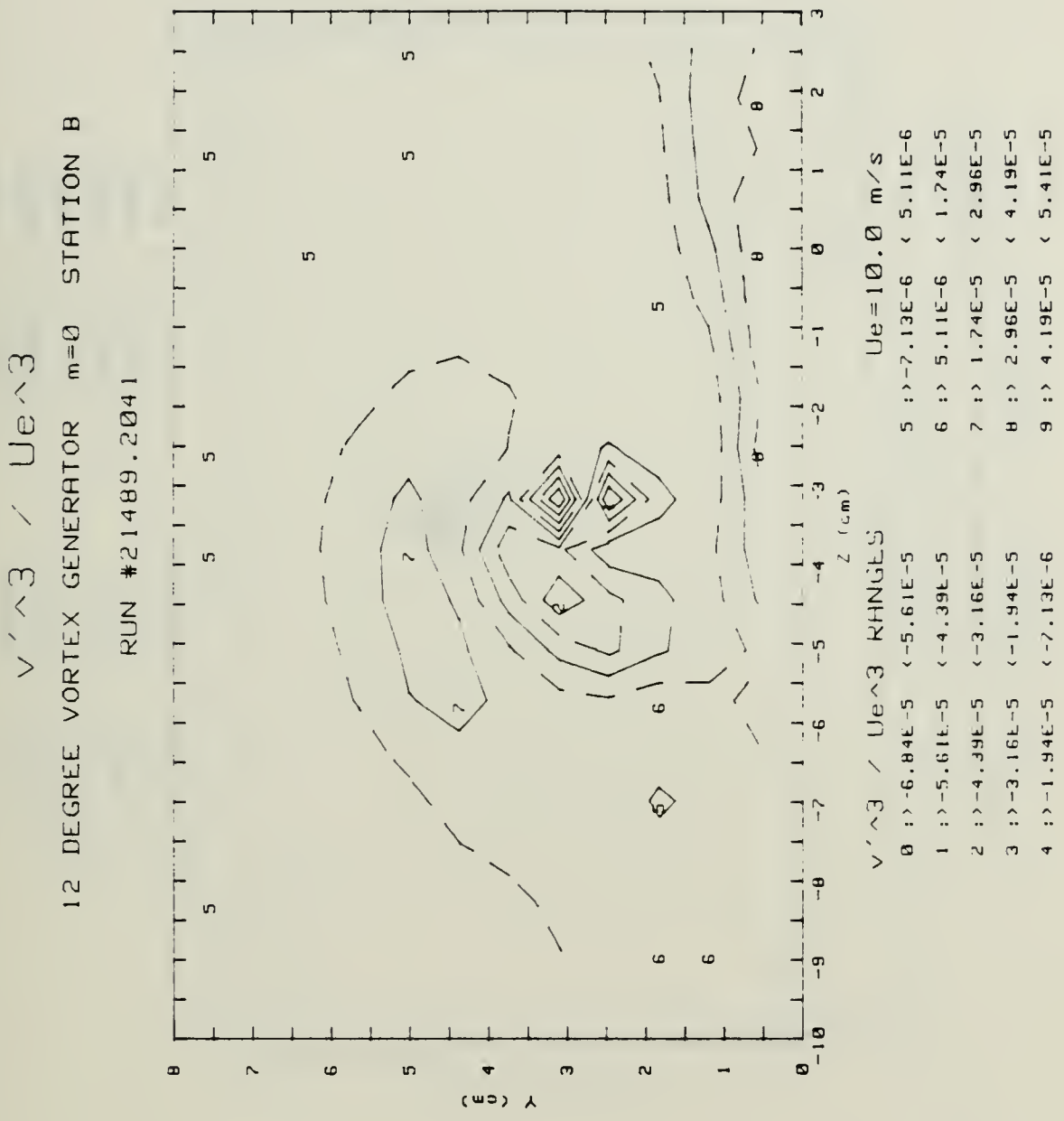

Figure 60. $\overline{v'^3}$ **(boundary layer / vortex, station B, Δ = 0.25 inches)**

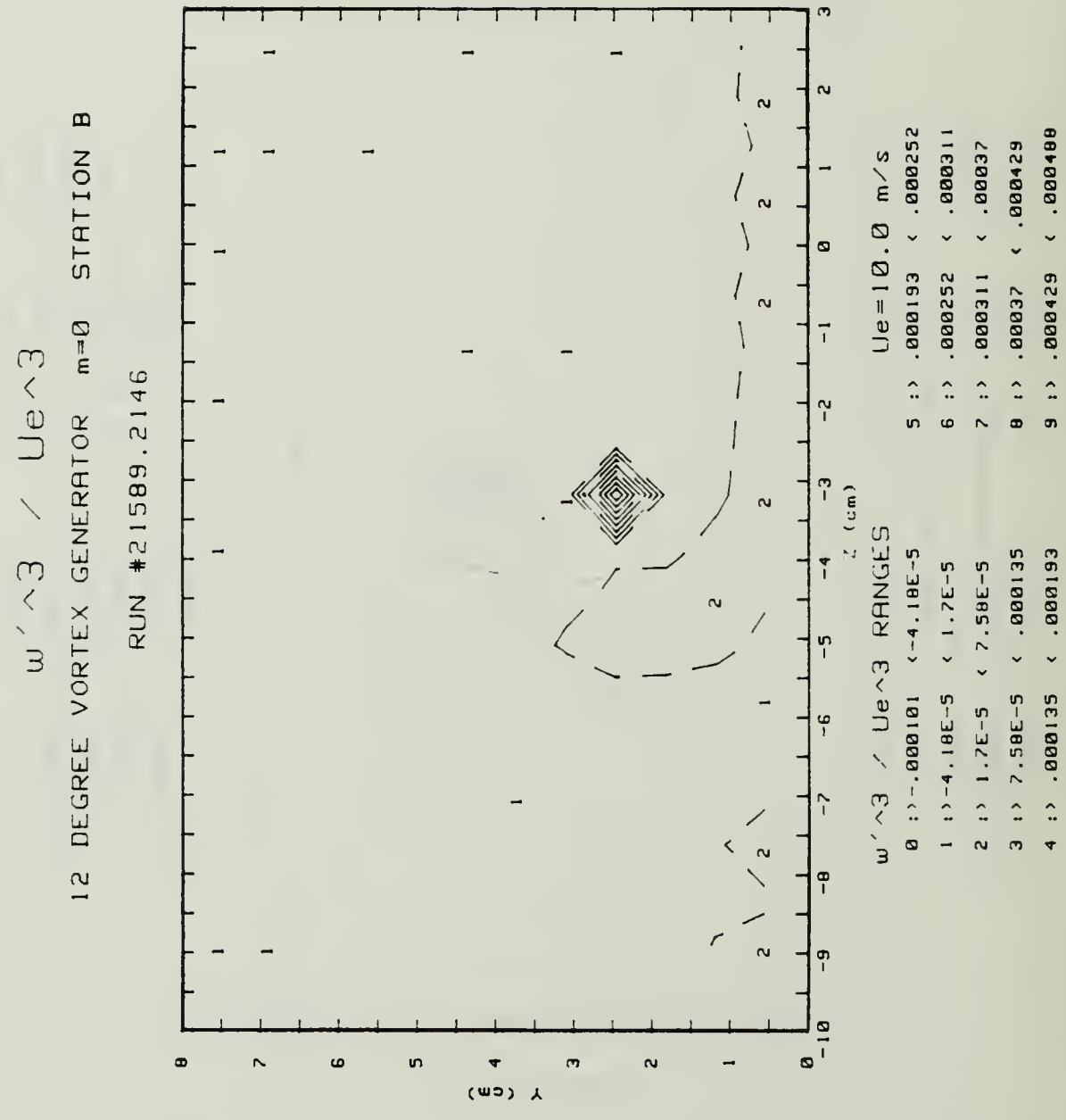

Figure 61. $\overline{w'^3}$ (boundary layer / vortex, station B, $\Delta = 0.25$ inches)

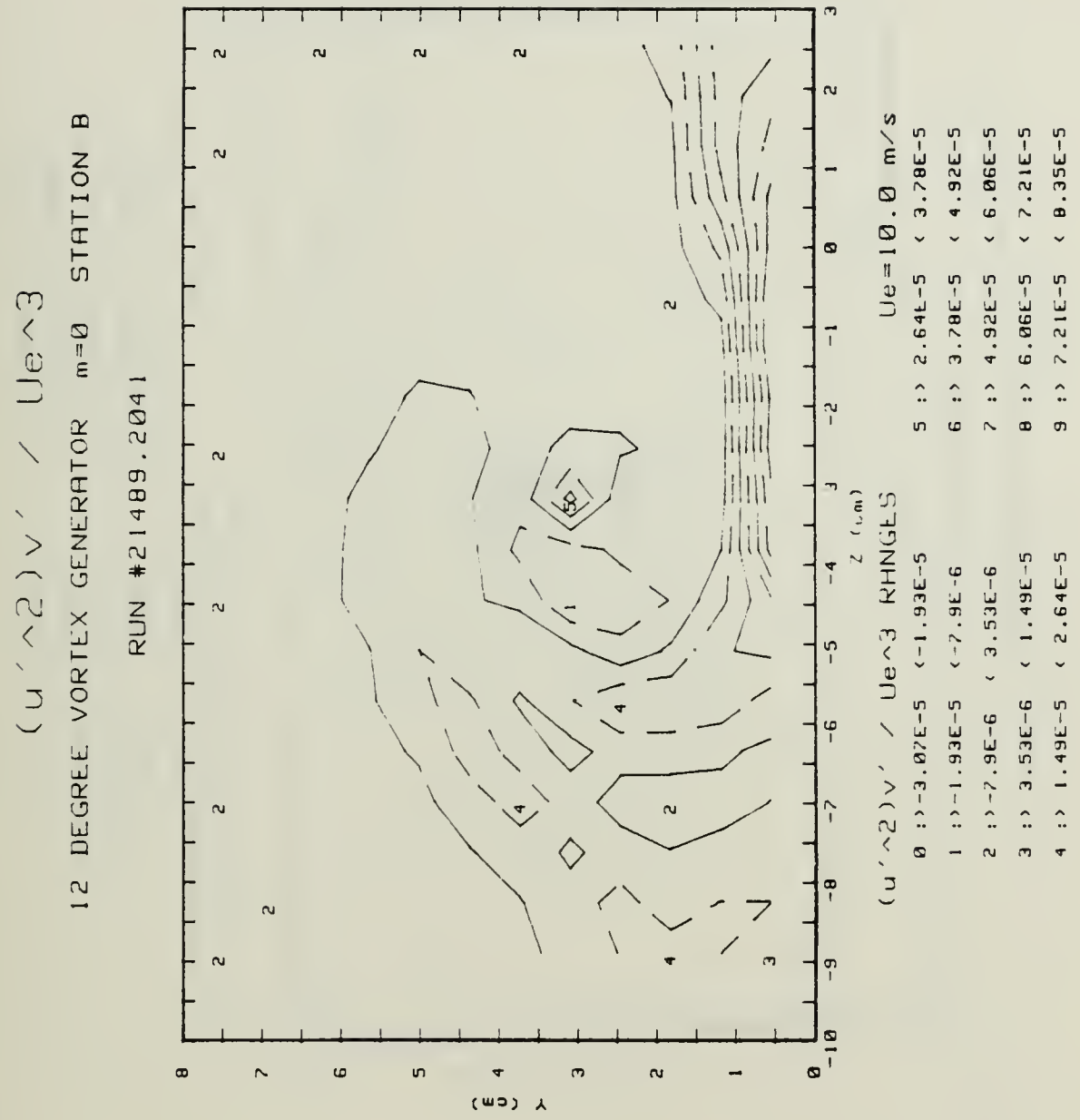

Figure 62. $\overline{u'^2v'}$ **(boundary layer / vortex, station B, Δ = 0.25 inches)**

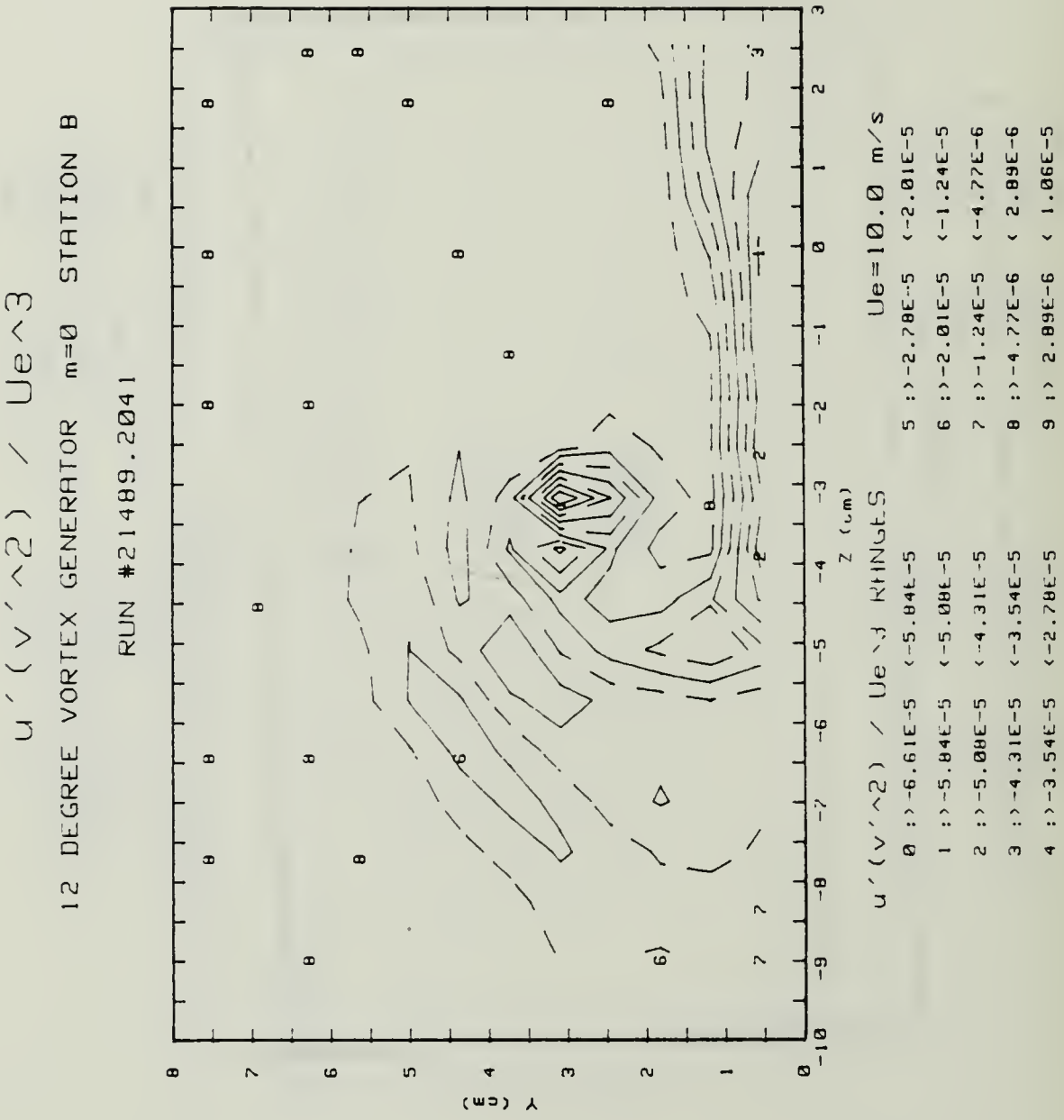

Figure 63. $\overline{u'v'^2}$ (boundary layer / vortex, station B, $\Delta = 0.25$ inches)

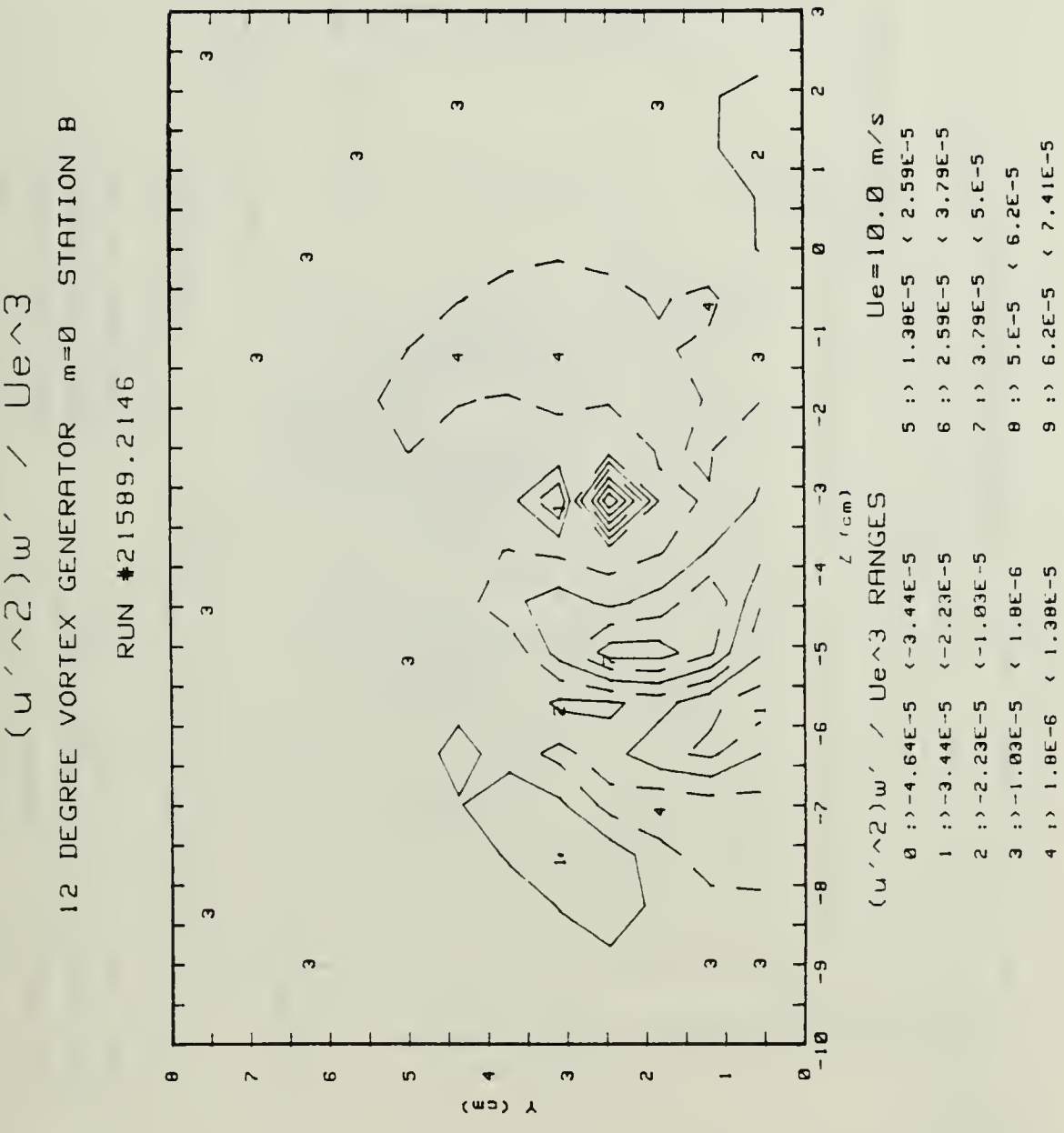

Figure 64. $\overline{u'^2w'}$ **(boundary layer / vortex, station B, Δ = 0.25 inches)**

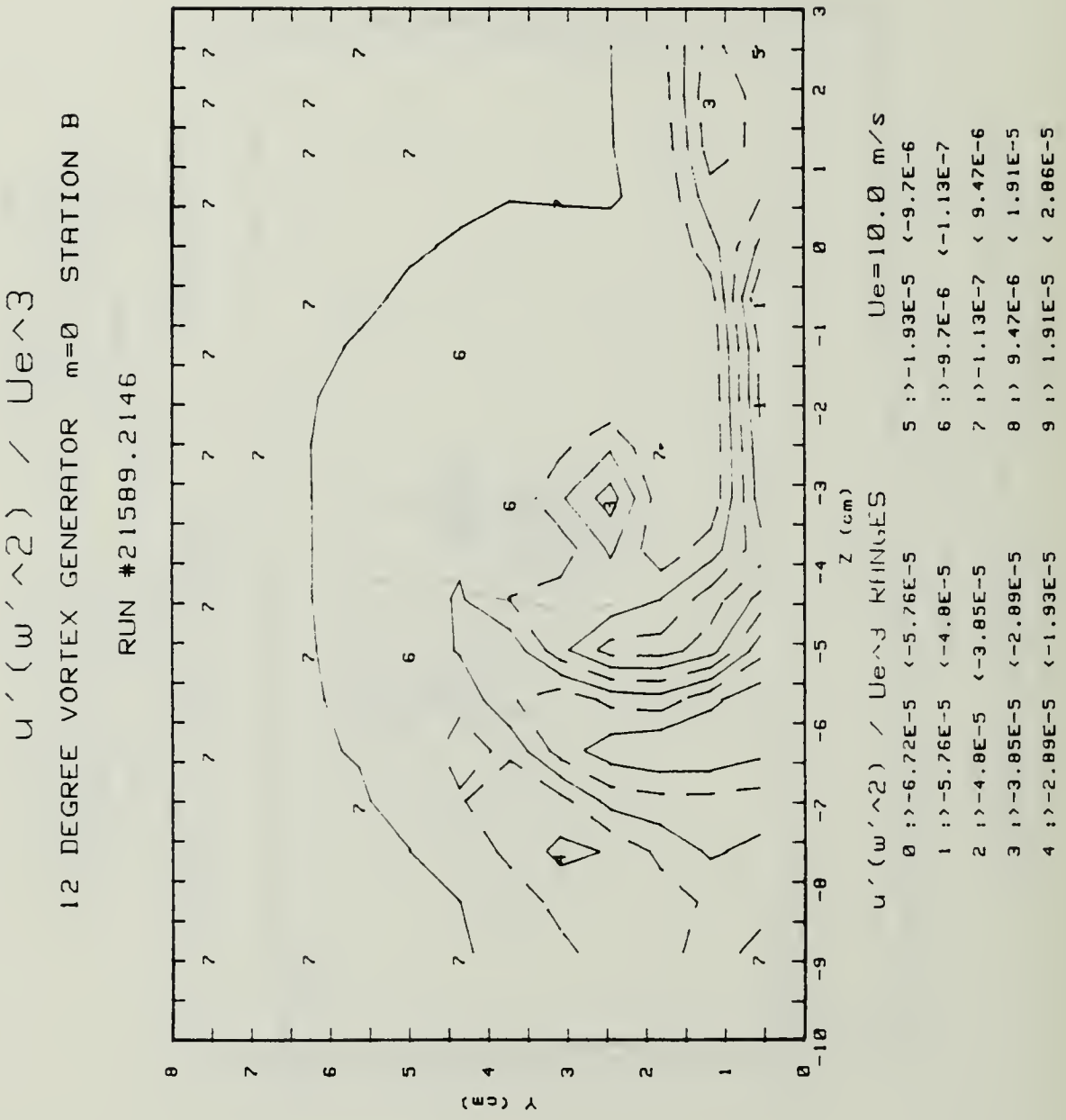

Figure 65. $\overline{u'w'^2}$ (boundary layer / vortex, station B, $\Delta = 0.25$ inches)

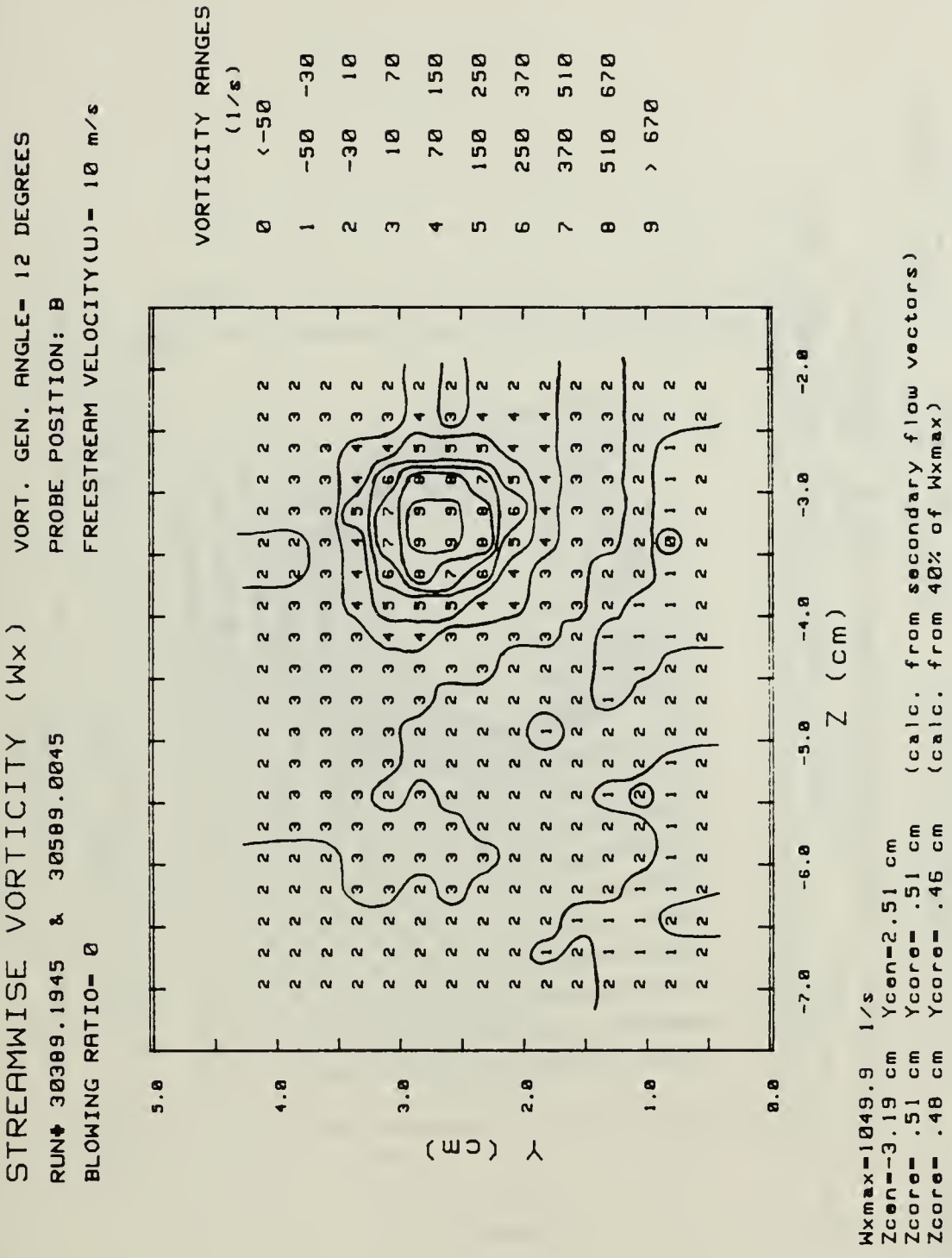

Figure 66. Streamwise Vorticity ω_x (boundary layer / vortex, station B, $\Delta = 0.10$ inches)

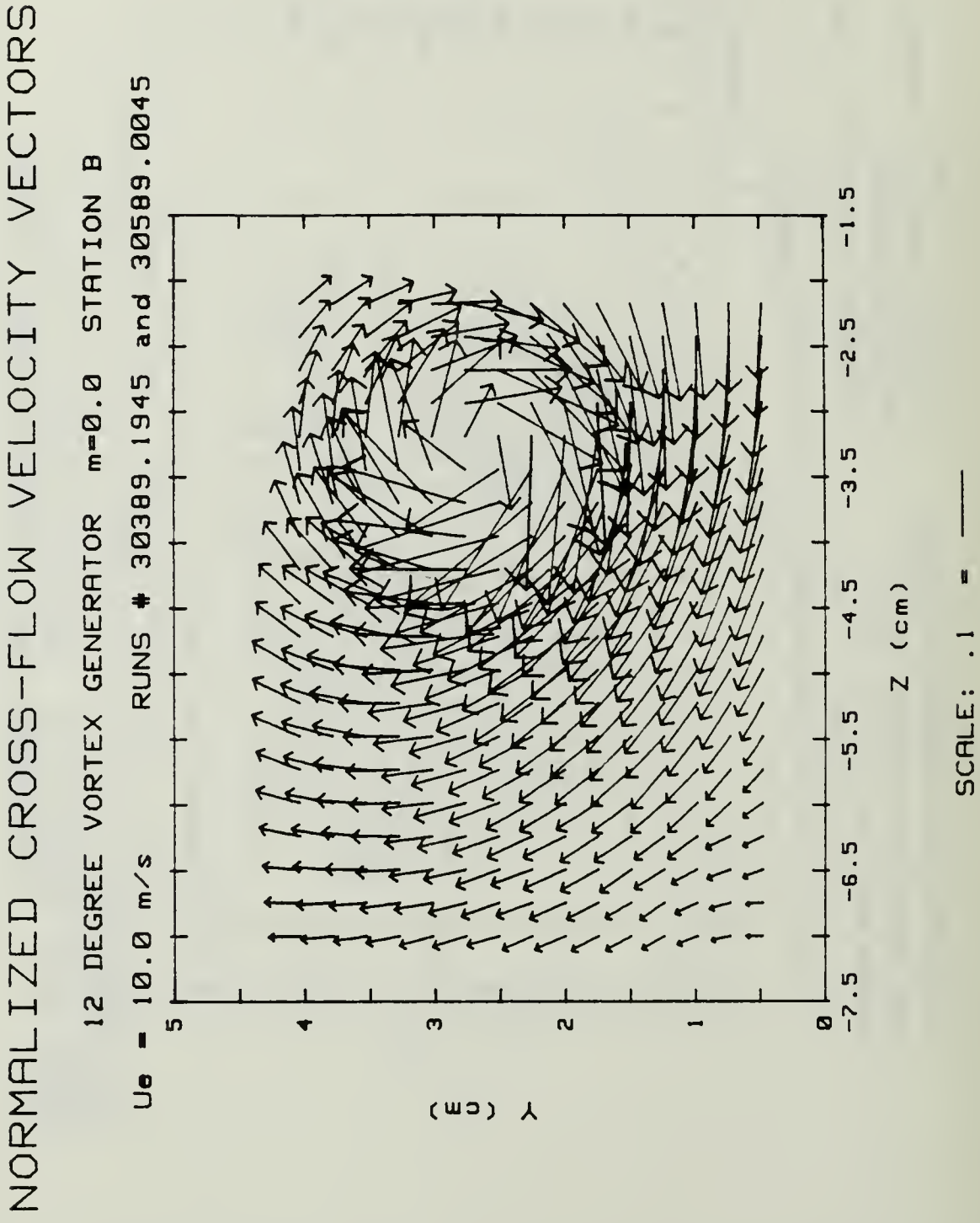

Figure 67. Secondary Flow Vectors (boundary layer / vortex, station B, $\Delta = 0.10$ inches)

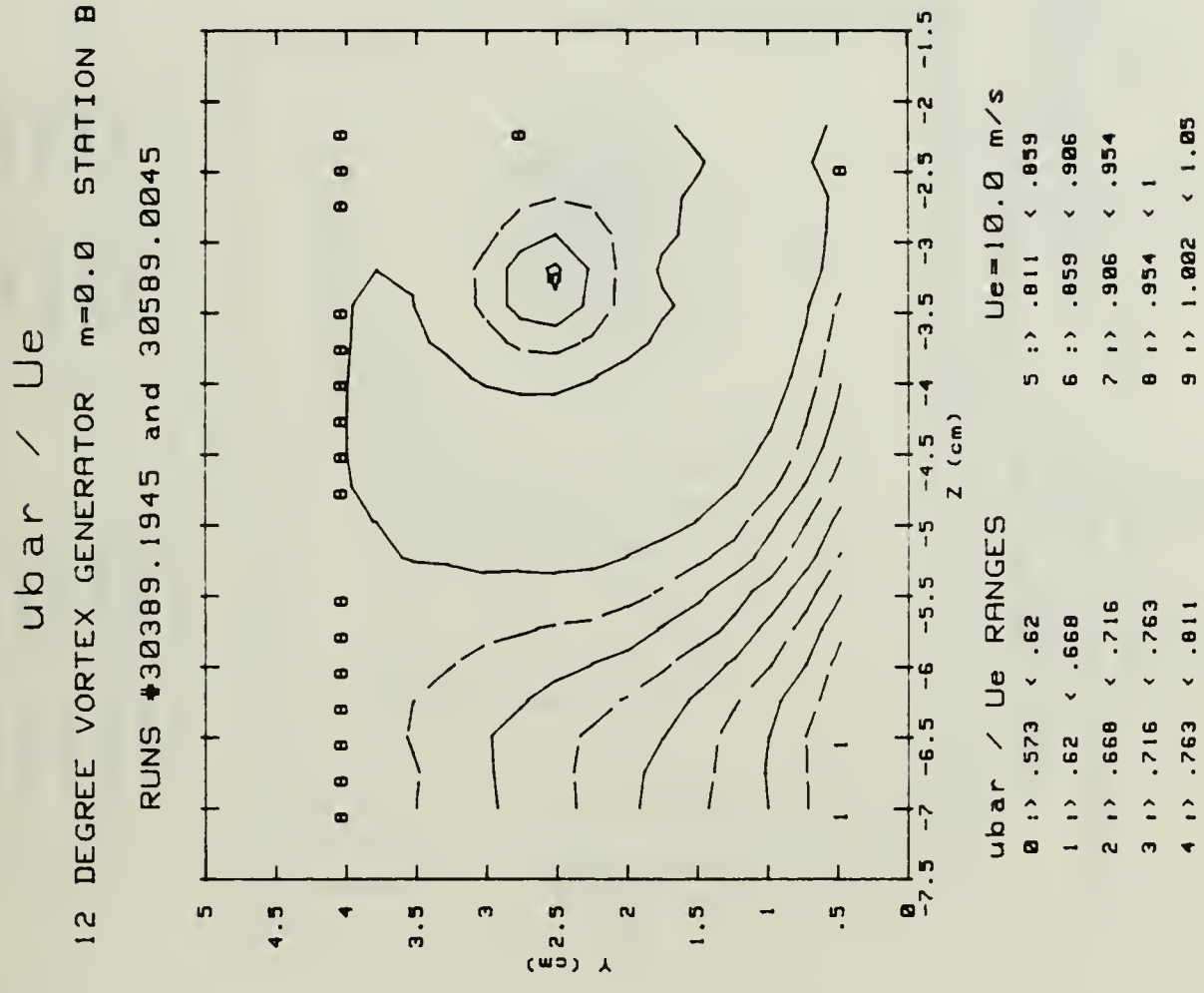

Figure 68. $\bar{u}$ (boundary layer / vortex, station B, $\Delta = 0.10$ inches)

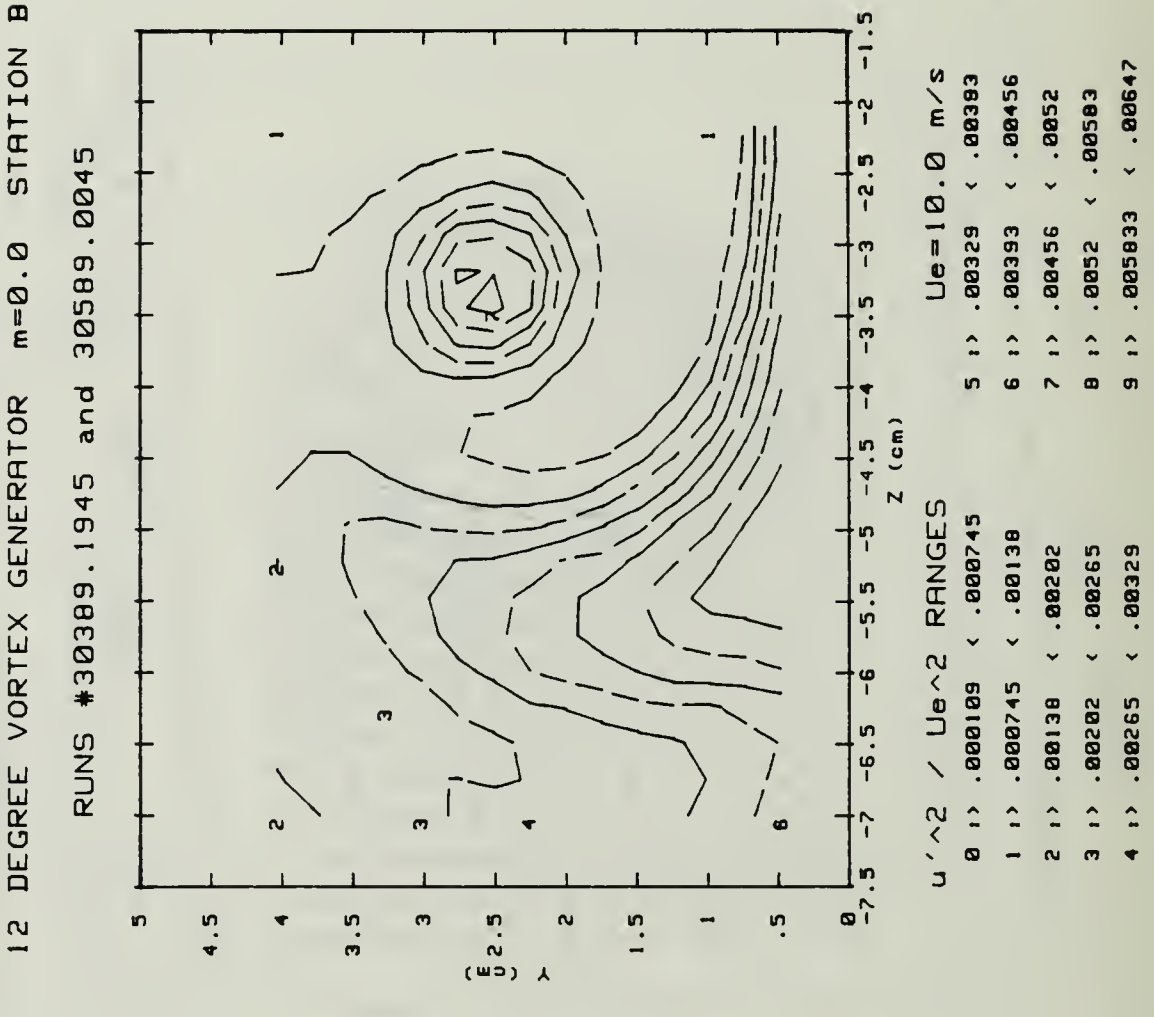

Figure 69. $\overline{u'^2}$ (boundary layer / vortex, station B, $\Delta = 0.10$ inches)

Figure 70. $\overline{v'^2}$ (boundary layer / vortex, station B, $\Delta = 0.10$ inches)

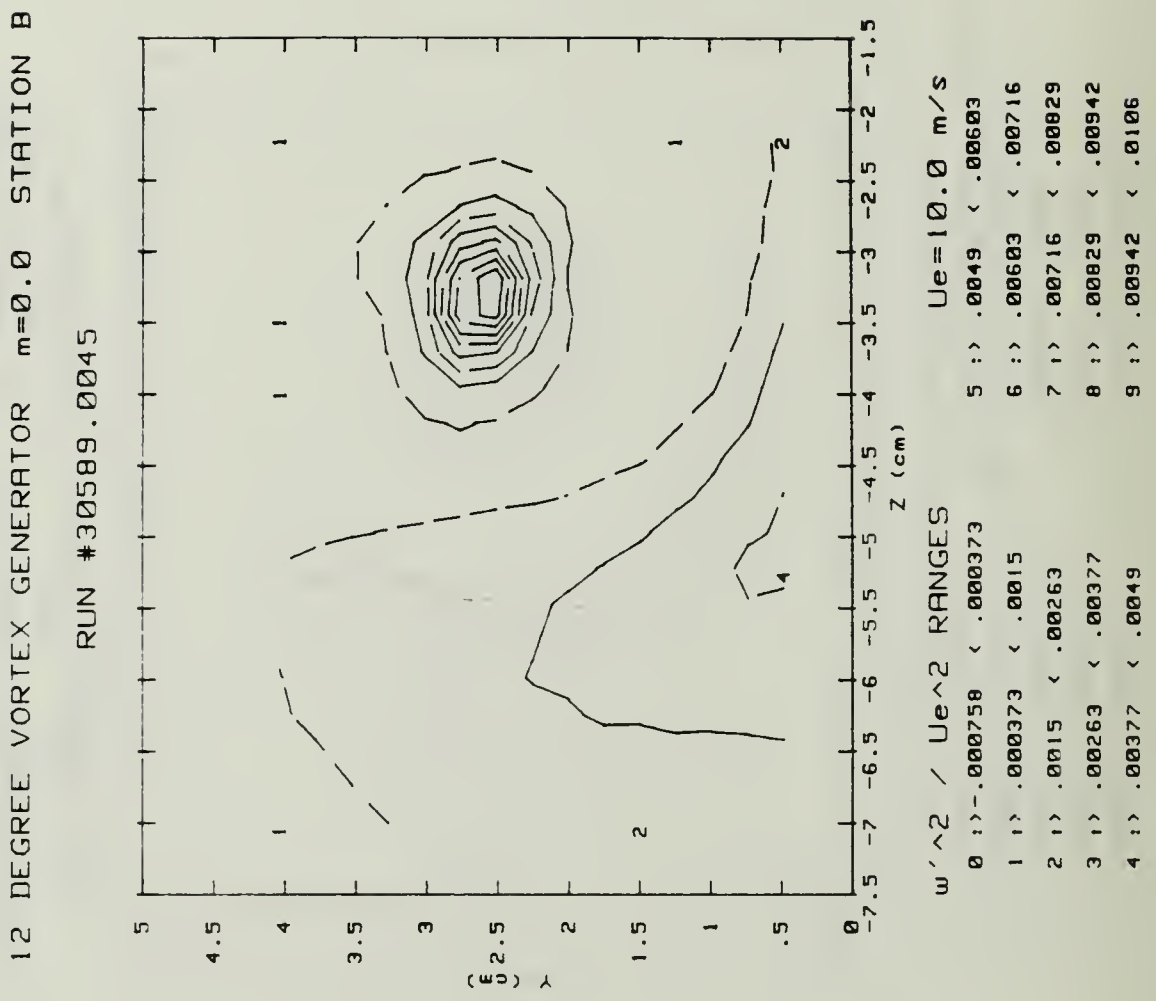

Figure 71. $\overline{w'^2}$ (boundary layer / vortex, station B, $\Delta = 0.10$ inches)

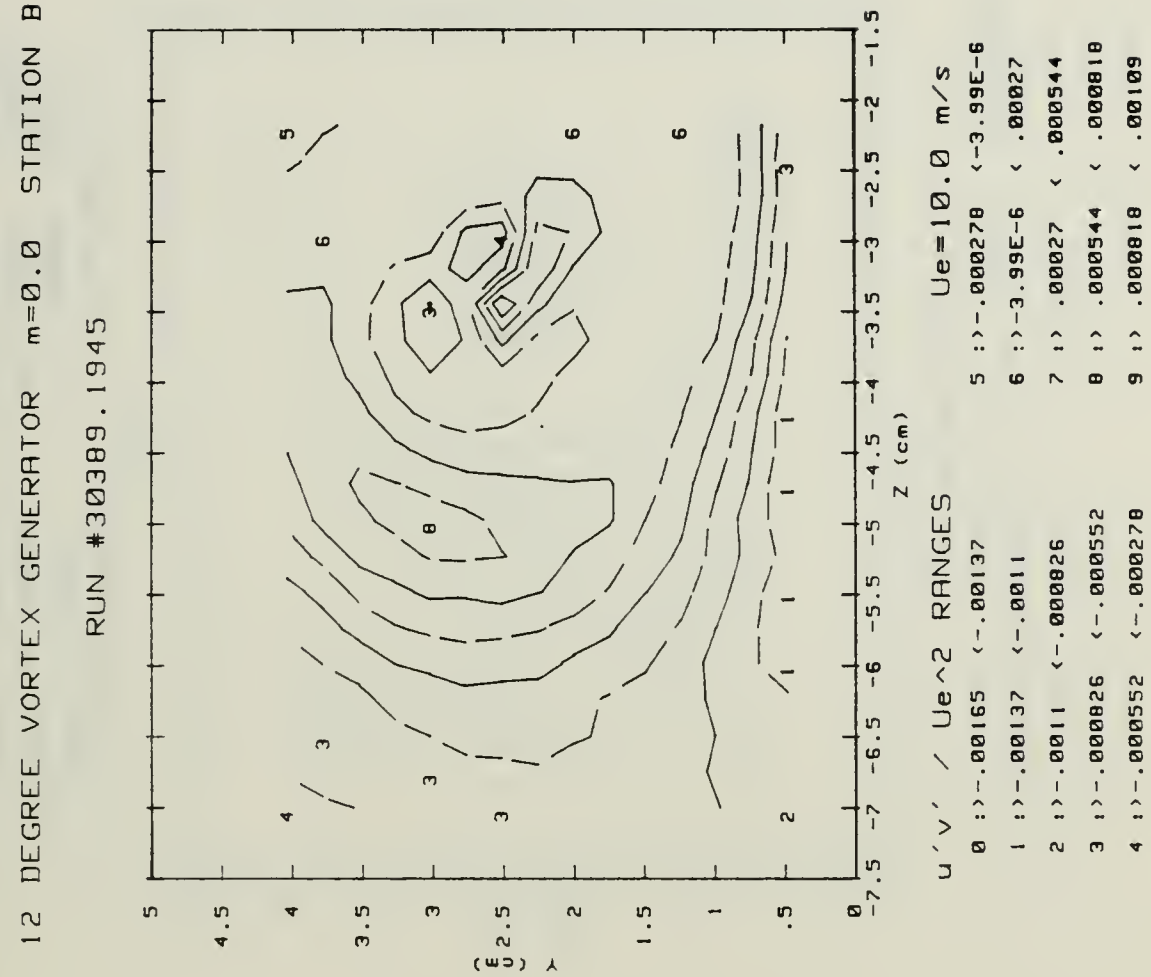

Figure 72. $\overline{u'v'}$ (boundary layer / vortex, station B, $\Delta = 0.10$ inches)

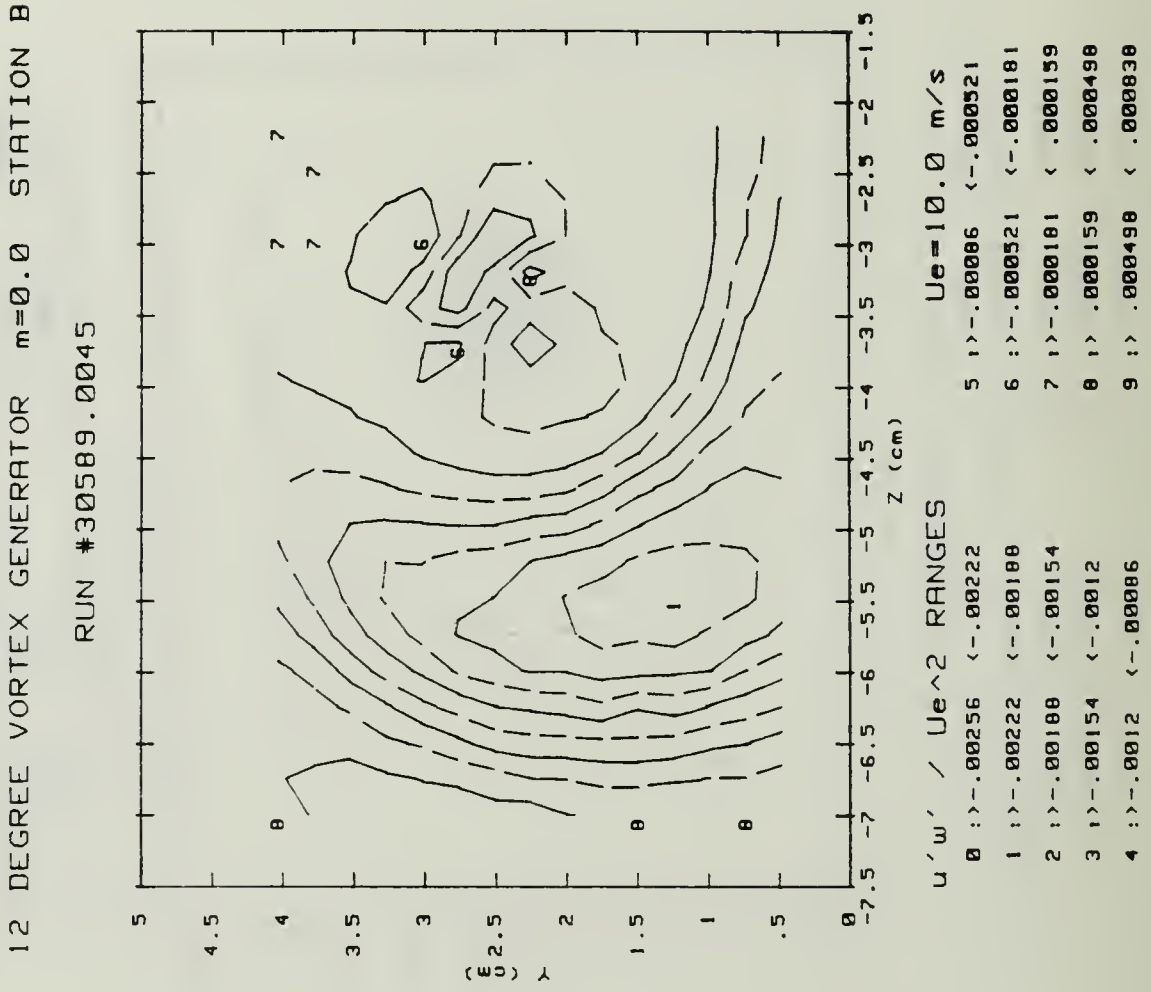

Figure 73. $\overline{u'w'}$ (boundary layer / vortex, station B, $\Delta = 0.10$ inches)

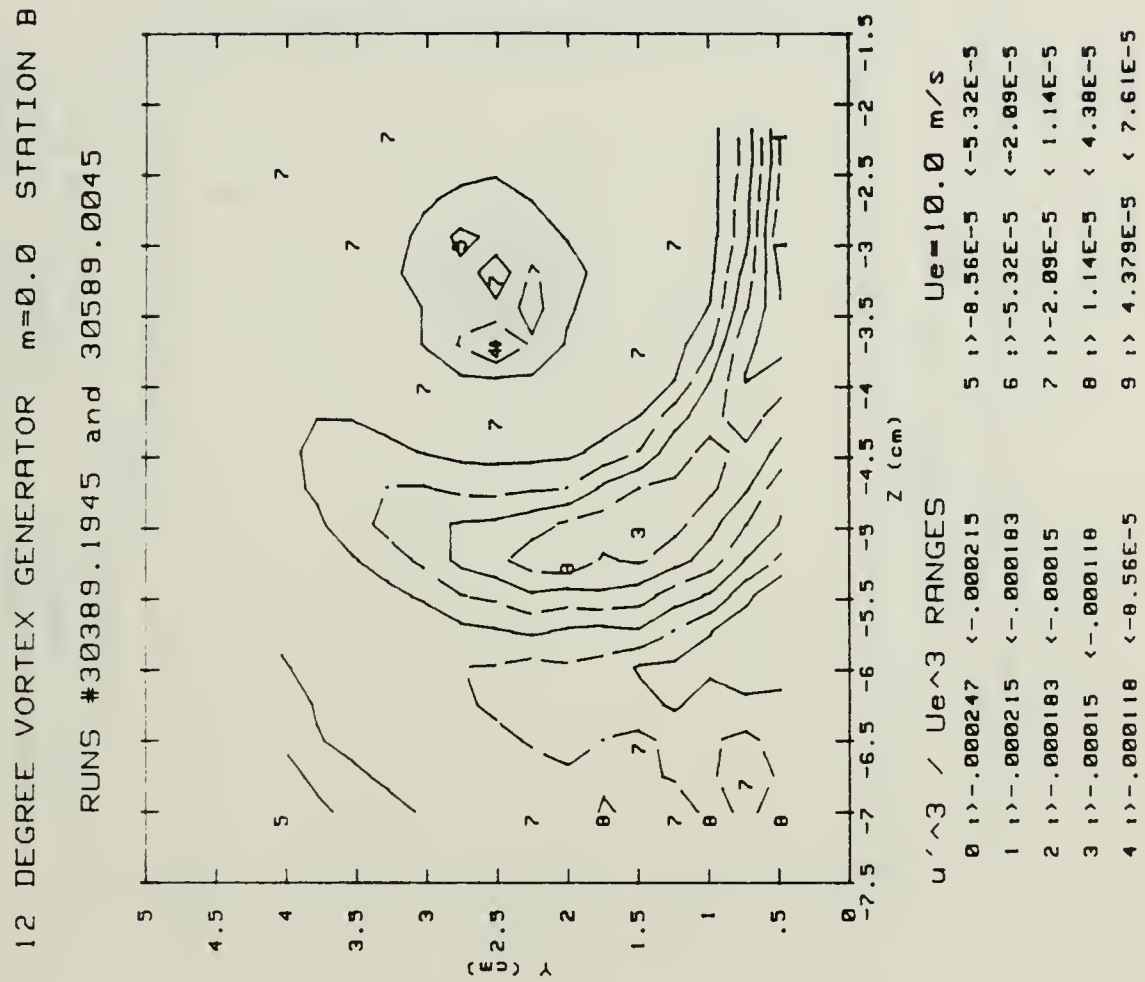

Figure 74. $\overline{u'^3}$ (boundary layer / vortex, station B, $\Delta = 0.10$ inches)

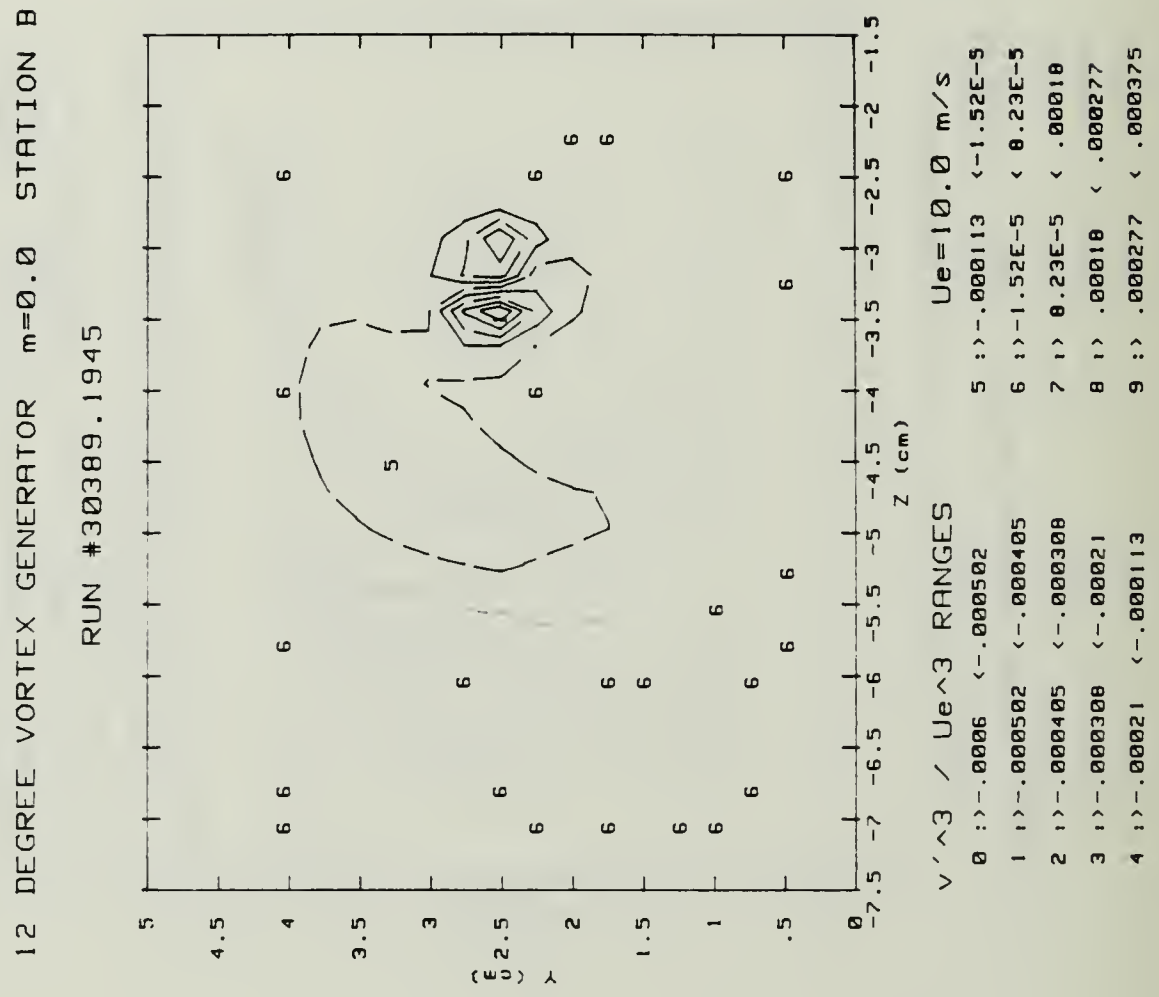

Figure 75. $\overline{v'^3}$ (boundary layer / vortex, station B, $\Delta = 0.10$ inches)

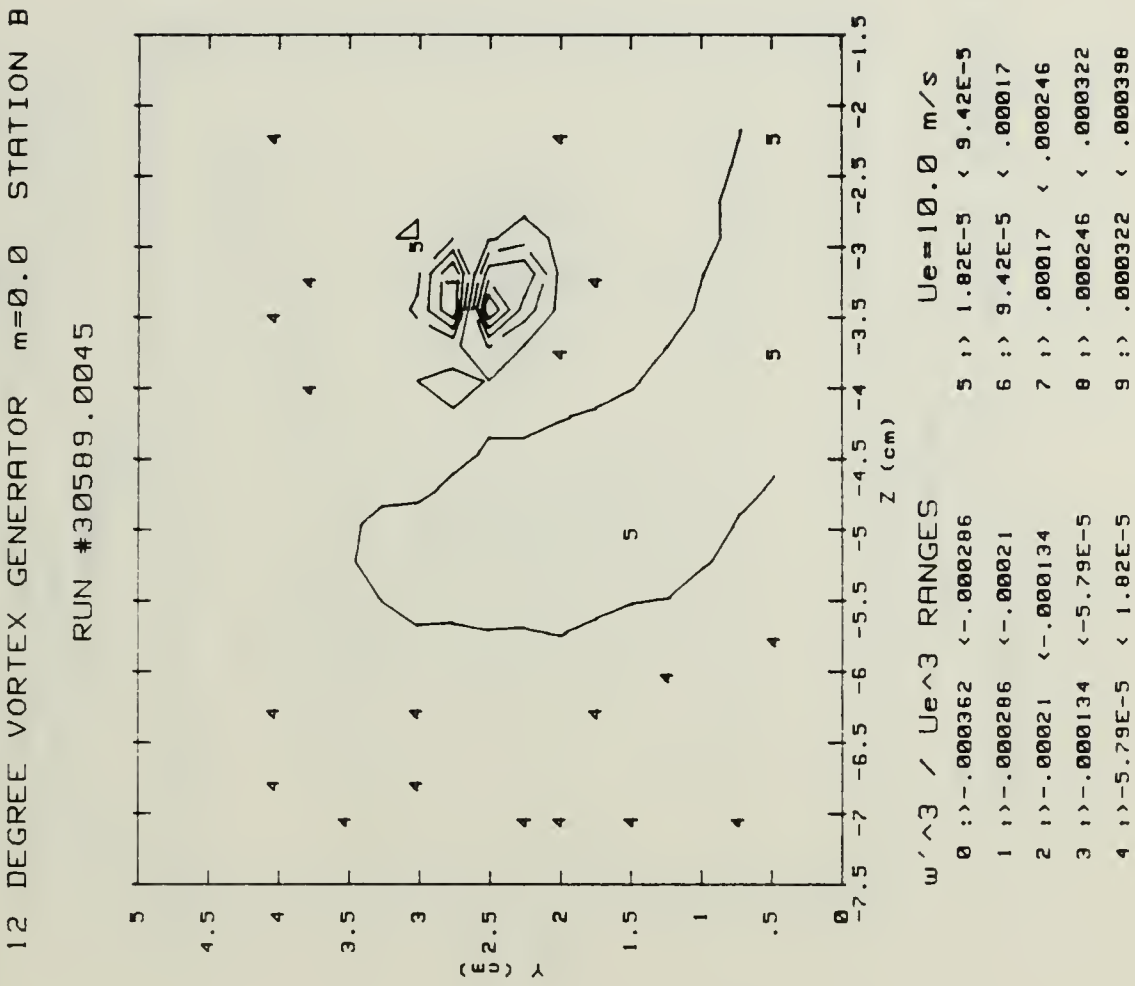

Figure 76. $\overline{w'^3}$ (boundary layer / vortex, station B, $\Delta = 0.10$ inches)

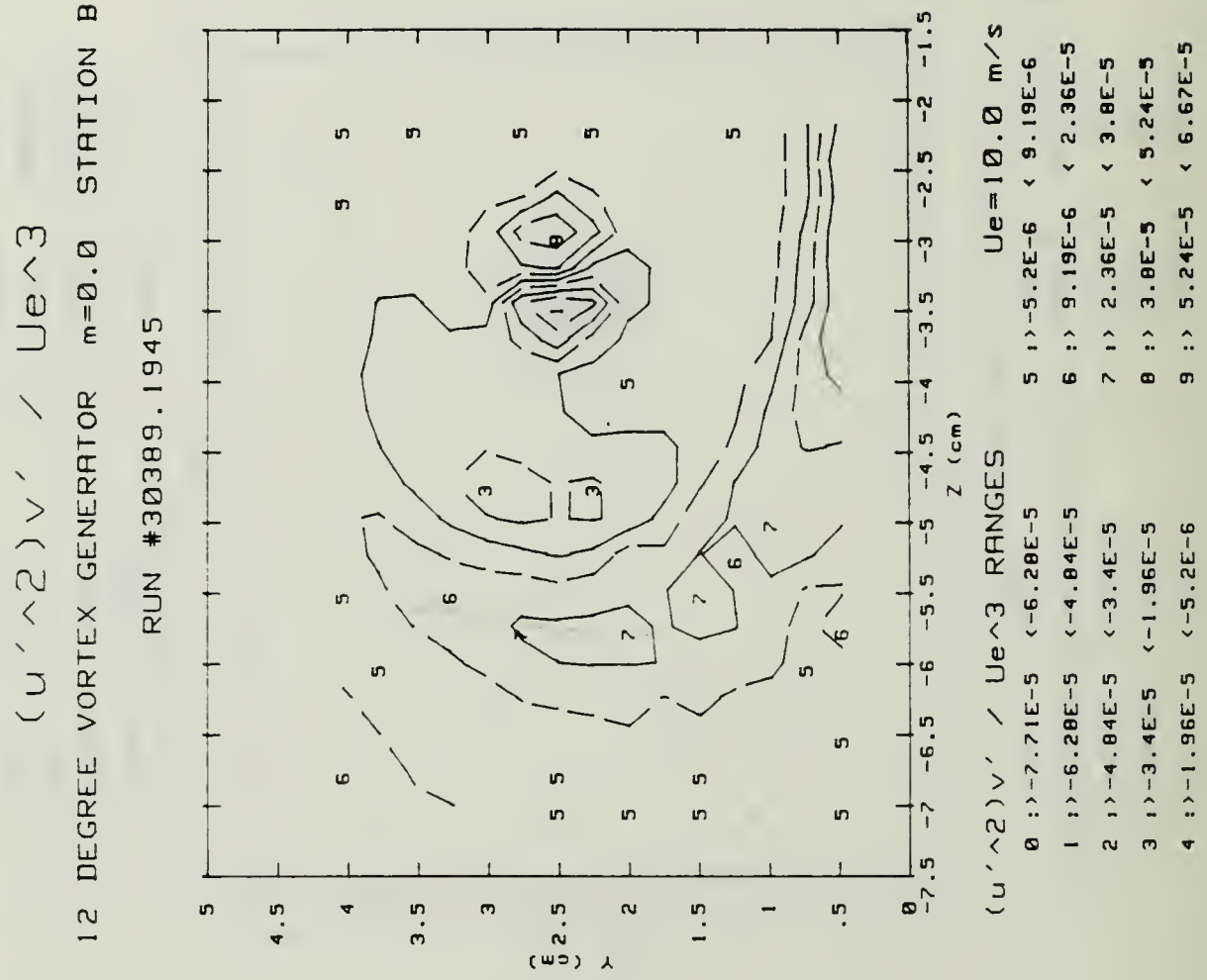

Figure 77. $\overline{u'^2v'}$ (boundary layer / vortex, station B, $\Delta = 0.10$ inches)

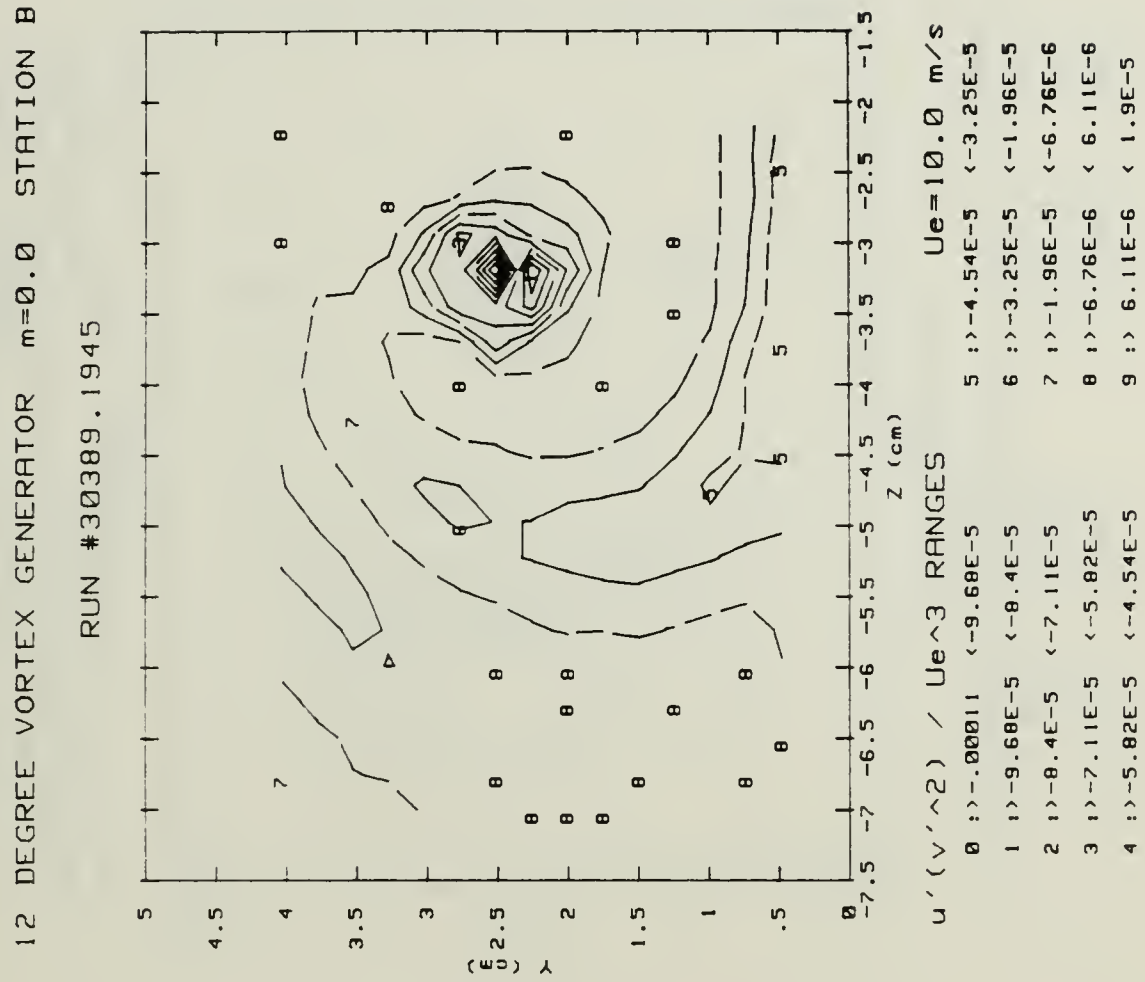

Figure 78. $\overline{u'v'^2}$ (boundary layer / vortex, station B, $\Delta = 0.10$ inches)

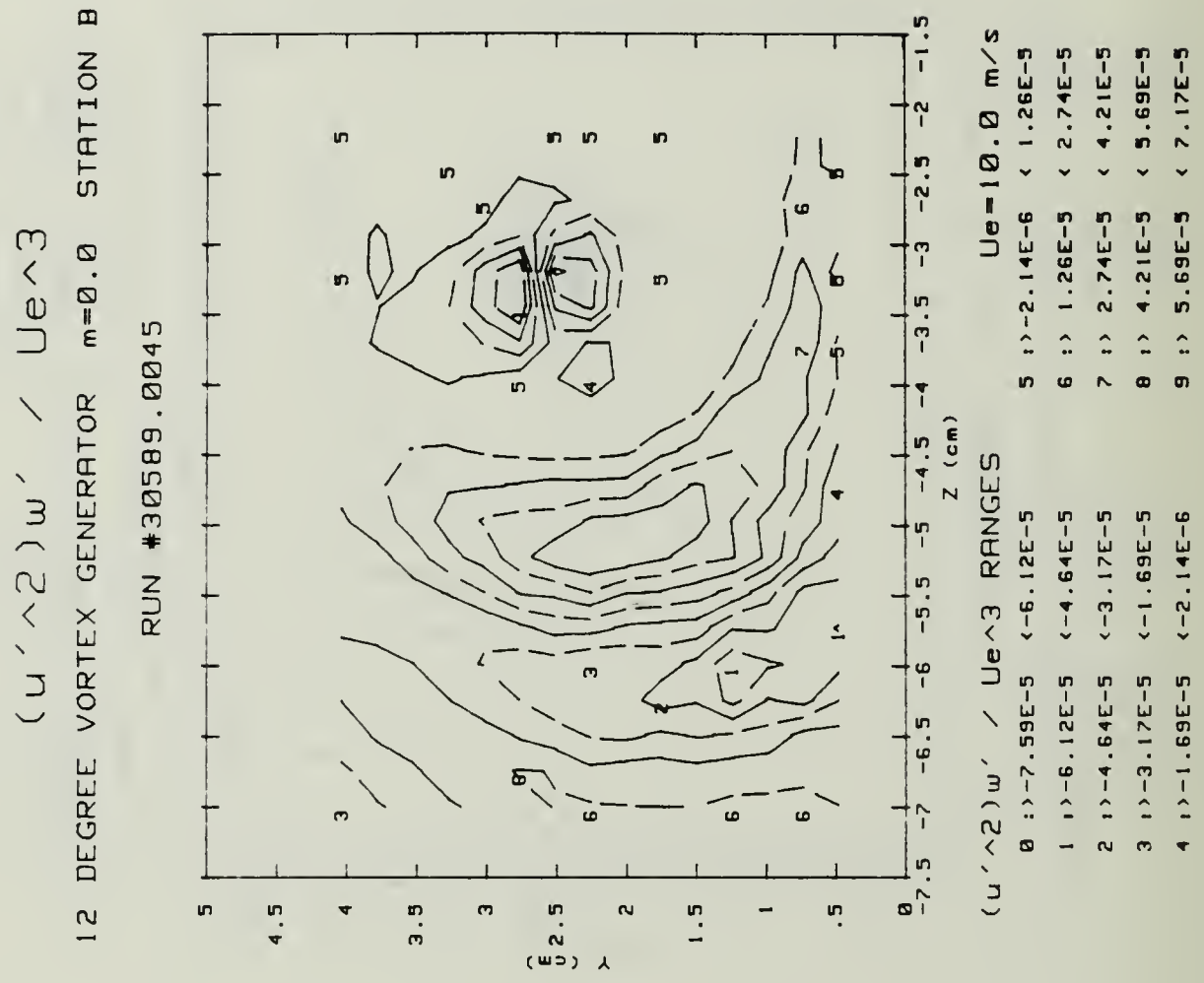

Figure 79. $\overline{u'^2w'}$ (boundary layer / vortex, station B, $\Delta = 0.10$ inches)

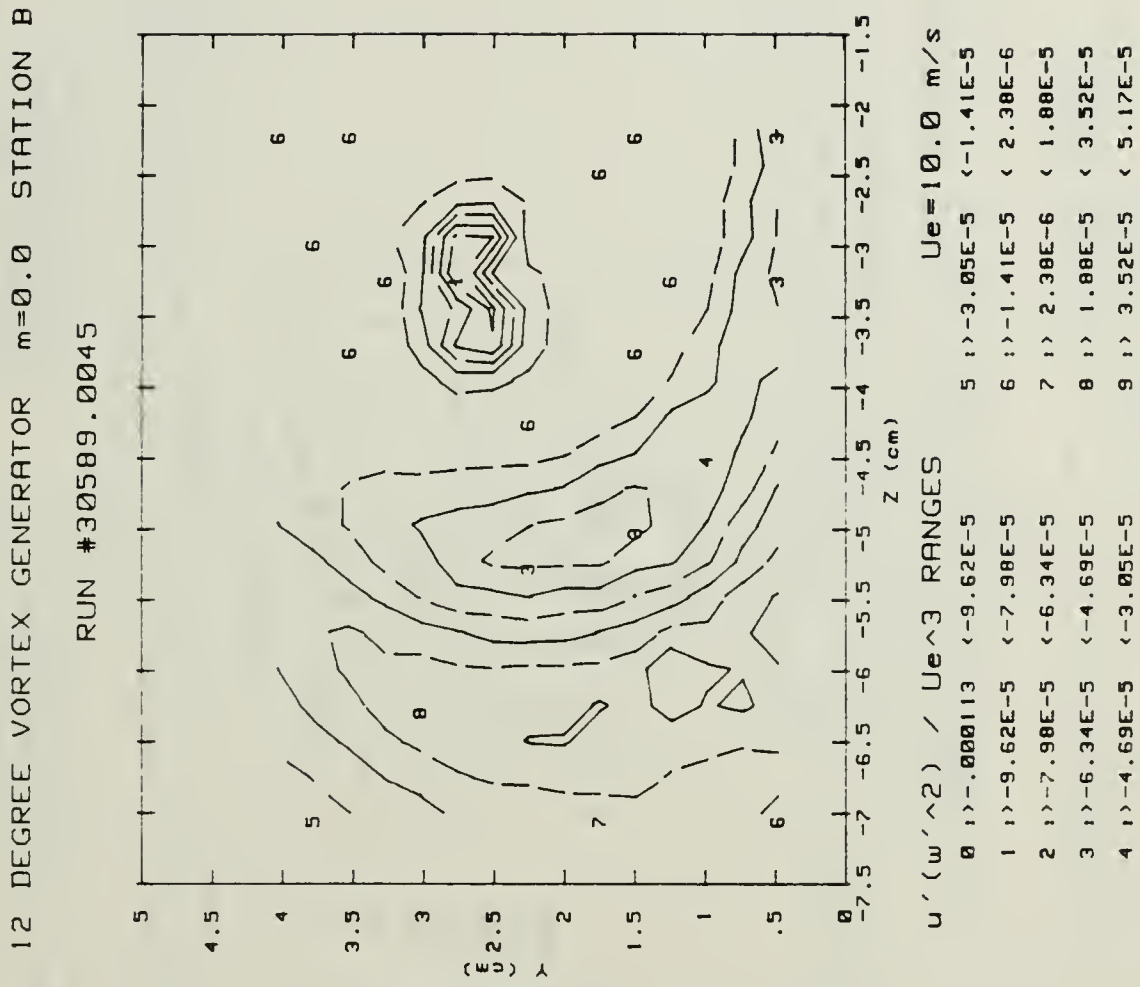

Figure 80. $\overline{u'w'^2}$ (boundary layer / vortex, station B, $\Delta = 0.10$ inches)

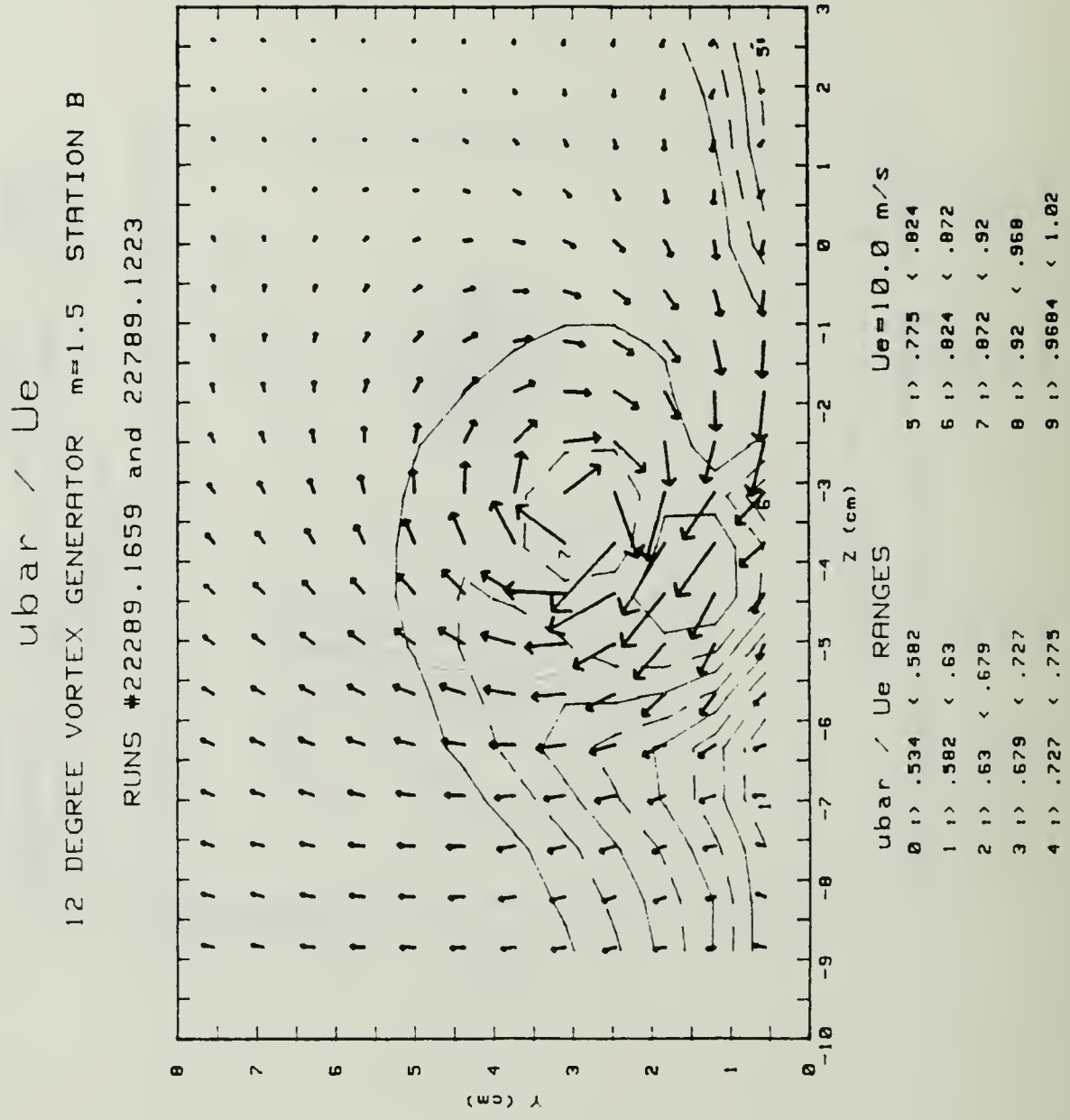

Figure 81. Mean Velocities (boundary layer / vortex / wall jet, station B, $\Delta = 0.25$ inches)

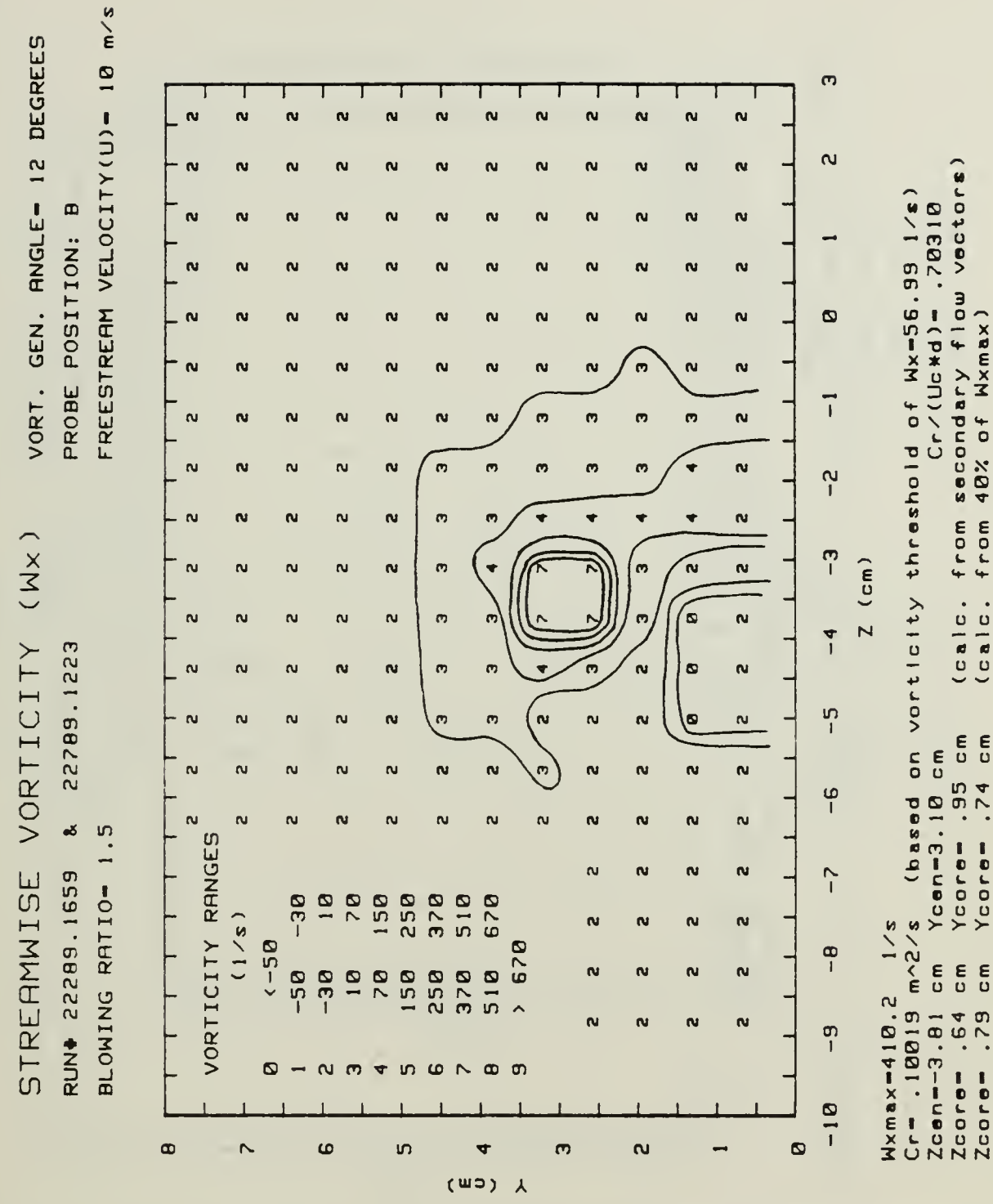

Figure 82. Streamwise Vorticity ω_x (boundary layer / vortex / wall jet, station B, $\Delta = 0.25$ inches)

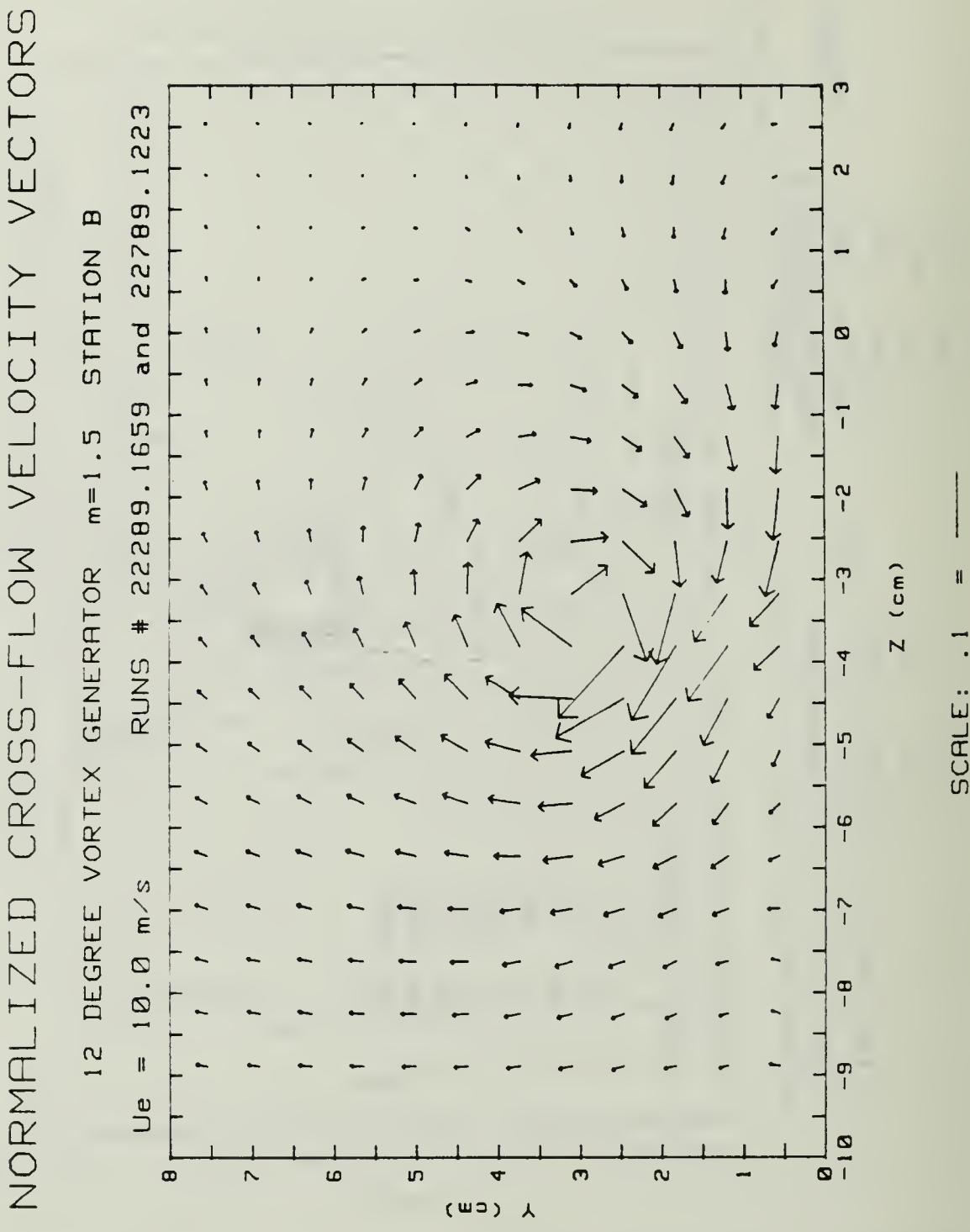

Figure 83. Secondary Flow Vectors (boundary layer / vortex / wall jet, station B, $\Delta = 0.25$ inches)

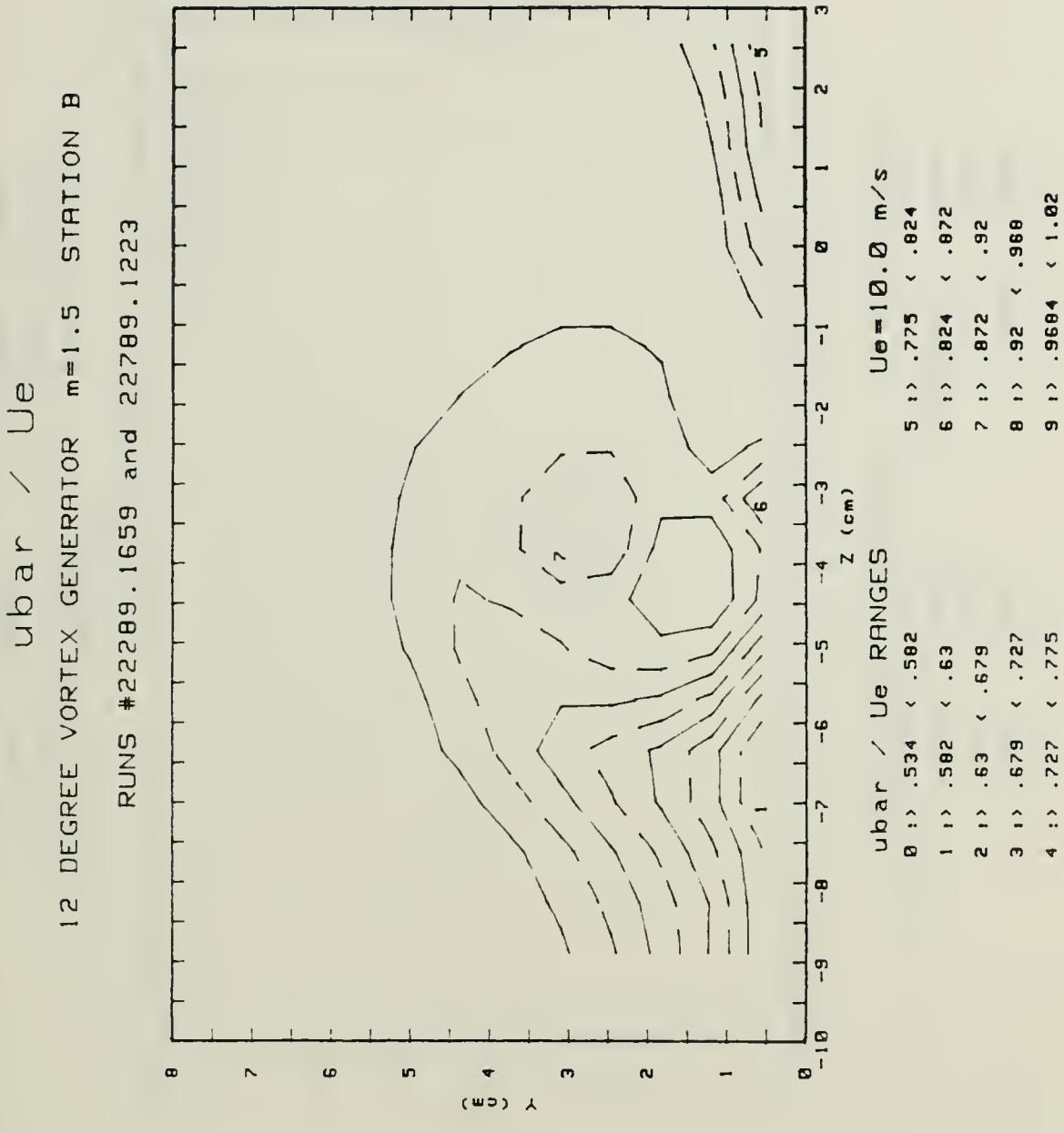

Figure 84. $\bar{u}$ (boundary layer / vortex / wall jet, station B, $\Delta = 0.25$ inches)

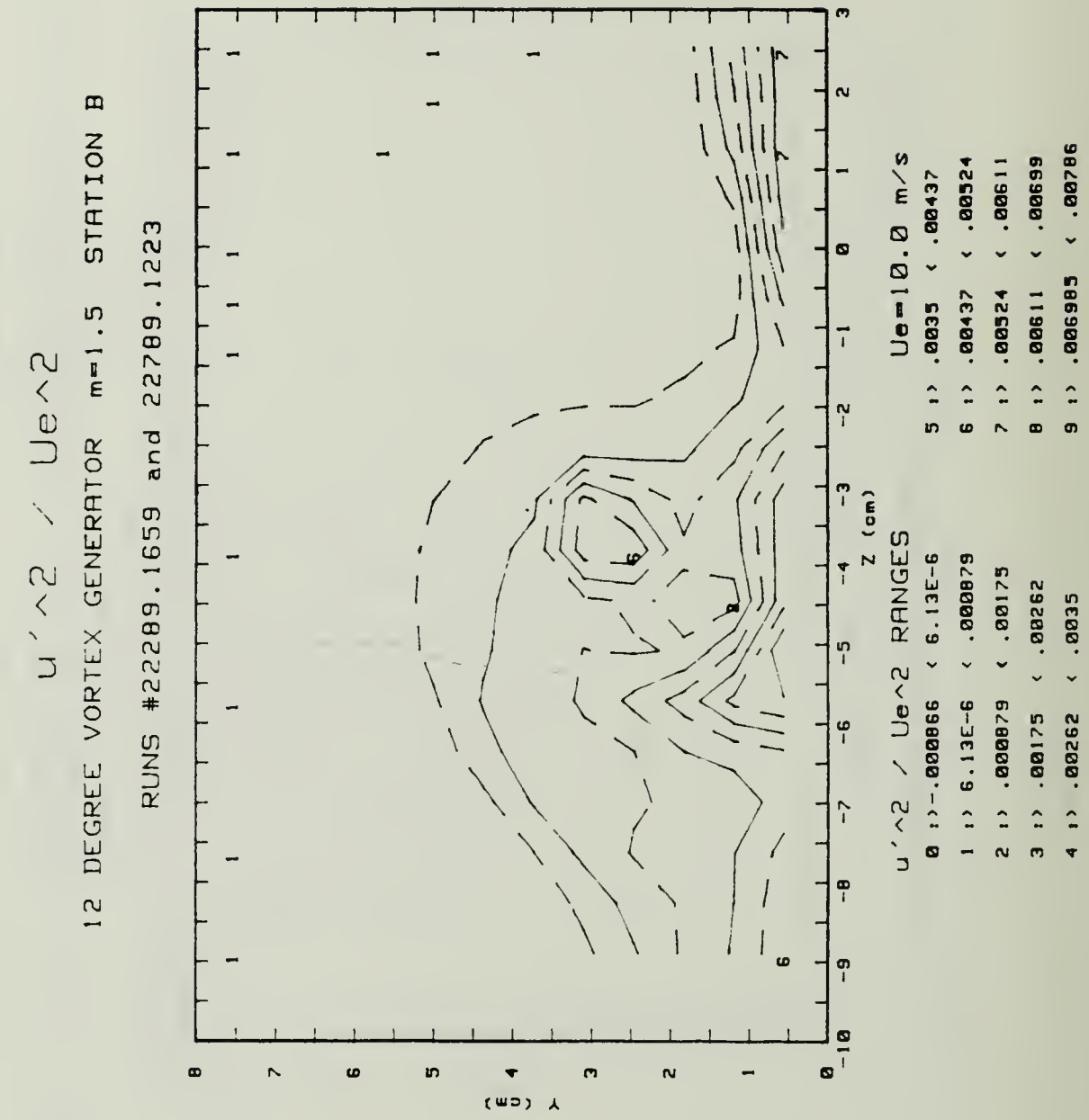

Figure 85. $\overline{u'^2}$ (boundary layer / vortex / wall jet, station B, $\Delta = 0.25$ inches)

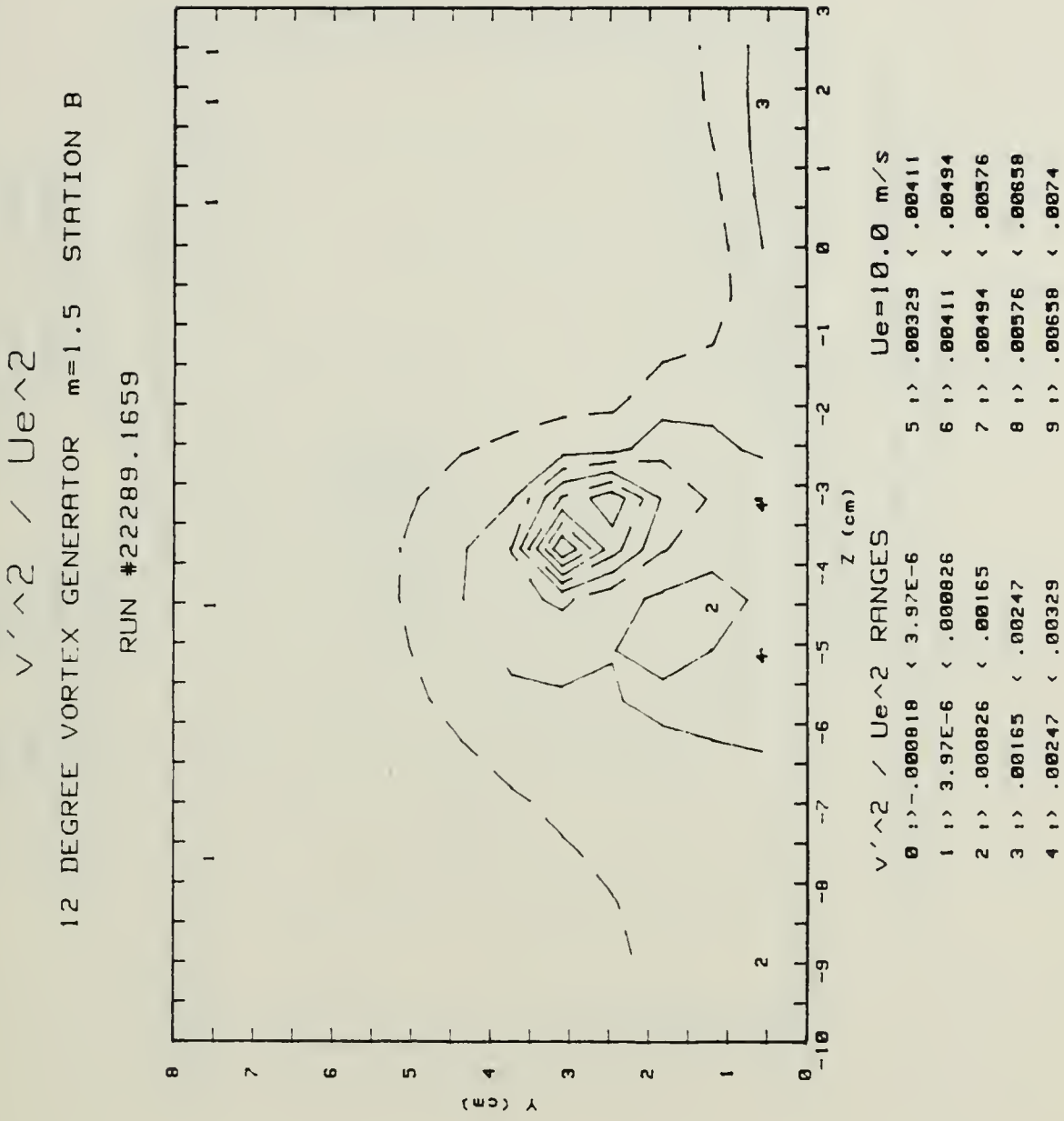

Figure 86. $\overline{v'^2}$ (boundary layer / vortex / wall jet, station B, $\Delta = 0.25$ inches)

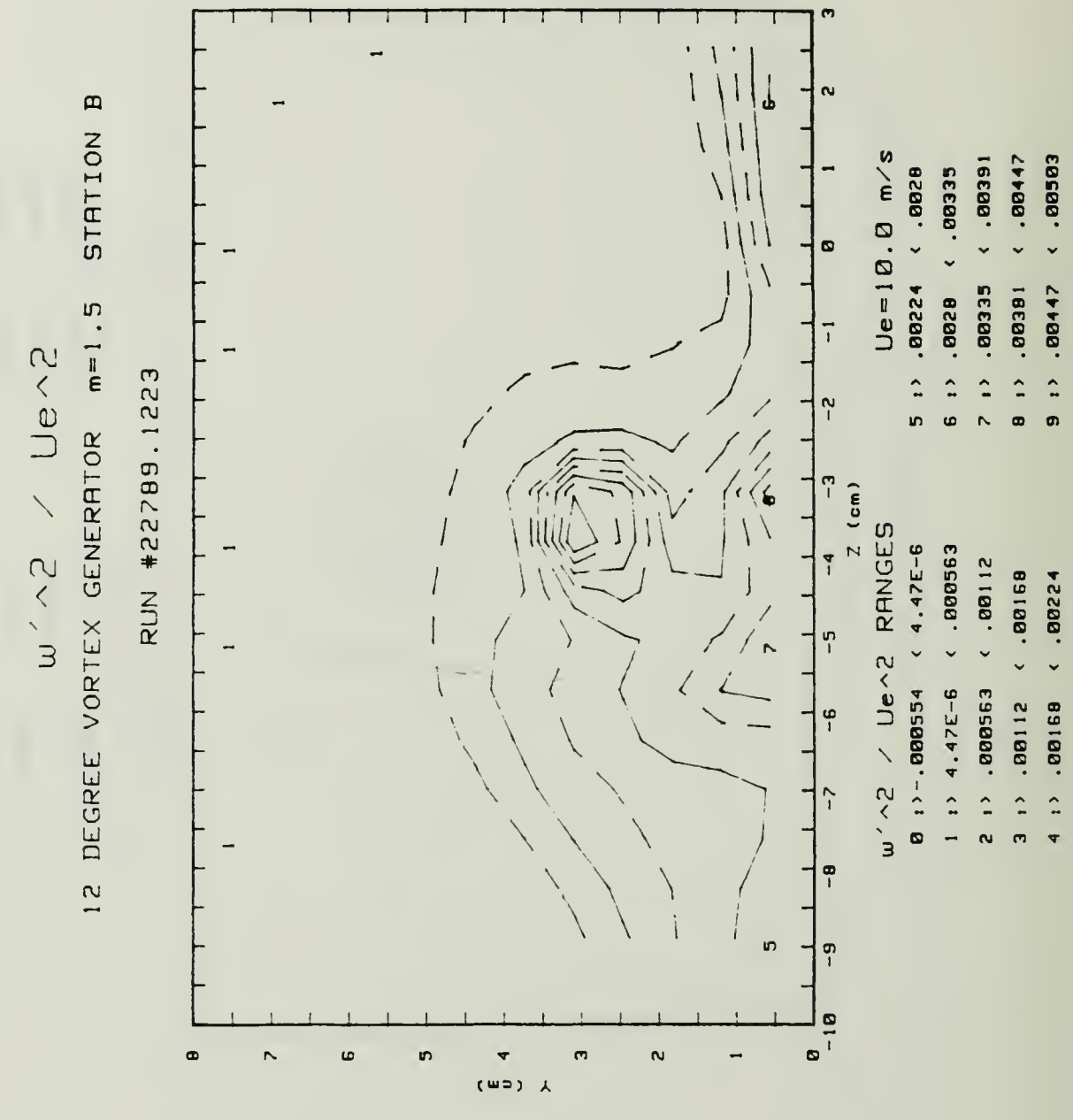

Figure 87. $\overline{w'^2}$ (boundary layer / vortex / wall jet, station B, $\Delta = 0.25$ inches)

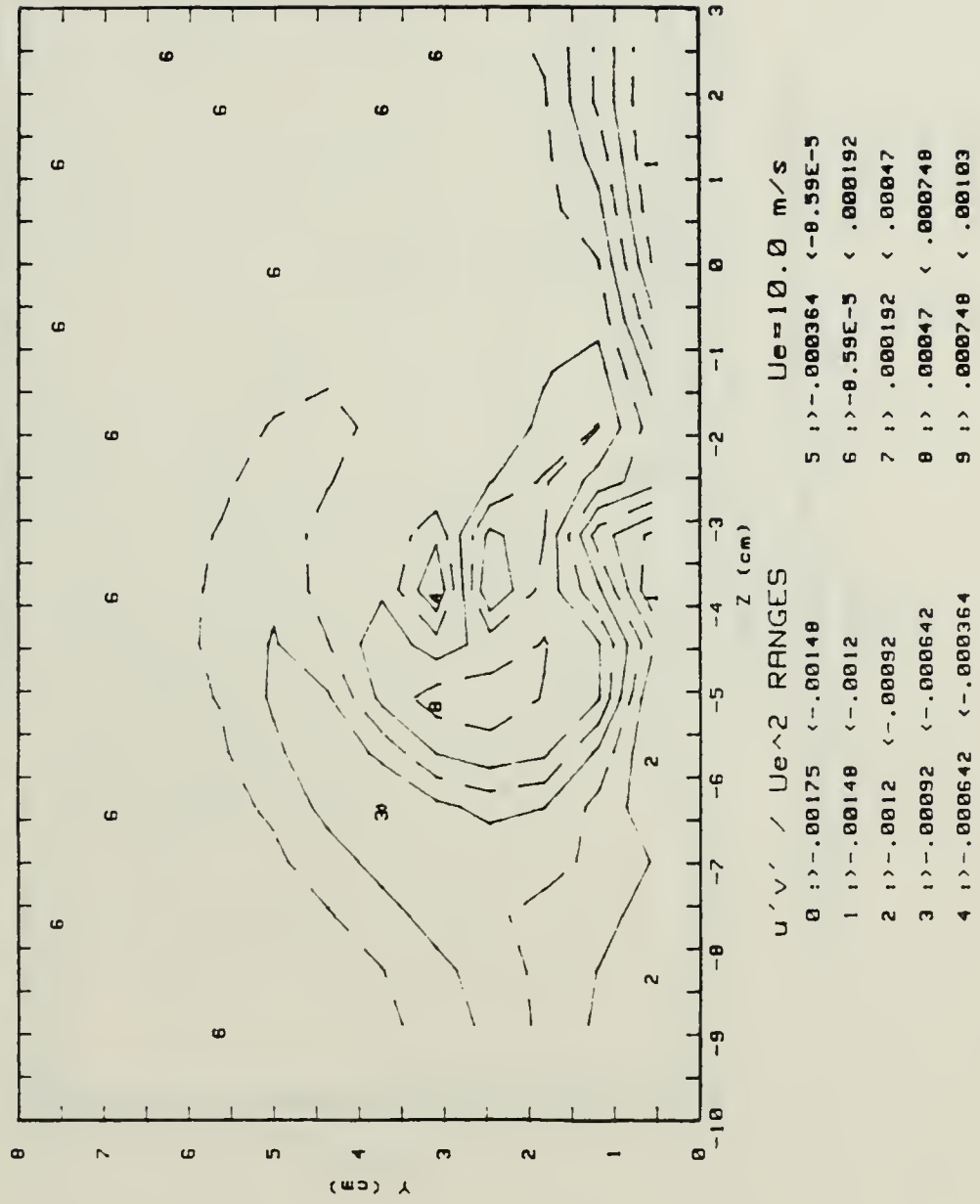

Figure 88. $\overline{u'v'}$ (boundary layer / vortex / wall jet, station B, $\Delta = 0.25$ inches)

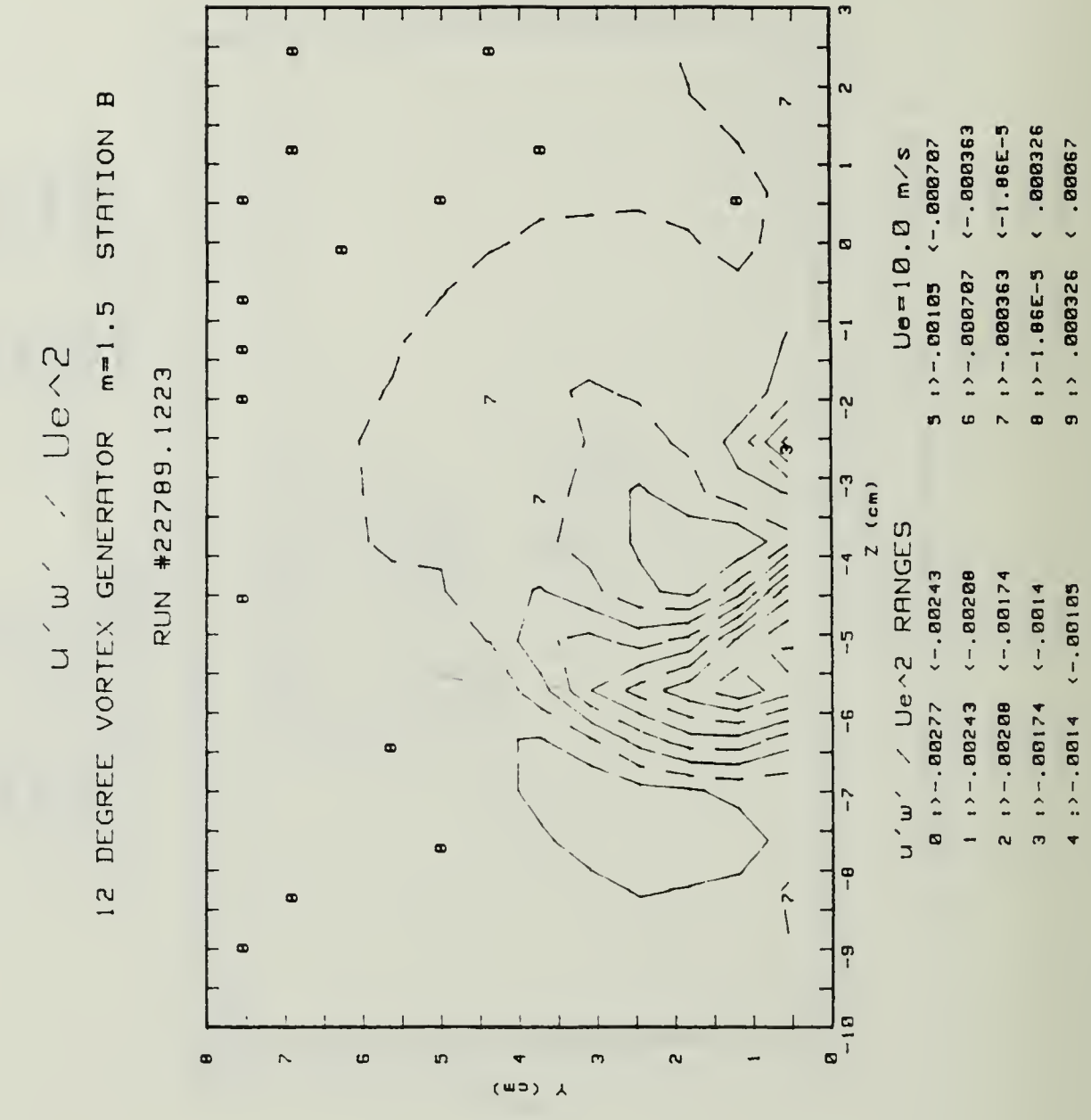

Figure 89. $\overline{u'w'}$ (boundary layer / vortex / wall jet, station B, $\Delta = 0.25$ inches)

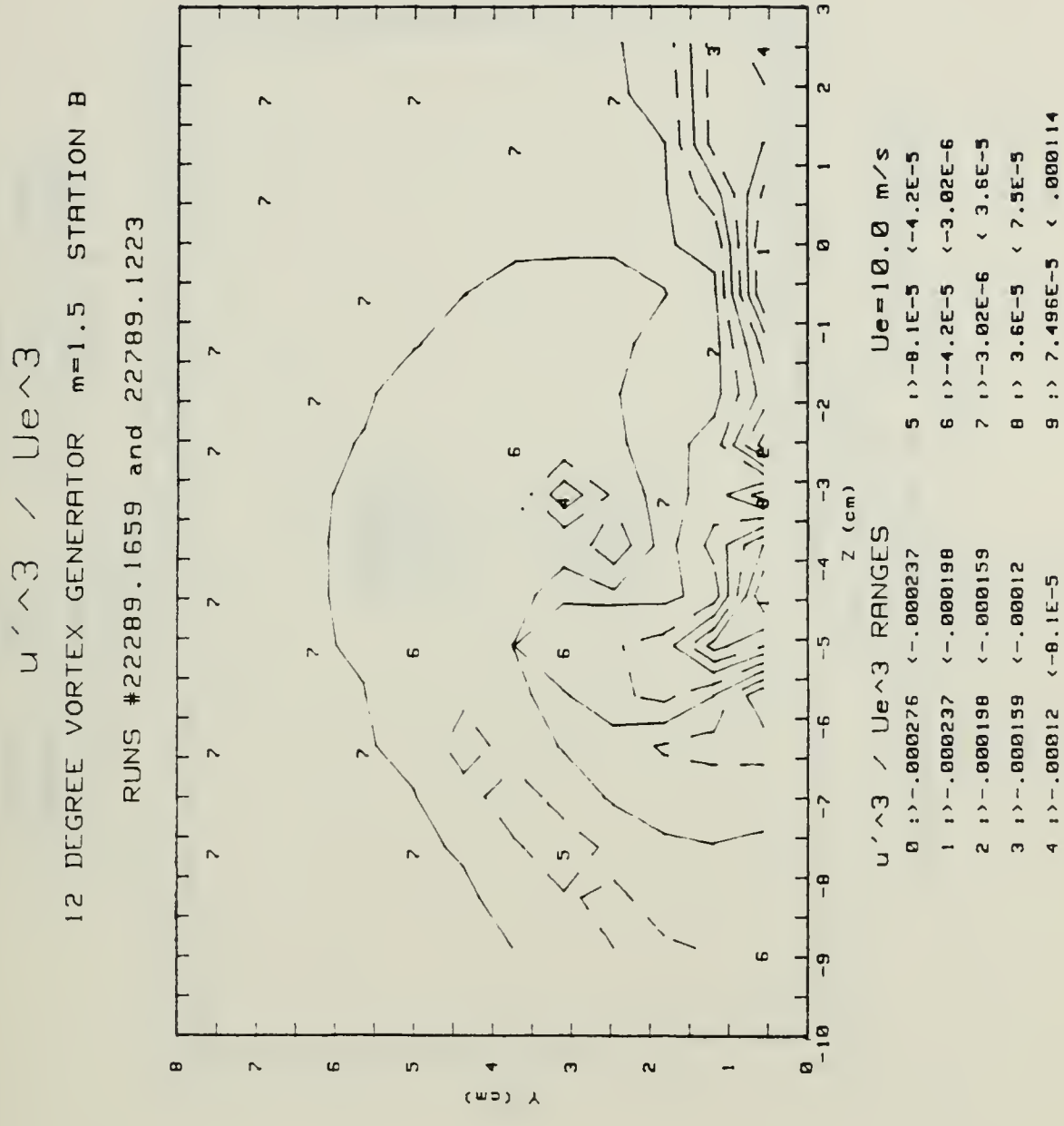

Figure 90. $\overline{u'^3}$ (boundary layer / vortex / wall jet, station B, $\Delta = 0.25$ inches)

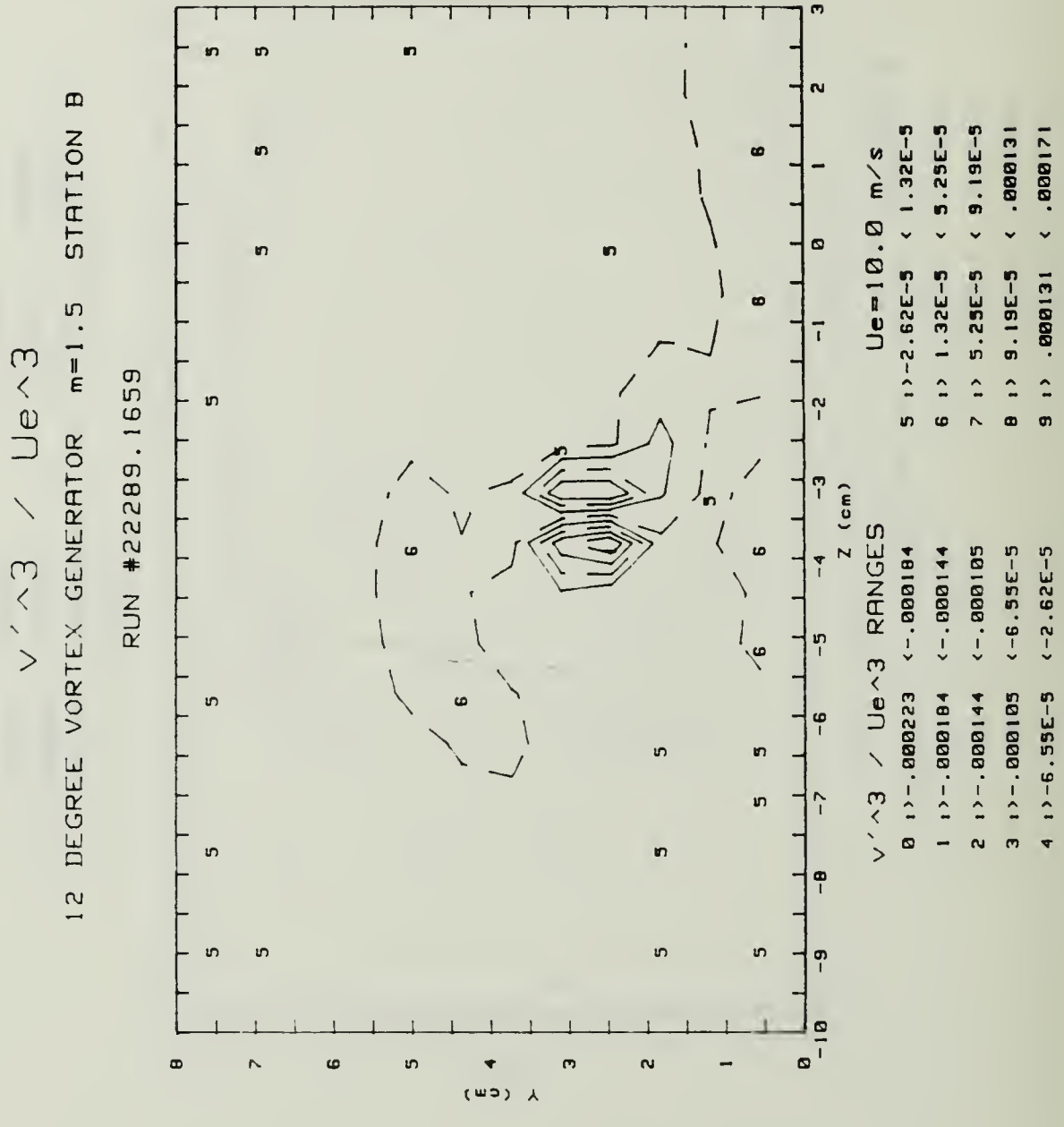

Figure 91. $\overline{v'^3}$ (boundary layer / vortex / wall jet, station B, $\Delta = 0.25$ inches)

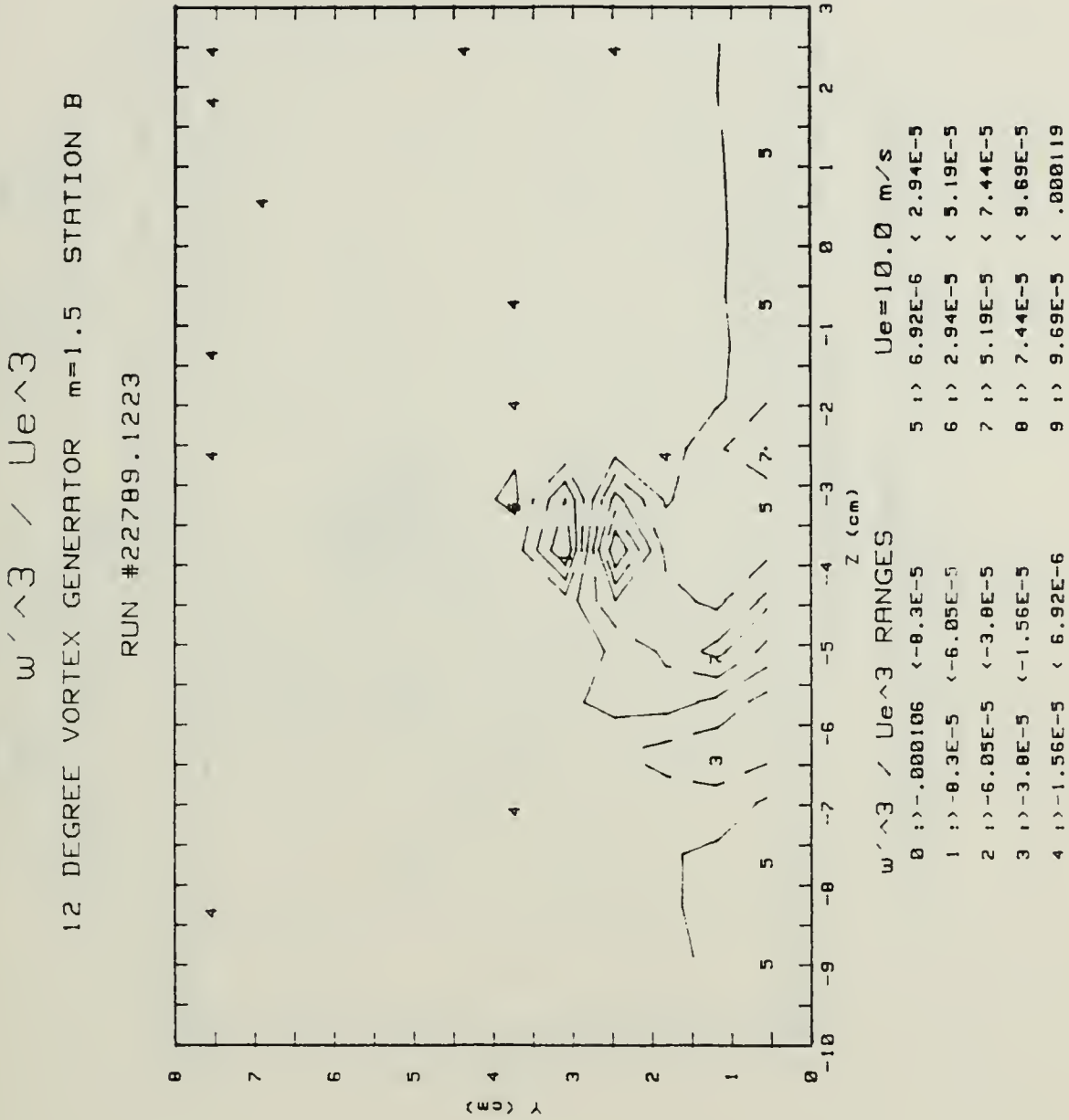

Figure 92. $\overline{w'^3}$ (boundary layer / vortex / wall jet, station B, $\Delta = 0.25$ inches)

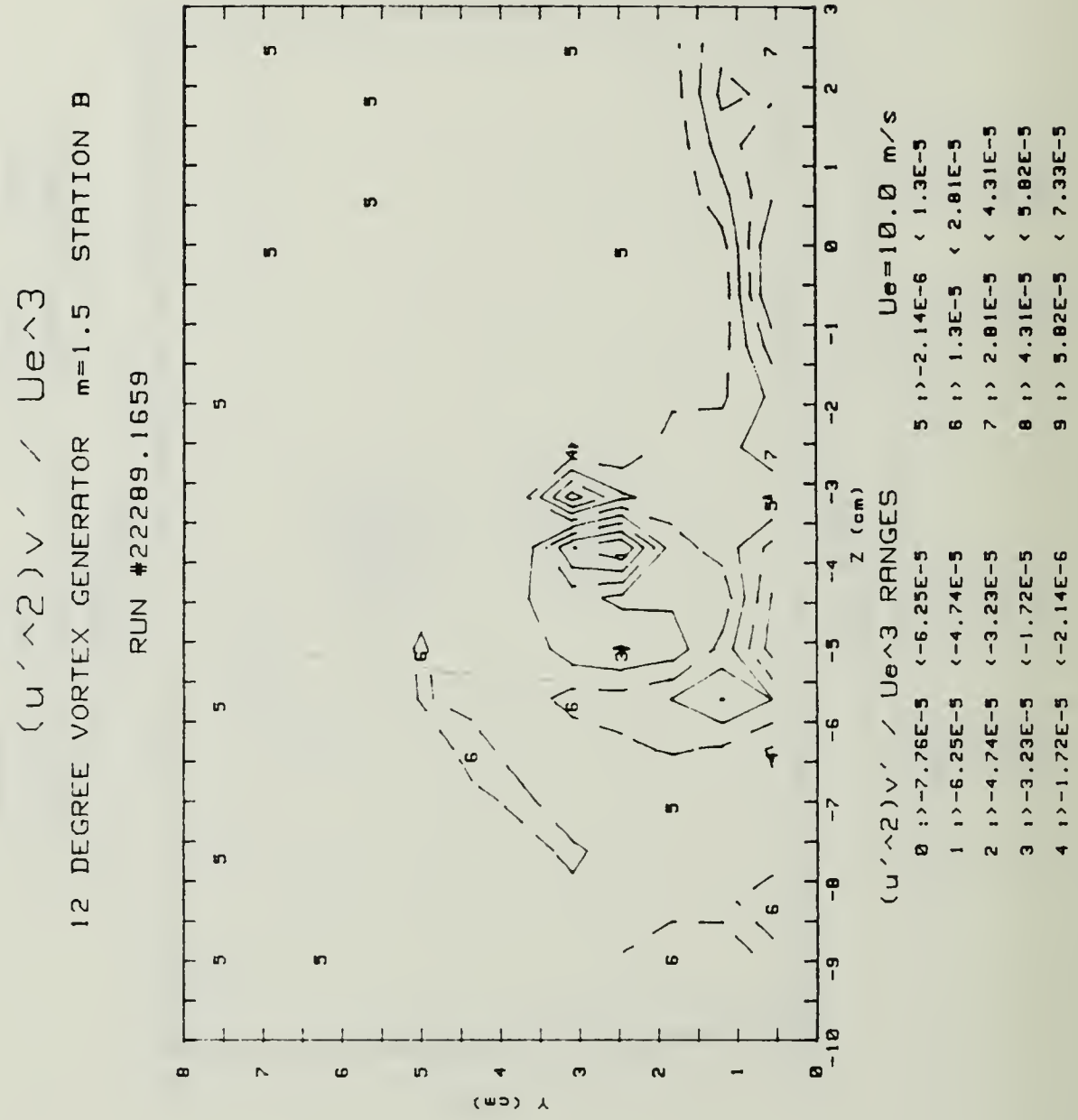

Figure 93. $\overline{u'^2v'}$ (boundary layer / vortex / wall jet, station B, $\Delta = 0.25$ inches)

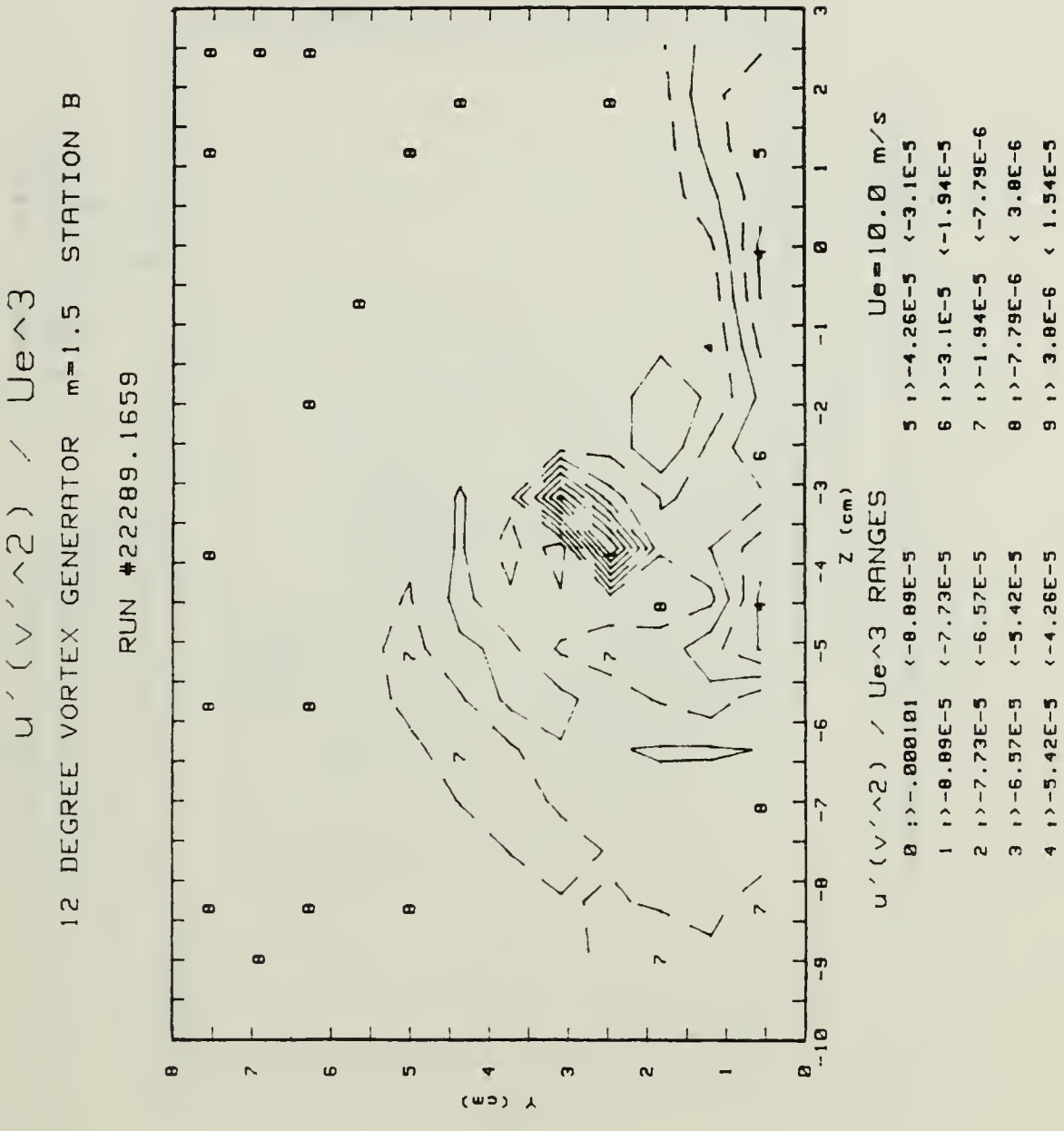

Figure 94. $\overline{u'v'^2}$ (boundary layer / vortex / wall jet, station B, $\Delta = 0.25$ inches)

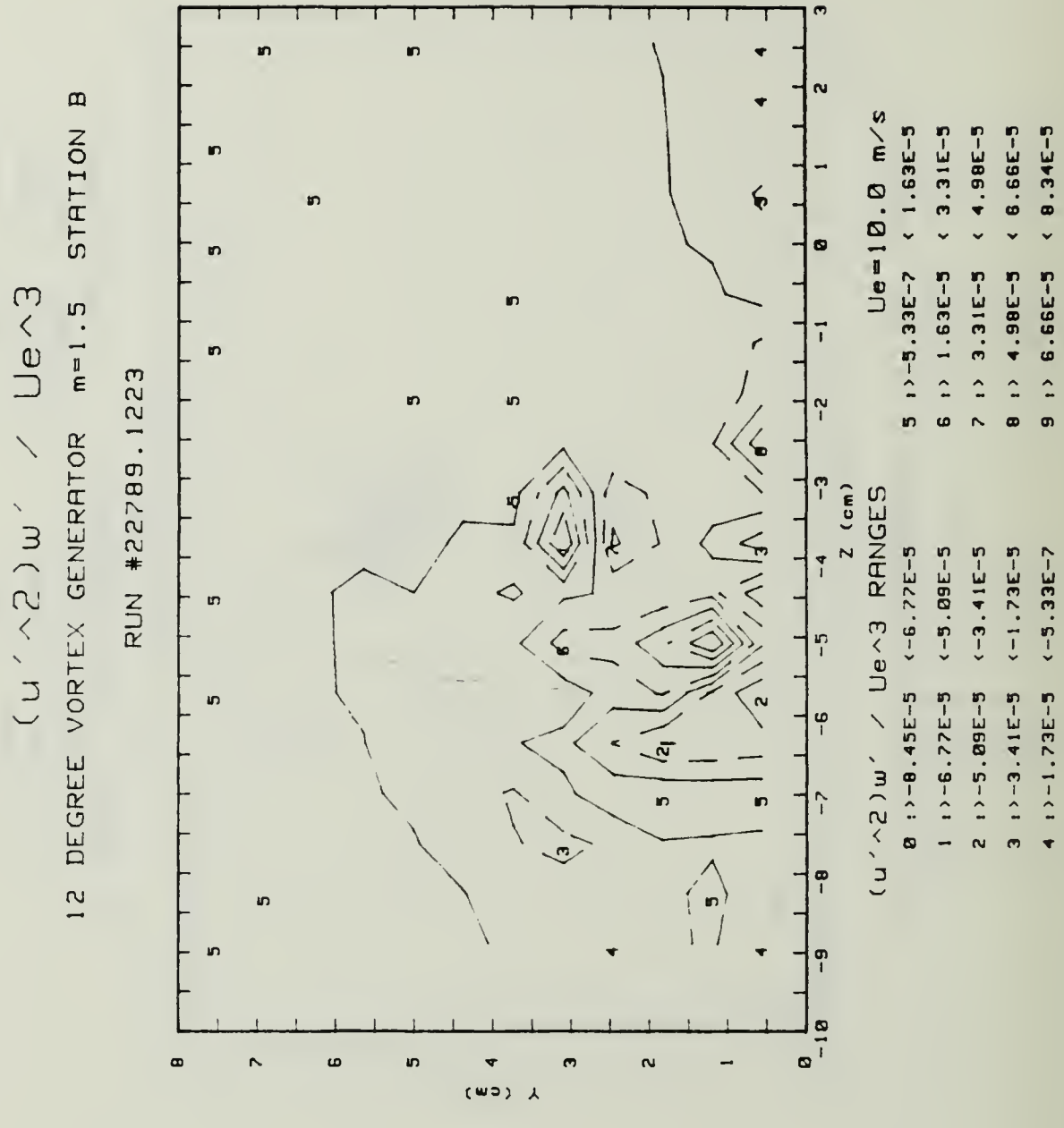

Figure 95. $\overline{u'^2w'}$ (boundary layer / vortex / wall jet, station B, $\Delta = 0.25$ inches)

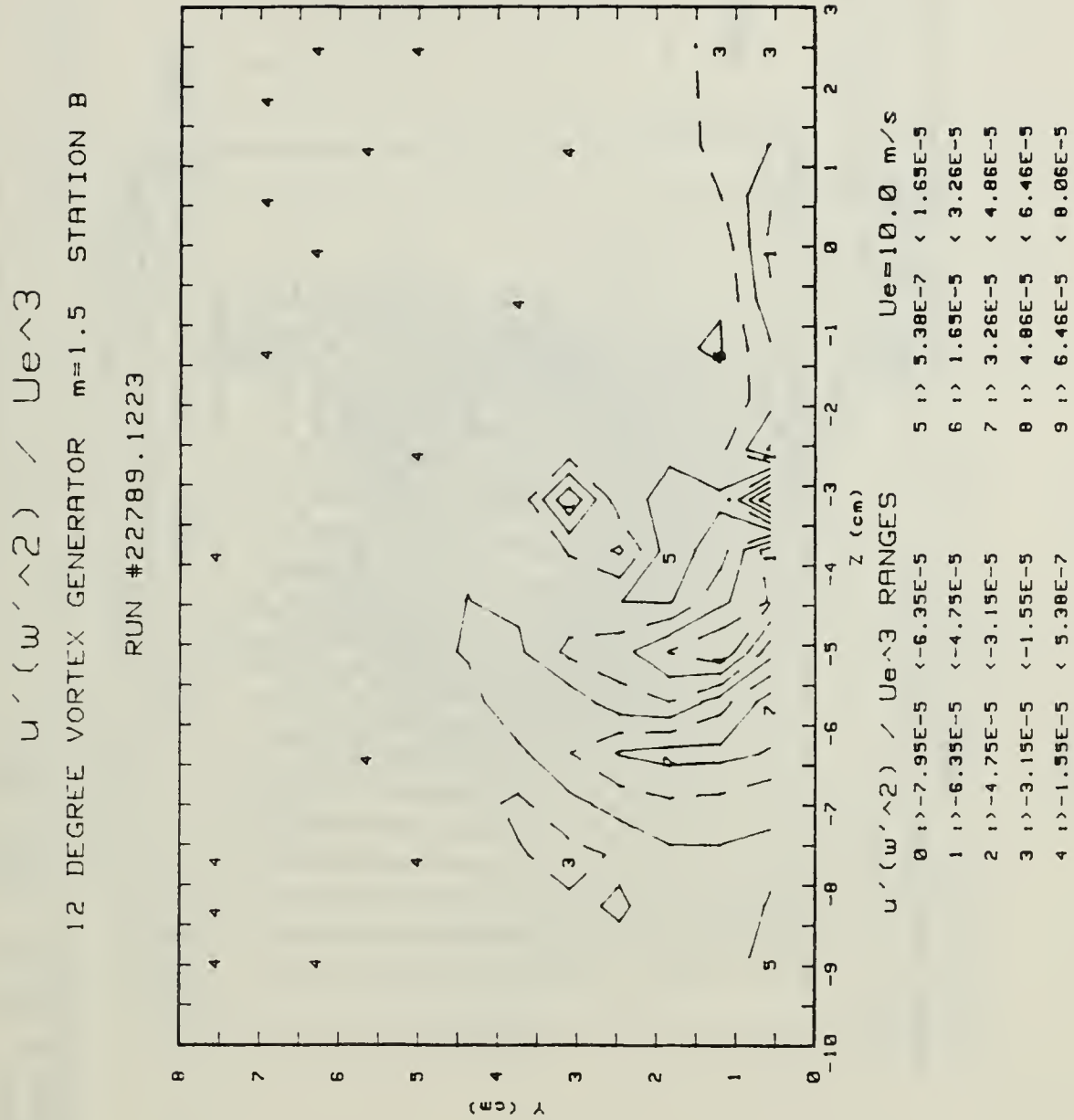

Figure 96. $\overline{u'w'^2}$ (boundary layer / vortex / wall jet, station B, $\Delta = 0.25$ inches)

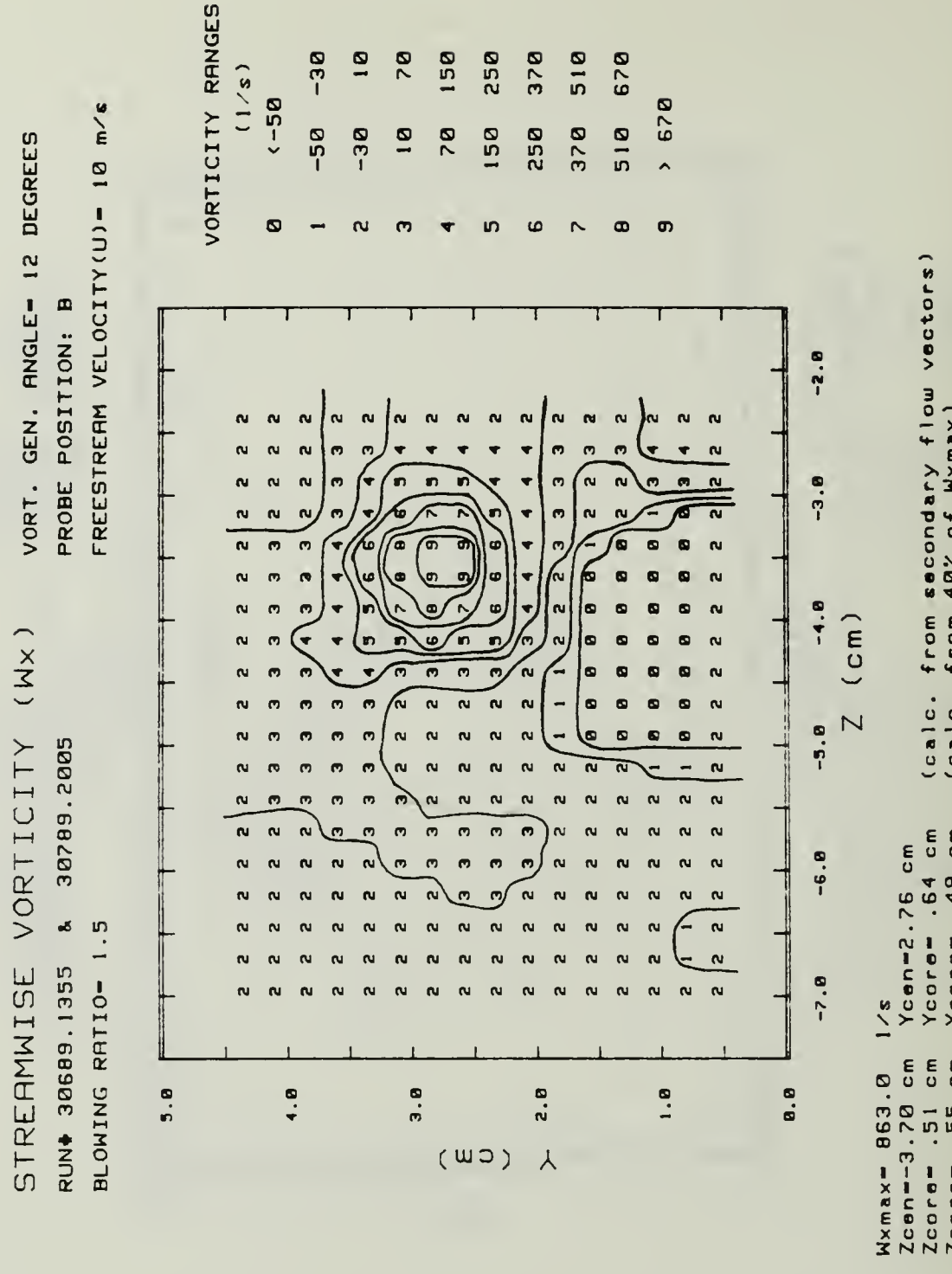

Figure 97. Streamwise Vorticity ω_x (boundary layer / vortex / wall jet, station B, $\Delta = 0.10$ inches)

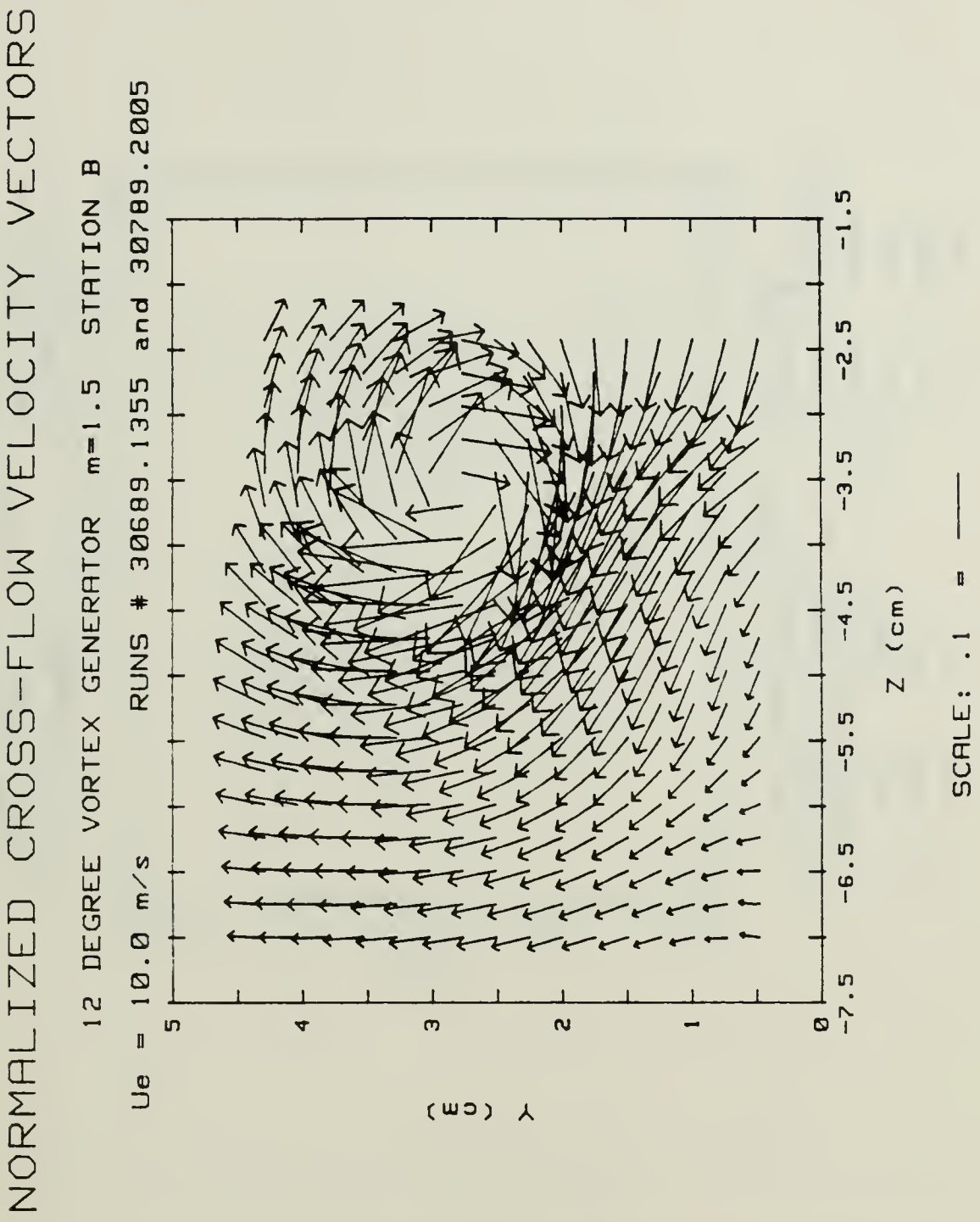
NORMALIZED CROSS-FLOW VELOCITY VECTORS
12 DEGREE VORTEX GENERATOR m=1.5 STATION B
Ue = 10.0 m/s RUNS # 30689.1355 and 30789.2005
Y (cm)
Z (cm)
SCALE: .1 =

Figure 98. Secondary Flow Vectors (boundary layer / vortex / wall jet, station B, $\Delta = 0.10$ inches)

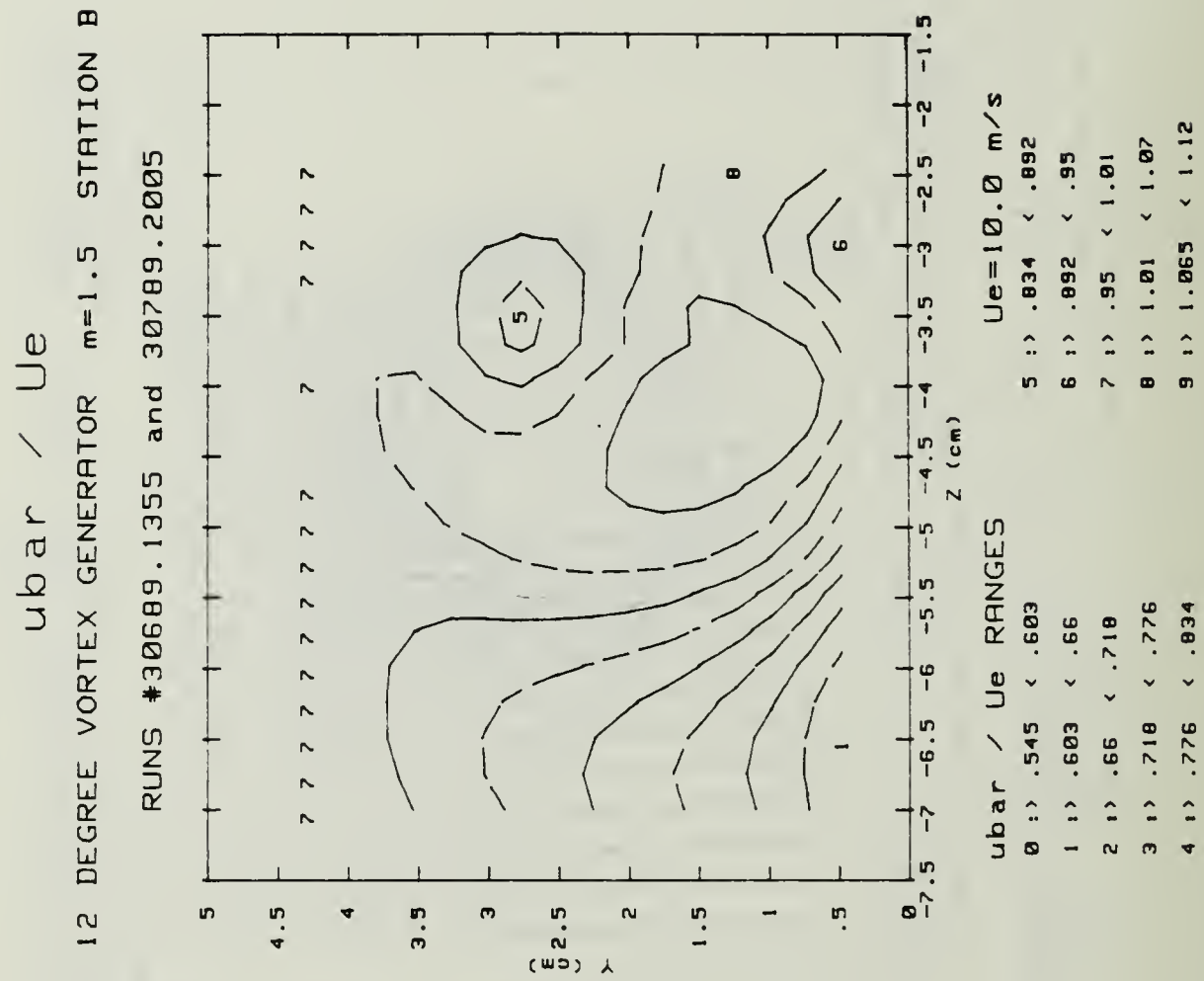

Figure 99. $\bar{u}$ (boundary layer / vortex / wall jet, station B, $\Delta = 0.10$ inches)

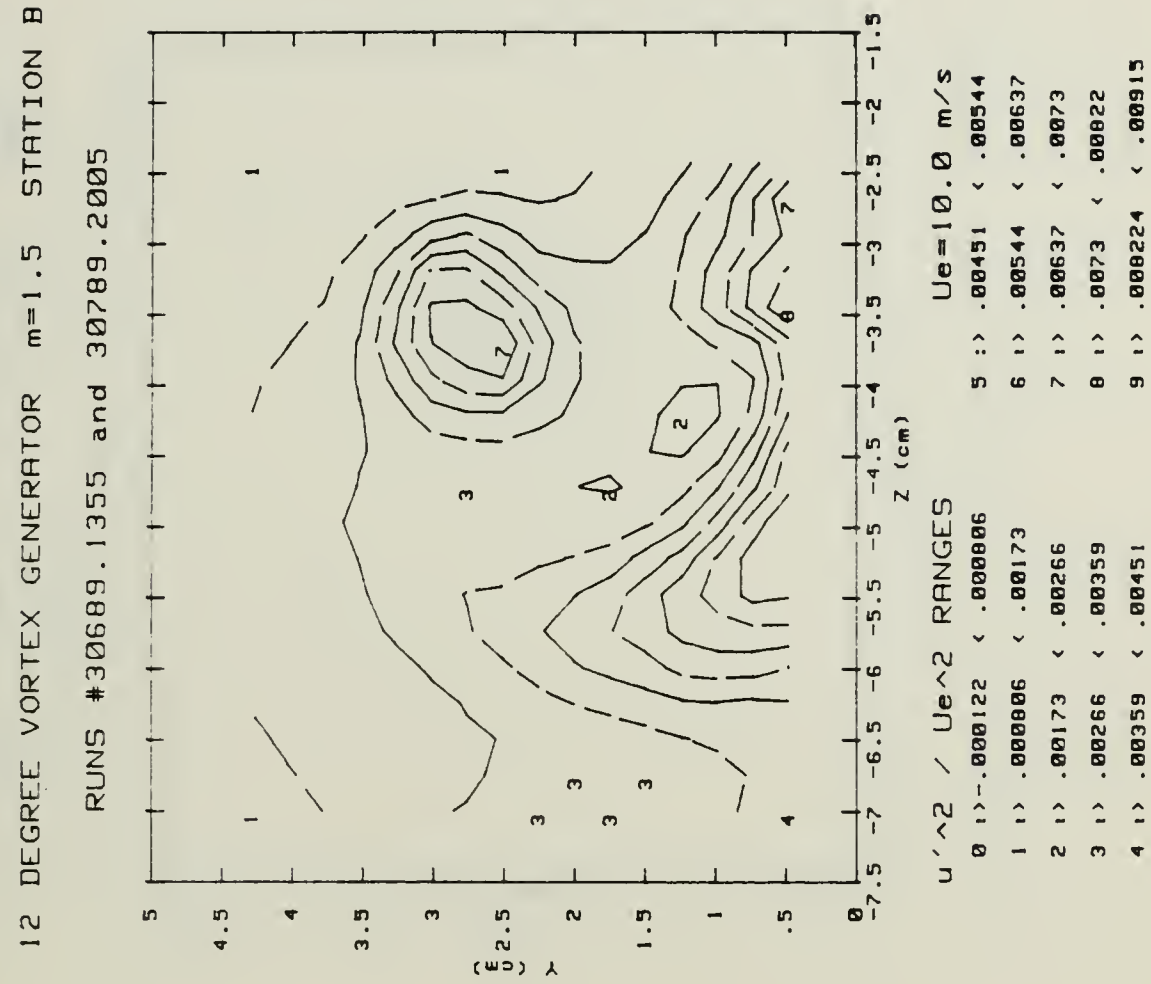

Figure 100. $\overline{u'^2}$ (boundary layer / vortex / wall jet, station B, $\Delta = 0.10$ inches)

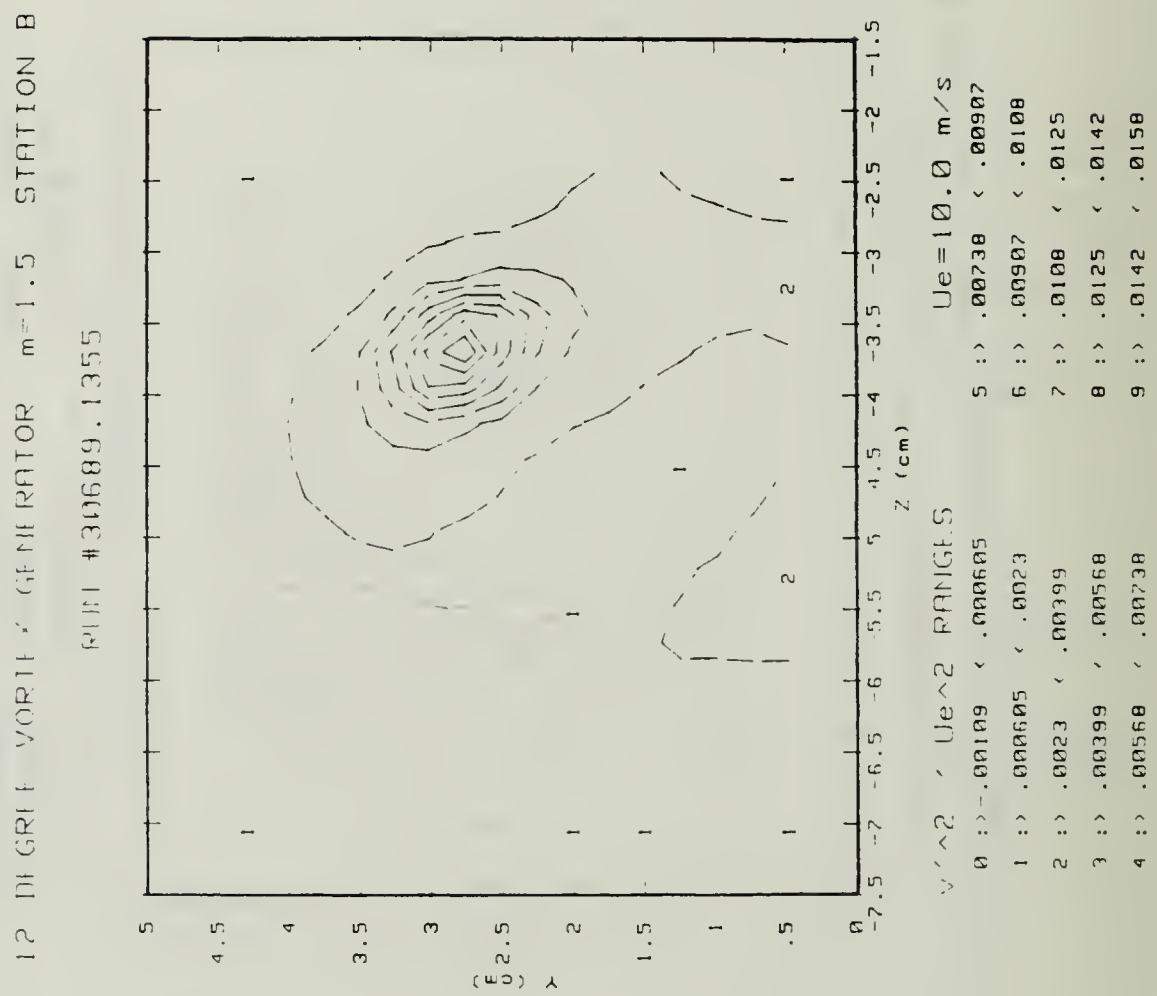

Figure 101. $\overline{v'^2}$ (boundary layer / vortex / wall jet, station B, $\Delta = 0.10$ inches)

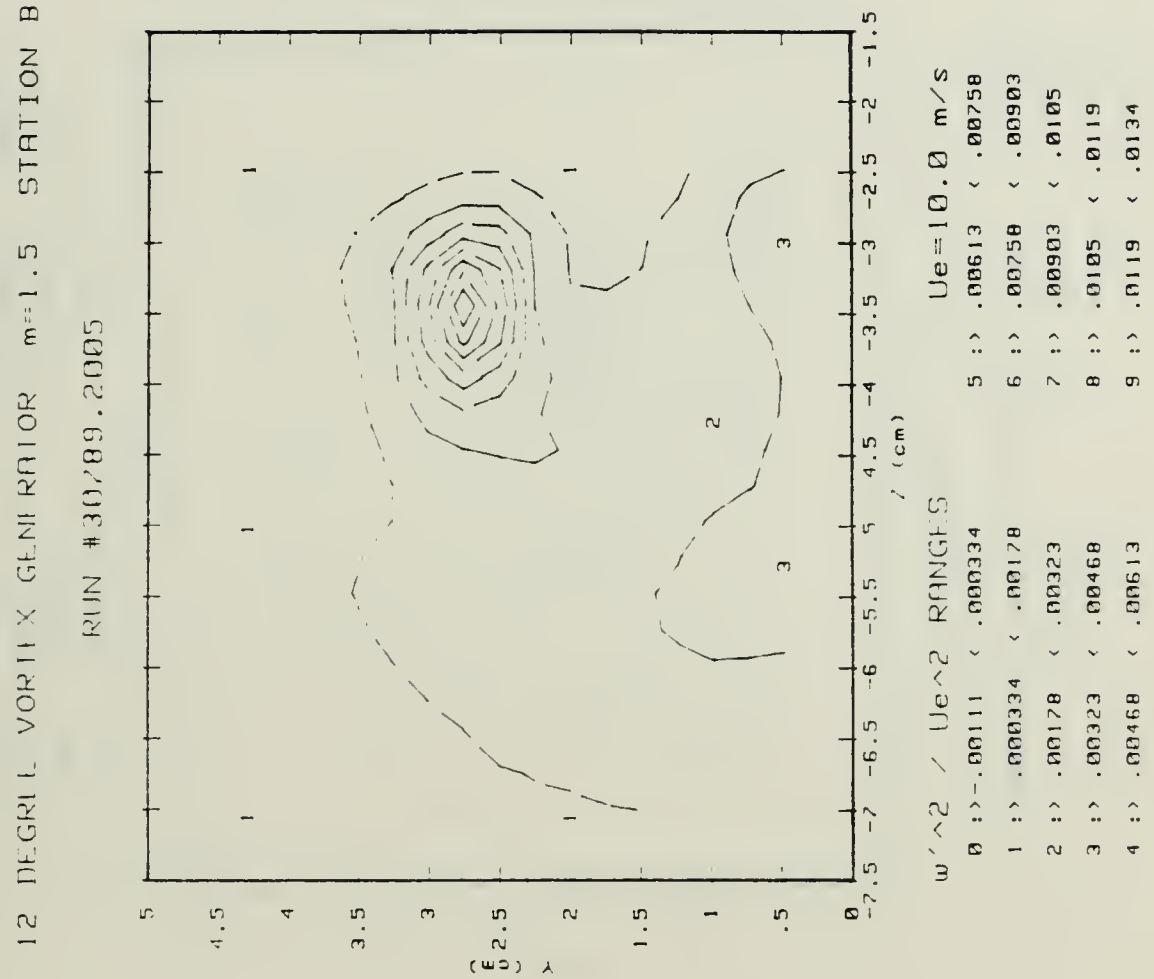

Figure 102. $\overline{w'^2}$ (boundary layer / vortex / wall jet, station B, $\Delta = 0.10$ inches)

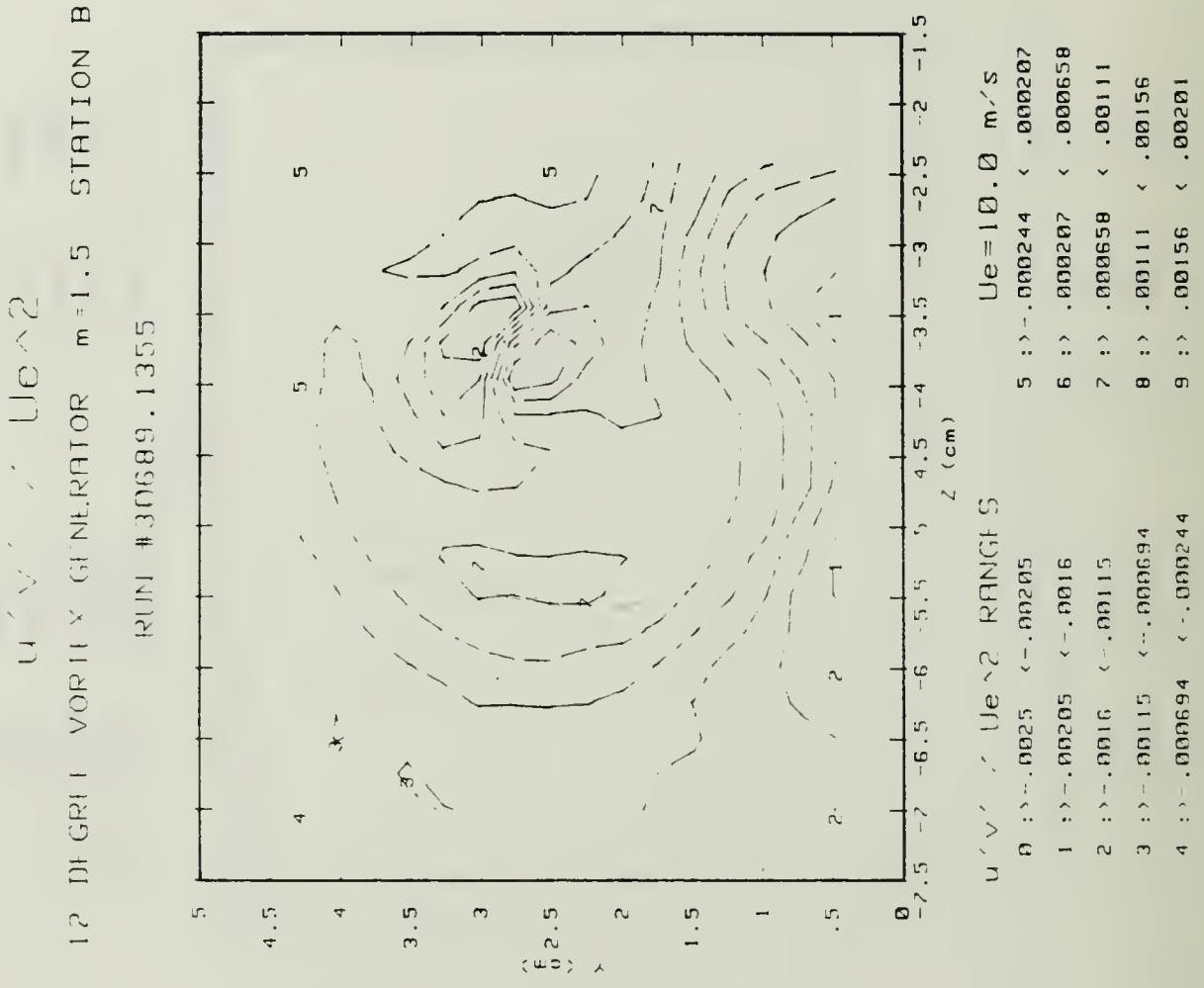

Figure 103. $\overline{u'v'}$ (boundary layer / vortex / wall jet, station B, Δ = 0.10 inches)

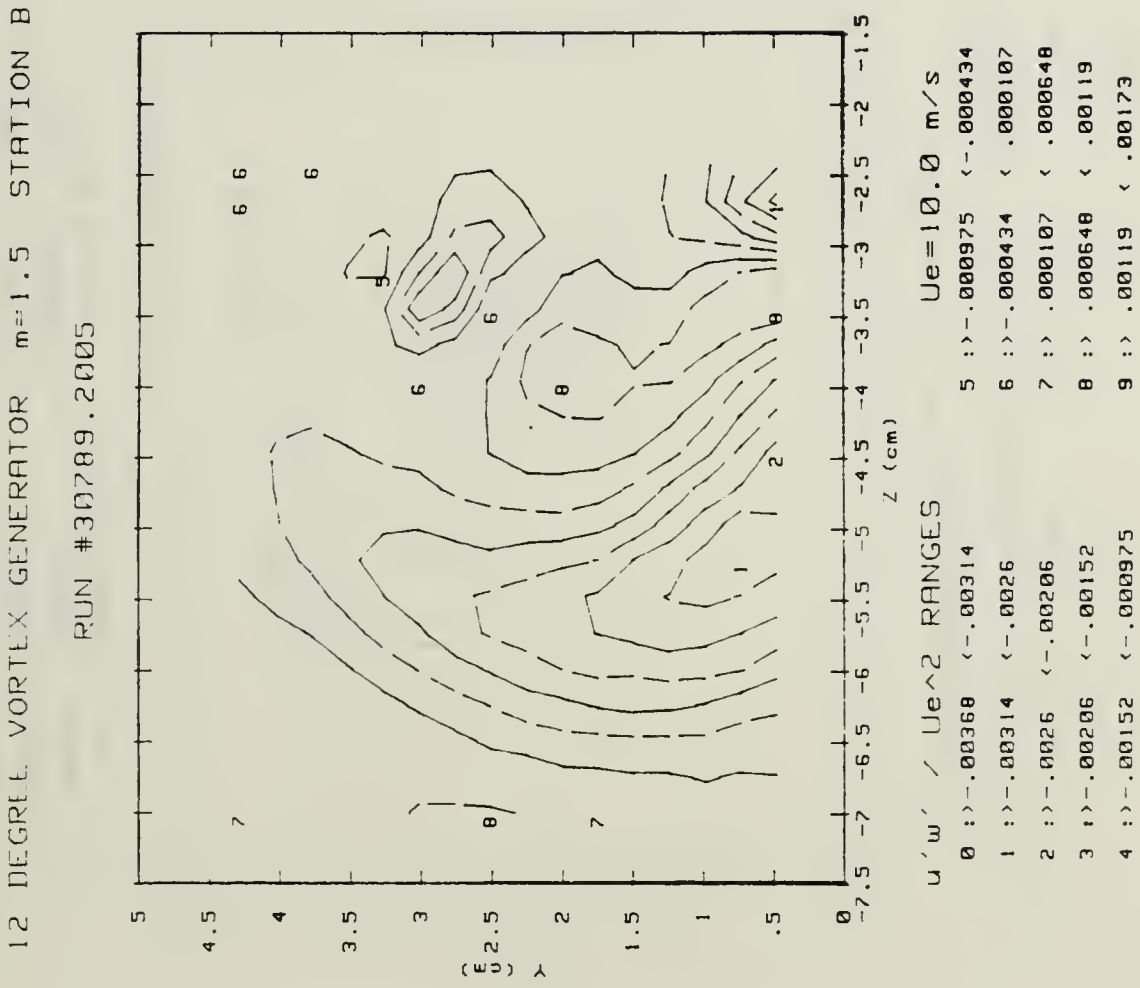

Figure 104. $\overline{u'w'}$ (boundary layer / vortex / wall jet, station B, $\Delta = 0.10$ inches)

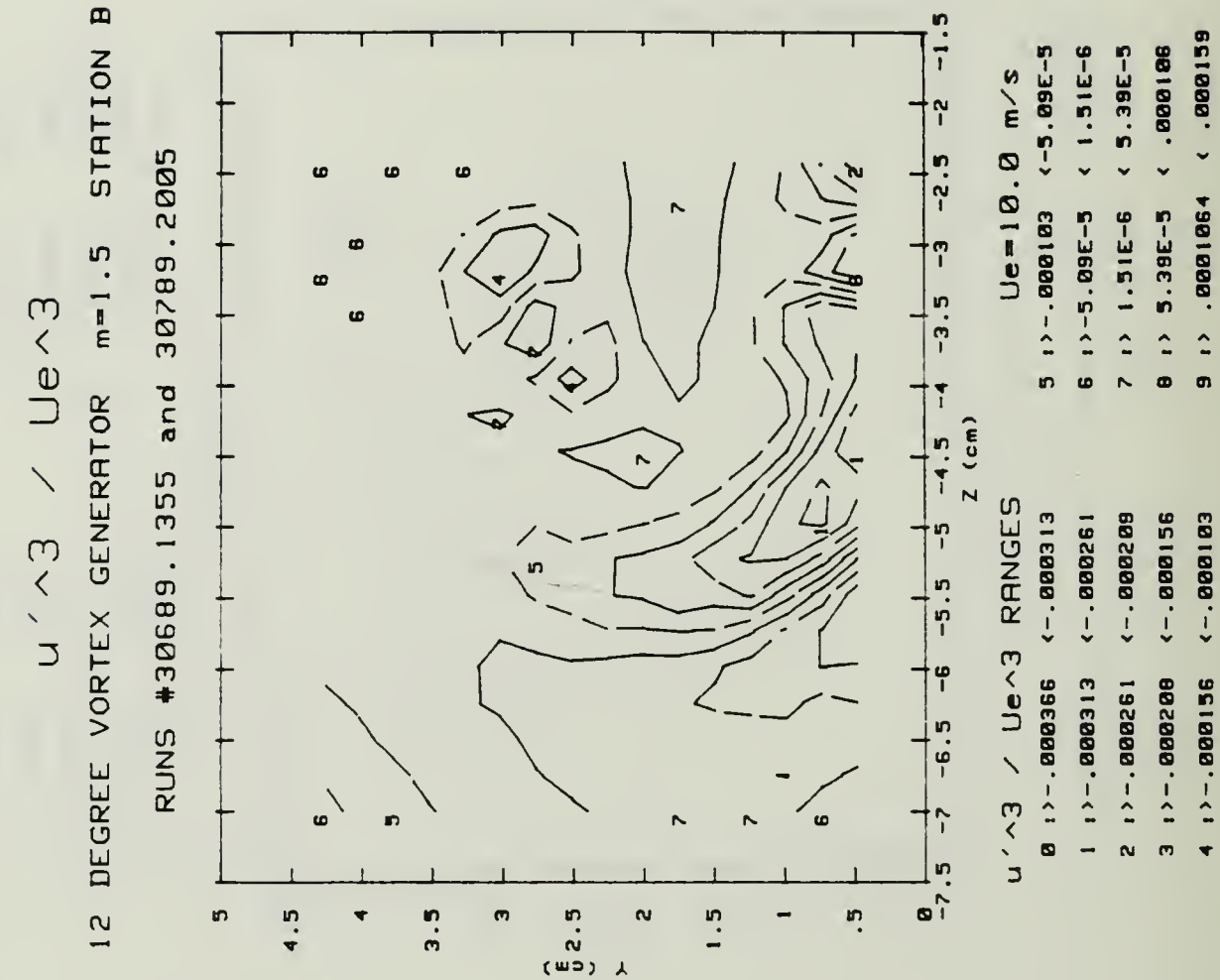

Figure 105. $\overline{u'^3}$ (boundary layer / vortex / wall jet, station B, $\Delta = 0.10$ inches)

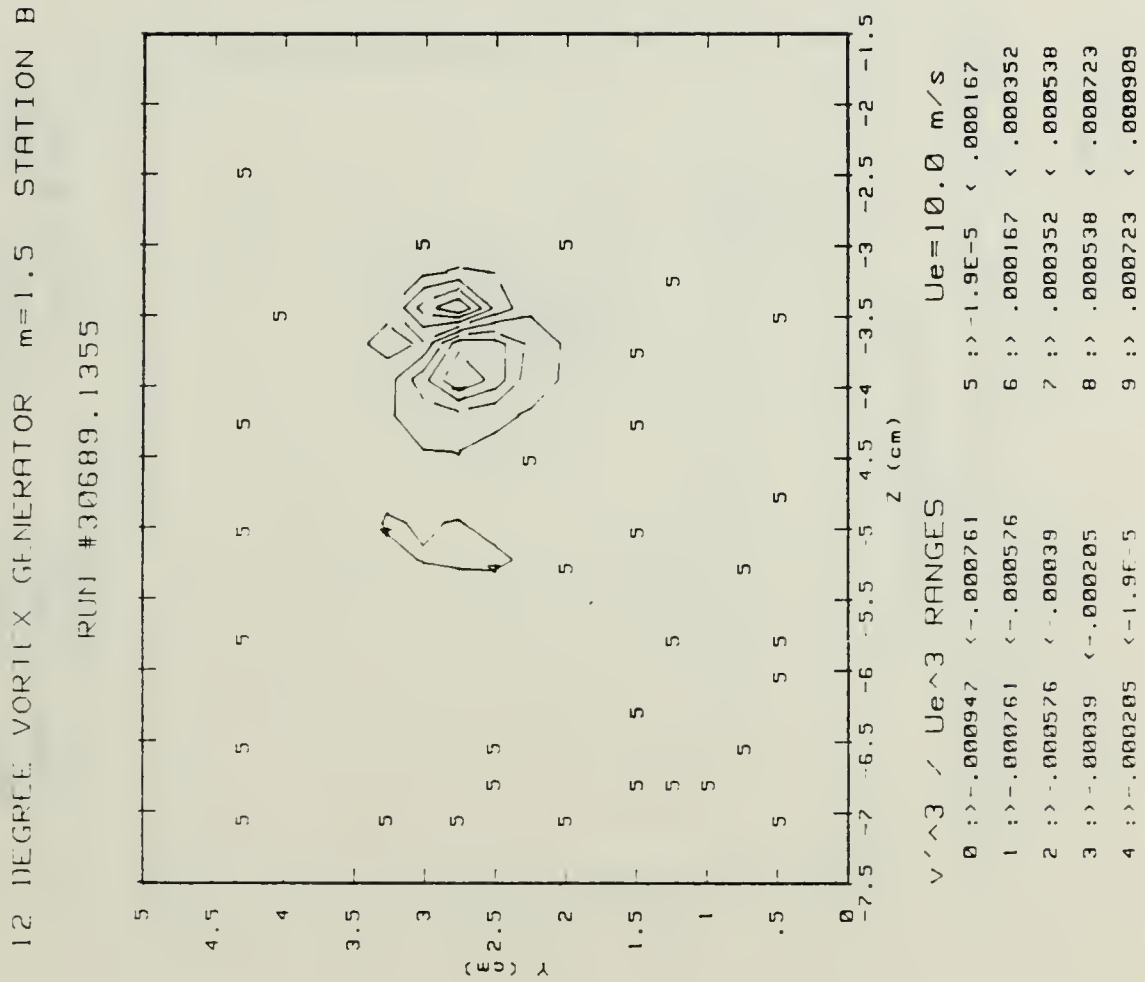

Figure 106. $\overline{v'^3}$ (boundary layer / vortex / wall jet, station B, $\Delta = 0.10$ inches)

Figure 107. $\overline{w'^3}$ (boundary layer / vortex / wall jet, station B, $\Delta = 0.10$ inches)

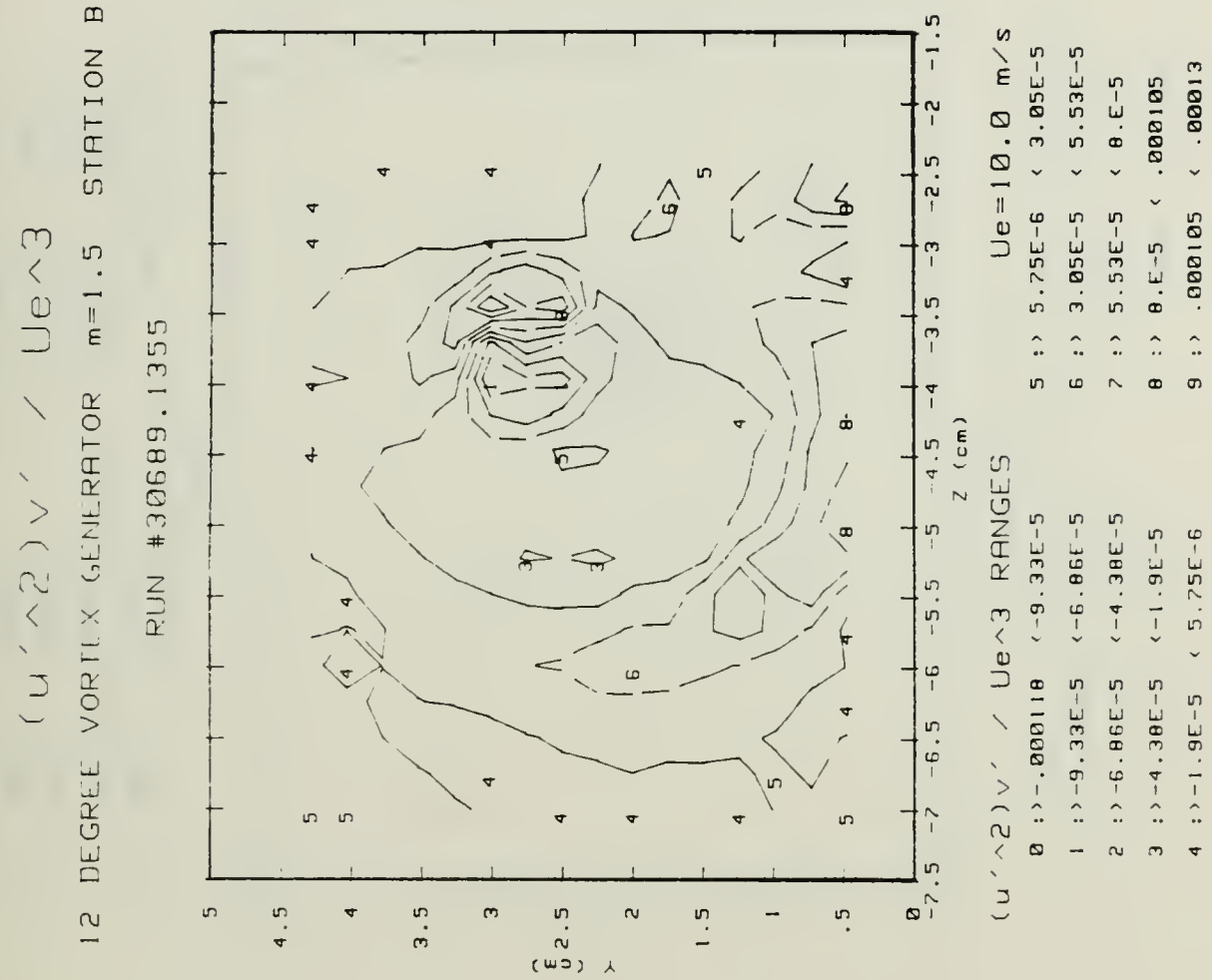

Figure 108. $\overline{u'^2v'}$ (boundary layer / vortex / wall jet, station B, $\Delta = 0.10$ inches)

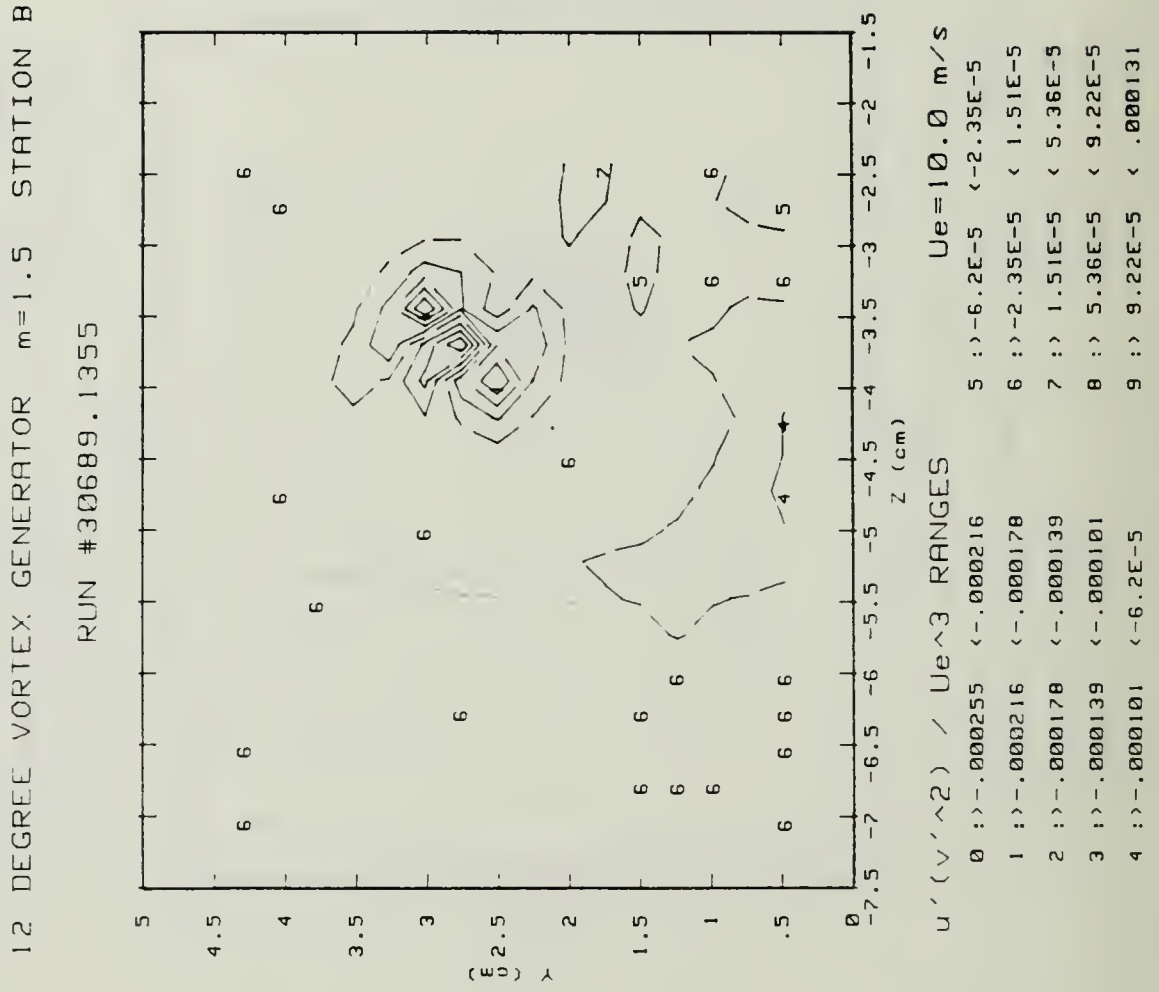

Figure 109. $\overline{u'v'^2}$ (boundary layer / vortex / wall jet, station B, $\Delta = 0.10$ inches)

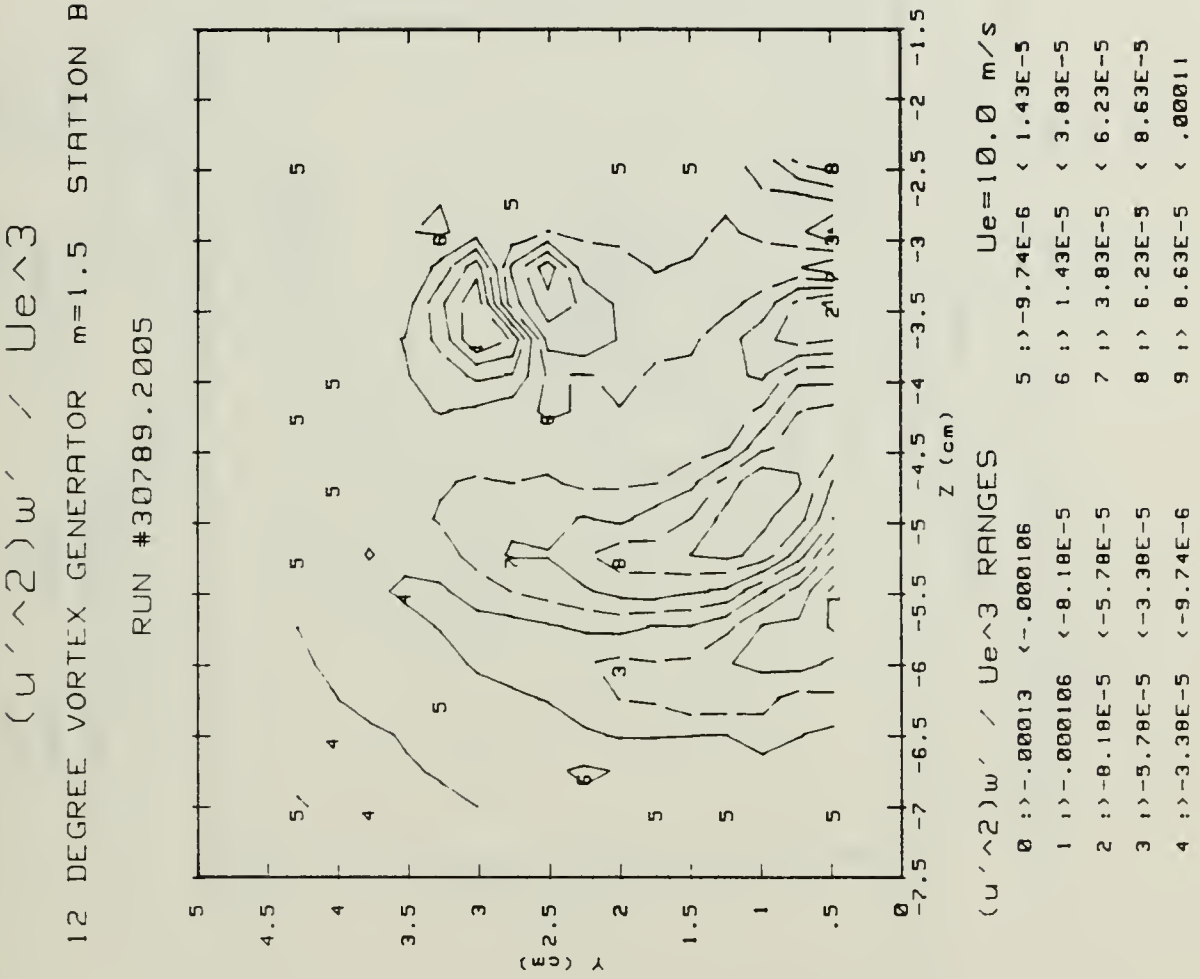

Figure 110. $\overline{u'^2w'}$ (boundary layer / vortex / wall jet, station B, $\Delta = 0.10$ inches)

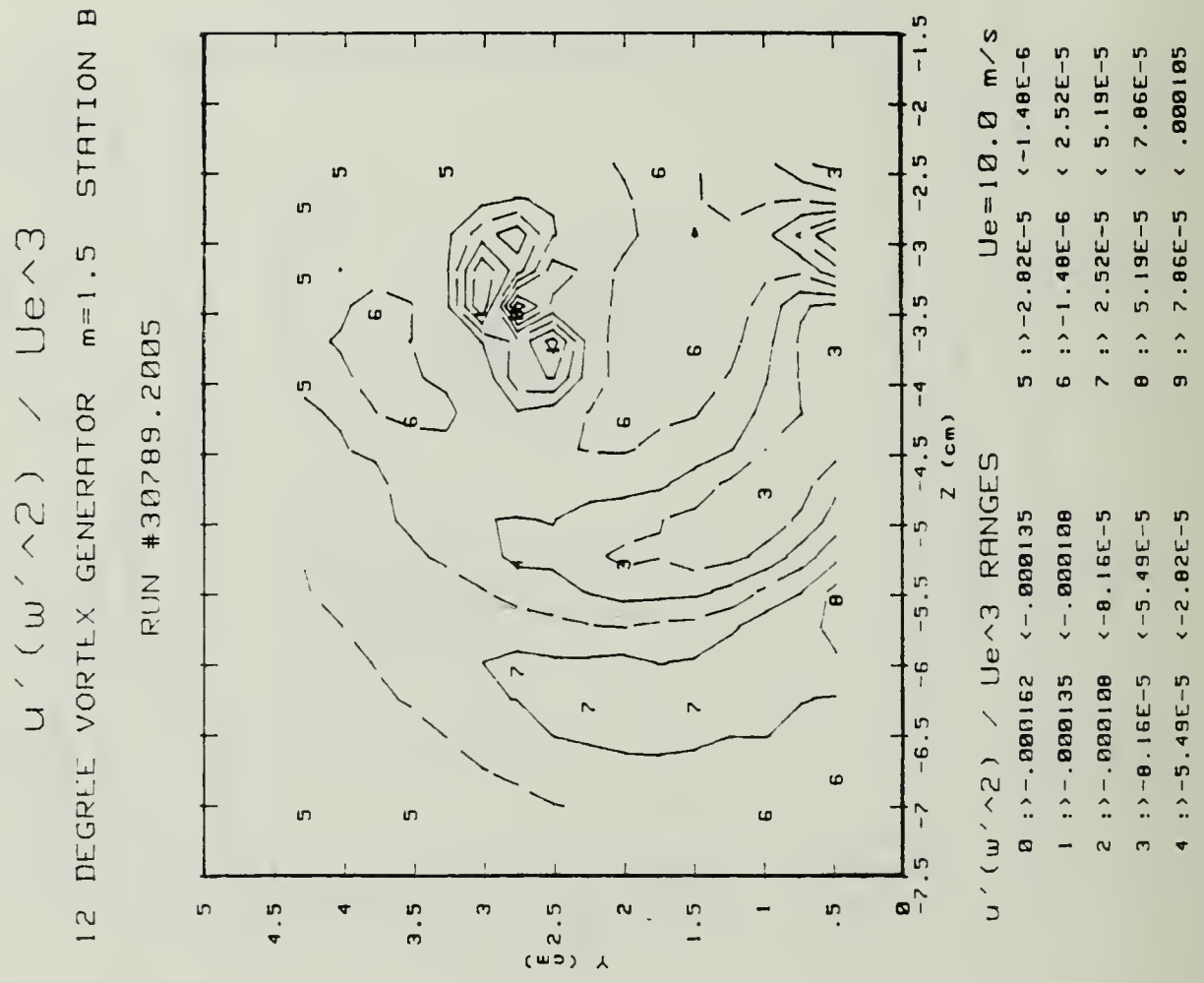

Figure 111. $\overline{u'w'^2}$ (boundary layer / vortex / wall jet, station B, $\Delta = 0.10$ inches)

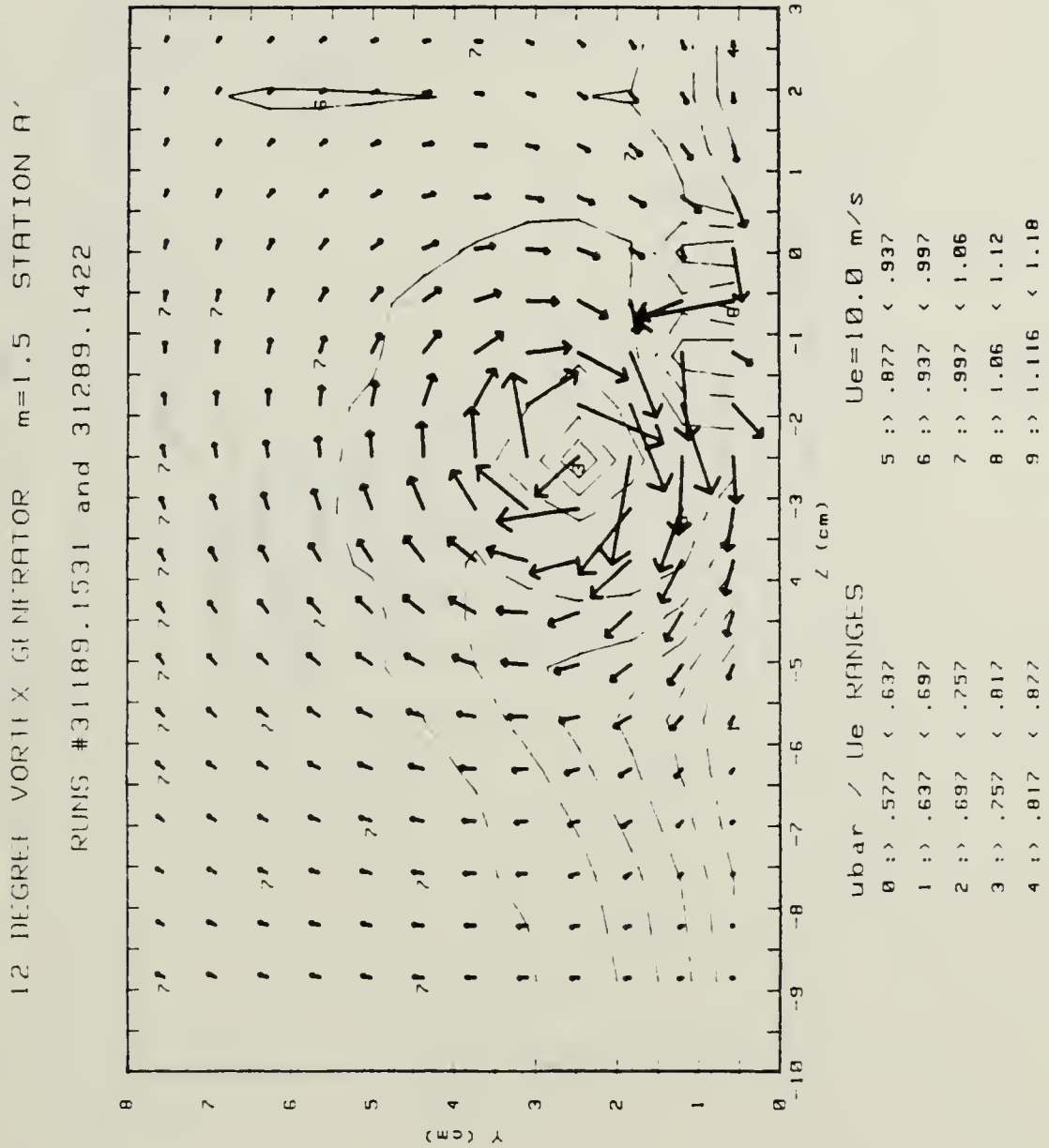

Figure 112. Mean Velocities (boundary layer / vortex / wall jet, station A′, $\Delta = 0.25$ inches)

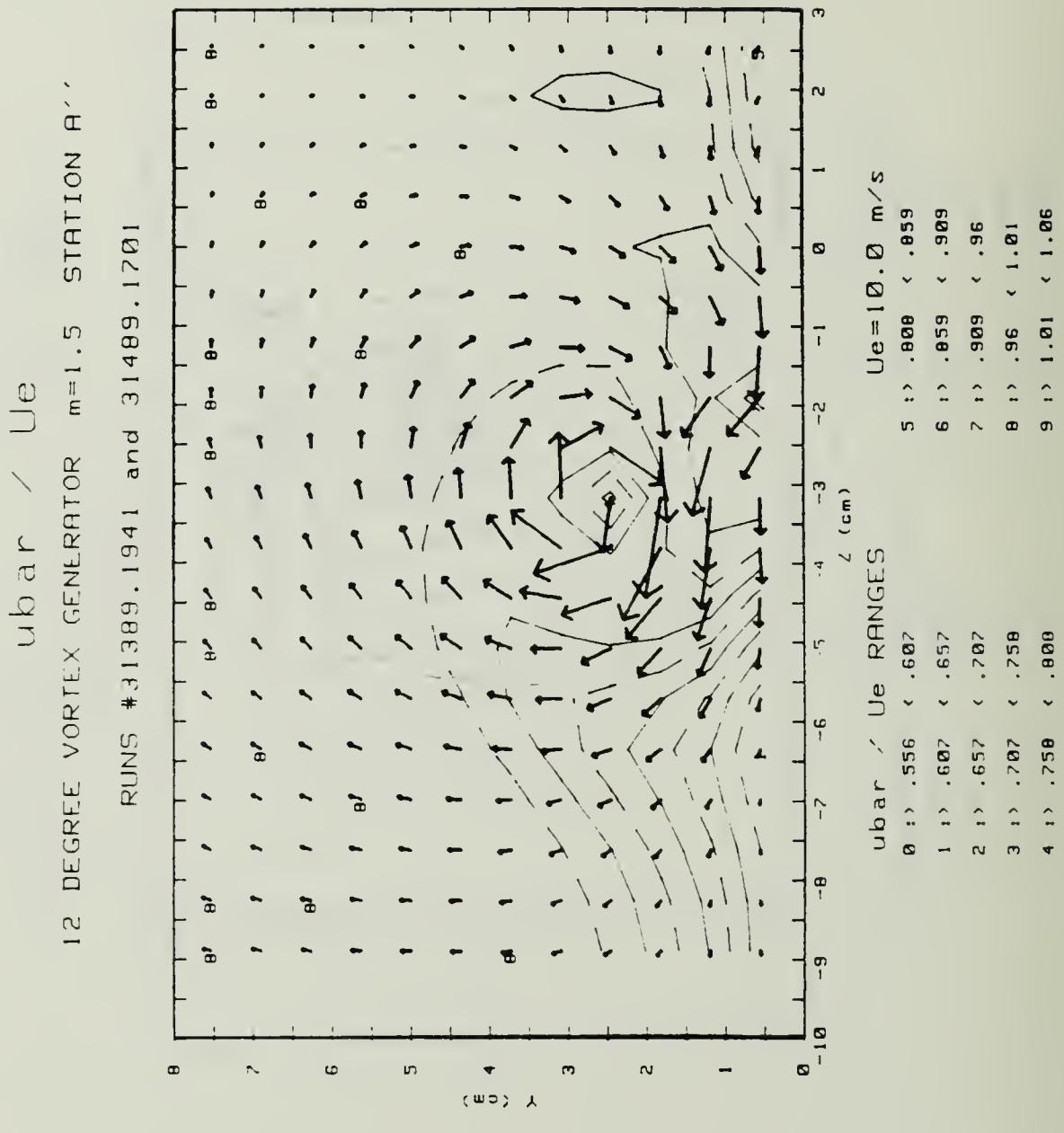

Figure 113. Mean Velocities (boundary layer / vortex / wall jet, station A″, $\Delta = 0.25$ inches)

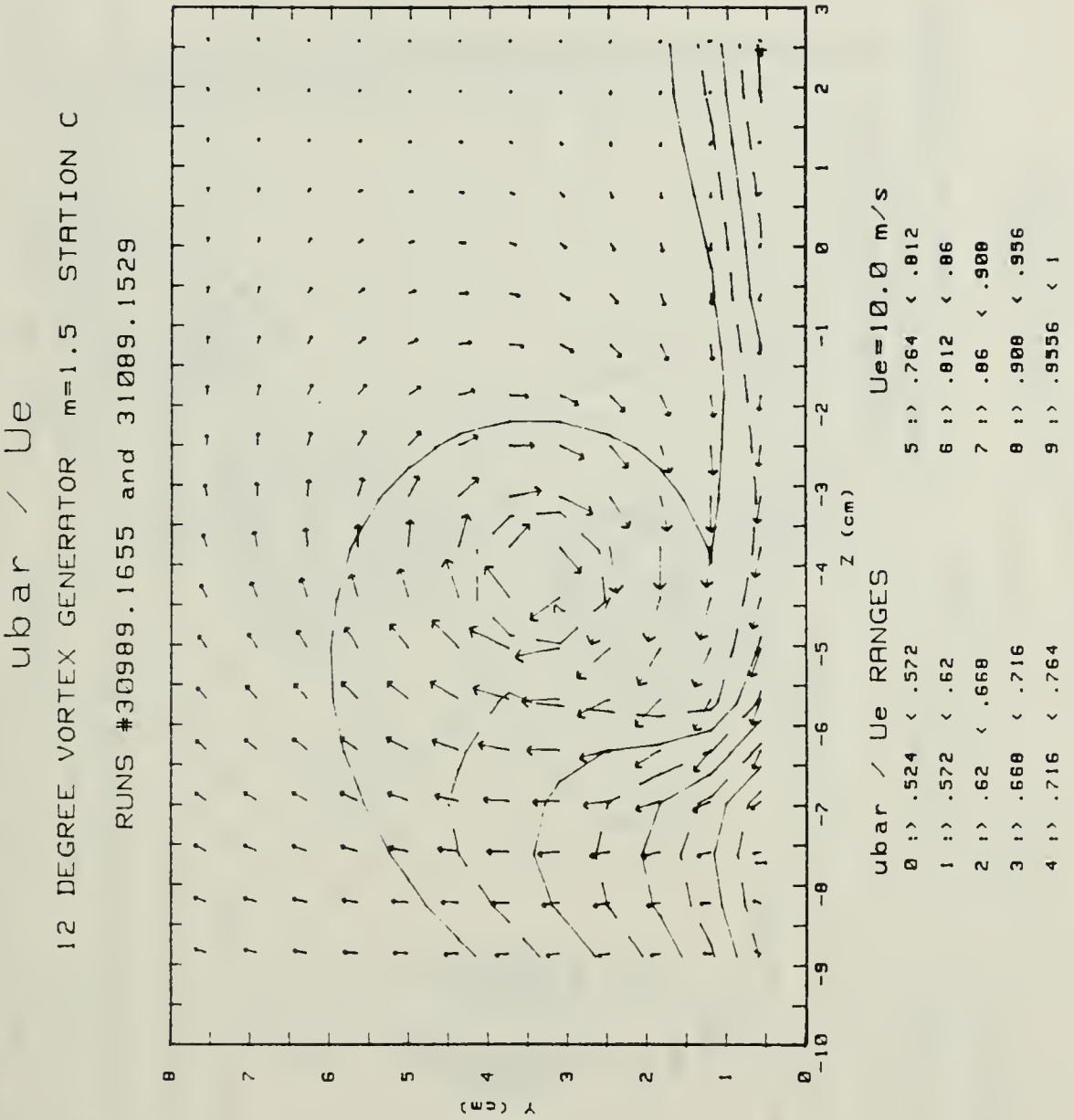

Figure 114. Mean Velocities (boundary layer / vortex / wall jet, station C, $\Delta = 0.25$ inches)

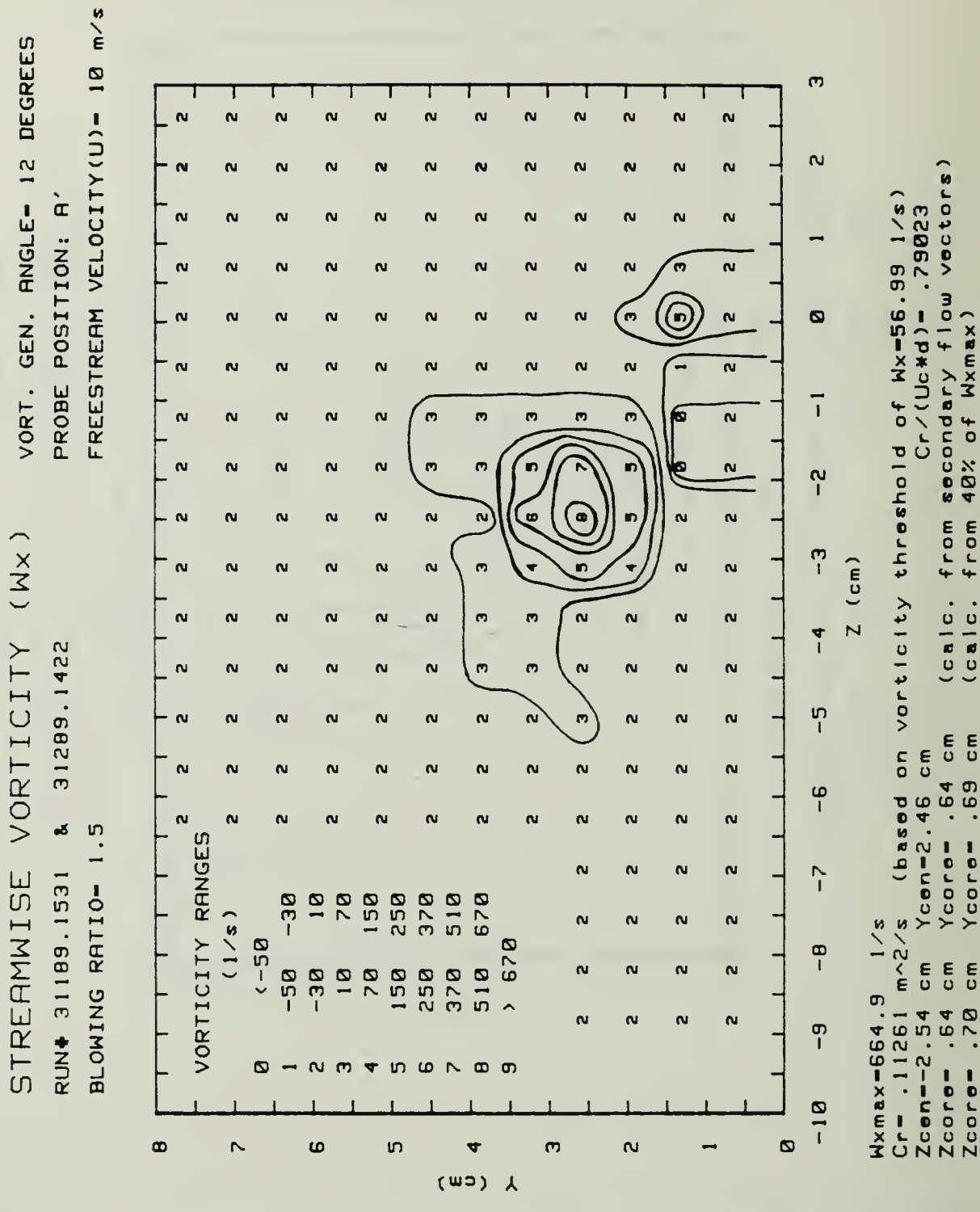

Figure 115. Streamwise Vorticity ω_x (boundary layer / vortex / wall jet, station A′, $\Delta = 0.25$ inches)

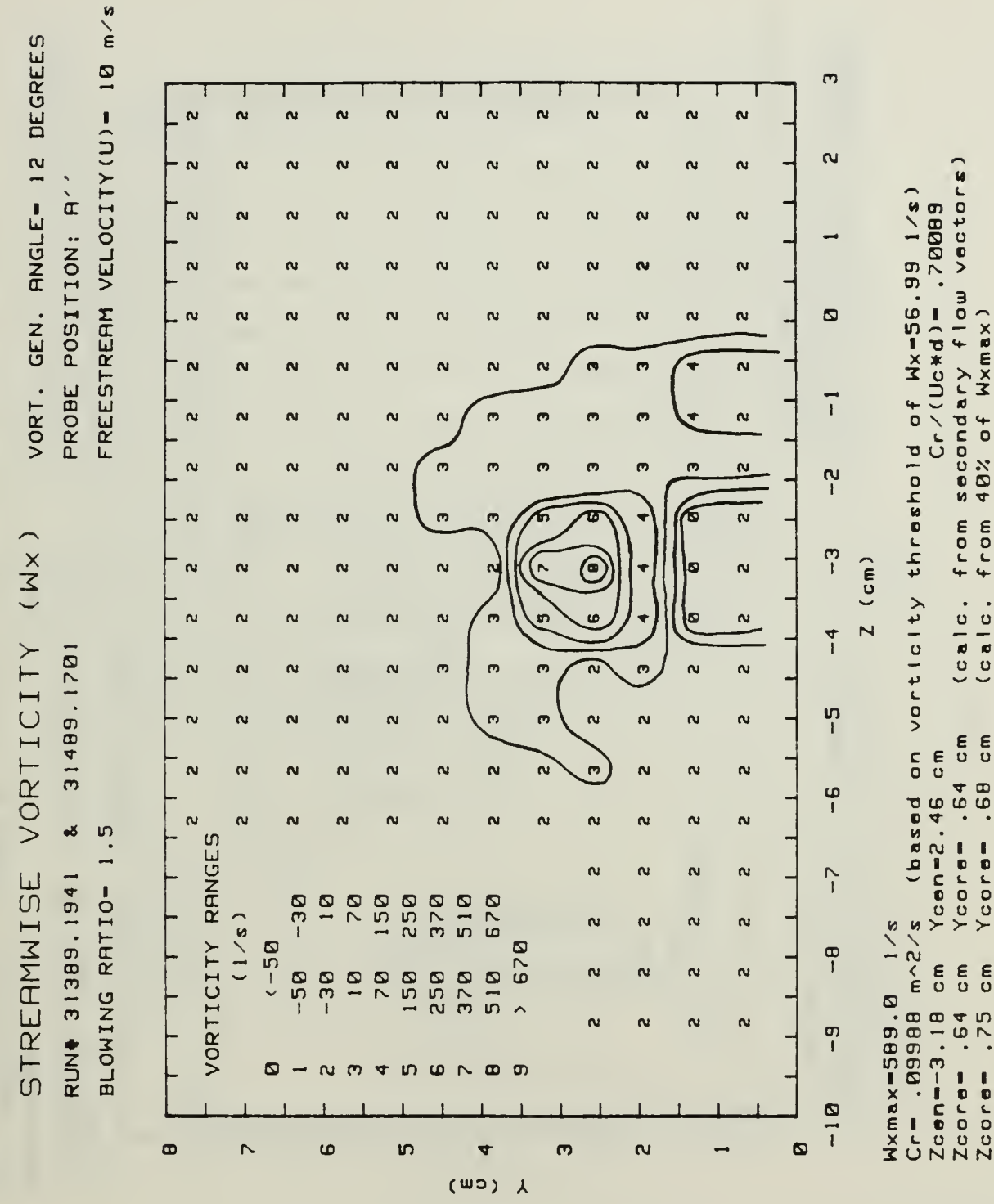

Figure 116. Streamwise Vorticity ω_x (boundary layer / vortex / wall jet, station A'', $\Delta = 0.25$ inches)

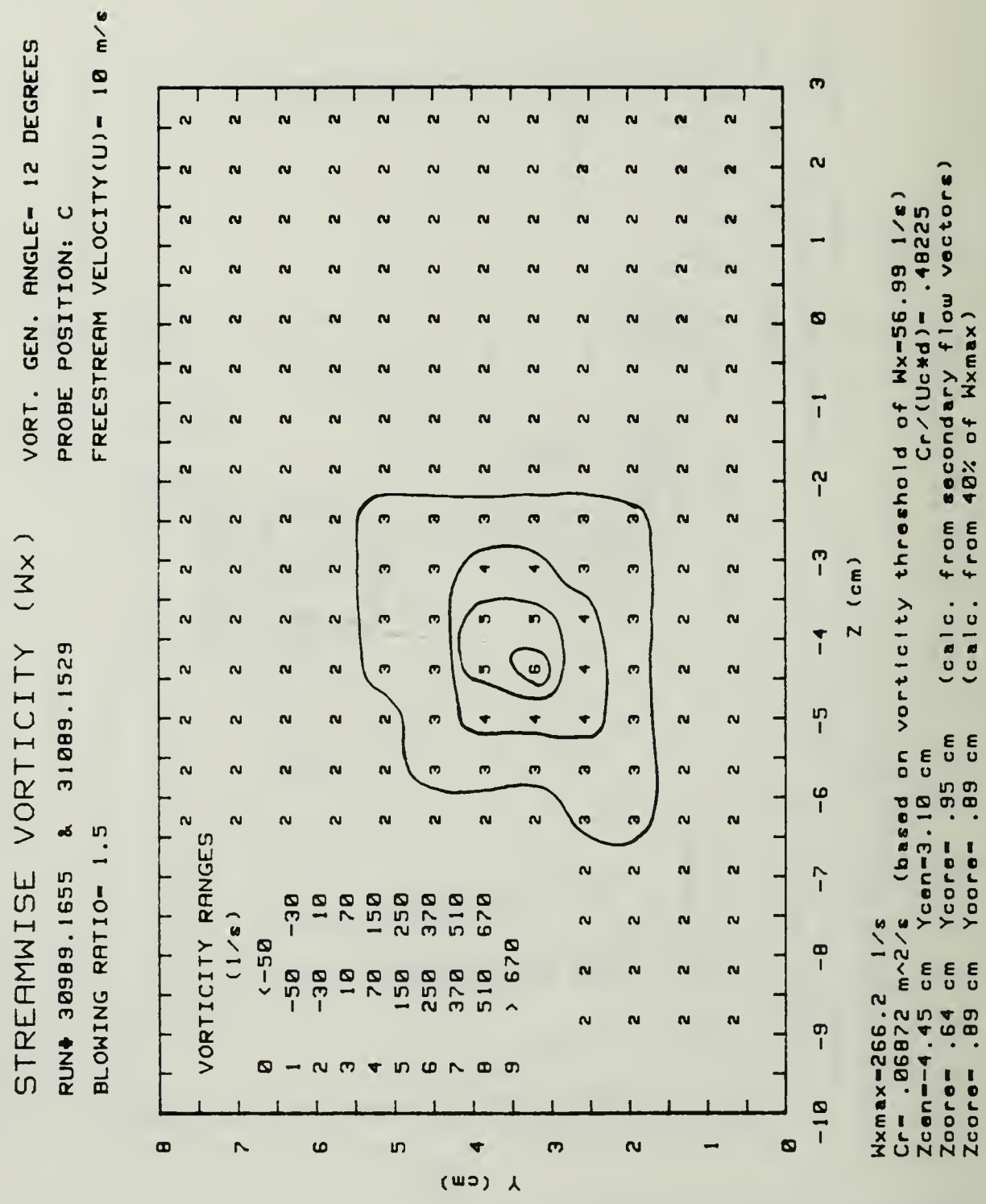

Figure 117. Streamwise Vorticity ω_x (boundary layer / vortex / wall jet, station C, $\Delta = 0.25$ inches)

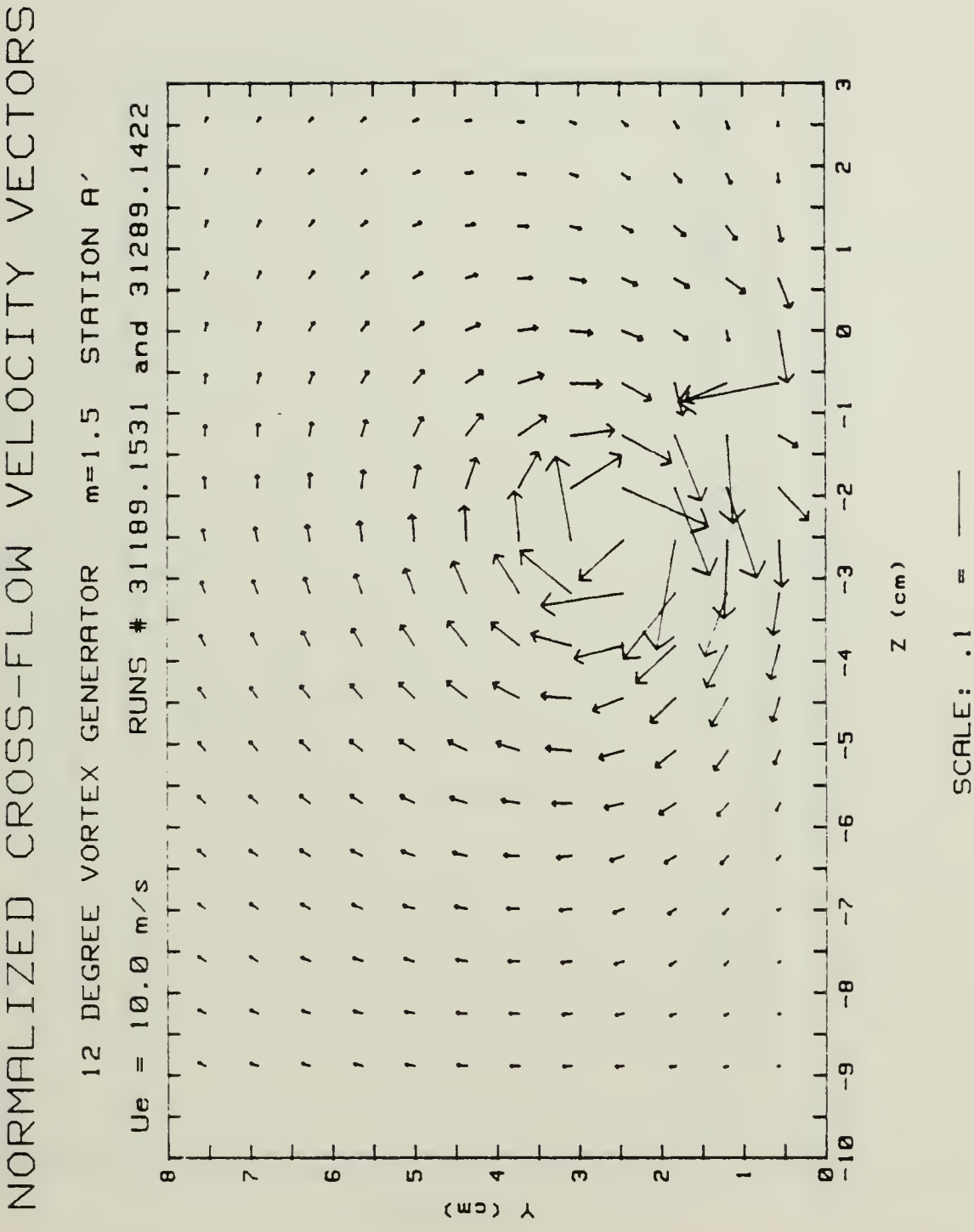
NORMALIZED CROSS-FLOW VELOCITY VECTORS
12 DEGREE VORTEX GENERATOR m=1.5 STATION A'
Ue = 10.0 m/s RUNS # 31189.1531 and 31289.1422
Y (cm)
Z (cm)
SCALE: .1 = ——

Figure 118. Secondary Flow Vectors (boundary layer / vortex / wall jet, station A′, $\Delta = 0.25$ inches)

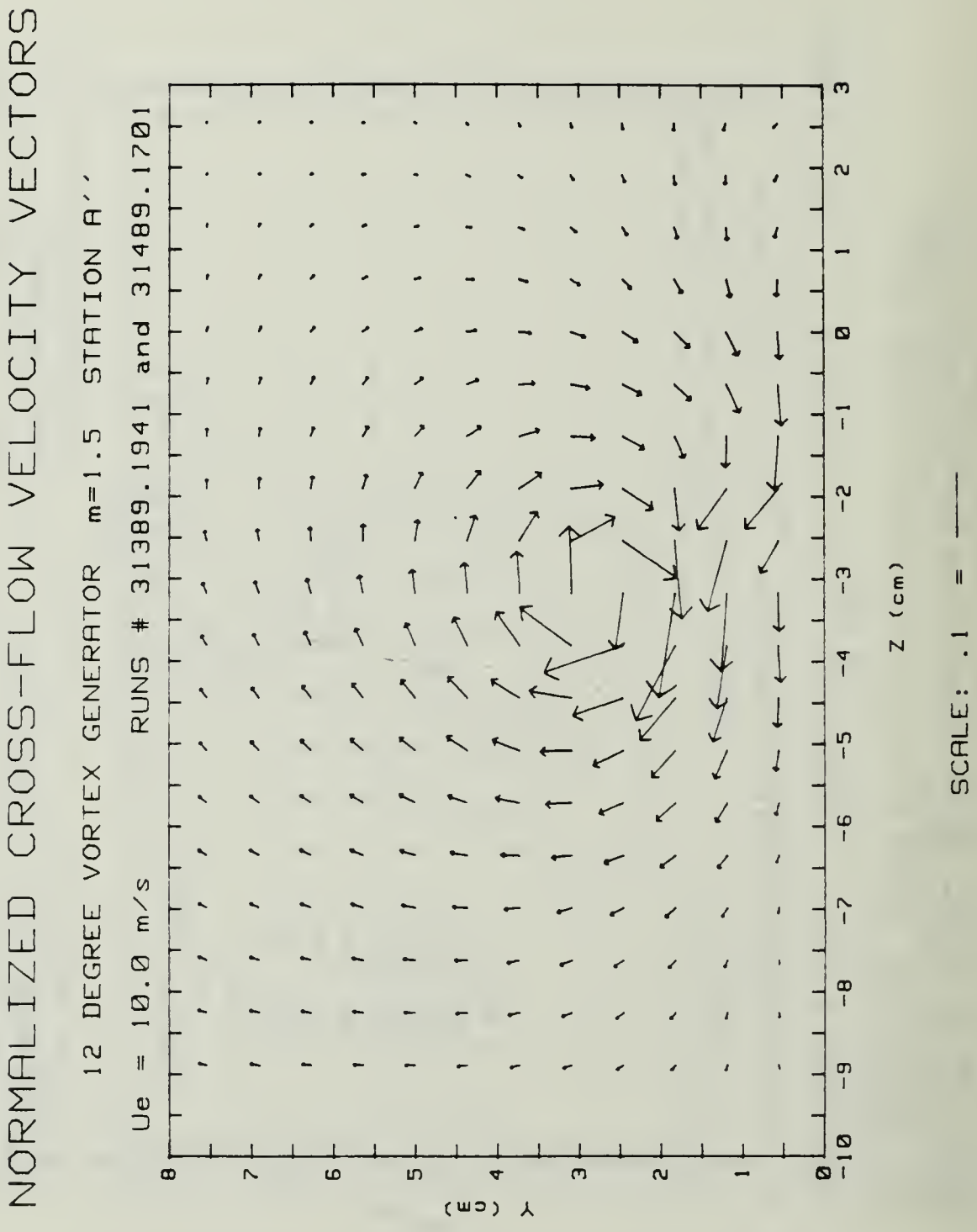
NORMALIZED CROSS-FLOW VELOCITY VECTORS
12 DEGREE VORTEX GENERATOR m=1.5 STATION A''
Ue = 10.0 m/s RUNS # 31389.1941 and 31489.1701
Y (cm)
Z (cm)
SCALE: .1 = ——

Figure 119. Secondary Flow Vectors (boundary layer / vortex / wall jet, station A″, Δ = 0.25 inches)

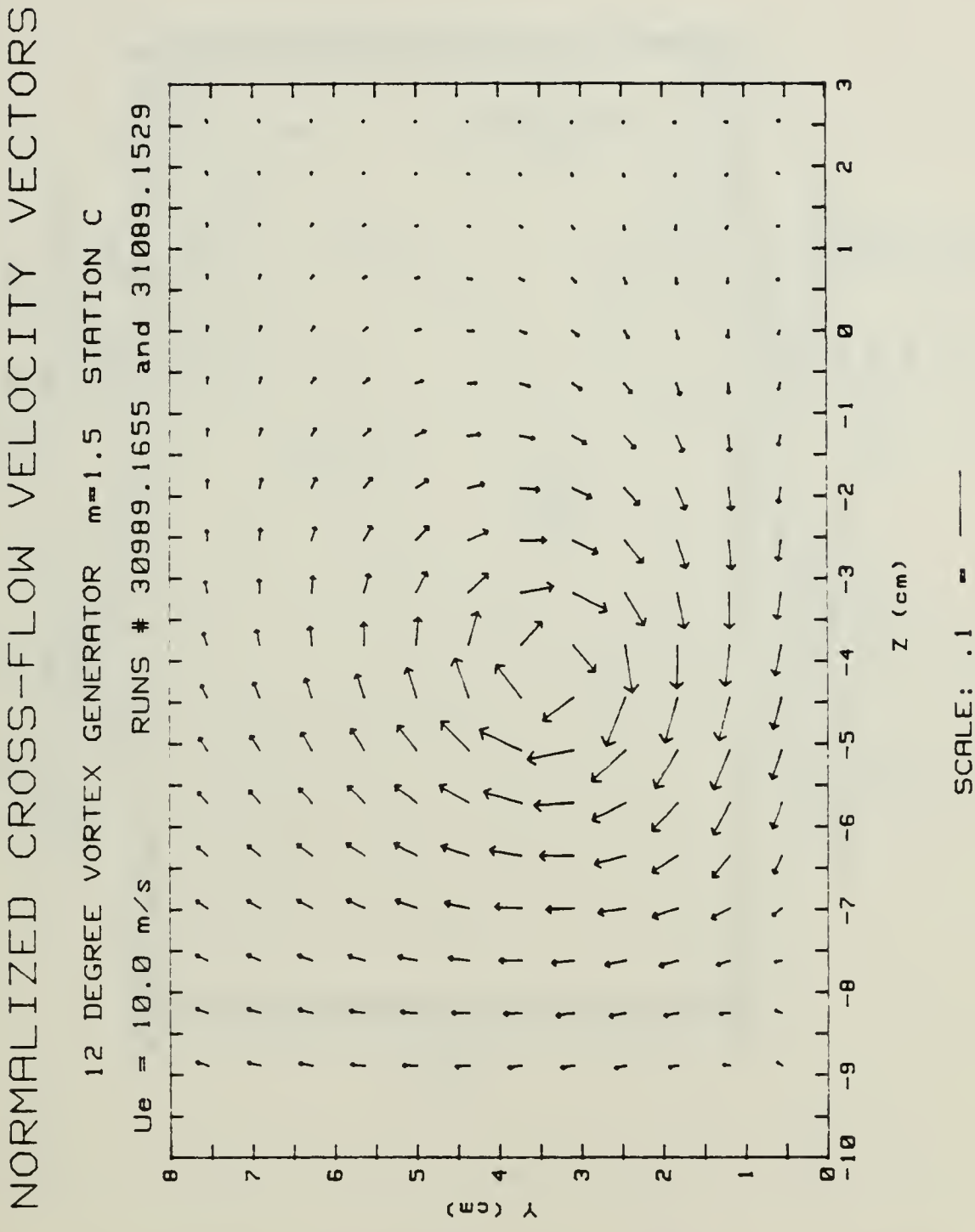
NORMALIZED CROSS-FLOW VELOCITY VECTORS
12 DEGREE VORTEX GENERATOR m=1.5 STATION C
Ue = 10.0 m/s RUNS # 30989.1655 and 31089.1529
Y (cm)
Z (cm)
SCALE: .1 = ——

Figure 120. Secondary Flow Vectors (boundary layer / vortex / wall jet, station C, $\Delta = 0.25$ inches)

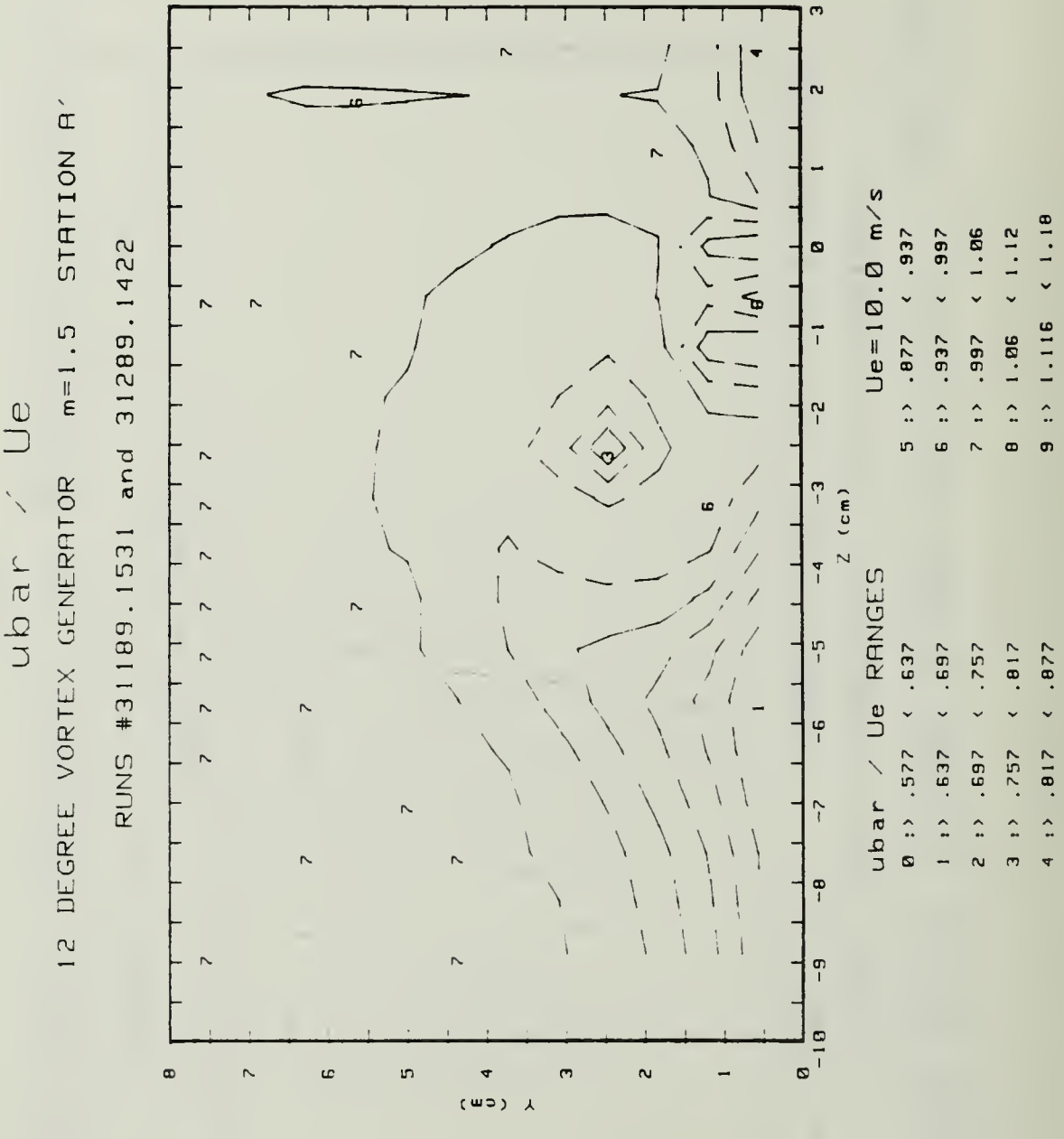

Figure 121. $\bar{u}$ (boundary layer / vortex / wall jet, station A′, $\Delta = 0.25$ inches)

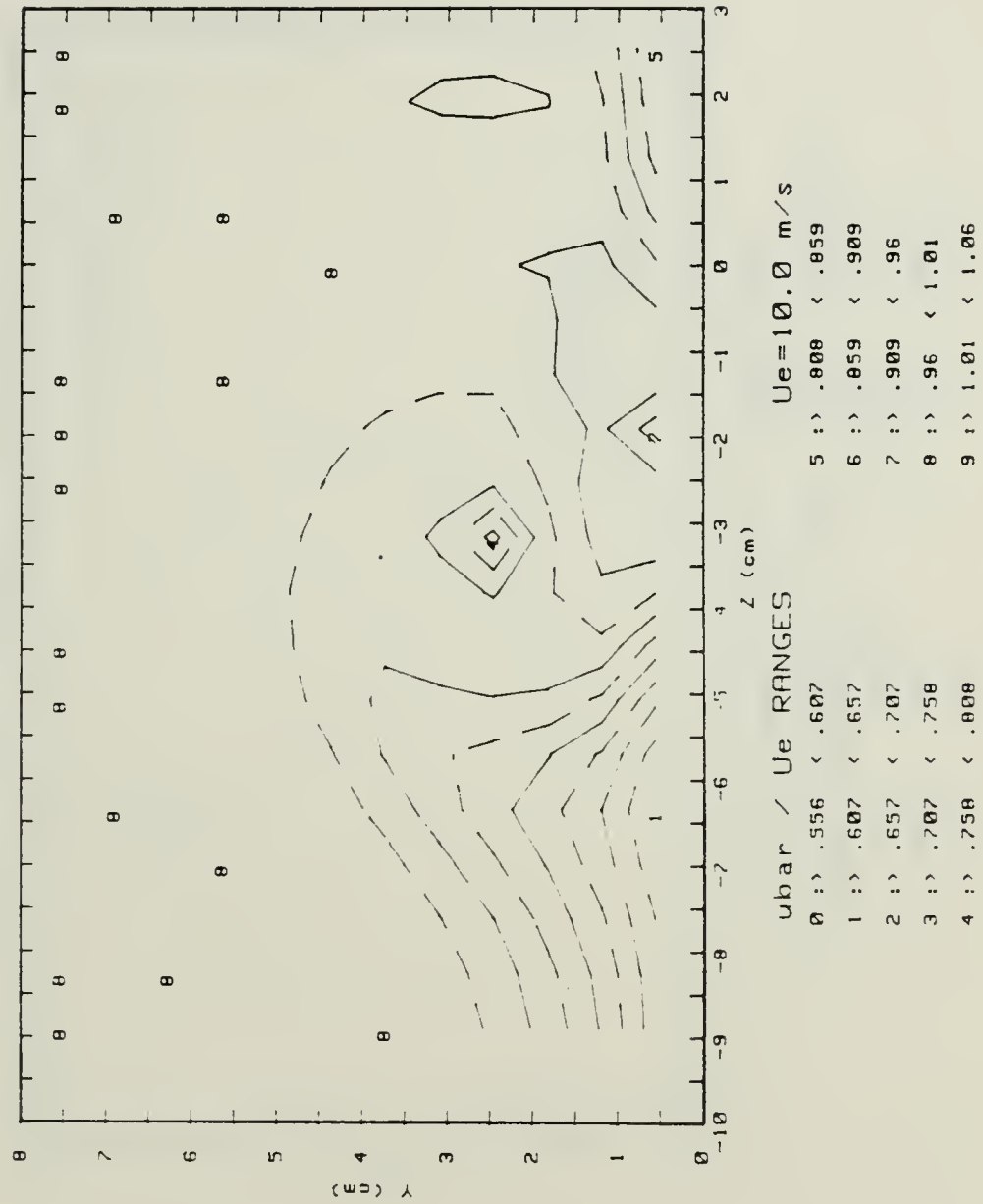

Figure 122. $\bar{u}$ (boundary layer / vortex / wall jet, station A″, Δ = 0.25 inches)

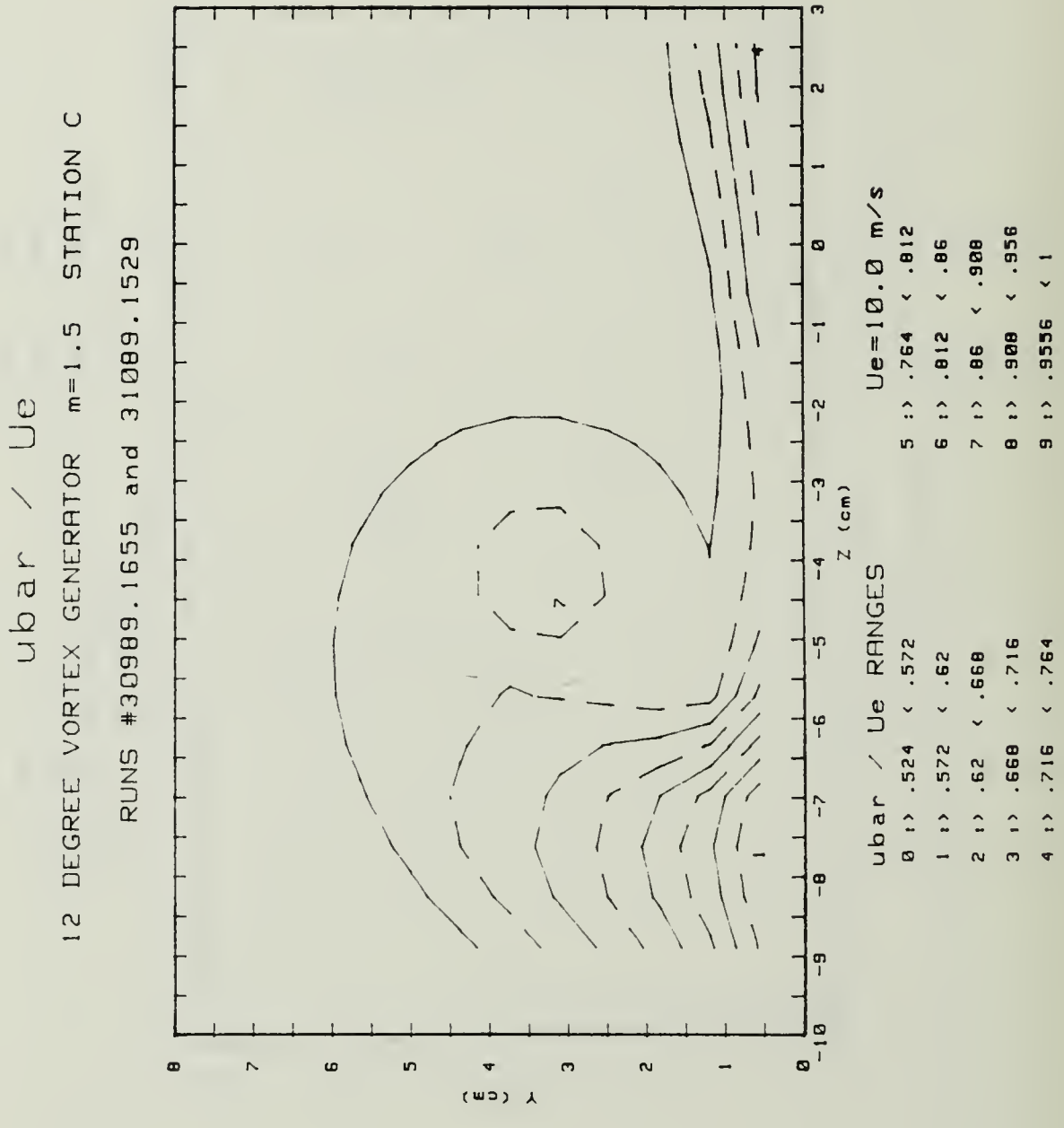

Figure 123. $\bar{u}$ (boundary layer / vortex / wall jet, station C, $\Delta = 0.25$ inches)

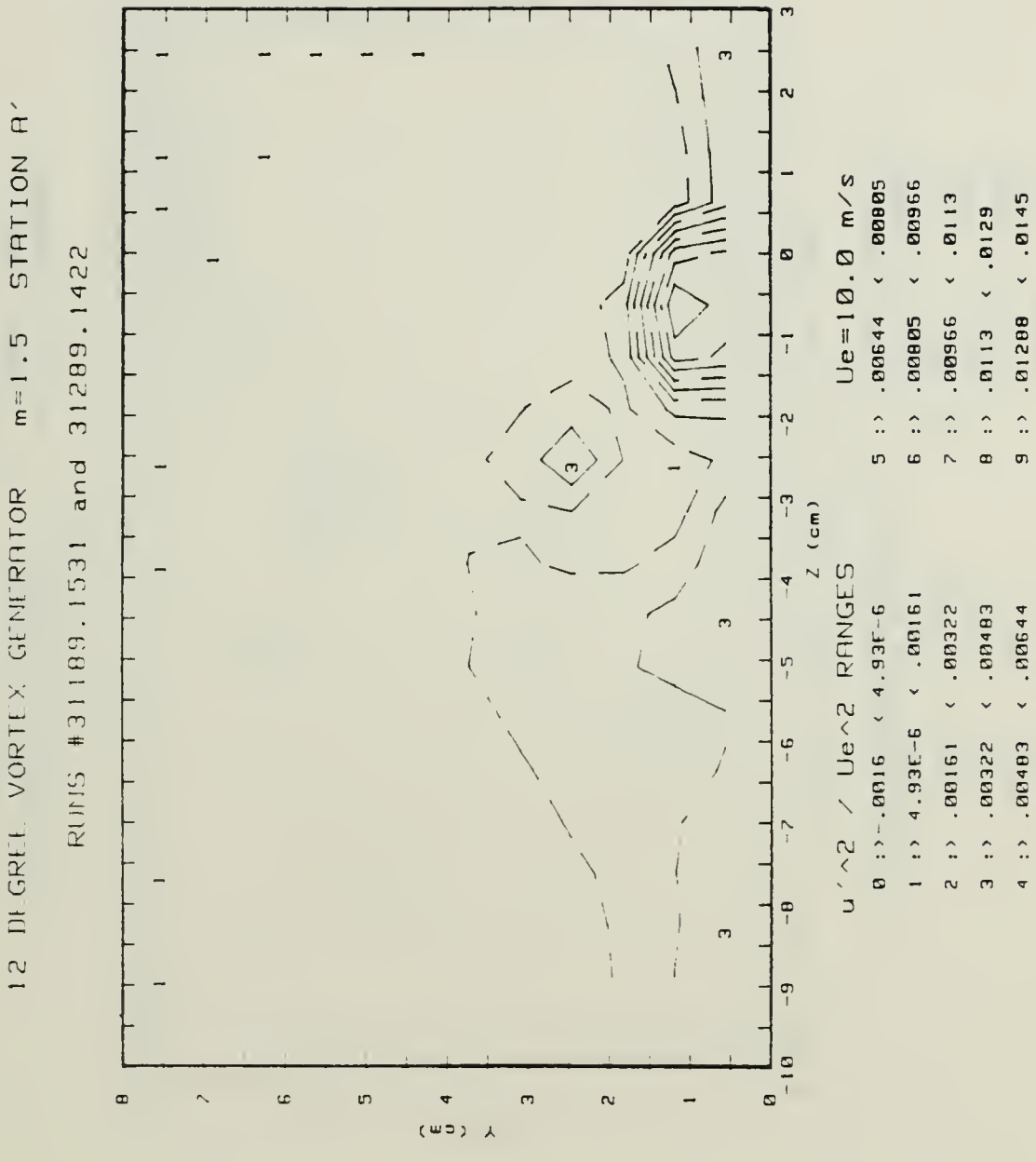

Figure 124. $\overline{u'^2}$ (boundary layer / vortex / wall jet, station A′, Δ = 0.25 inches)

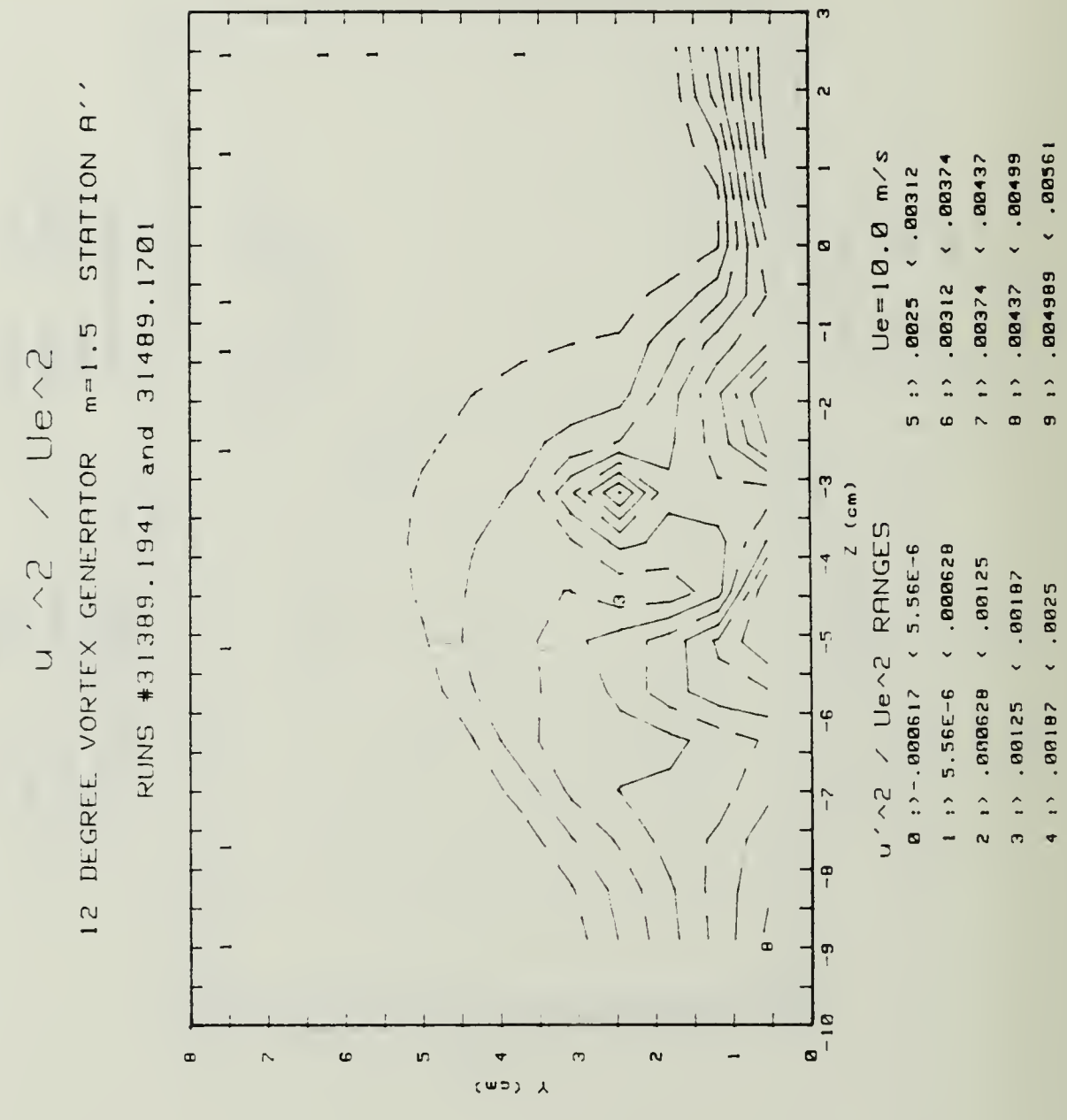

Figure 125. $\overline{u'^2}$ (boundary layer / vortex / wall jet, station A″, Δ = 0.25 inches)

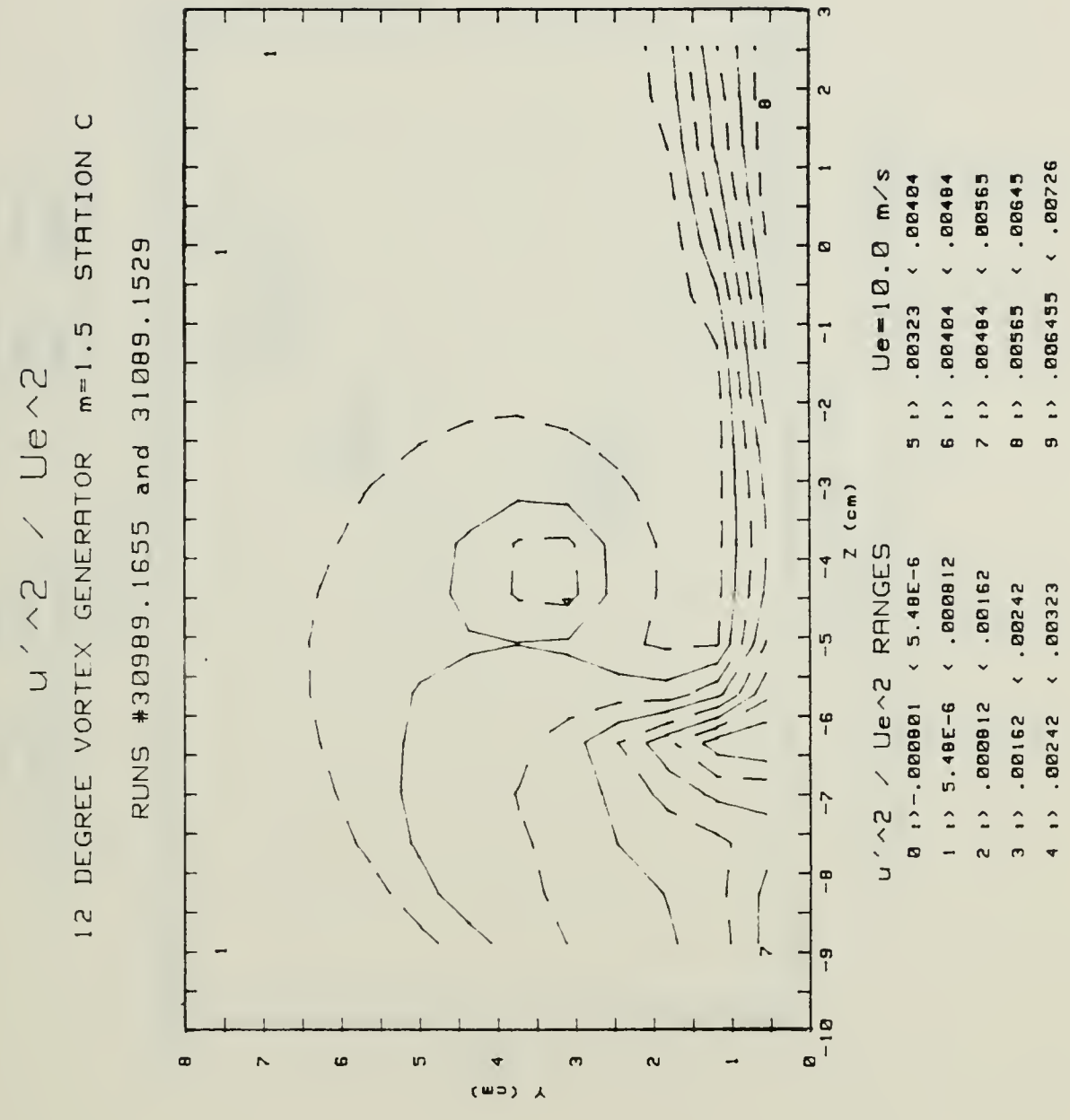

Figure 126. $\overline{u'^2}$ (boundary layer / vortex / wall jet, station C, $\Delta = 0.25$ inches)

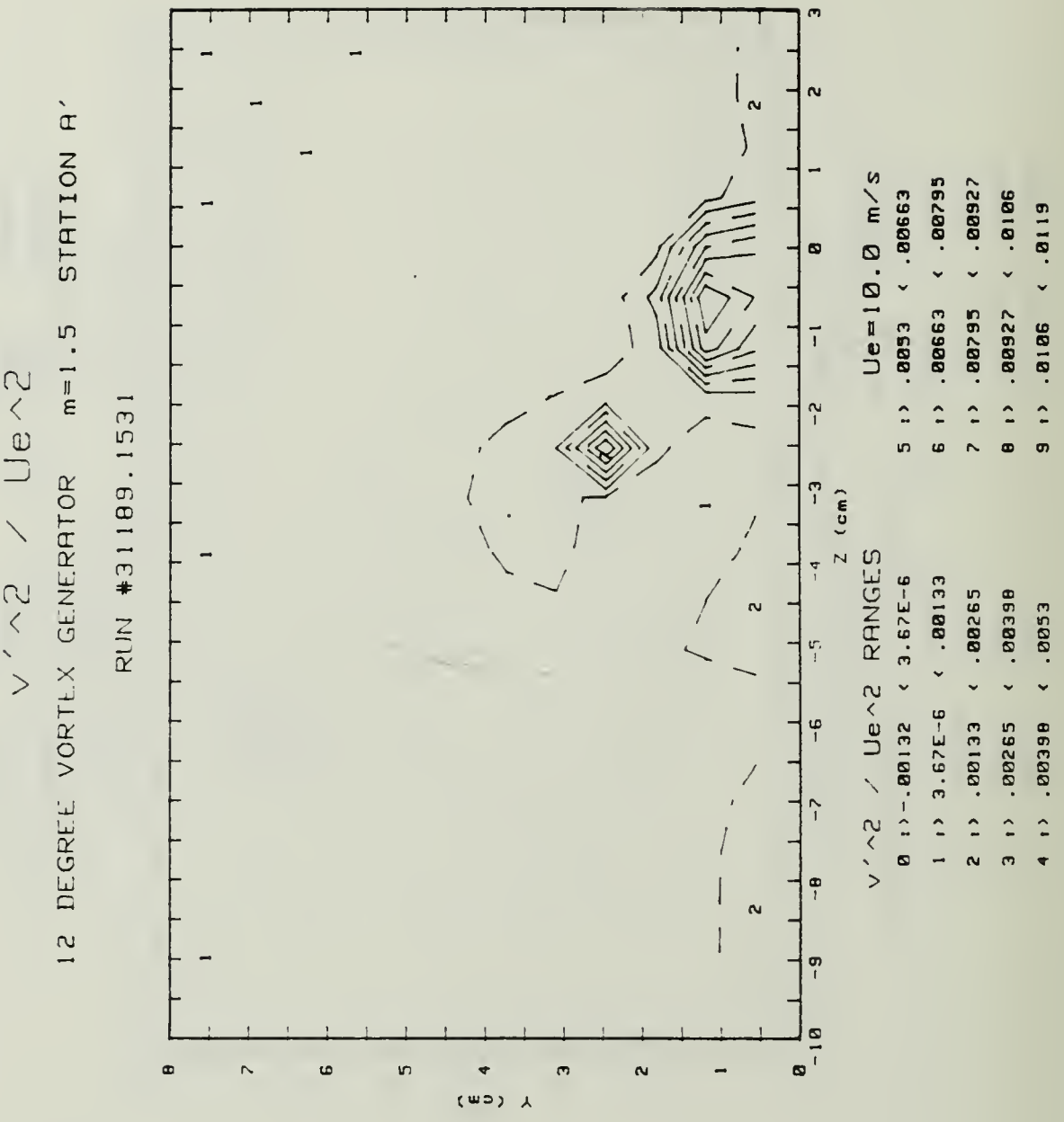

Figure 127. $\overline{v'^2}$ (boundary layer / vortex / wall jet, station A′, Δ = 0.25 inches)

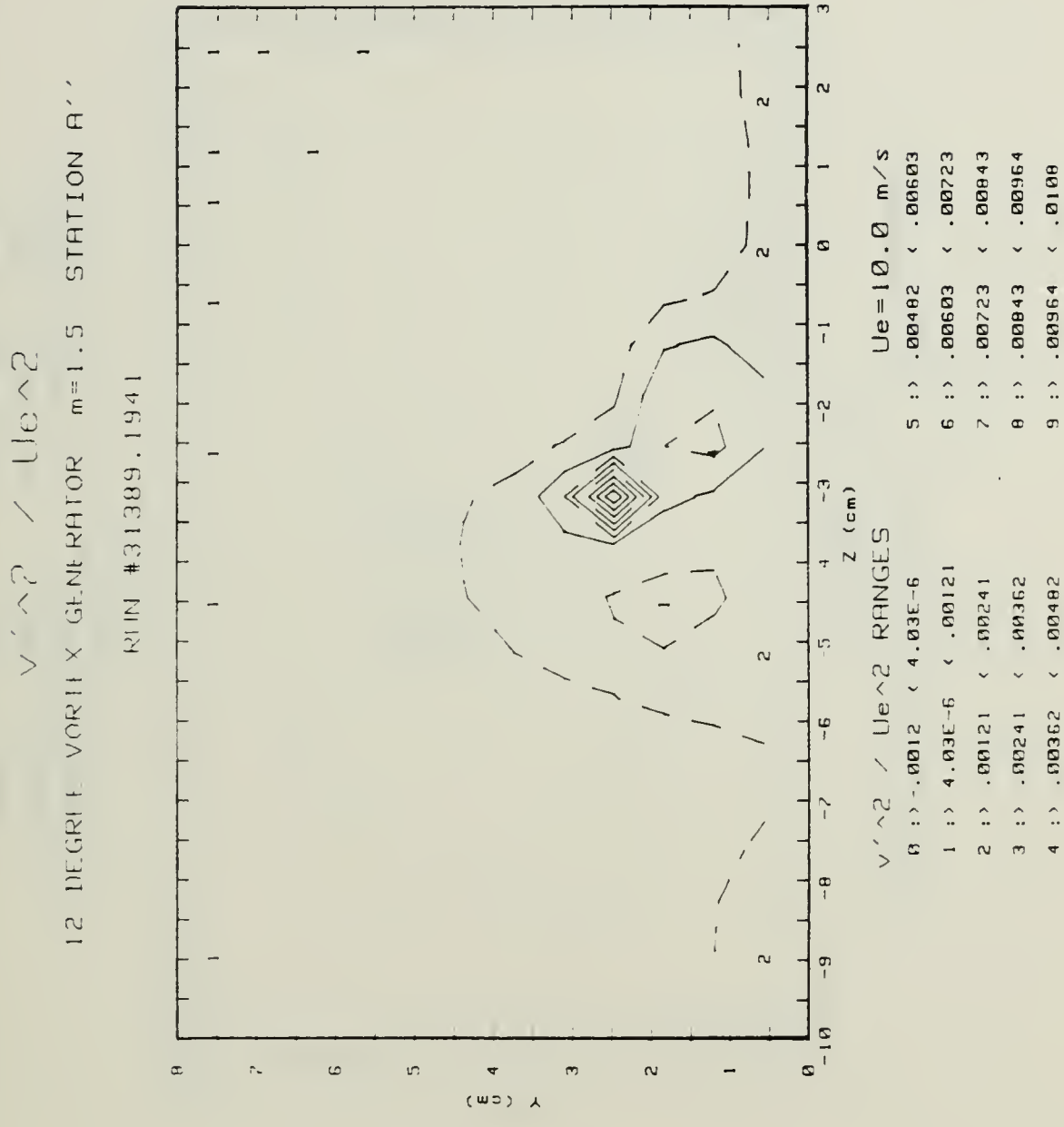

Figure 128. $\overline{v'^2}$ (boundary layer / vortex / wall jet, station A″, Δ = 0.25 inches)

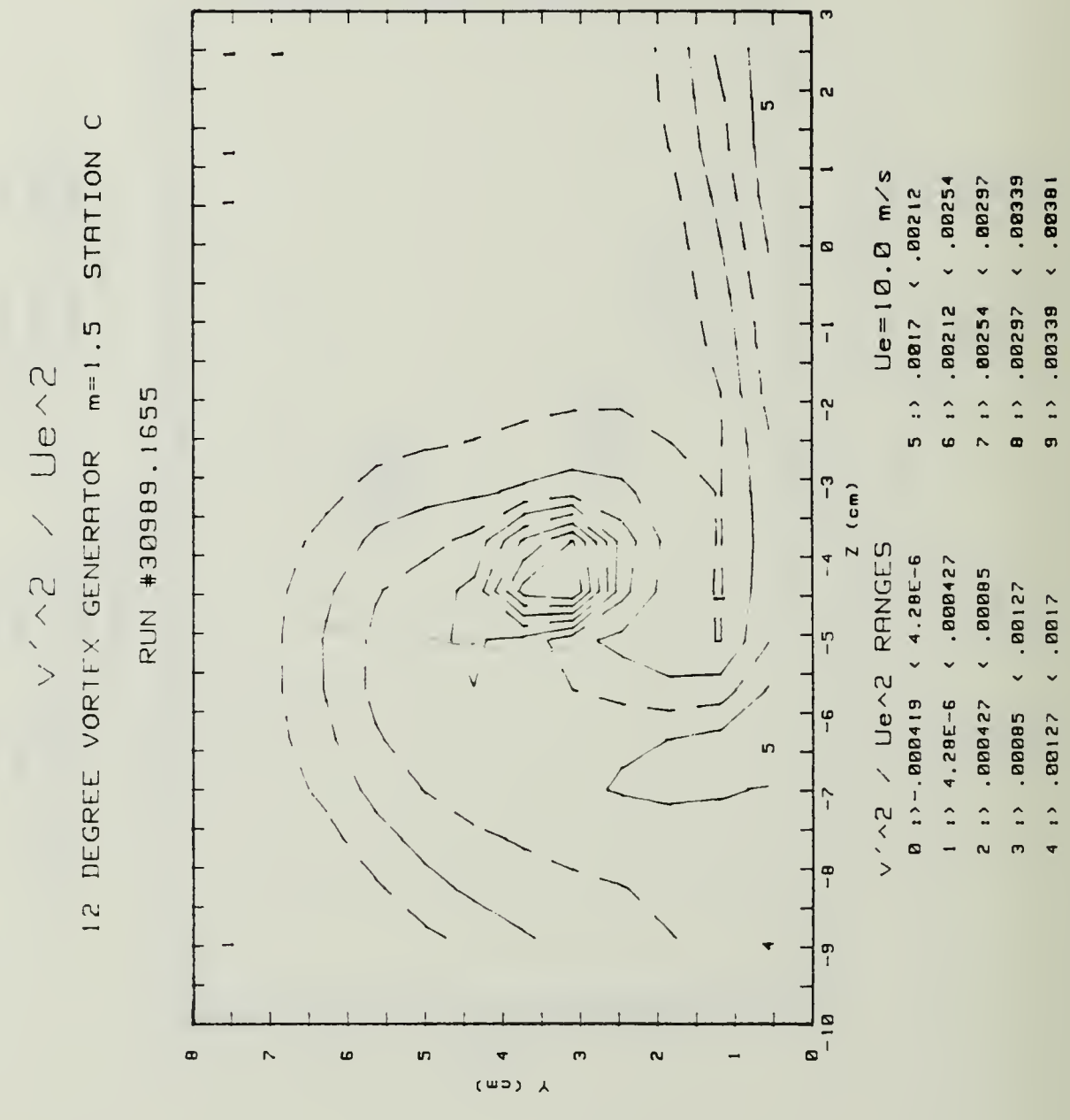

Figure 129. $\overline{v'^2}$ (boundary layer / vortex / wall jet, station C, $\Delta = 0.25$ inches)

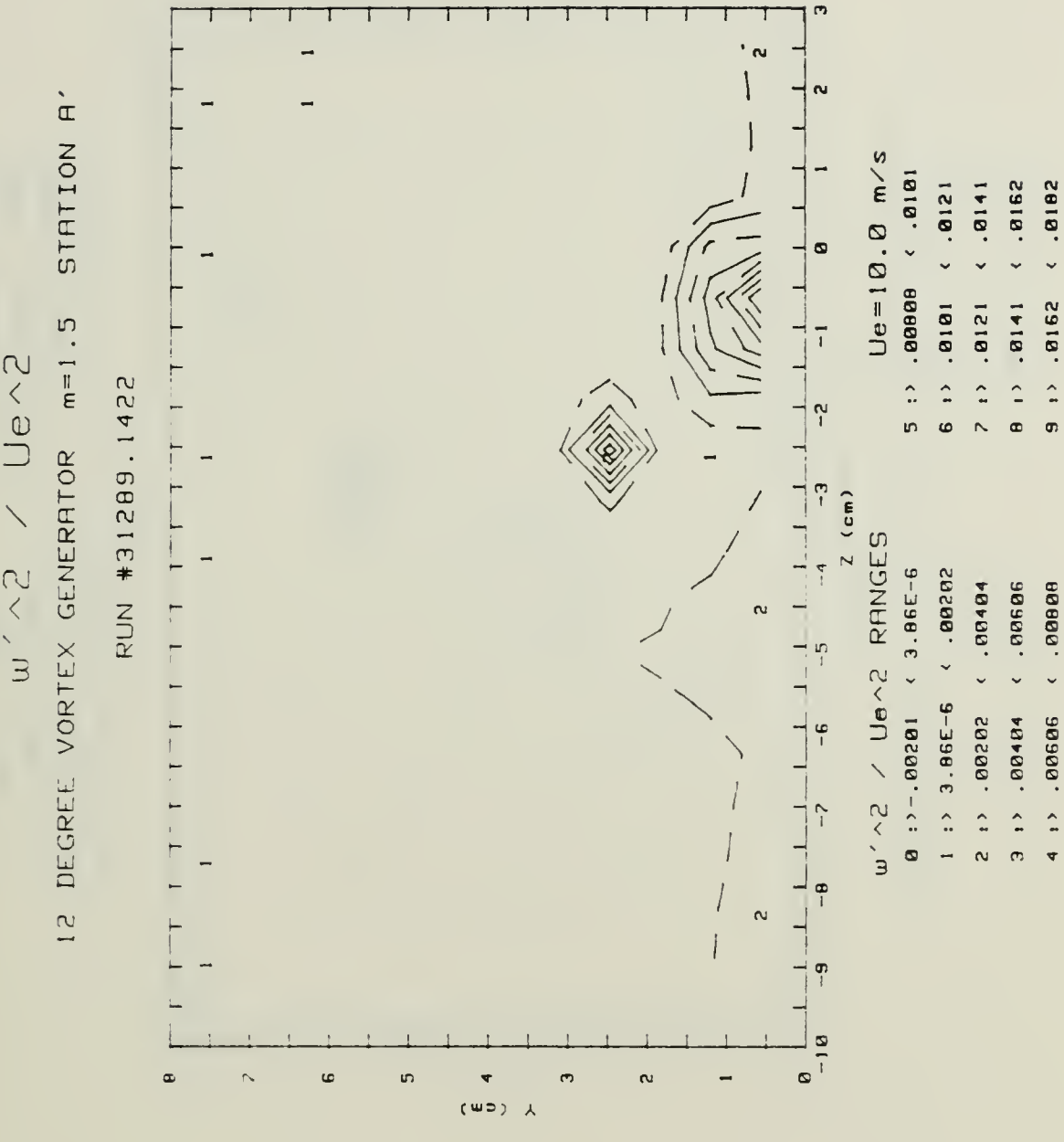

Figure 130. $\overline{w'^2}$ (boundary layer / vortex / wall jet, station A′, Δ = 0.25 inches)

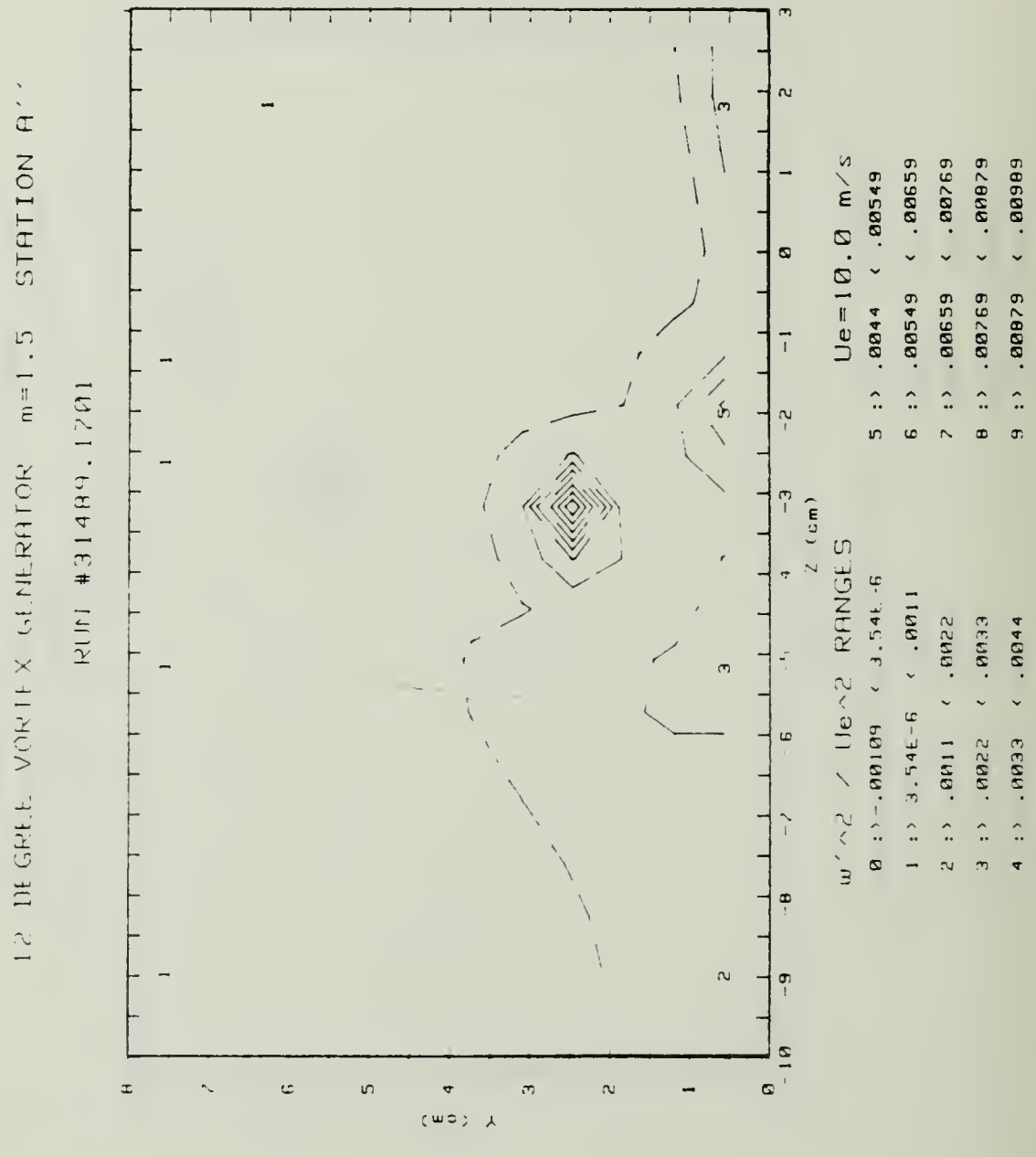

Figure 131. $\overline{w'^2}$ (boundary layer / vortex / wall jet, station A″, Δ = 0.25 inches)

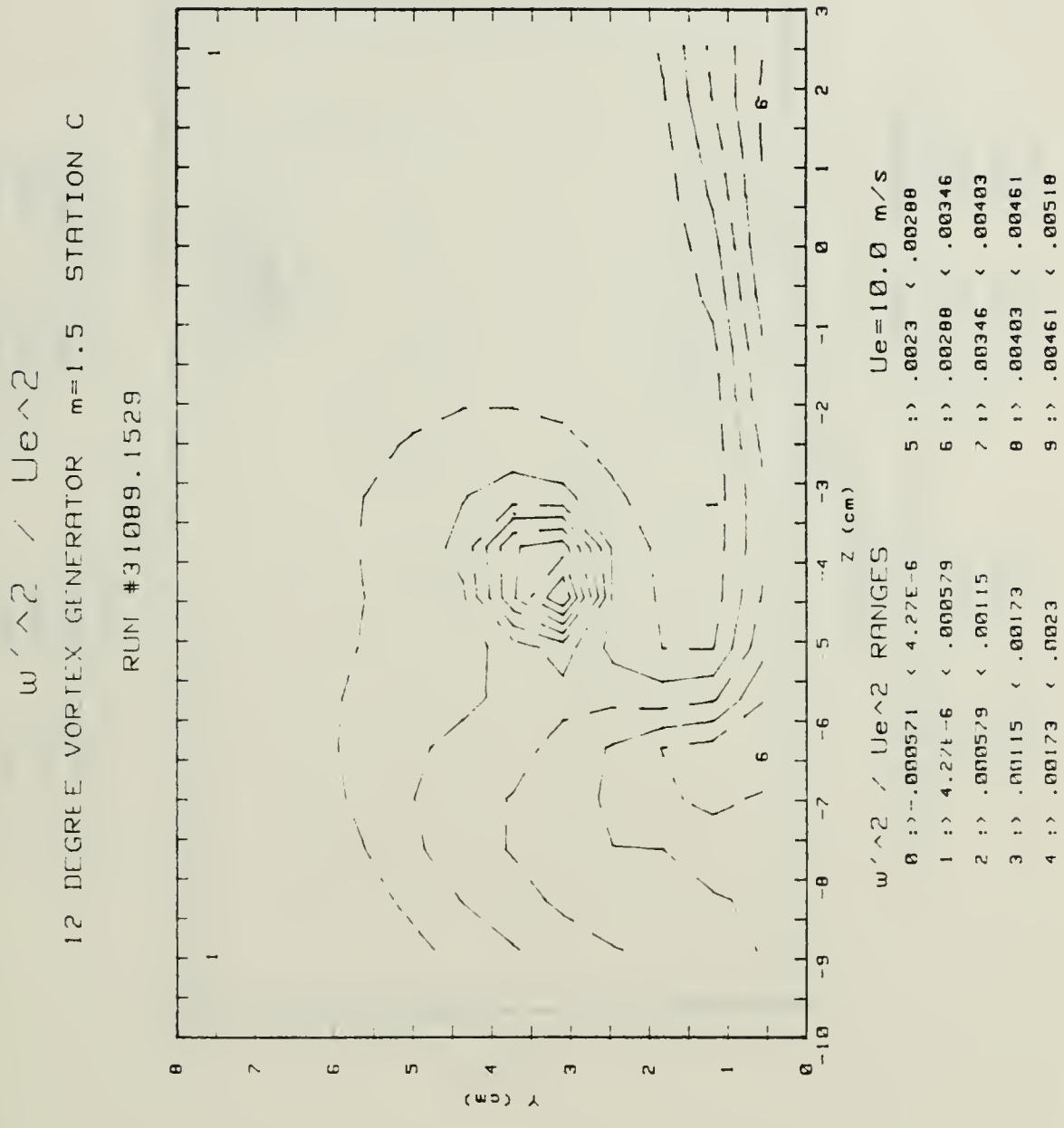

Figure 132. $\overline{w'^2}$ (boundary layer / vortex / wall jet, station C, $\Delta = 0.25$ inches)

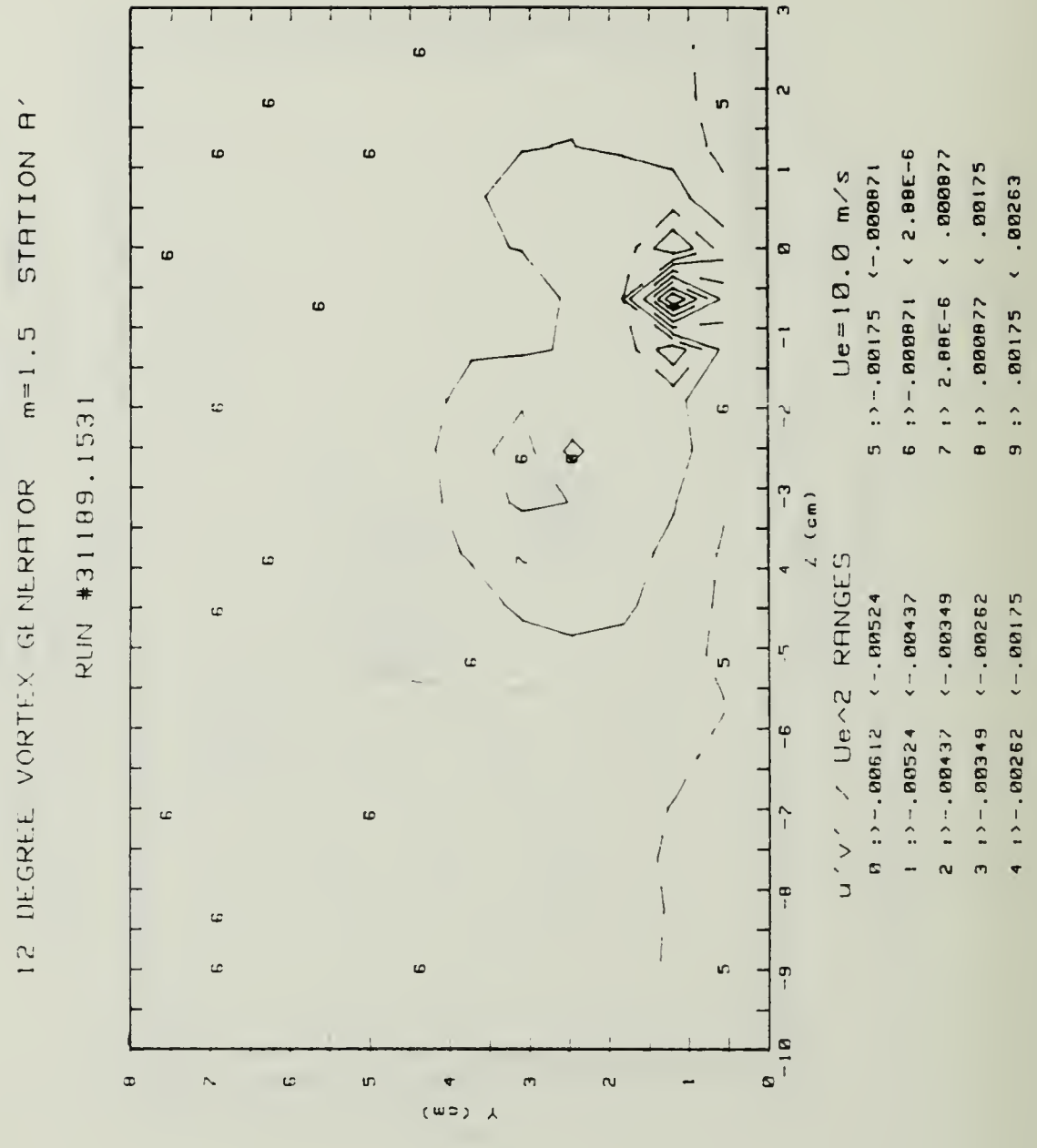

Figure 133. $\overline{u'v'}$ (boundary layer / vortex / wall jet, station A′, Δ = 0.25 inches)

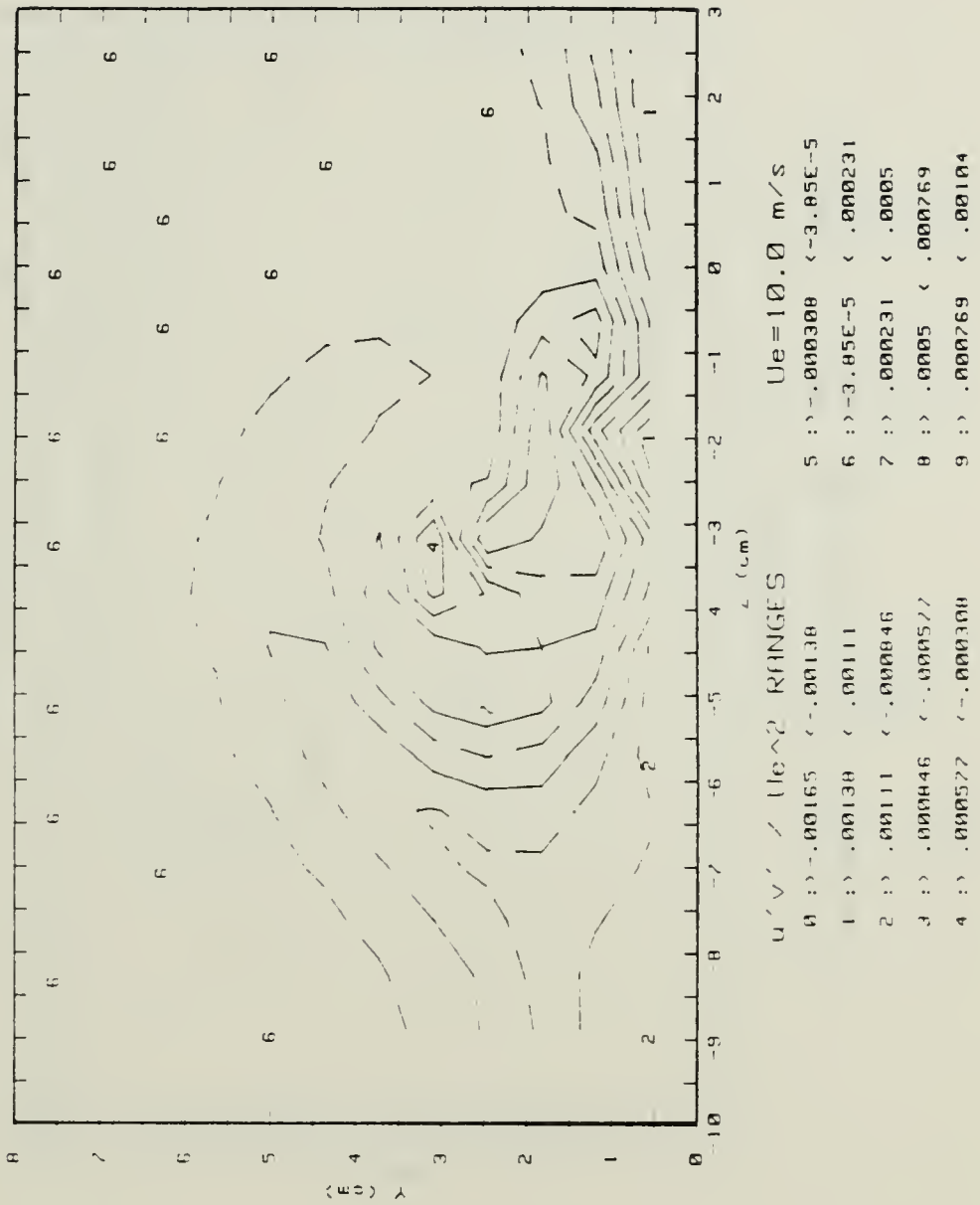

Figure 134. $\overline{u'v'}$ (boundary layer / vortex / wall jet, station A'', $\Delta = 0.25$ inches)

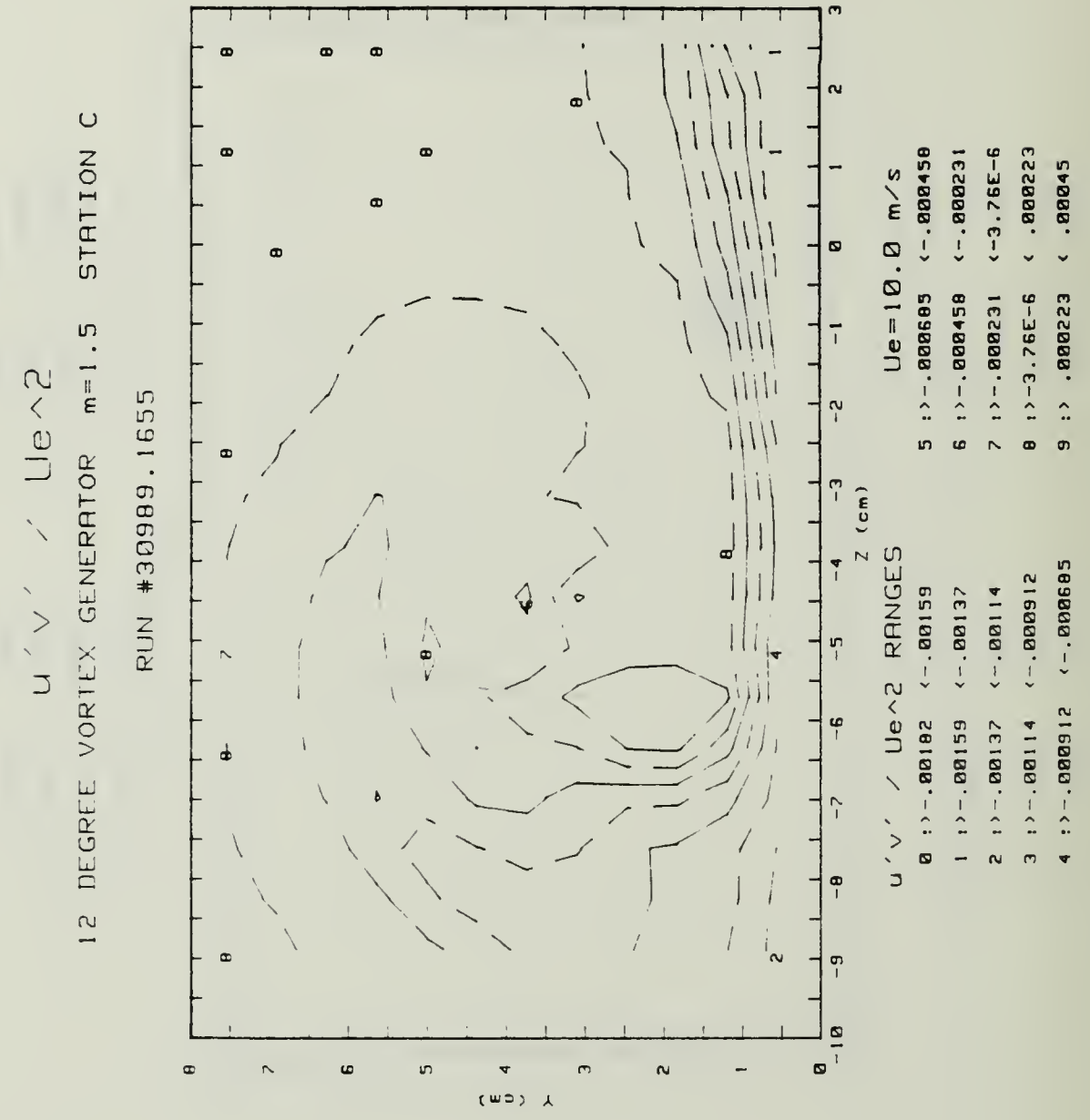

Figure 135. $\overline{u'v'}$ (boundary layer / vortex / wall jet, station C, $\Delta = 0.25$ inches)

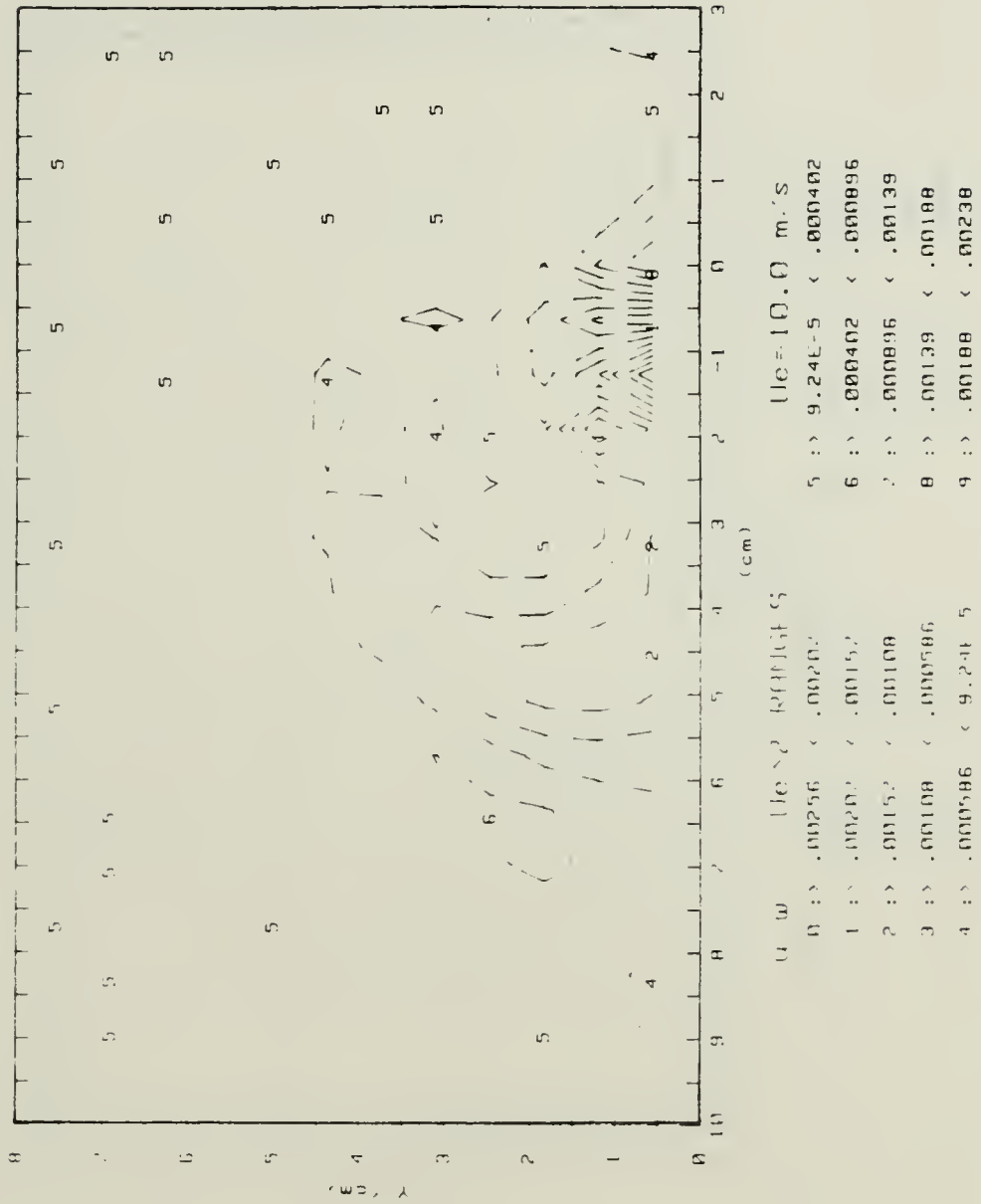

Figure 136. $\overline{u'w'}$ (boundary layer / vortex / wall jet, station A′, Δ = 0.25 inches)

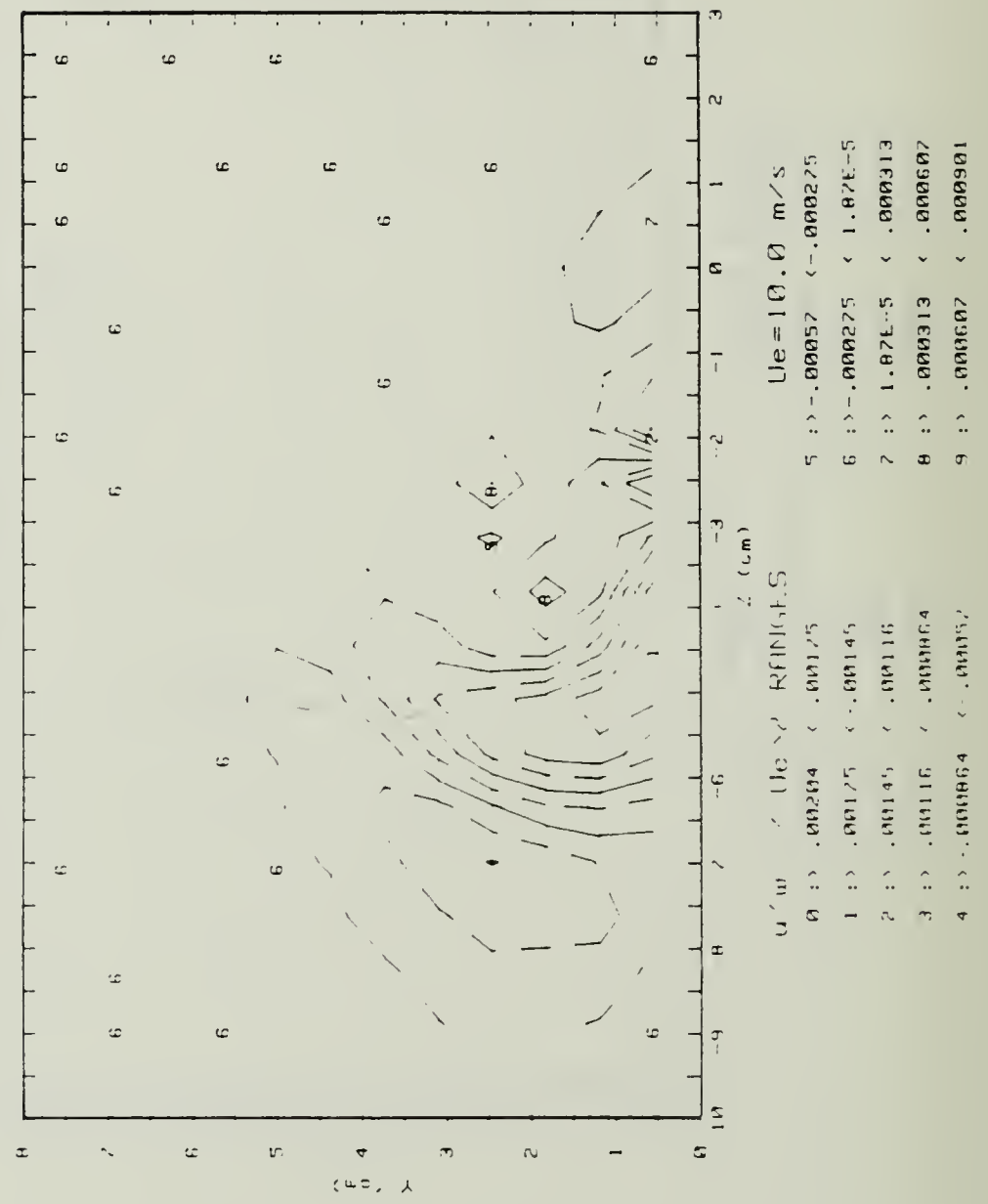

Figure 137. $\overline{u'w'}$ (boundary layer / vortex / wall jet, station A″, Δ = 0.25 inches)

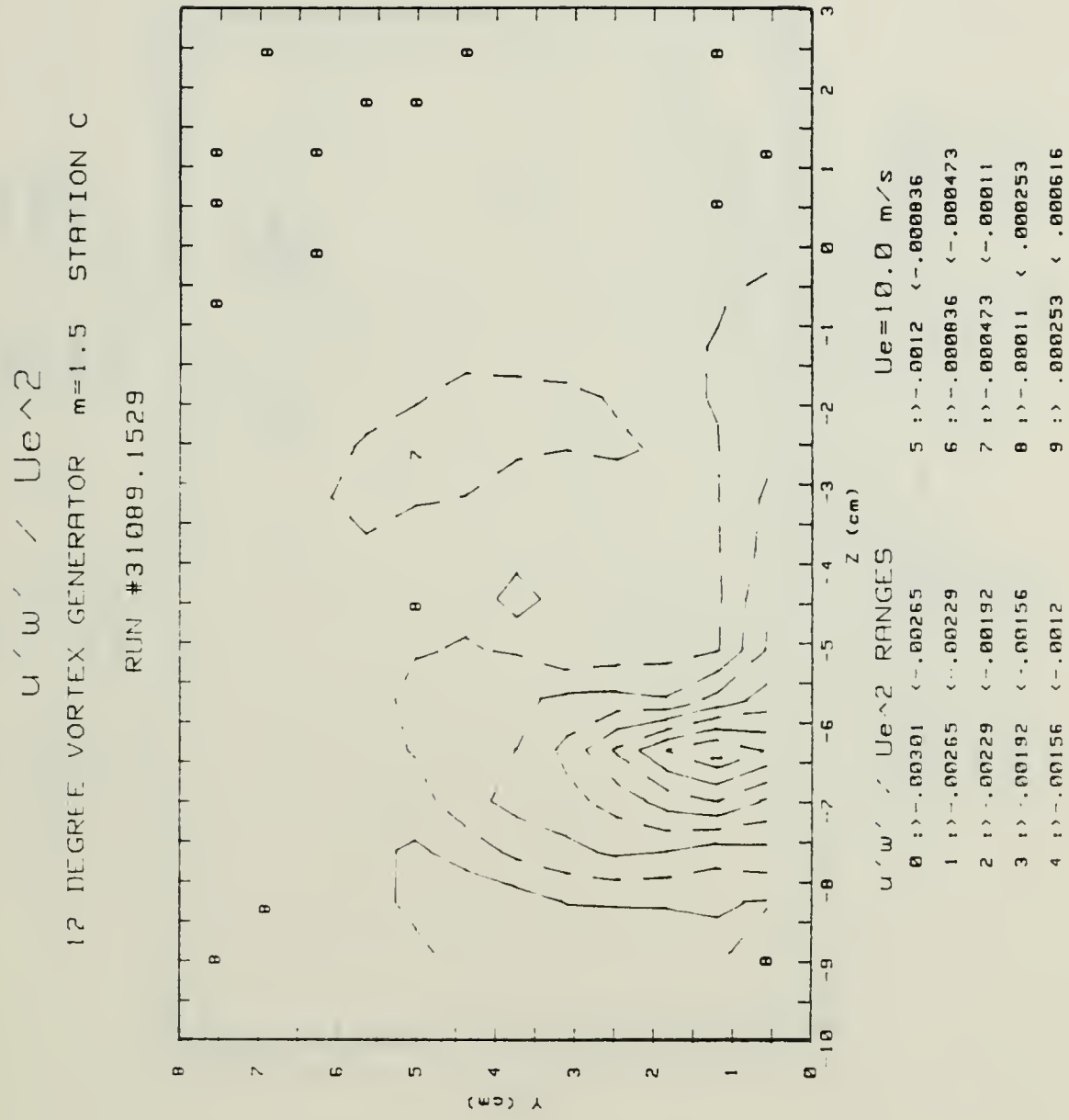

Figure 138. $\overline{u'w'}$ (boundary layer / vortex / wall jet, station C, $\Delta = 0.25$ inches)

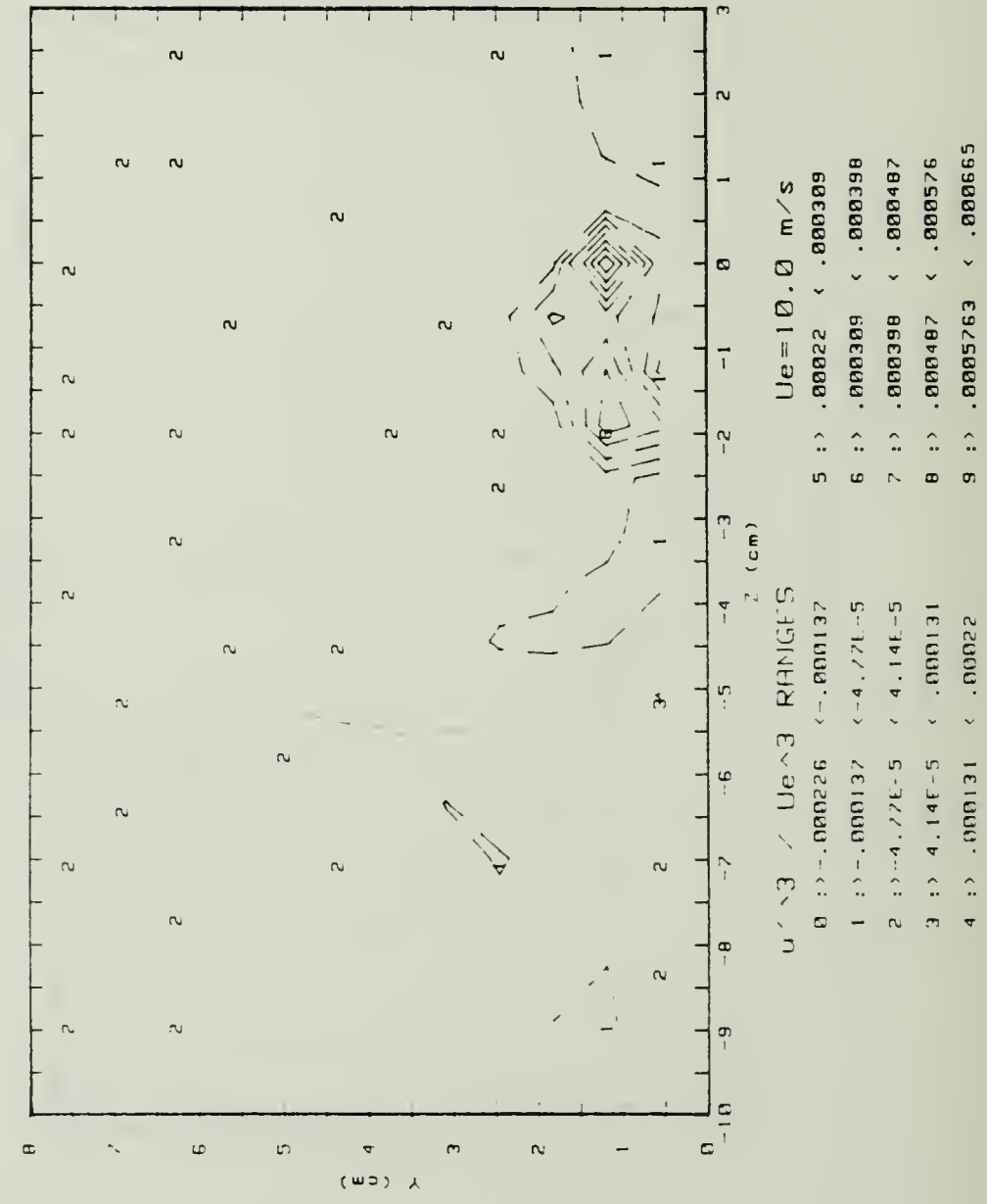

Figure 139. $\overline{u'^3}$ (boundary layer / vortex / wall jet, station A′, Δ = 0.25 inches)

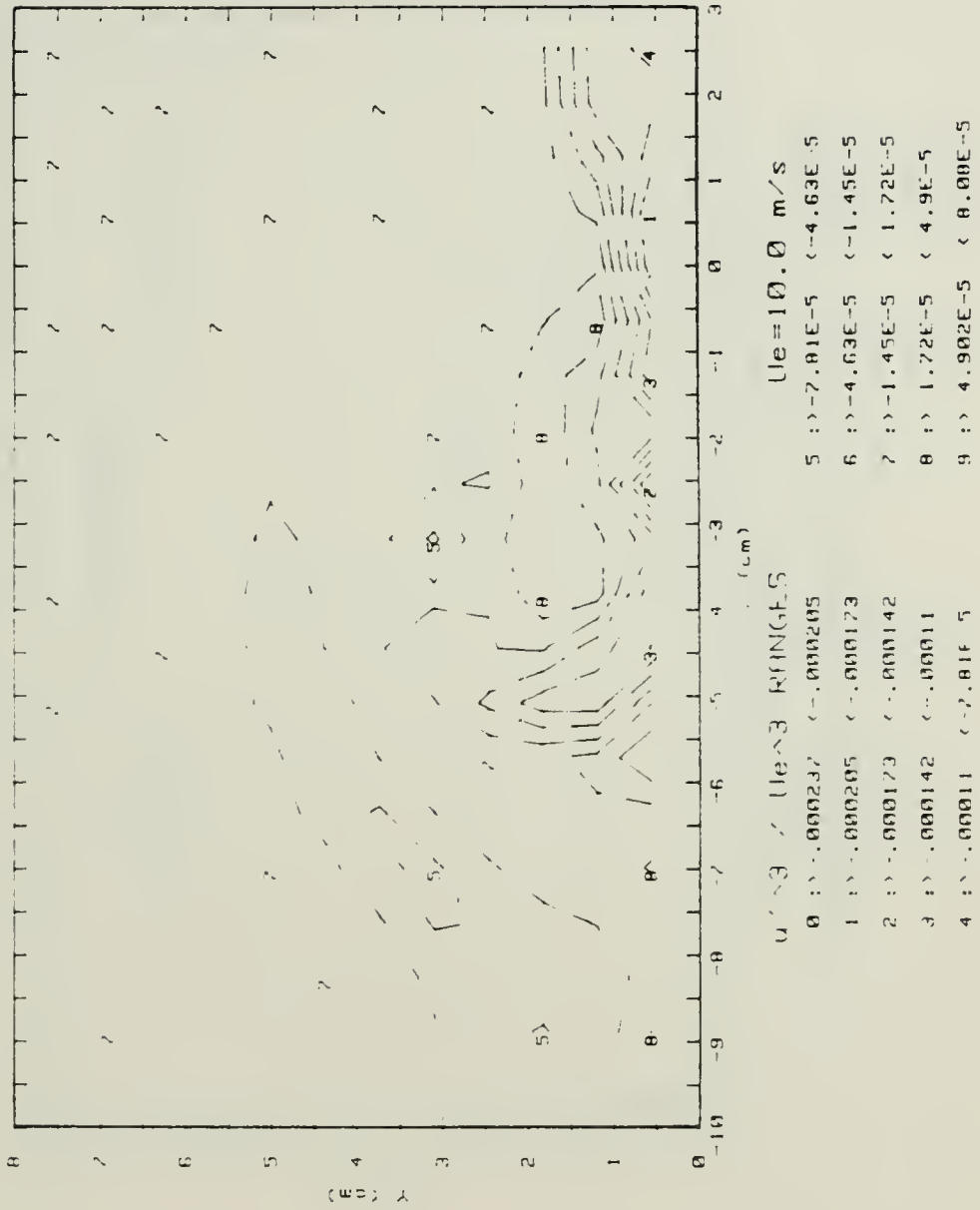

Figure 140. $\overline{u'^3}$ (boundary layer / vortex / wall jet, station A'', $\Delta = 0.25$ inches)

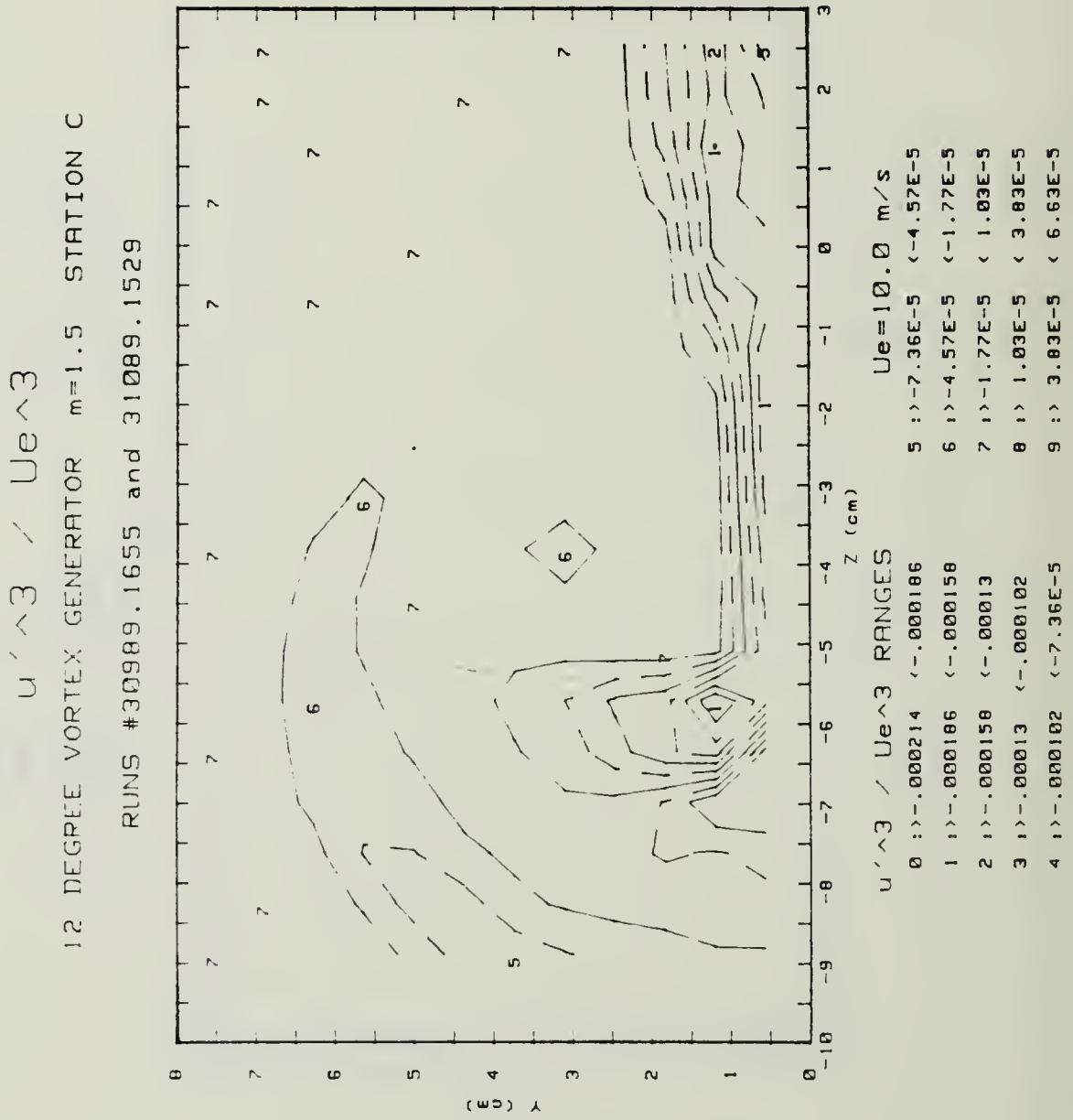

Figure 141. $\overline{u'^3}$ (boundary layer / vortex / wall jet, station C, $\Delta = 0.25$ inches)

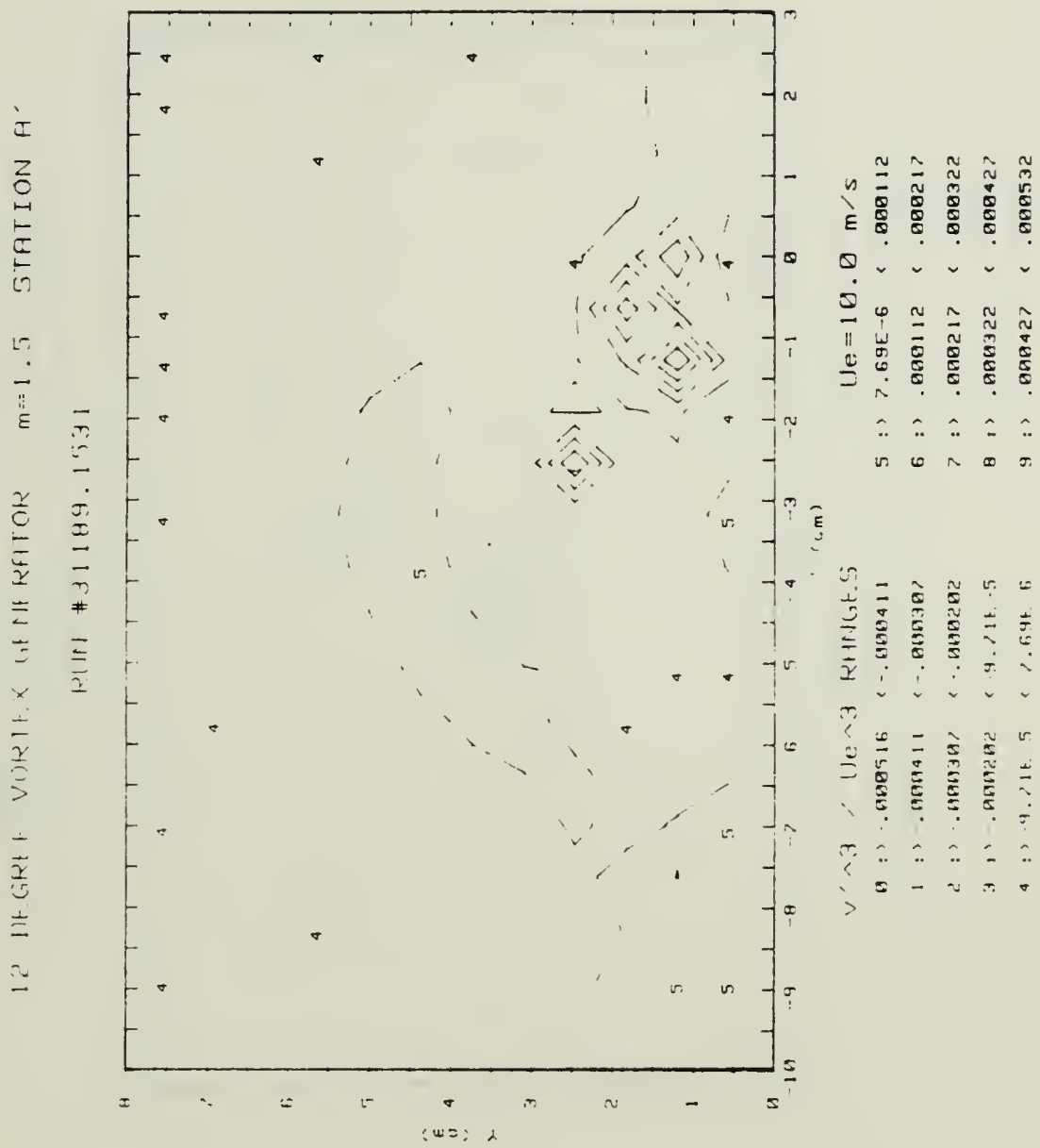

Figure 142. $\overline{v'^3}$ (boundary layer / vortex / wall jet, station A′, Δ = 0.25 inches)

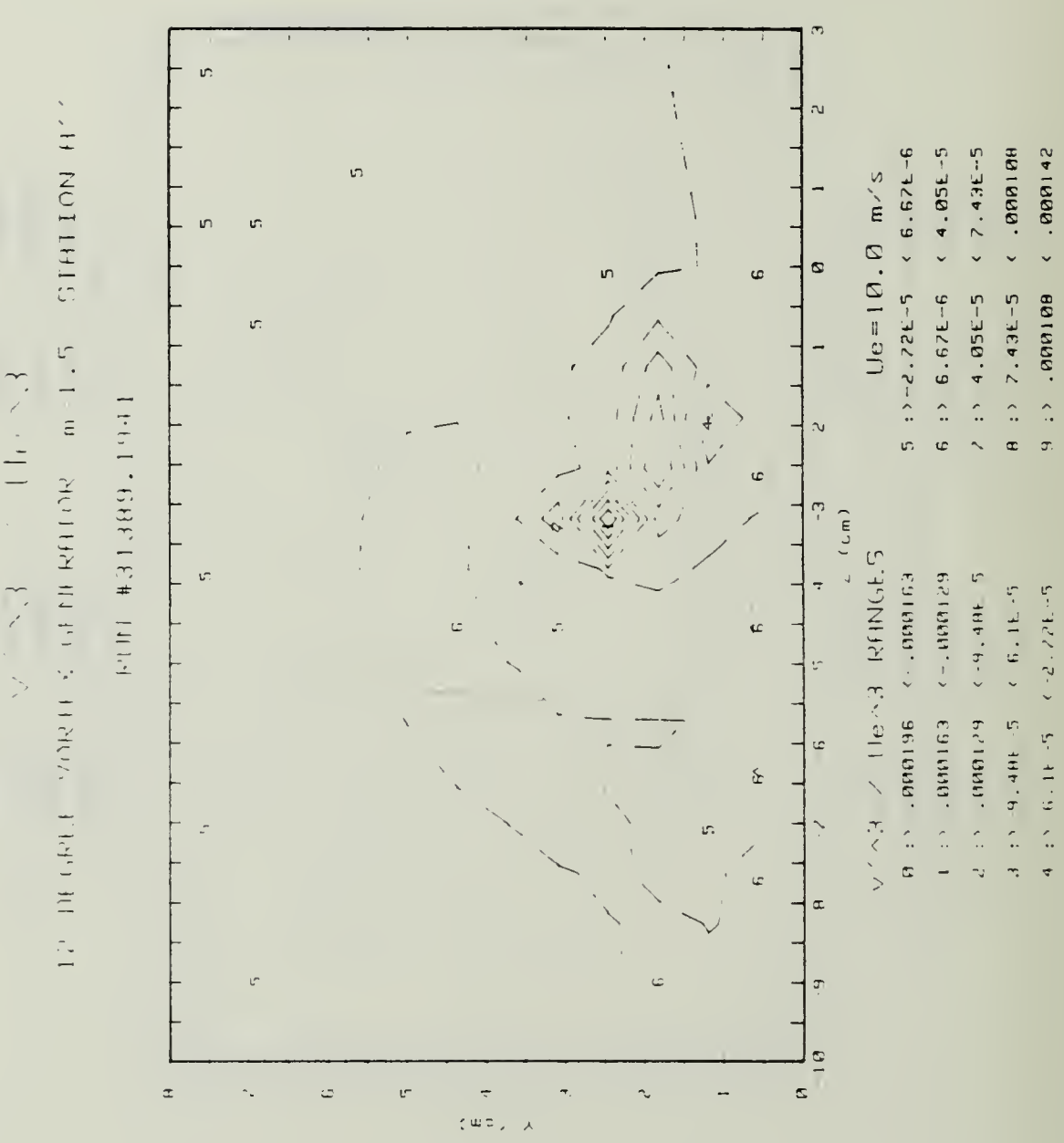

Figure 143. $\overline{v'^3}$ (boundary layer / vortex / wall jet, station A'', $\Delta = 0.25$ inches)

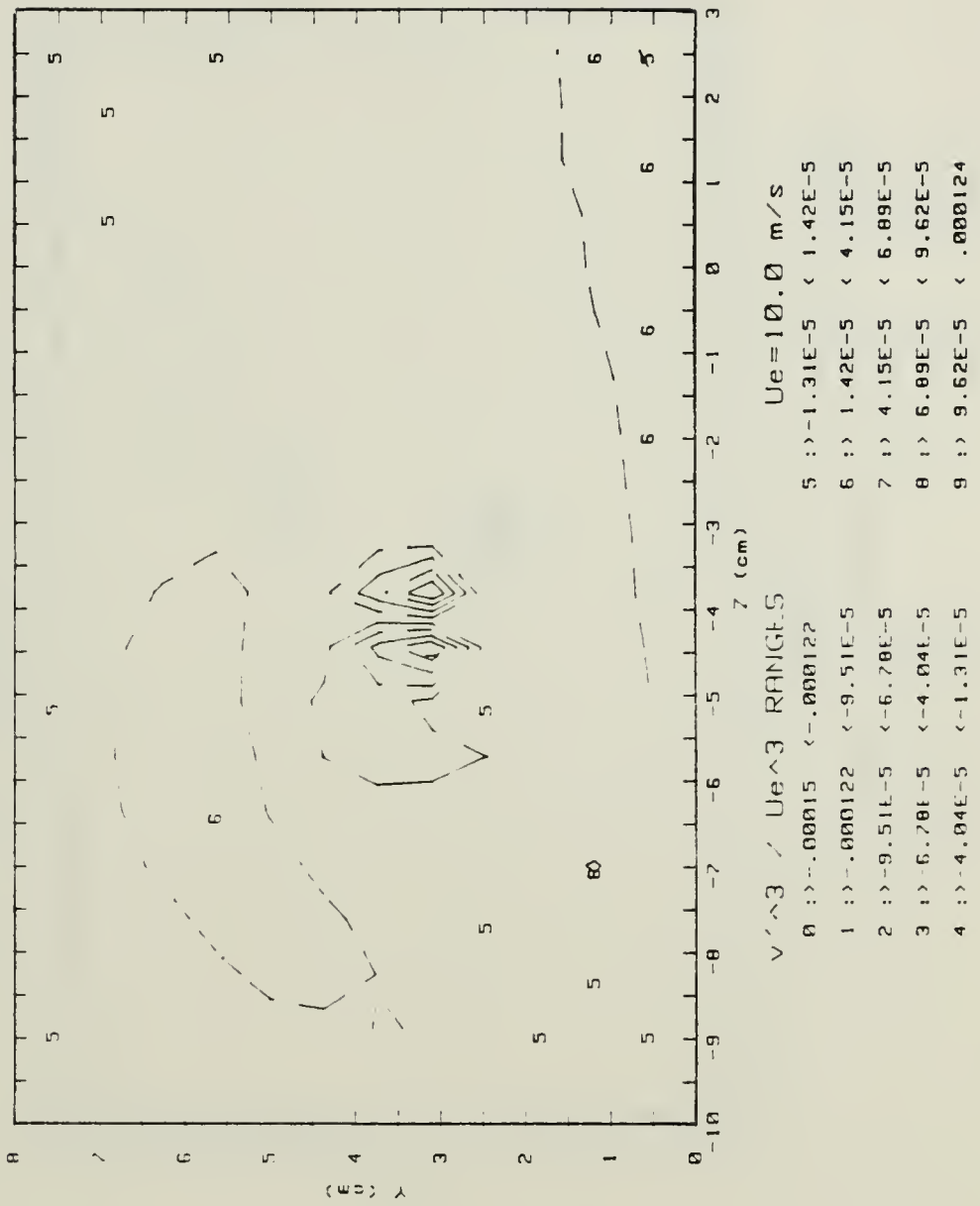

Figure 144. $\overline{v'^3}$ (boundary layer / vortex / wall jet, station C, $\Delta = 0.25$ inches)

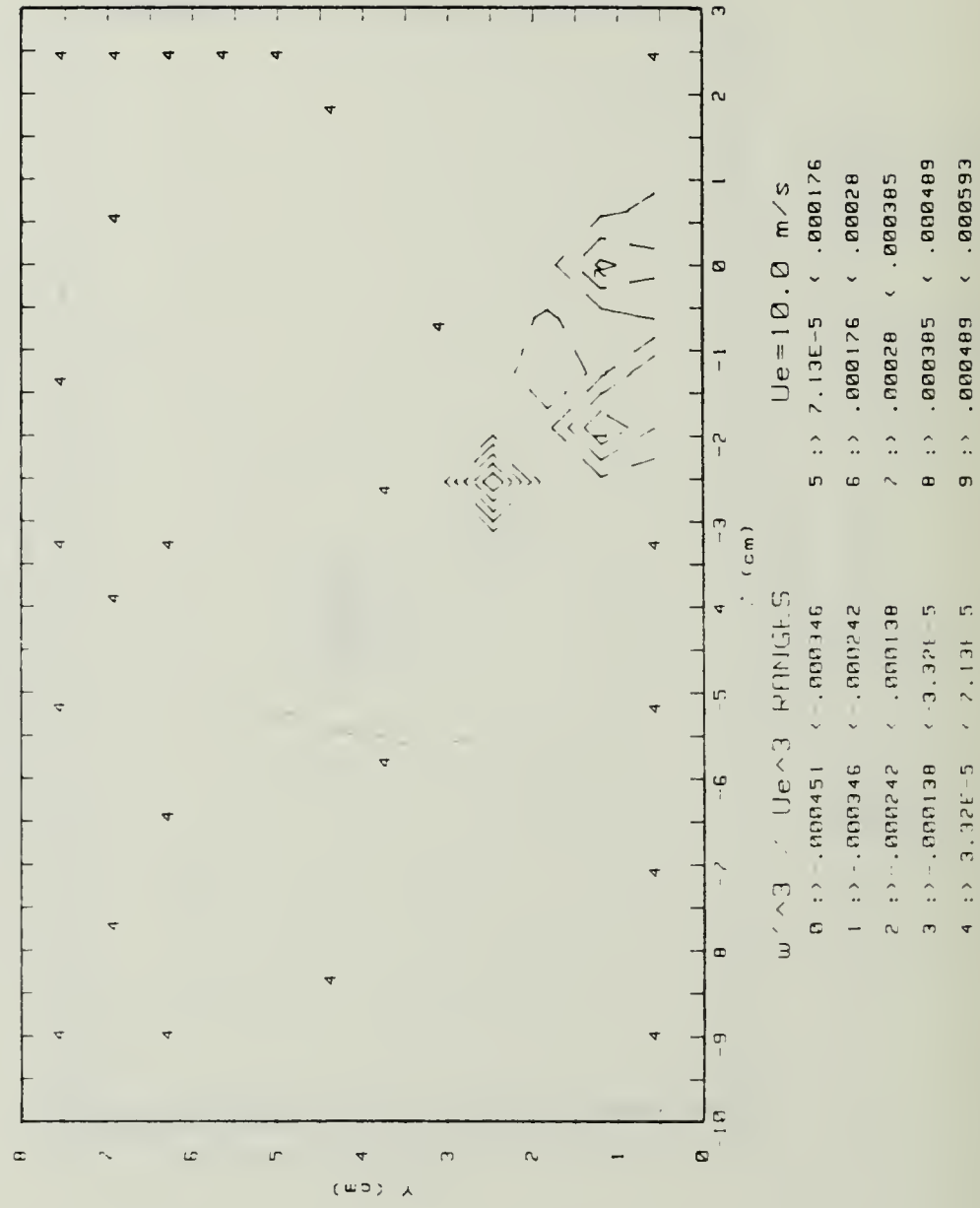

Figure 145. $\overline{w'^3}$ (boundary layer / vortex / wall jet, station A′, Δ = 0.25 inches)

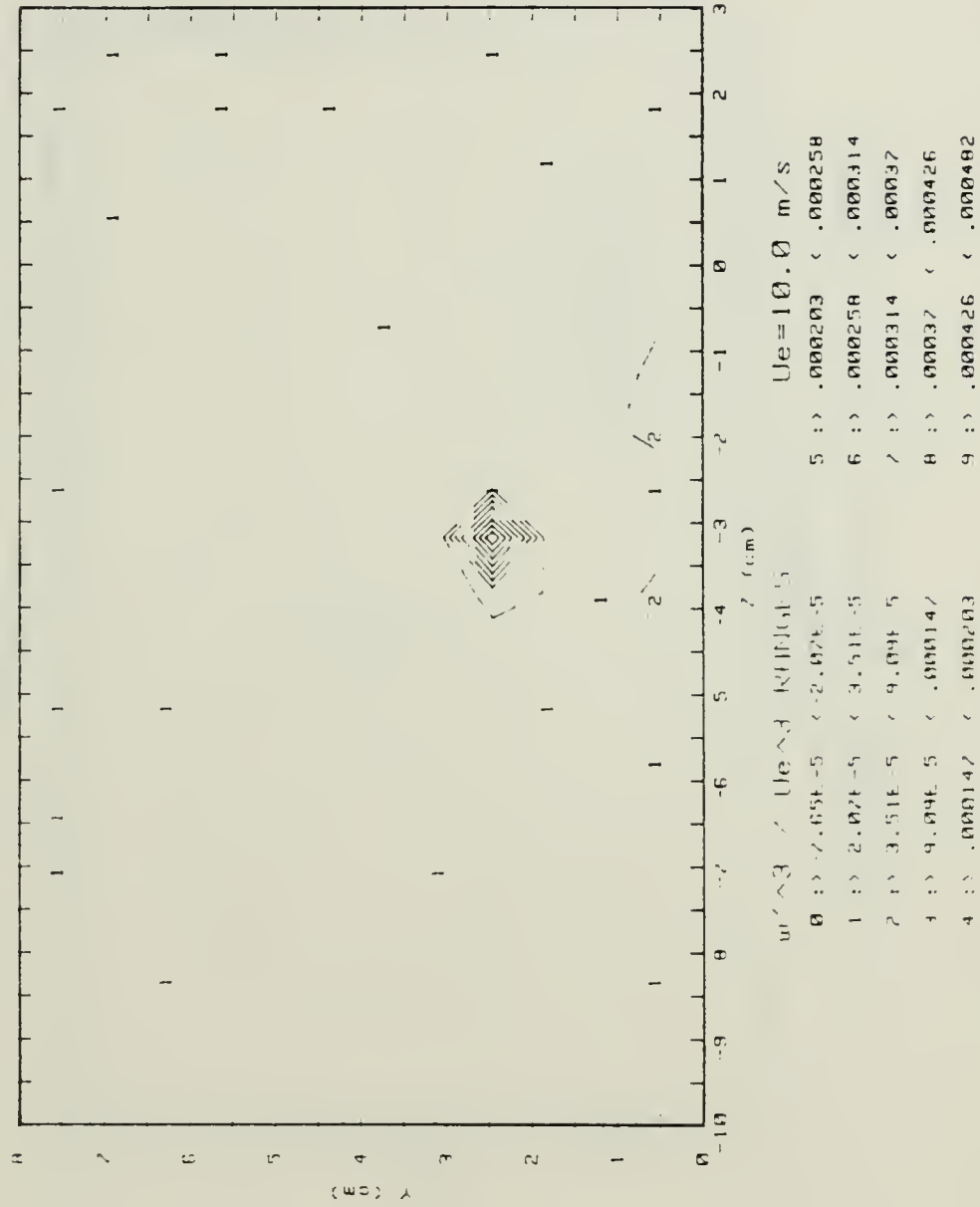

Figure 146. $\overline{w'^3}$ (boundary layer / vortex / wall jet, station A″, Δ = 0.25 inches)

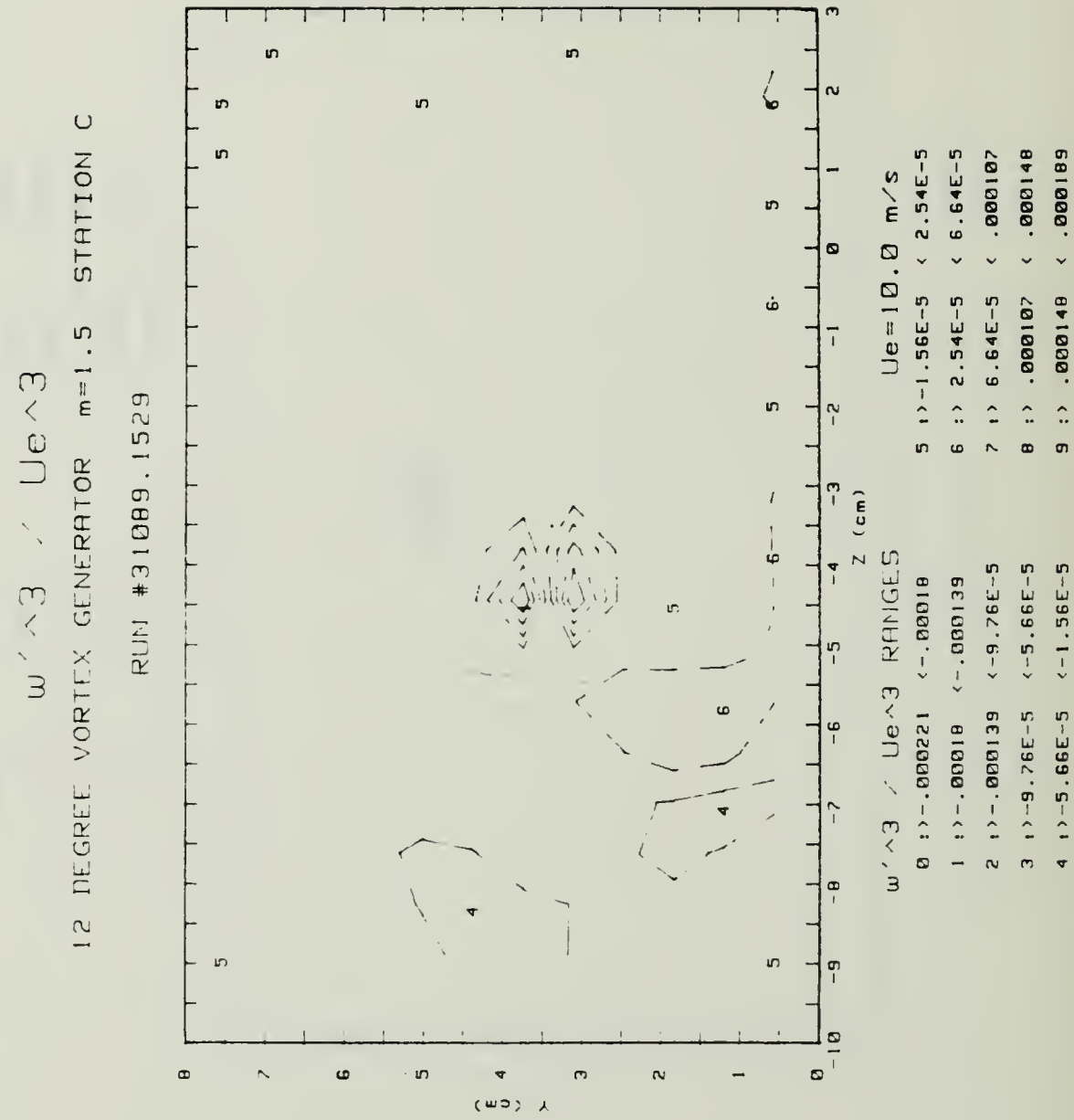

Figure 147. $\overline{w'^3}$ (boundary layer / vortex / wall jet, station C, Δ = 0.25 inches)

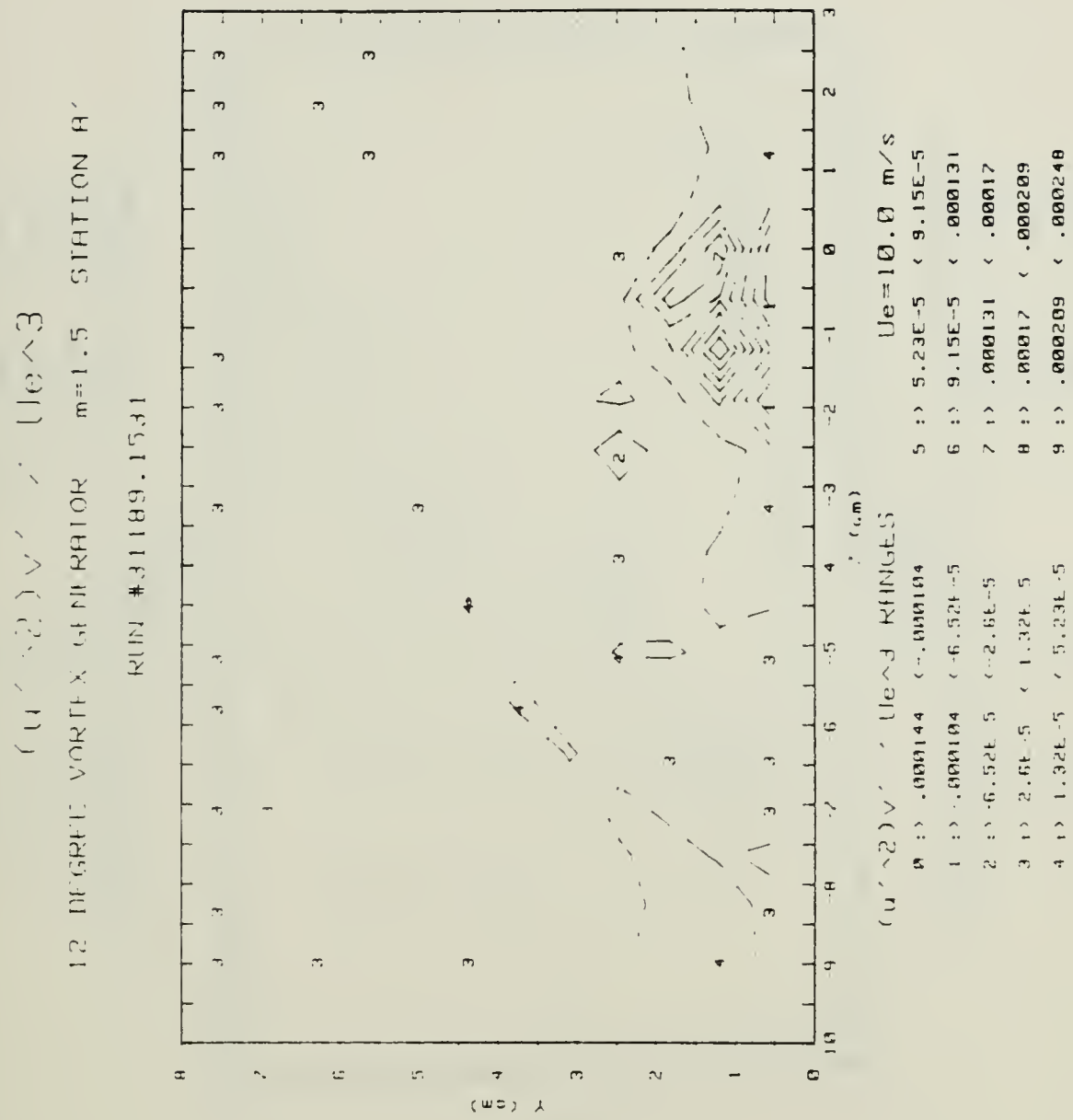

Figure 148. $\overline{u'v'}$ (boundary layer / vortex / wall jet, station A', $\Delta = 0.25$ inches)

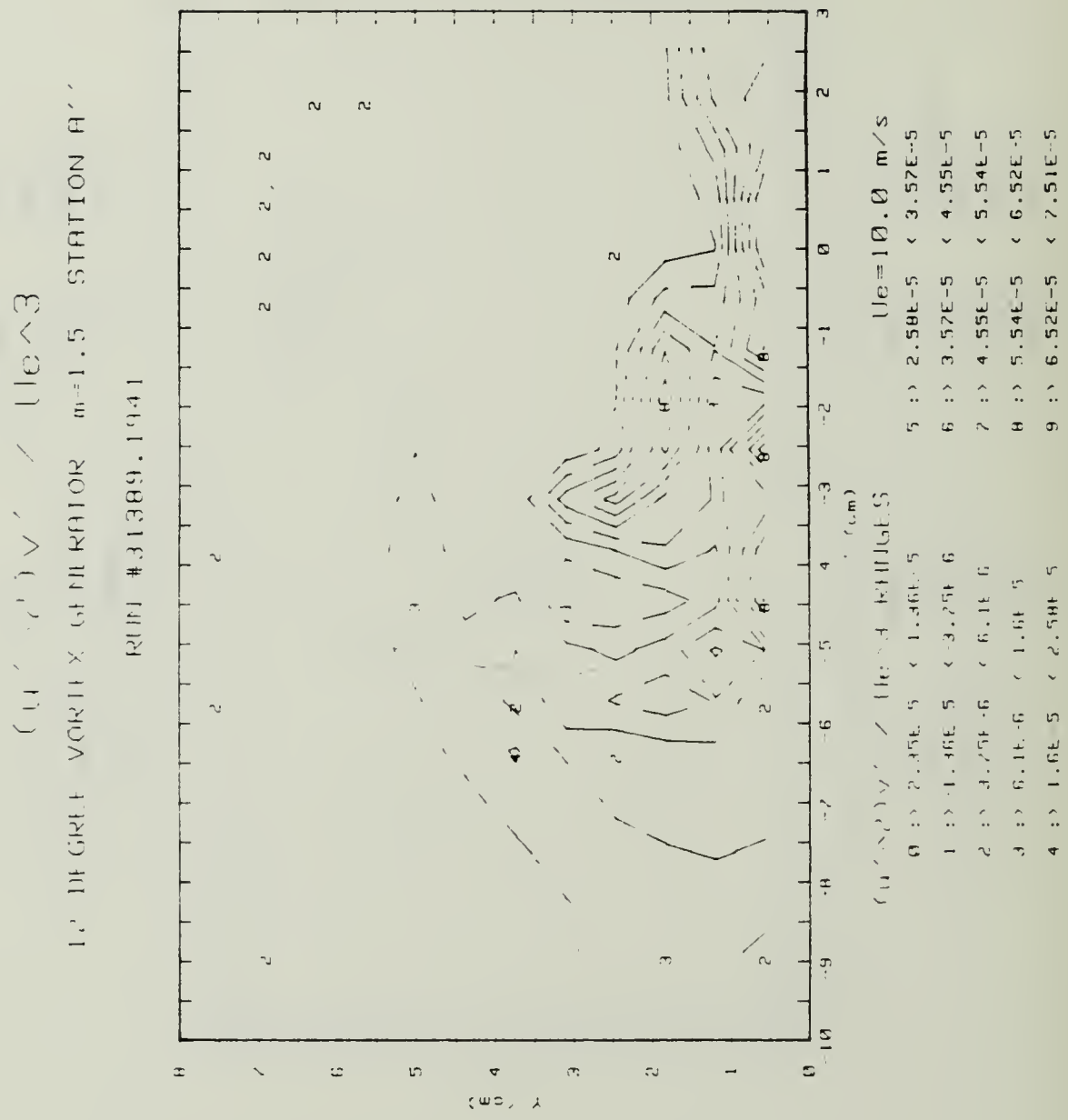

Figure 149. $\overline{u'v'}$ (boundary layer / vortex / wall jet, station A'', $\Delta = 0.25$ inches)

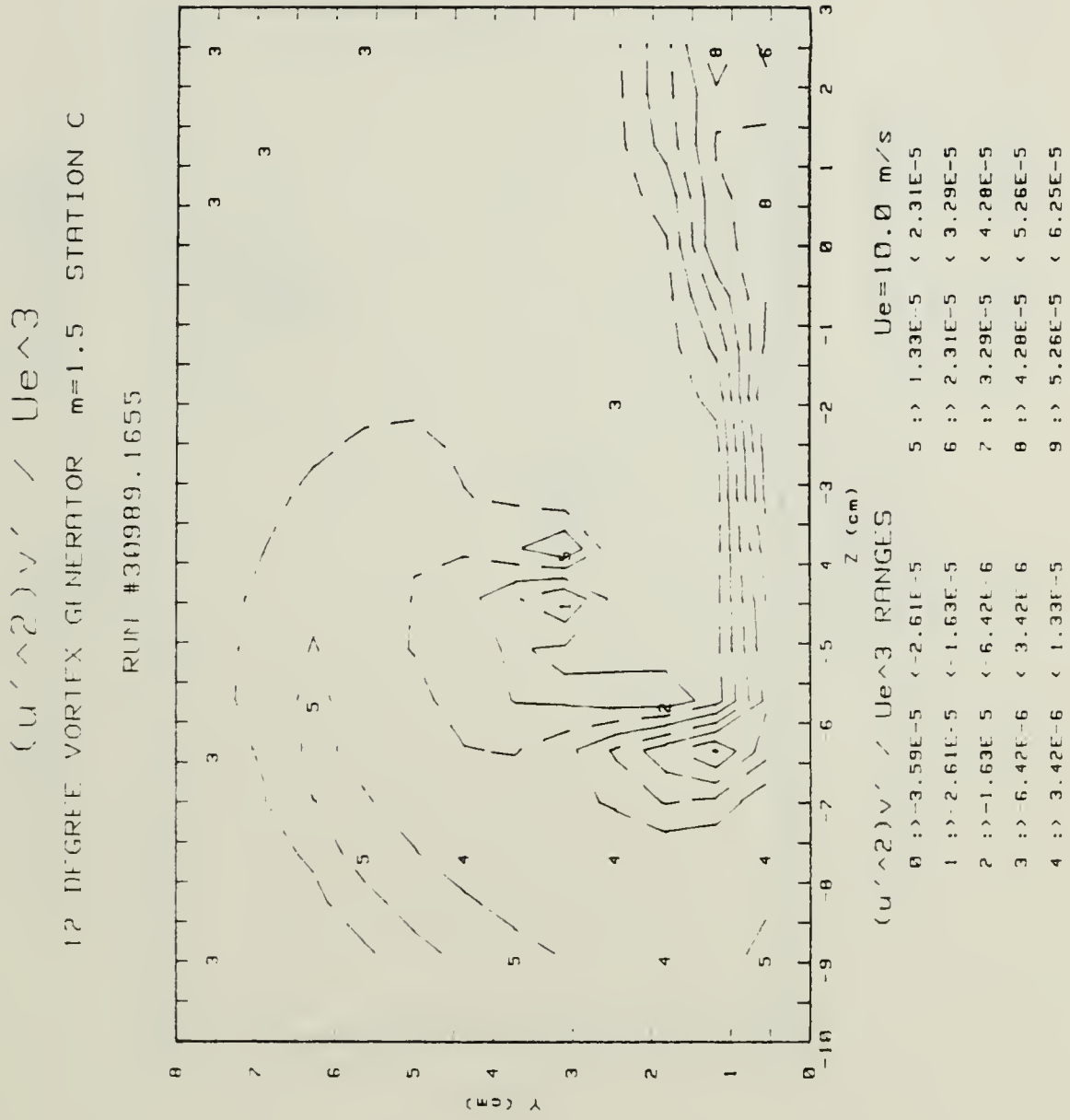

Figure 150. $\overline{u'v'}$ (boundary layer / vortex / wall jet, station C, $\Delta = 0.25$ inches)

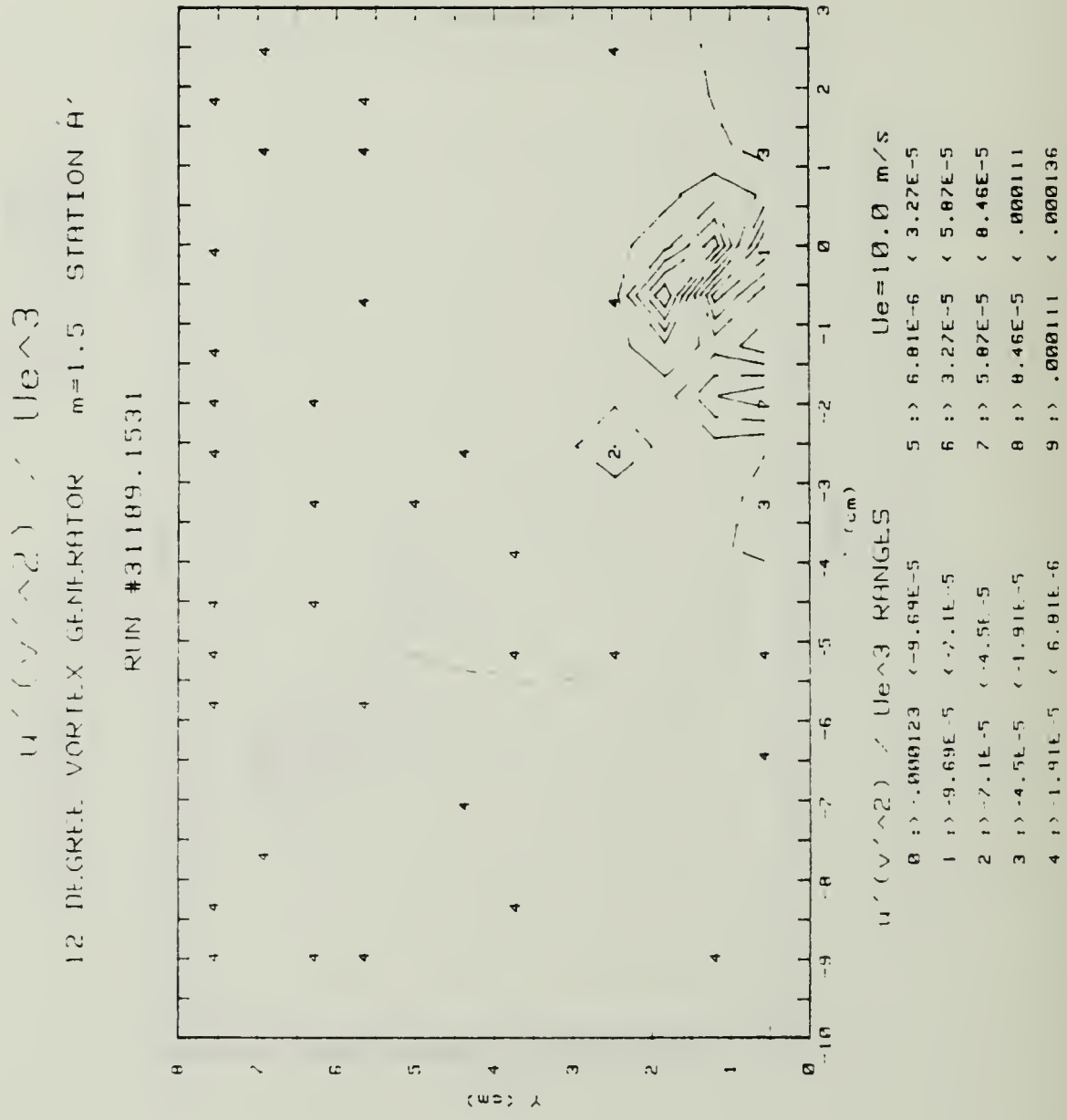

Figure 151. $\overline{u'v'^2}$ (boundary layer / vortex / wall jet, station A′, Δ = 0.25 inches)

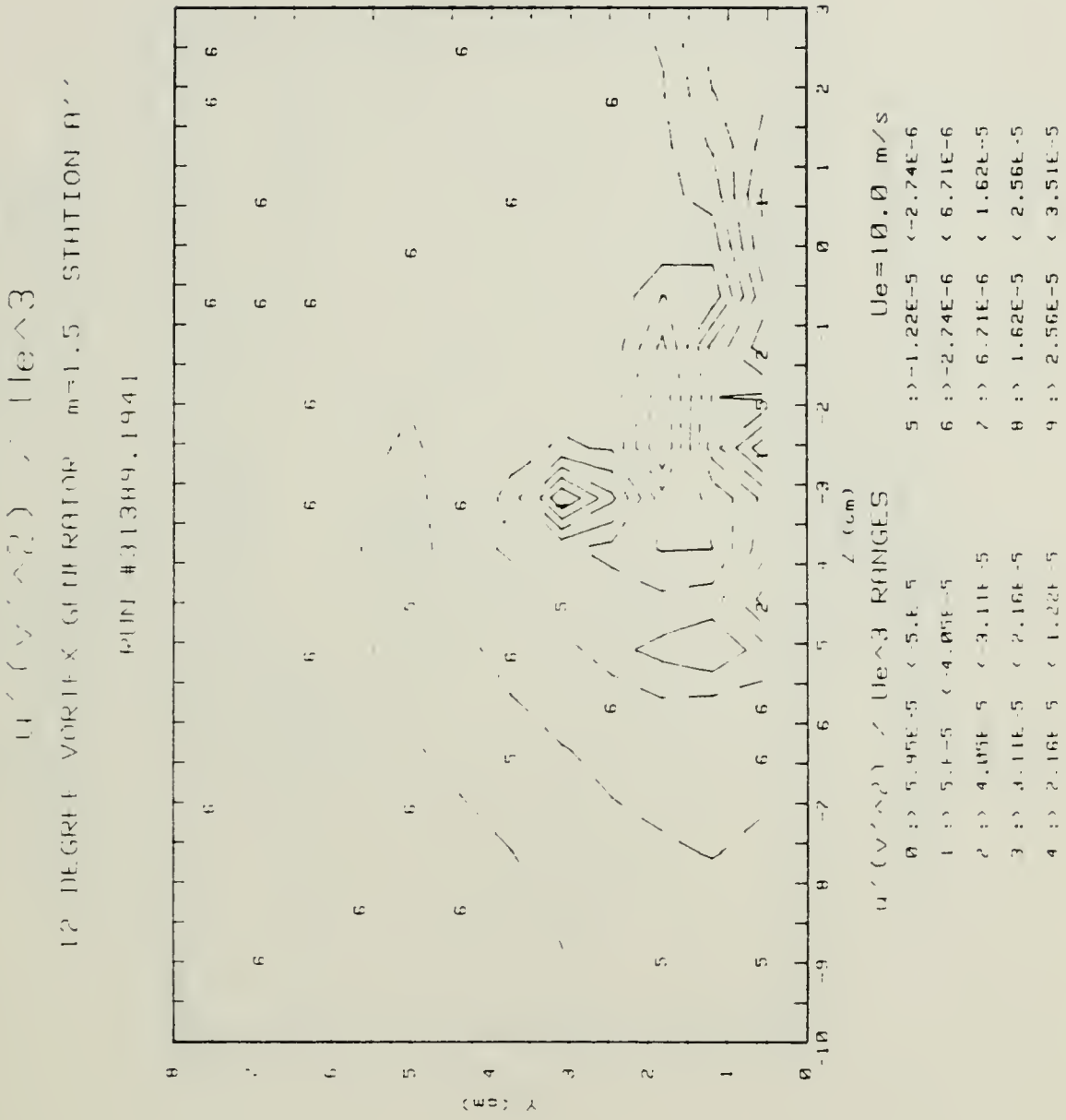

Figure 152. $\overline{u'v'}$ (boundary layer / vortex / wall jet, station A″, Δ = 0.25 inches)

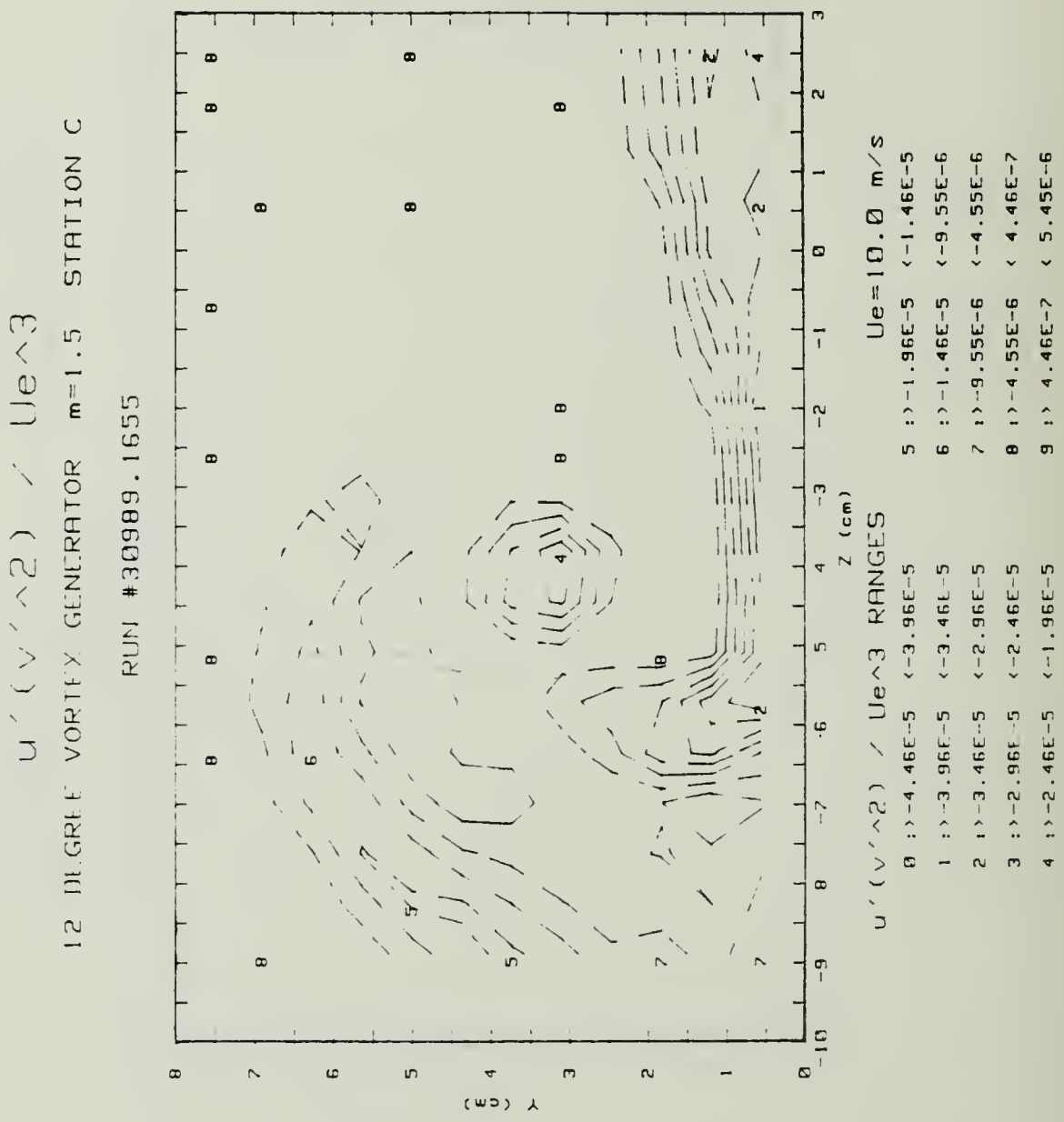

Figure 153. $\overline{u'v'^2}$ (boundary layer / vortex / wall jet, station C, $\Delta = 0.25$ inches)

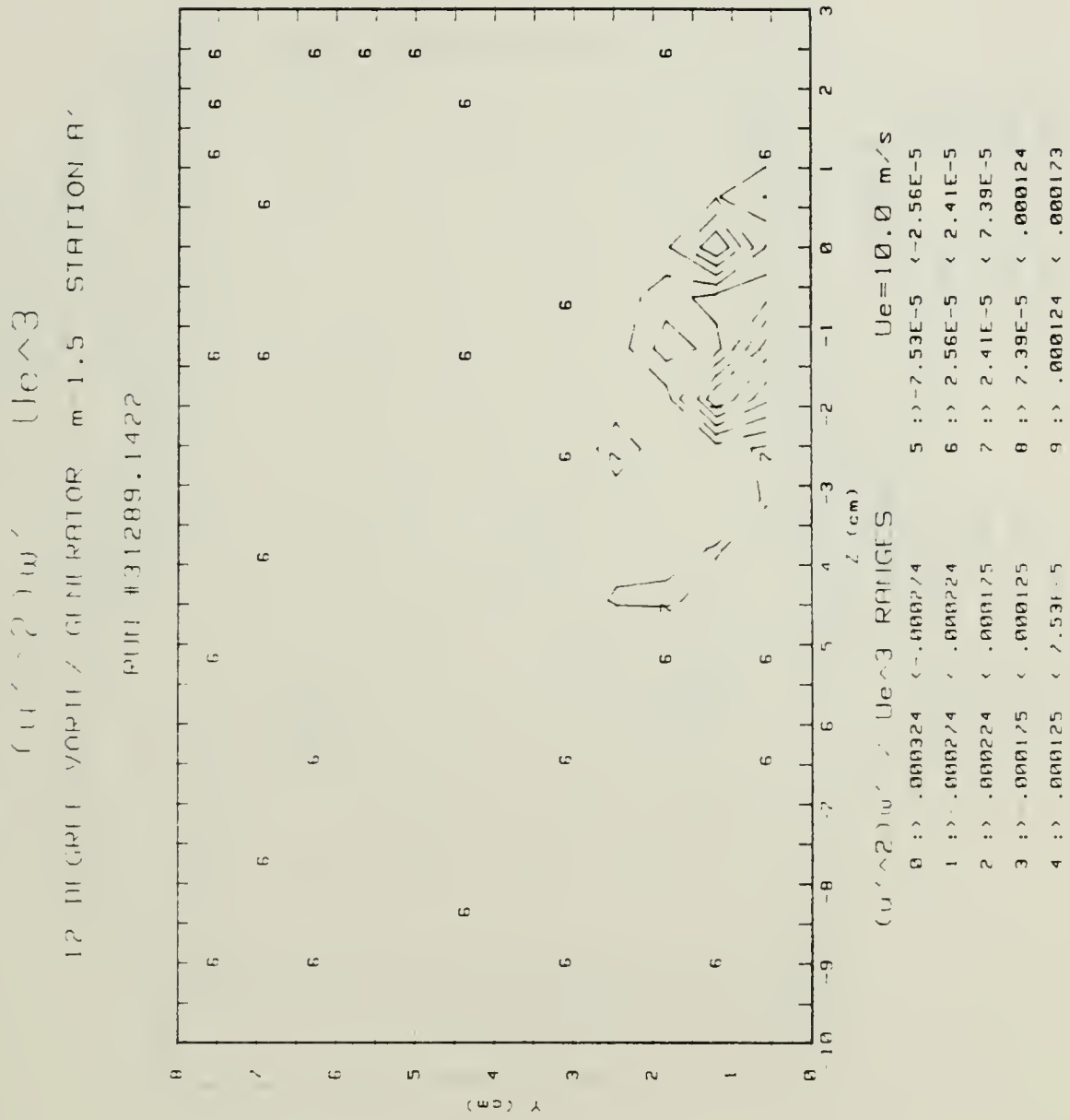

Figure 154. $\overline{u'w'}$ (boundary layer / vortex / wall jet, station A′, Δ = 0.25 inches)

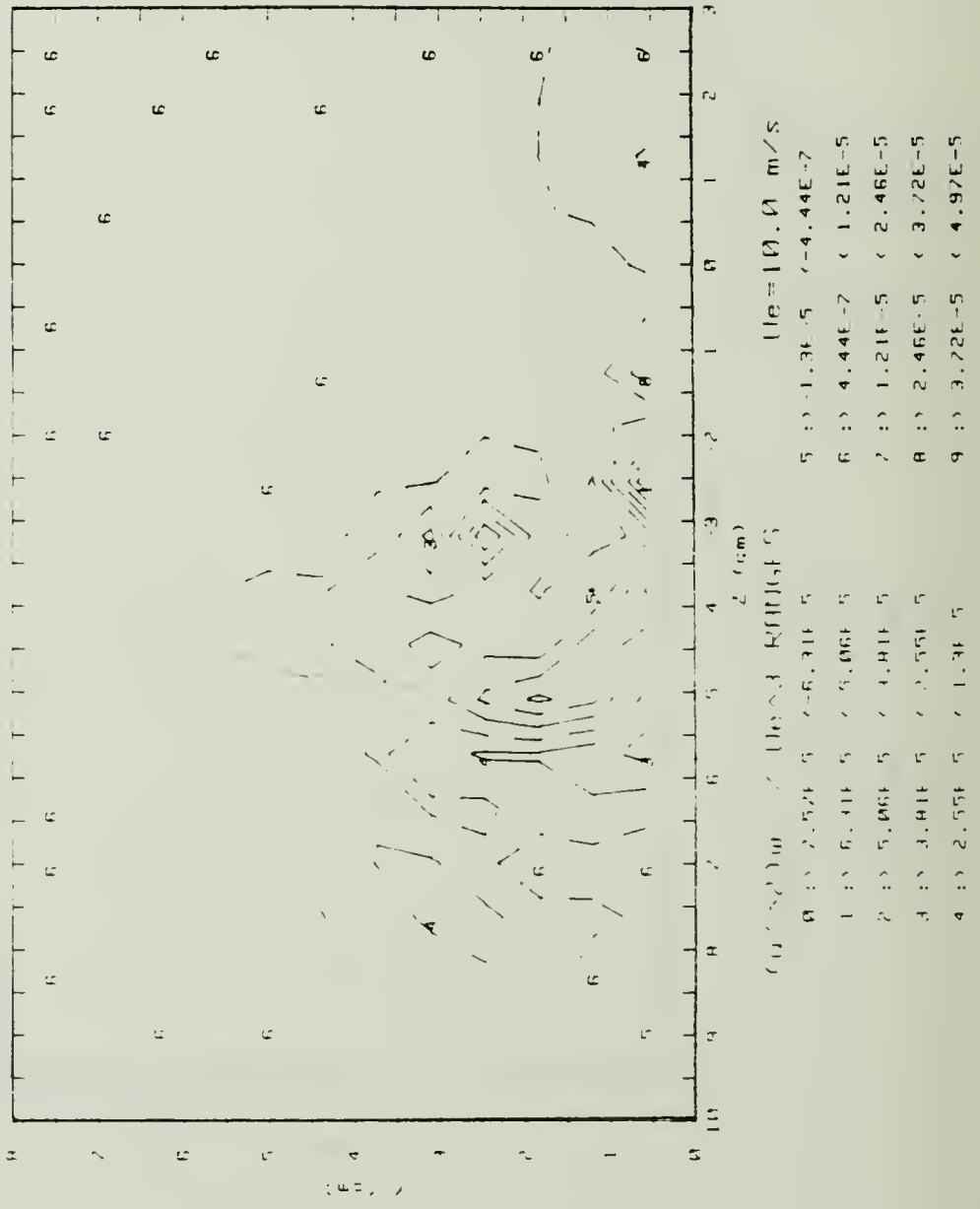

Figure 155. $\overline{u'w'}$ (boundary layer / vortex / wall jet, station A'', $\Delta = 0.25$ inches)

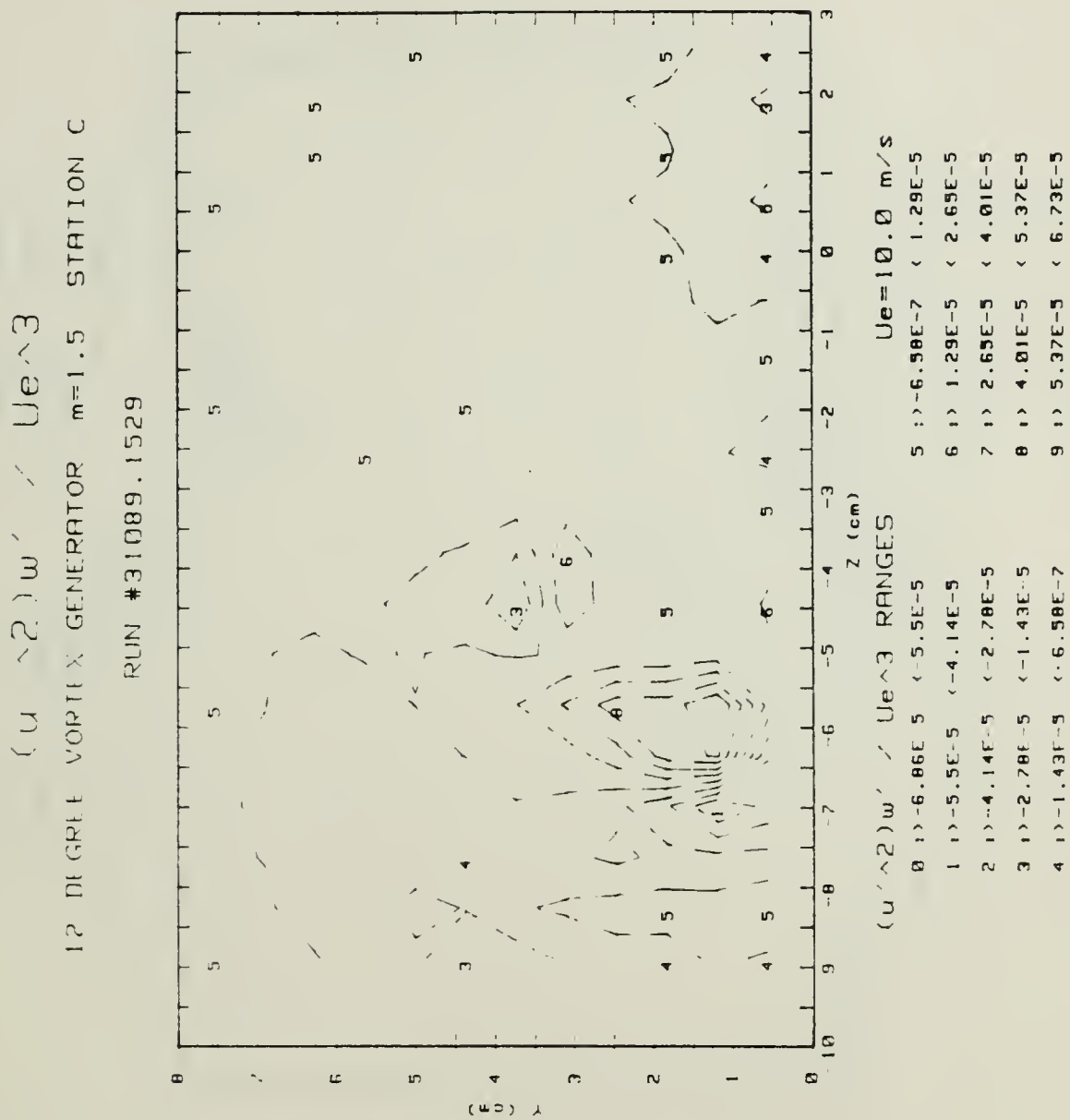

Figure 156. $\overline{u'^2w'}$ (boundary layer / vortex / wall jet, station C, $\Delta = 0.25$ inches)

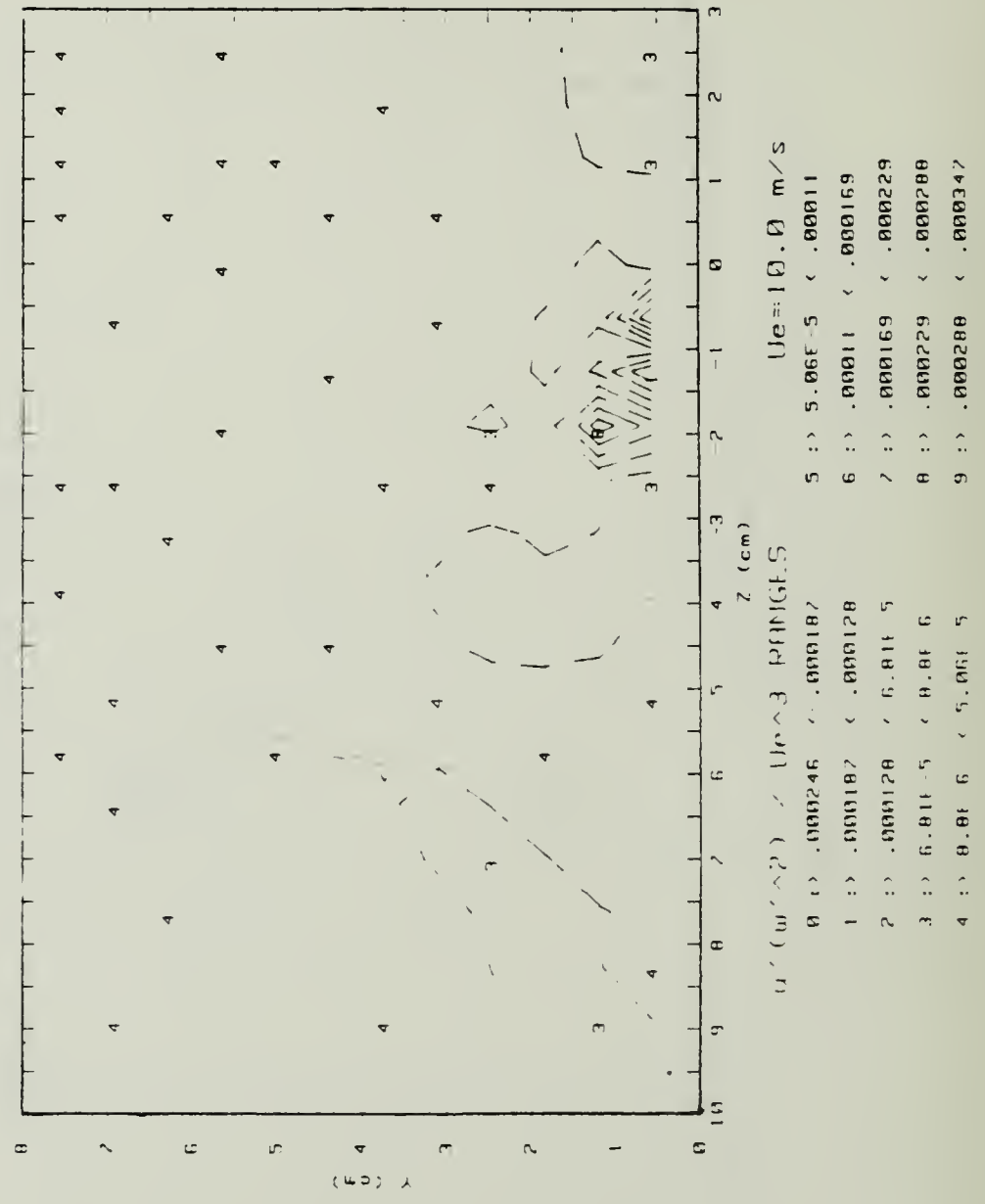

Figure 157. $\overline{u'w'}$ (boundary layer / vortex / wall jet, station A', Δ = 0.25 inches)

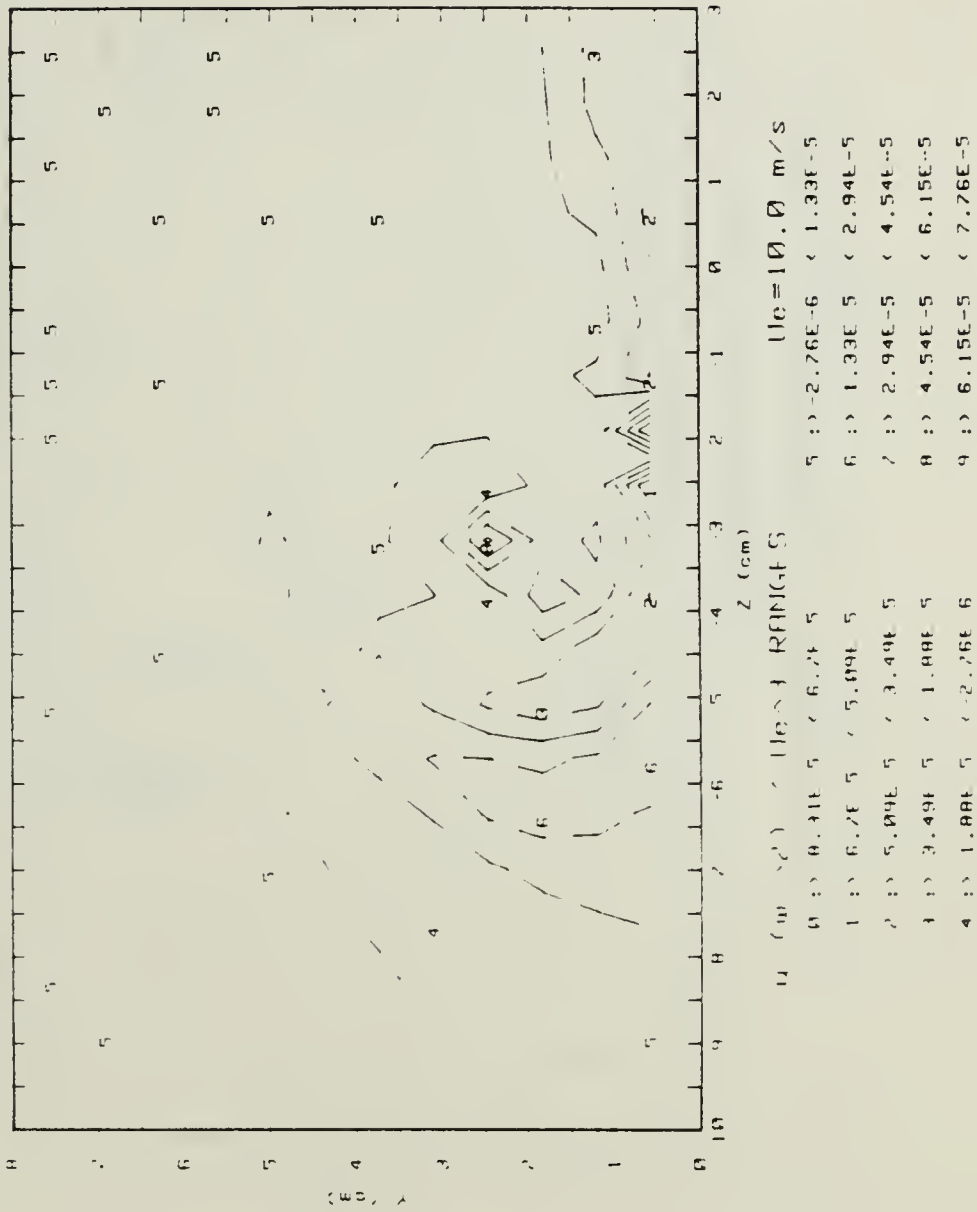

Figure 158. $\overline{u'w'}$ (boundary layer / vortex / wall jet, station A'', Δ = 0.25 inches)

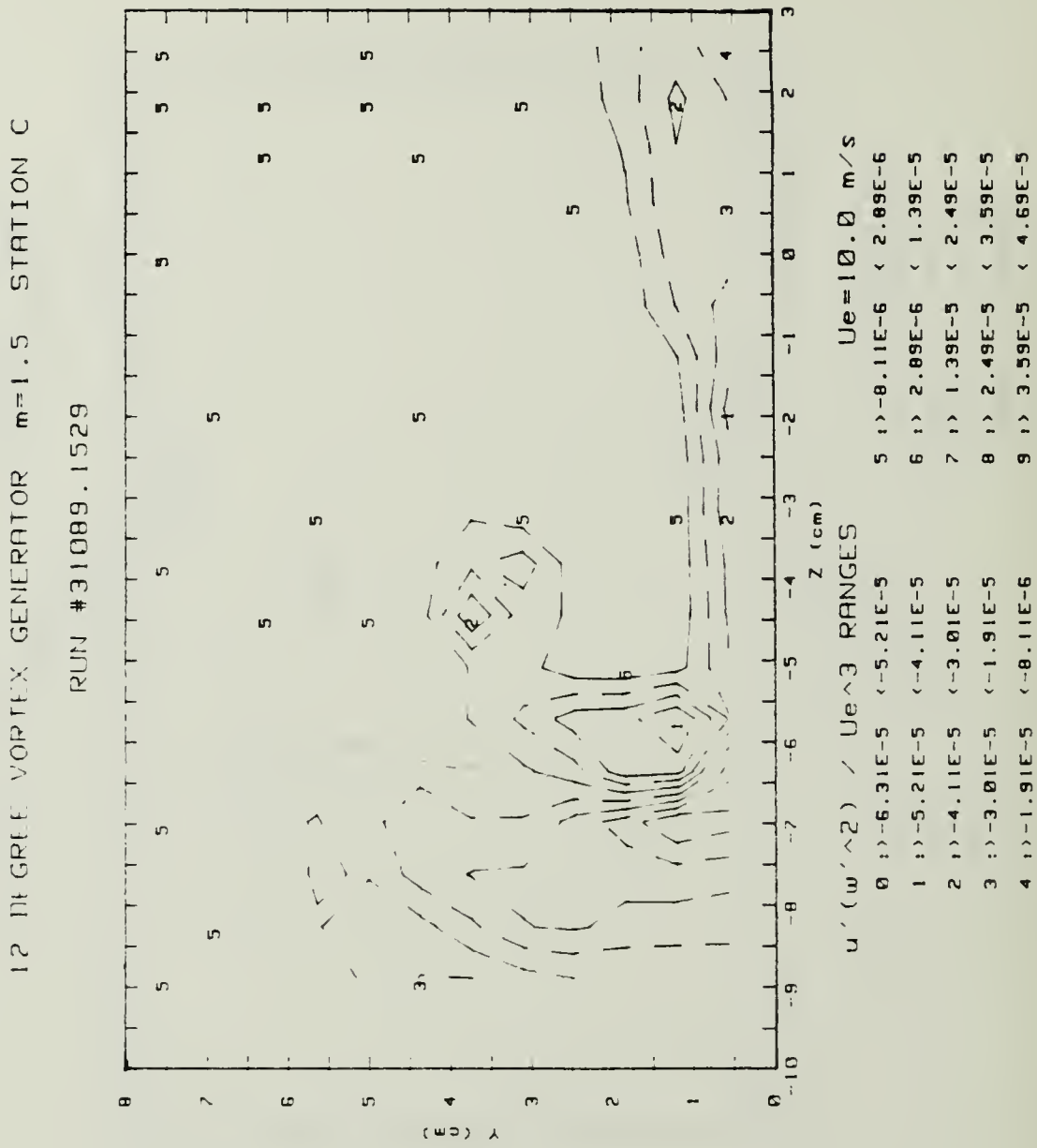

Figure 159. $\overline{u'w'^2}$ (boundary layer / vortex / wall jet, station C, $\Delta = 0.25$ inches)

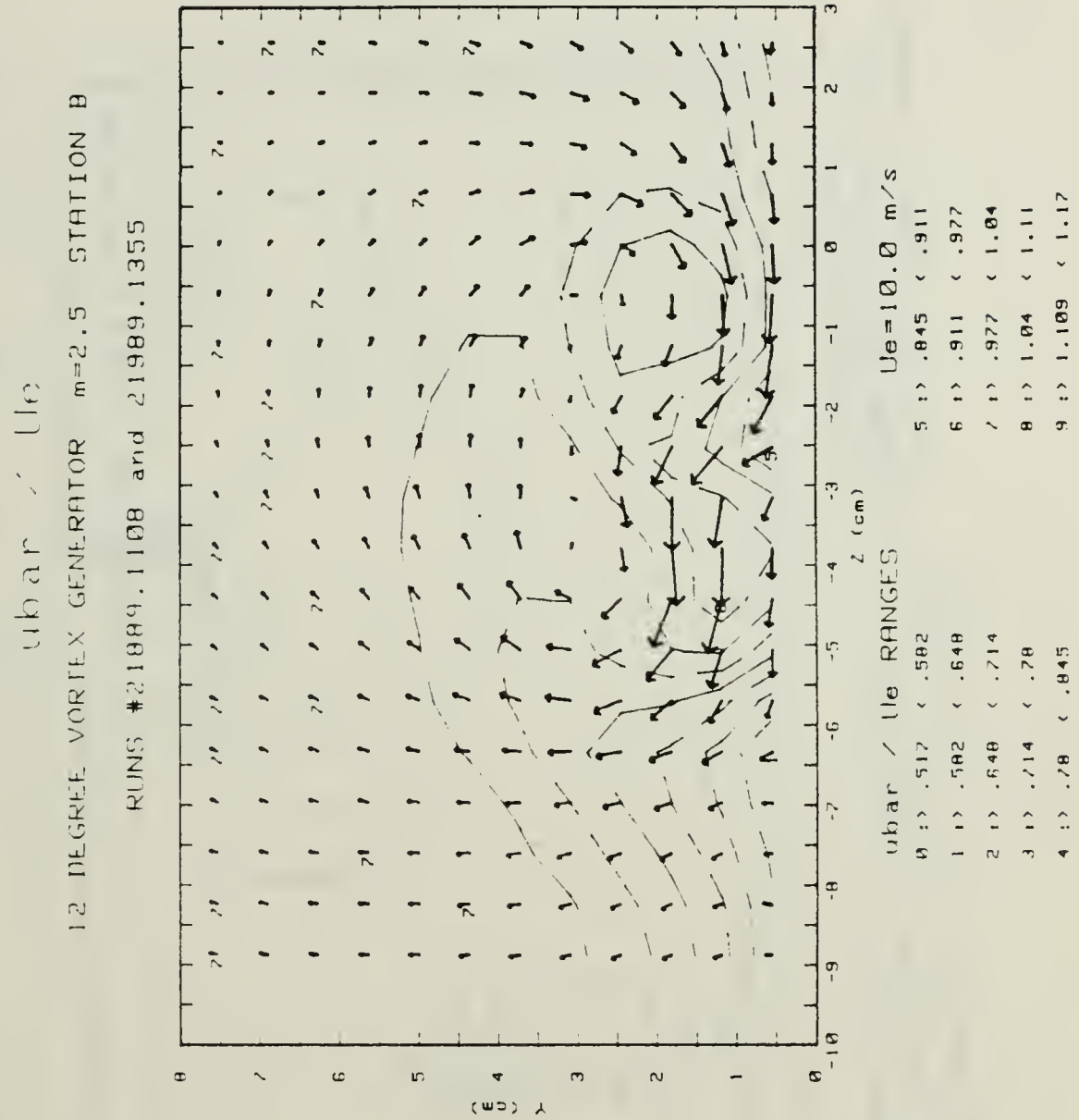

Figure 160. Mean Velocities (boundary layer / vortex / wall jet, station B, $\Delta = 0.25$ inches, m = 2.5)

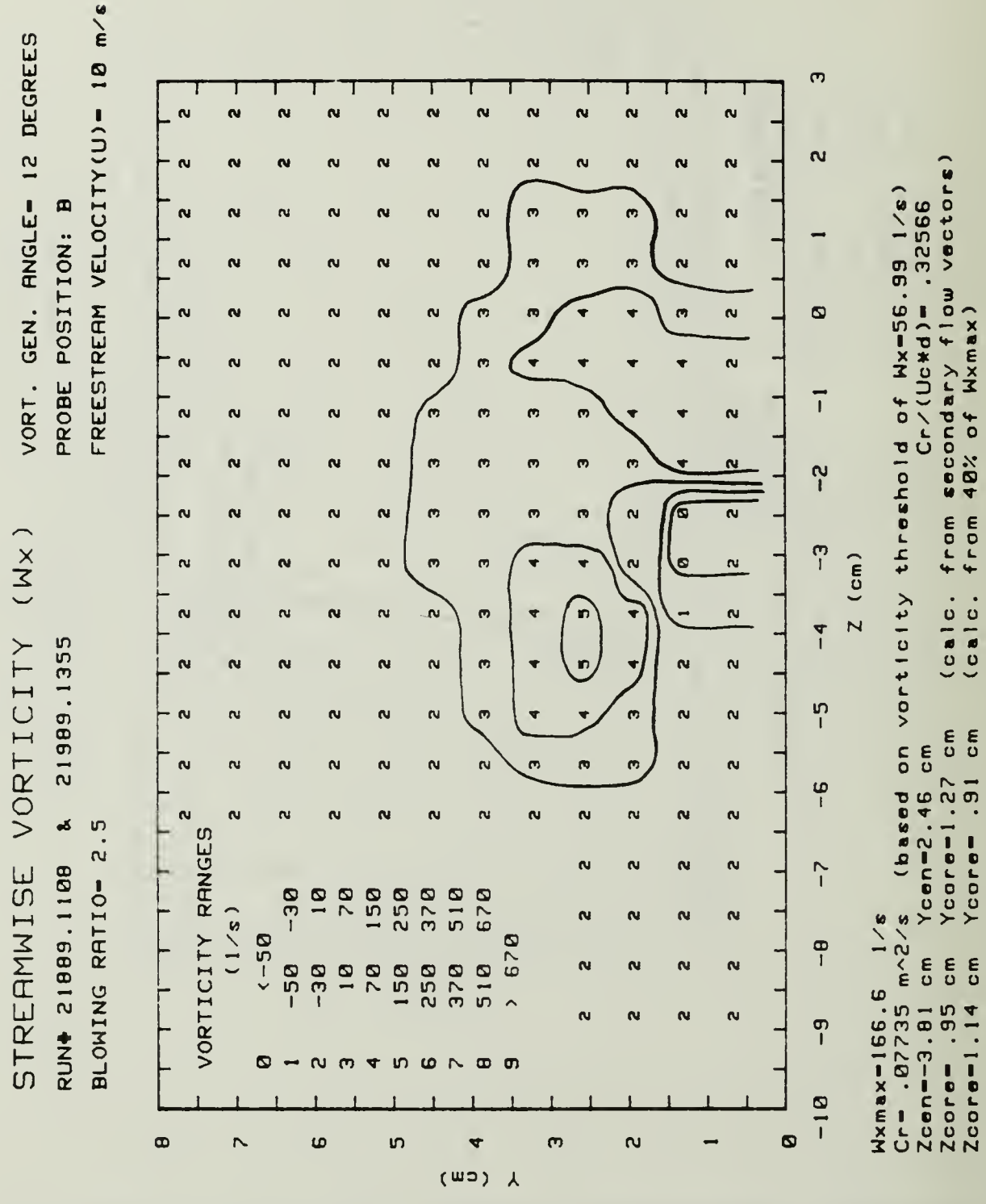

Figure 161. Streamwise Vorticity ω_x (boundary layer / vortex / wall jet, station B, $\Delta = 0.25$ inches, m = 2.5)

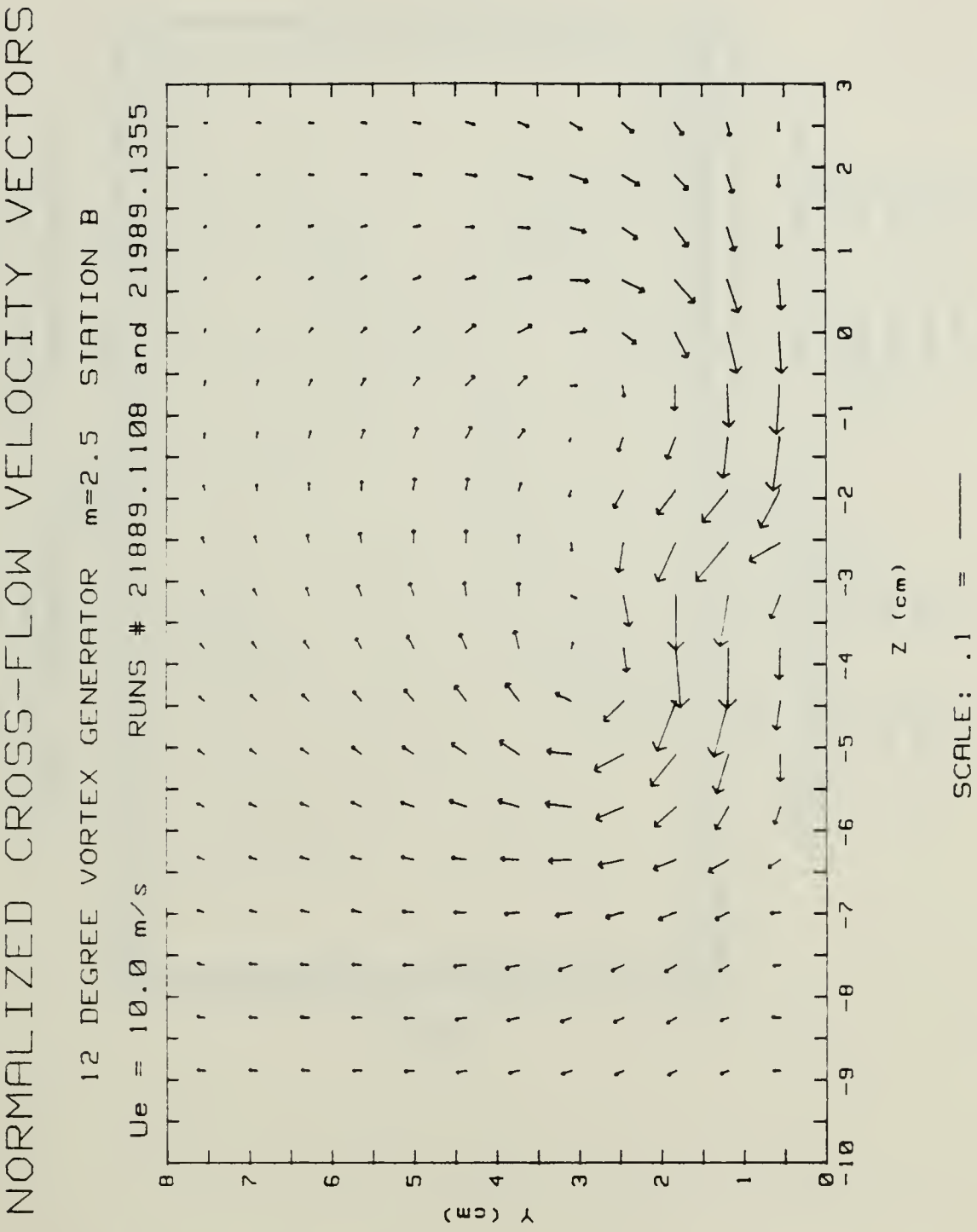
NORMALIZED CROSS-FLOW VELOCITY VECTORS
12 DEGREE VORTEX GENERATOR m=2.5 STATION B
Ue = 10.0 m/s RUNS # 21889.1108 and 21989.1355
Y (cm)
Z (cm)
SCALE: .1 = ——

Figure 162. Secondary Flow Vectors (boundary layer / vortex / wall jet, station B, $\Delta = 0.25$ inches, $m = 2.5$)

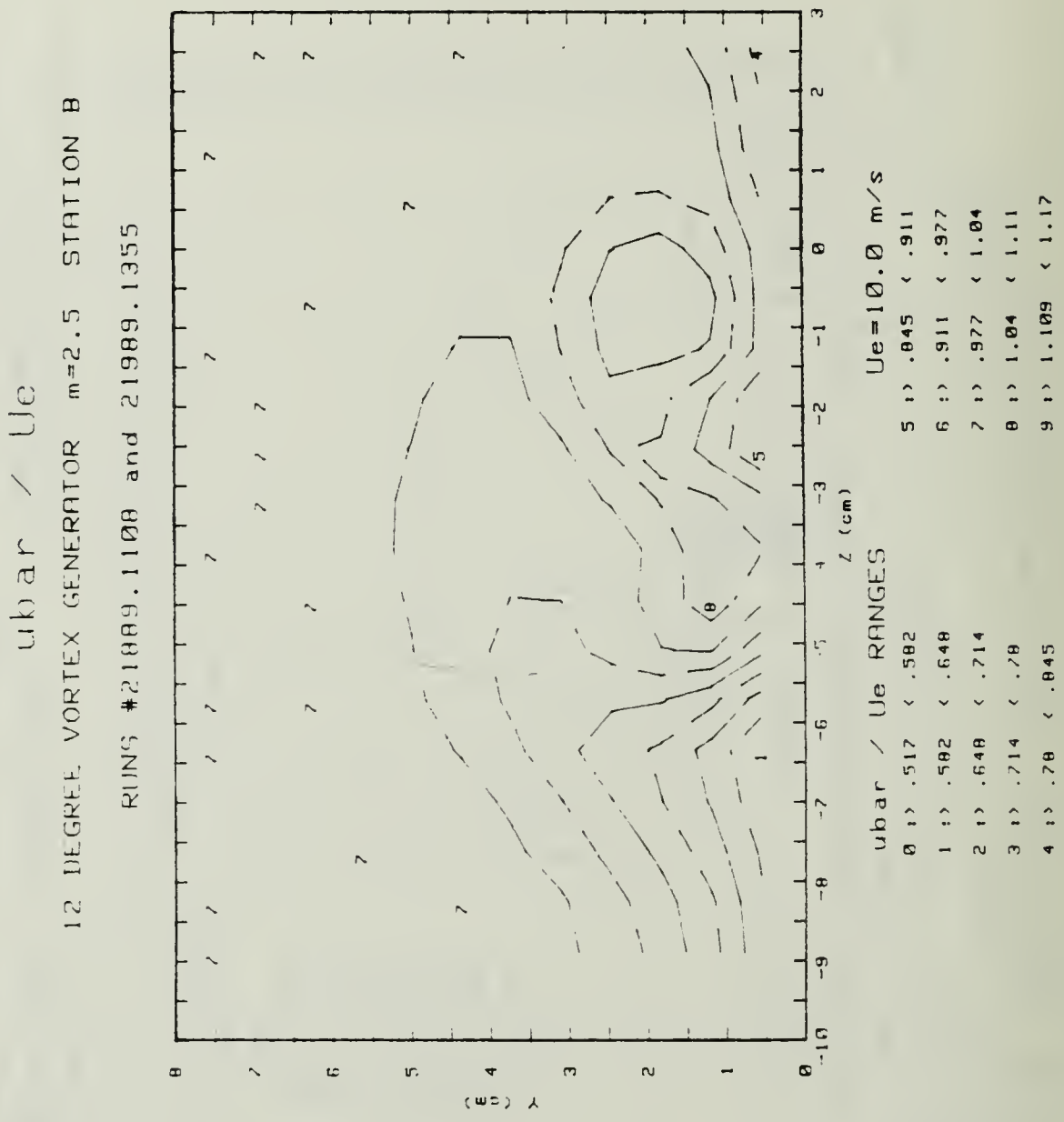

Figure 163. $\bar{u}$ (boundary layer / vortex / wall jet, station B, $\Delta = 0.25$ inches, $m = 2.5$)

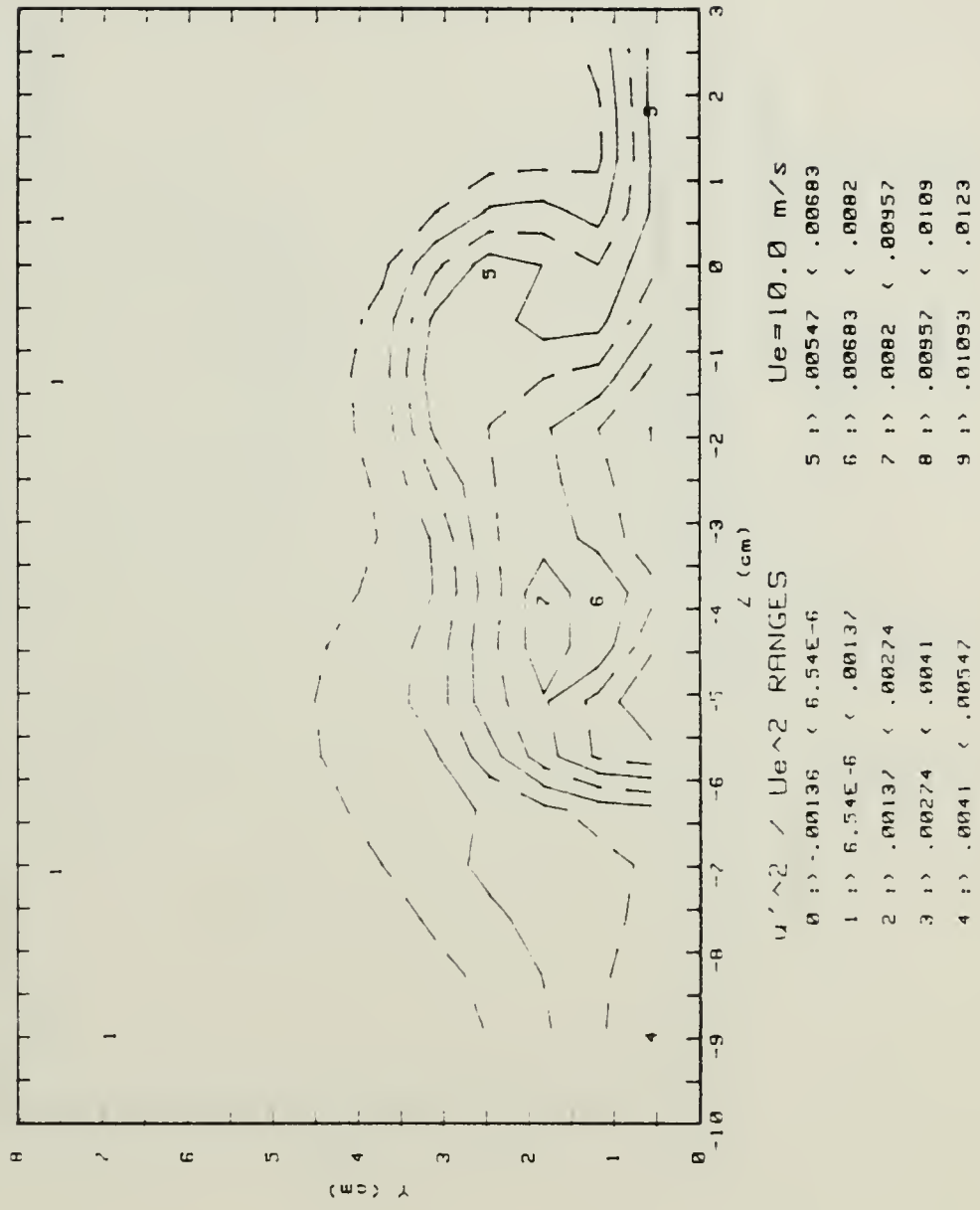

Figure 164. $\overline{u'^2}$ (boundary layer / vortex / wall jet, station B, $\Delta = 0.25$ inches, m = 2.5)

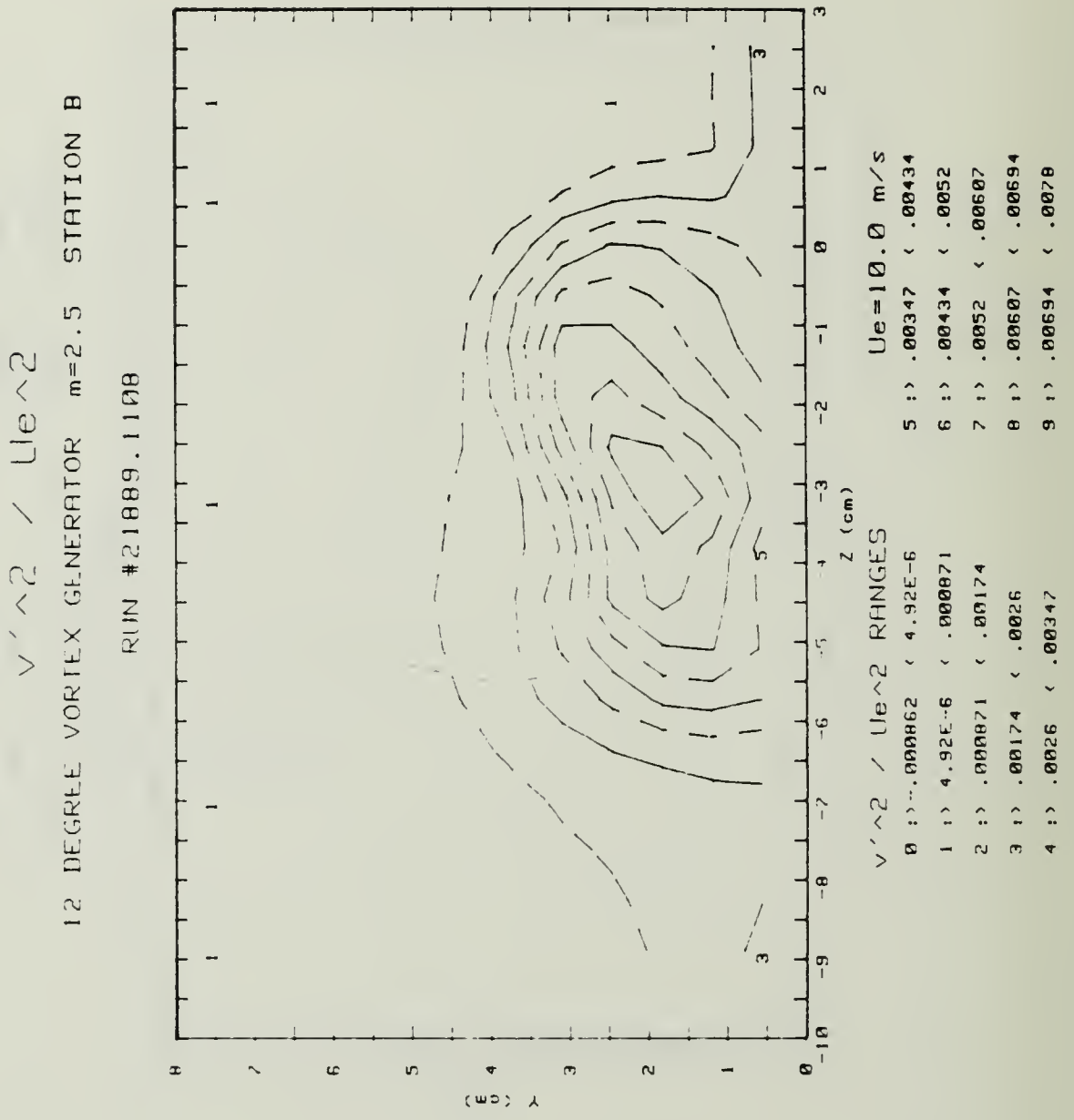

Figure 165. $\overline{v'^2}$ (boundary layer / vortex / wall jet, station B, $\Delta = 0.25$ inches, $m = 2.5$)

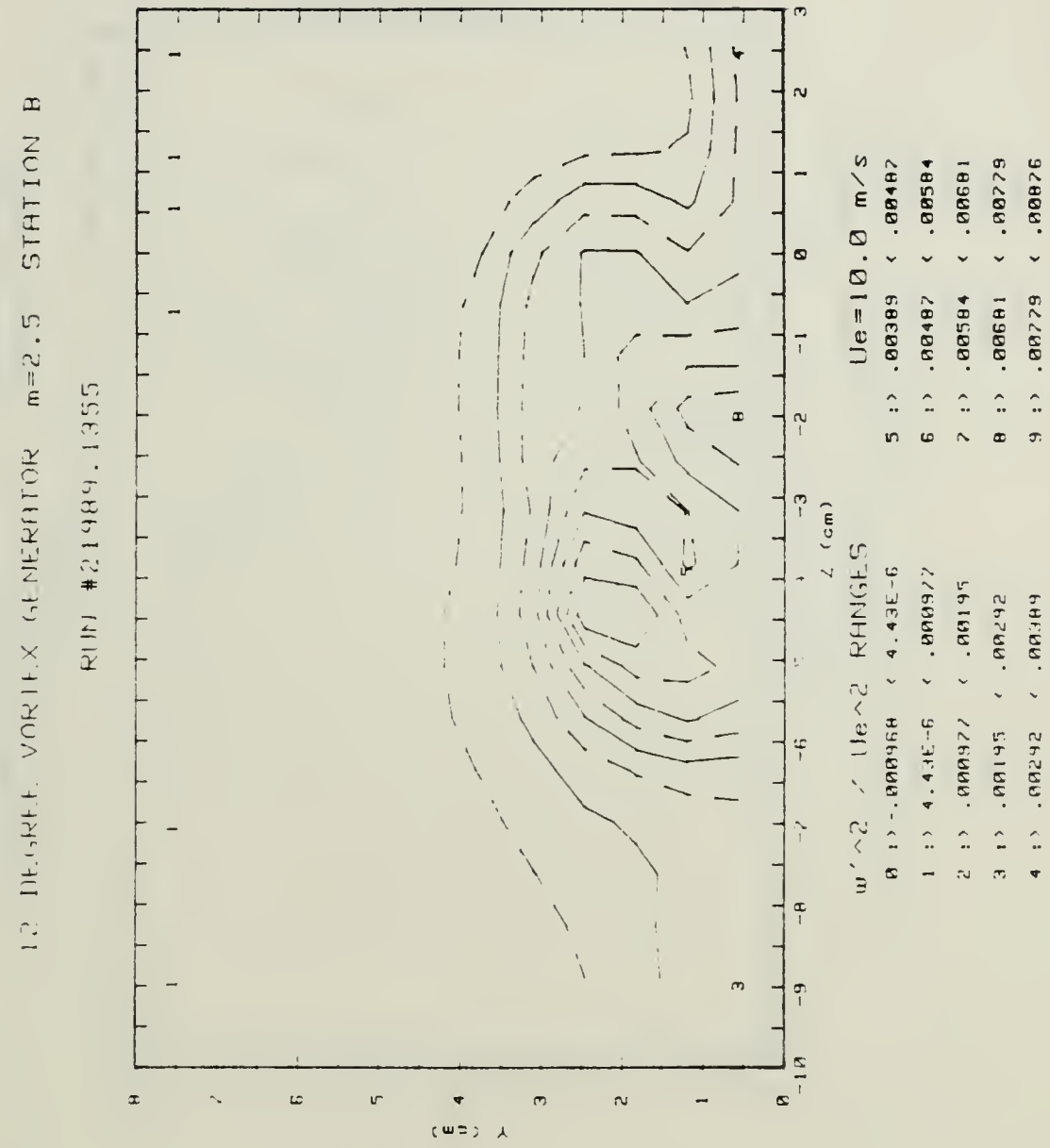

Figure 166. $\overline{w'^2}$ (boundary layer / vortex / wall jet, station B, $\Delta = 0.25$ inches, $m = 2.5$)

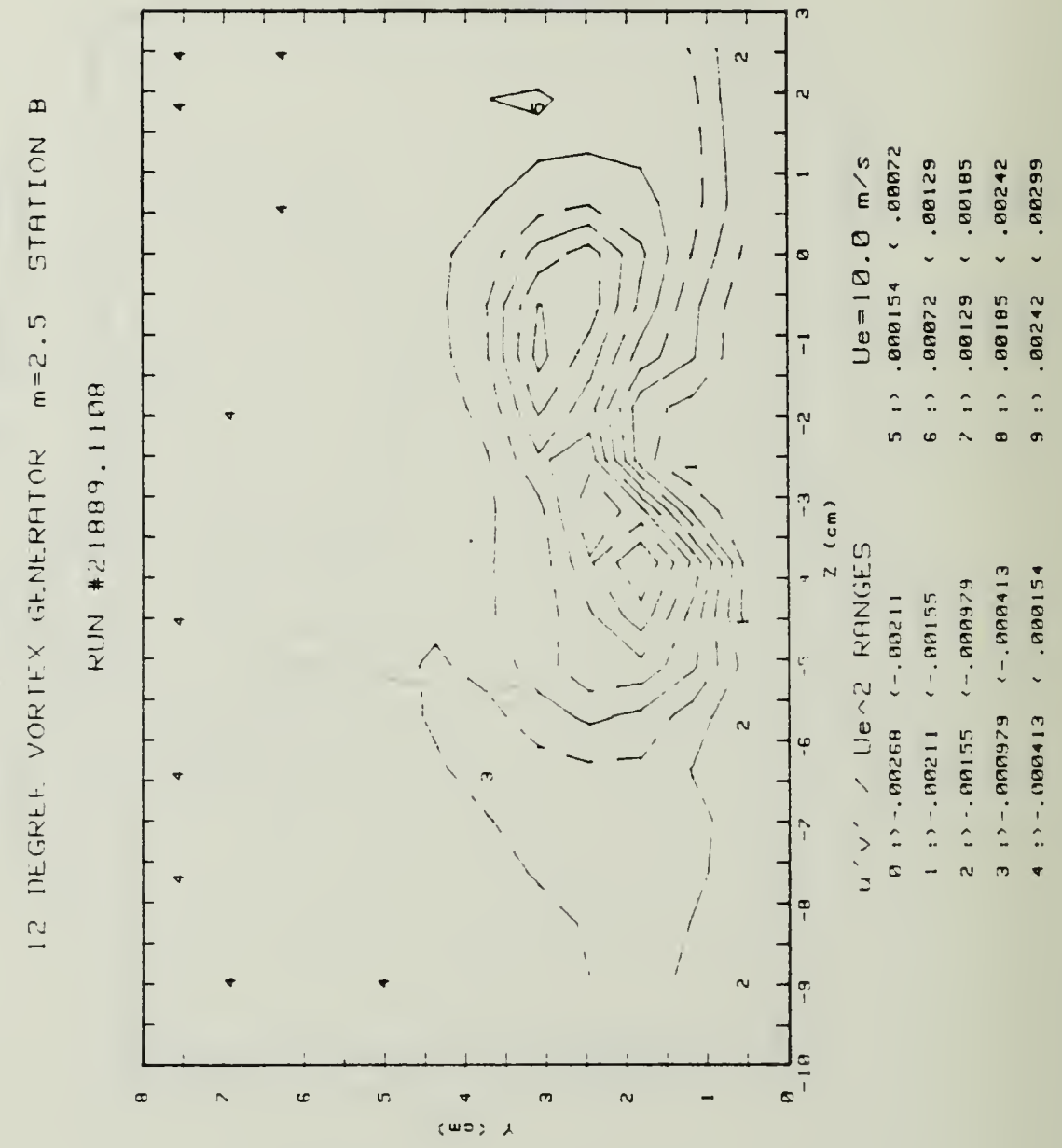

Figure 167. $\overline{u'v'}$ (boundary layer / vortex / wall jet, station B, $\Delta = 0.25$ inches, m = 2.5)

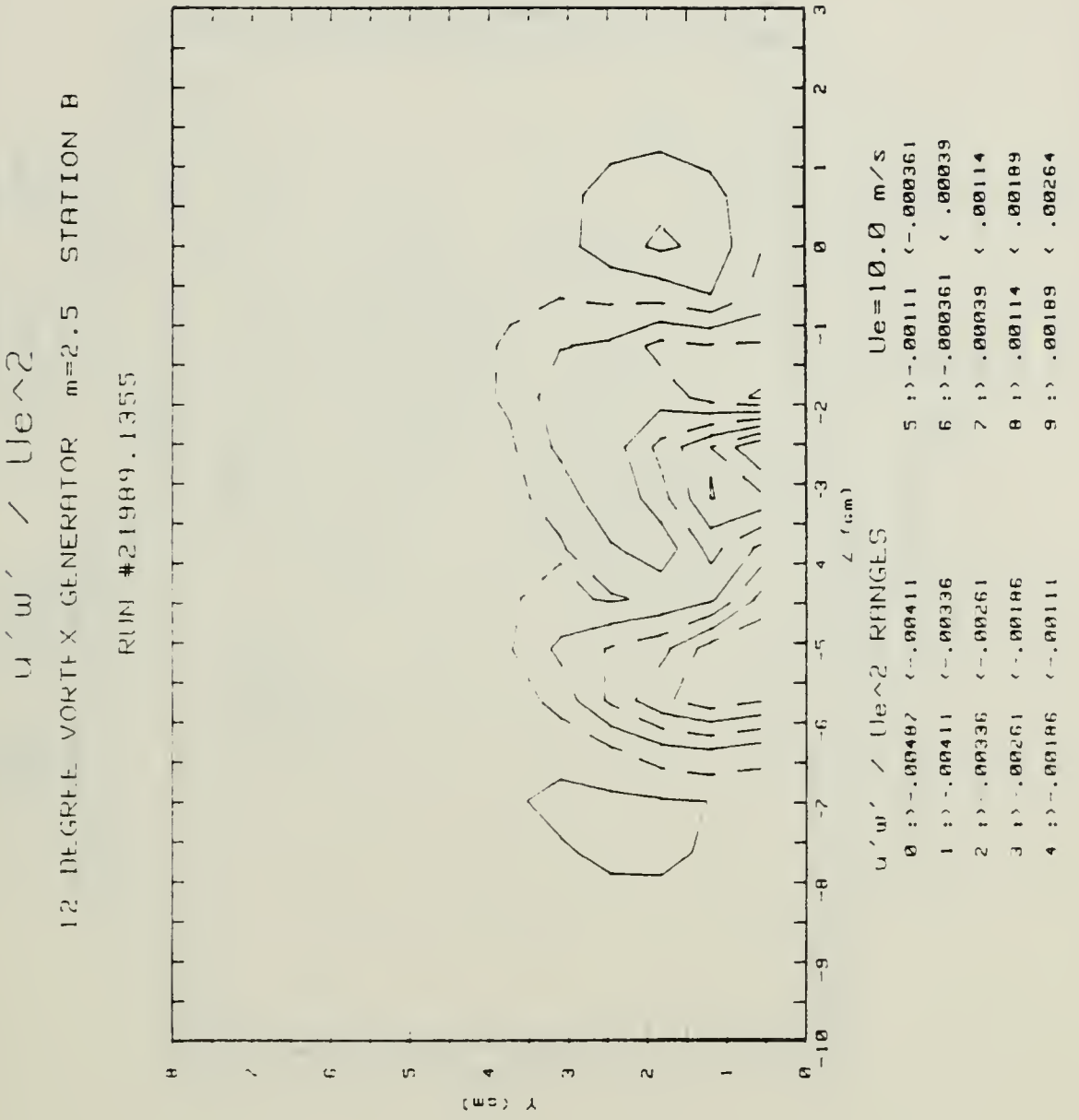

Figure 168. $\overline{u'w'}$ (boundary layer / vortex / wall jet, station B, $\Delta = 0.25$ inches, $m = 2.5$)

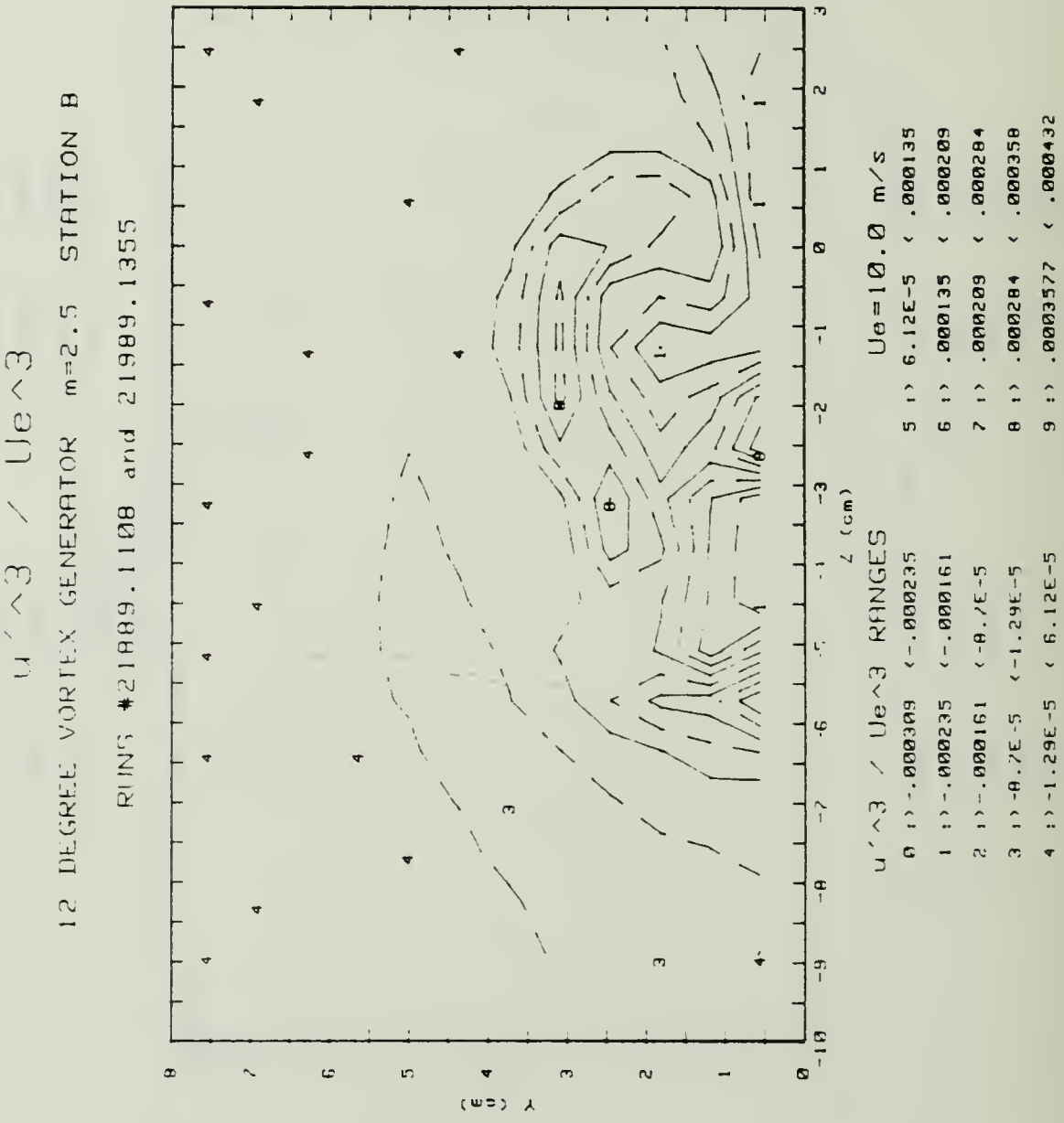

Figure 169. $\overline{u'^3}$ (boundary layer / vortex / wall jet, station B, $\Delta = 0.25$ inches, m = 2.5)

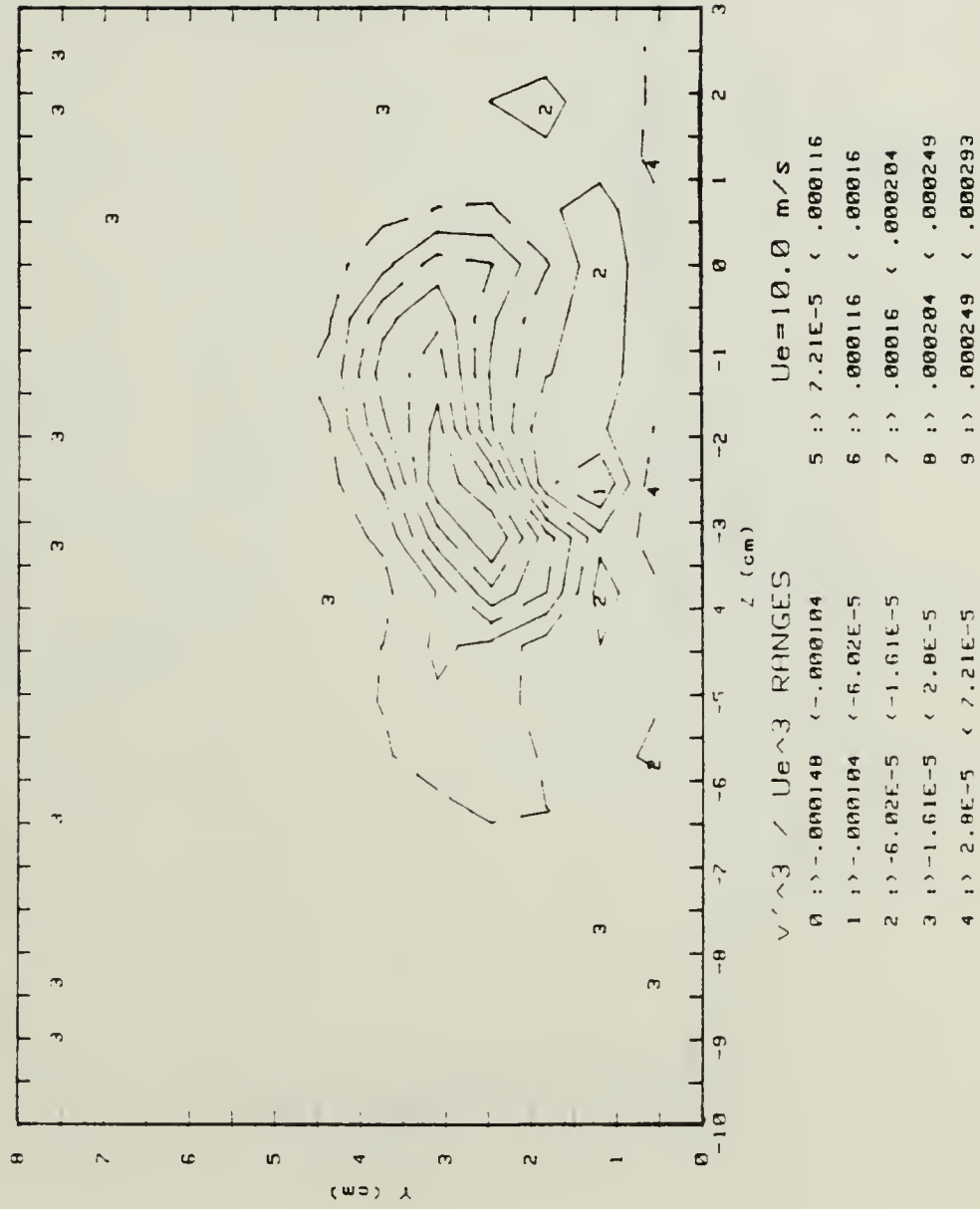

Figure 170. $\overline{v'^3}$ (boundary layer / vortex / wall jet, station B, $\Delta = 0.25$ inches, $m = 2.5$)

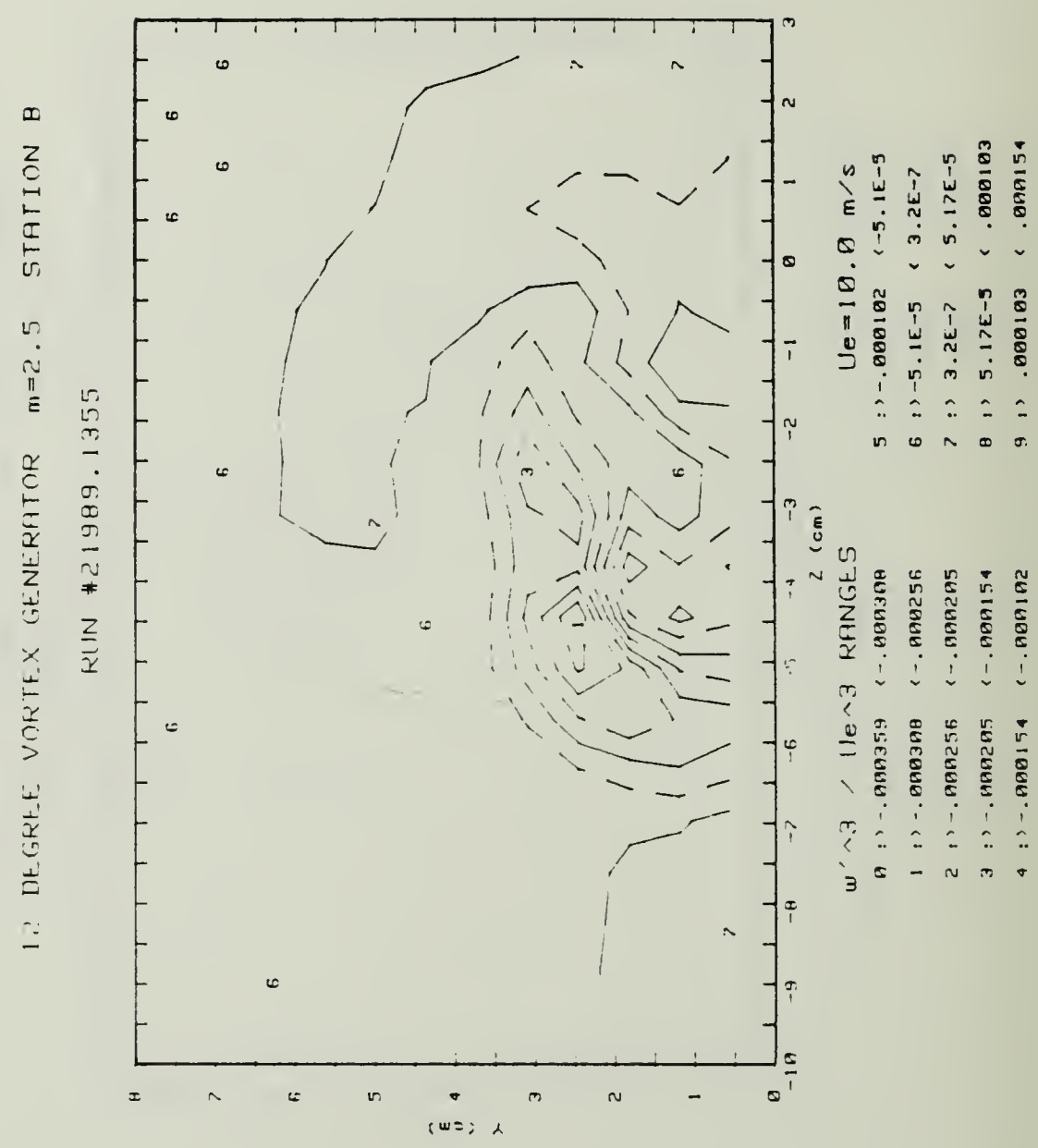

Figure 171. $\overline{w'^3}$ (boundary layer / vortex / wall jet, station B, $\Delta = 0.25$ inches, $m = 2.5$)

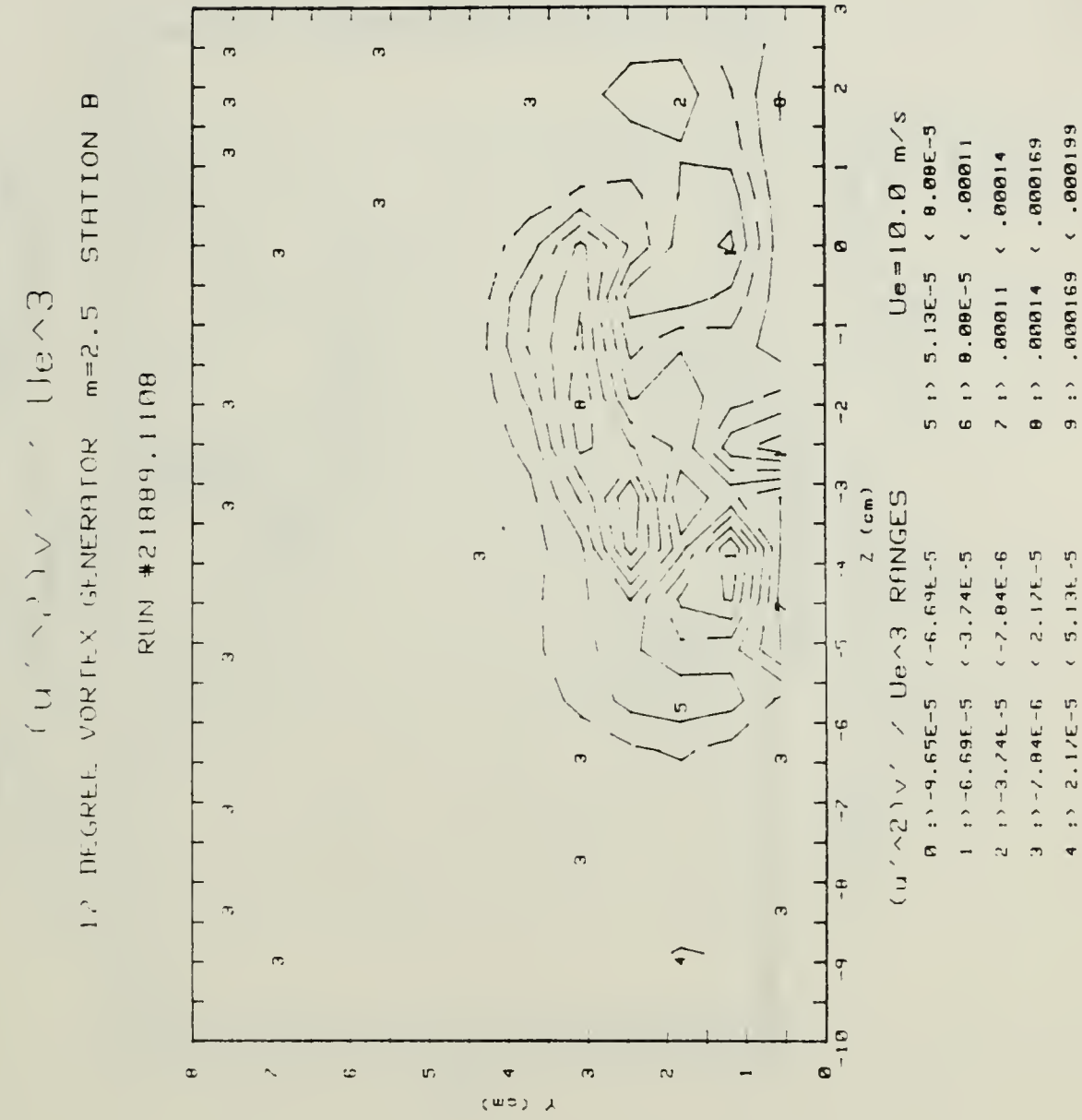

Figure 172. $\overline{u'^2v'}$ (boundary layer / vortex / wall jet, station B, $\Delta = 0.25$ inches, m = 2.5)

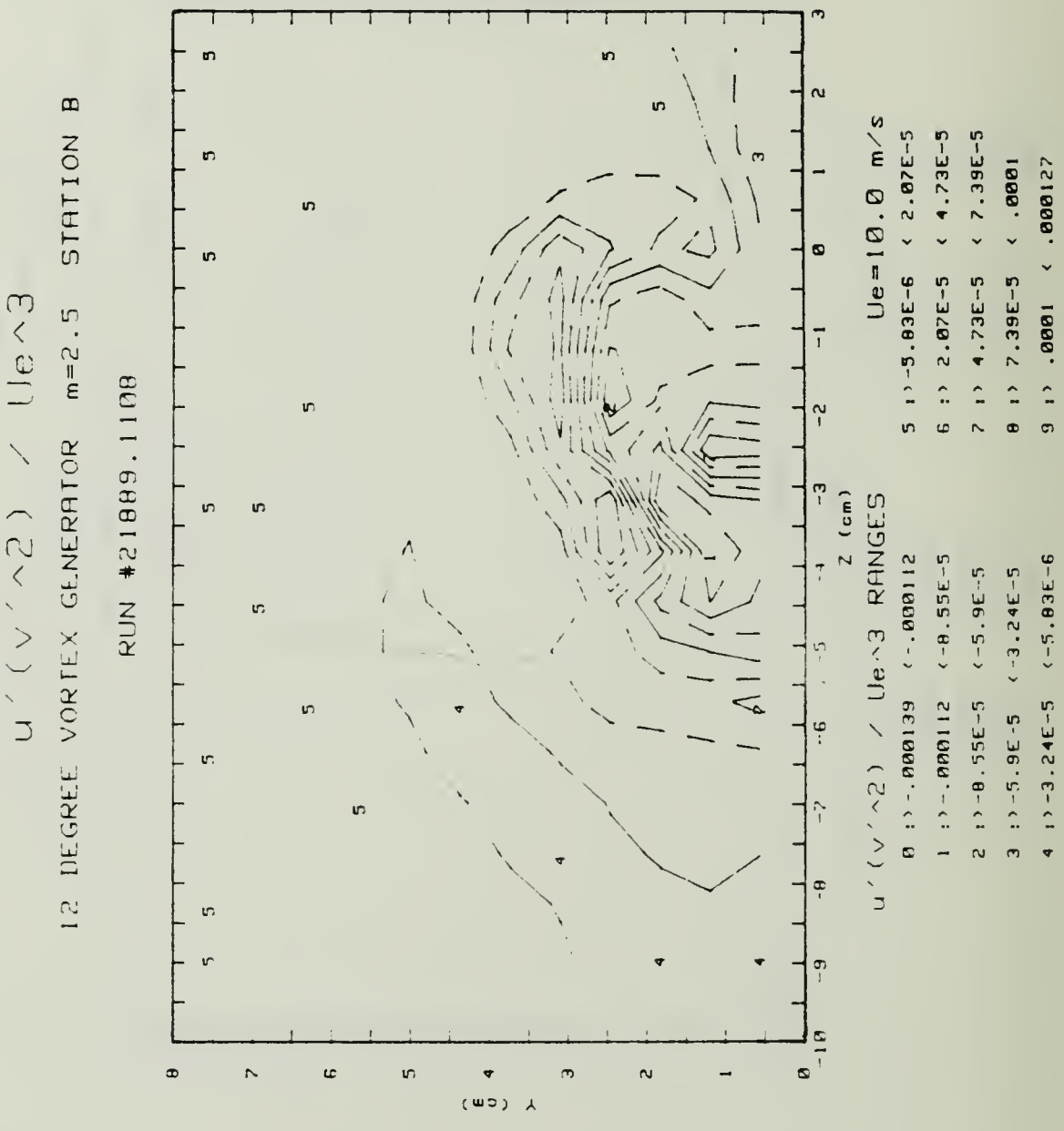

Figure 173. $\overline{u'v'^2}$ (boundary layer / vortex / wall jet, station B, $\Delta = 0.25$ inches, m = 2.5)

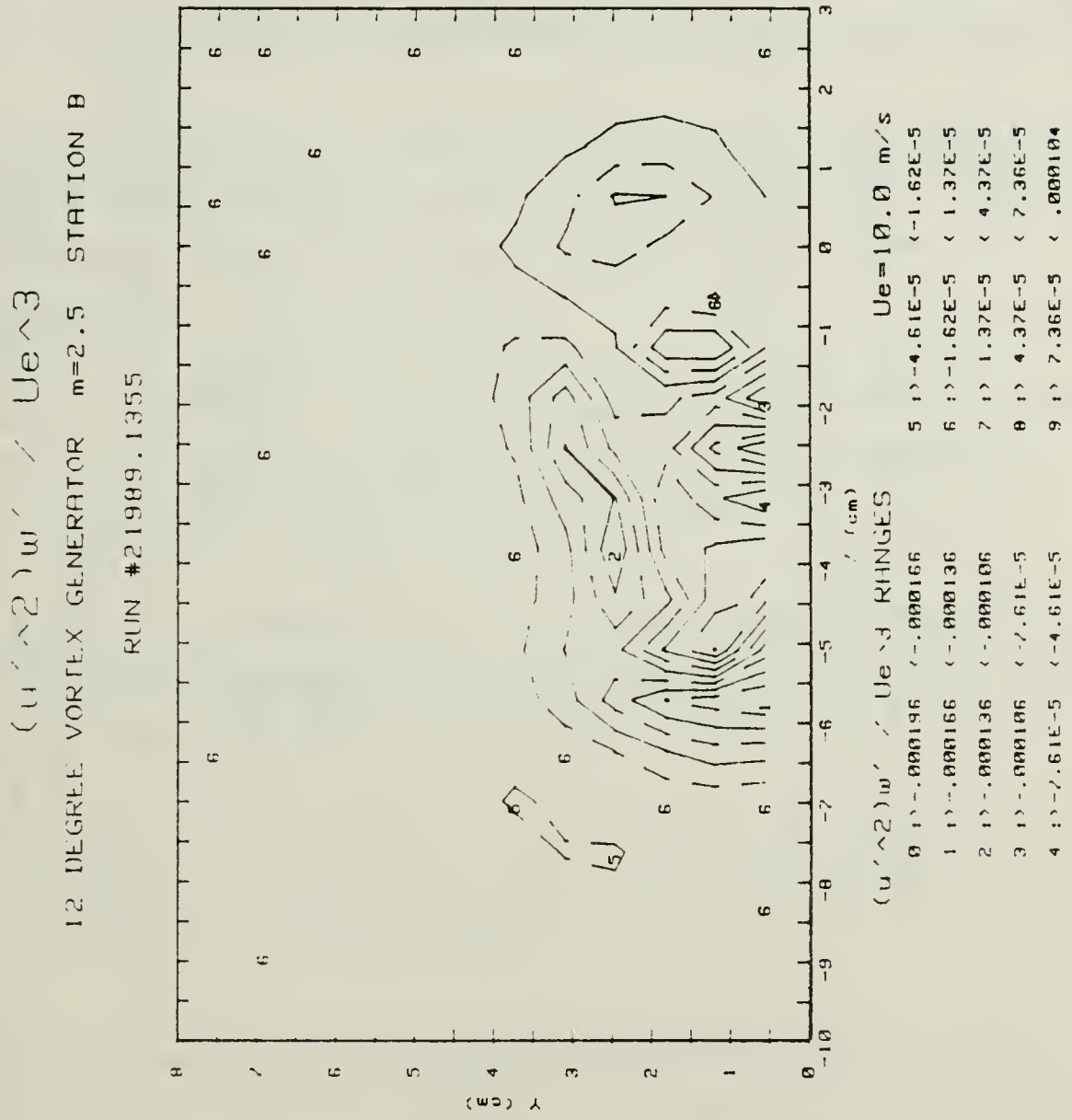

Figure 174. $\overline{u'^2w'}$ (boundary layer / vortex / wall jet, station B, $\Delta = 0.25$ inches, $m = 2.5$)

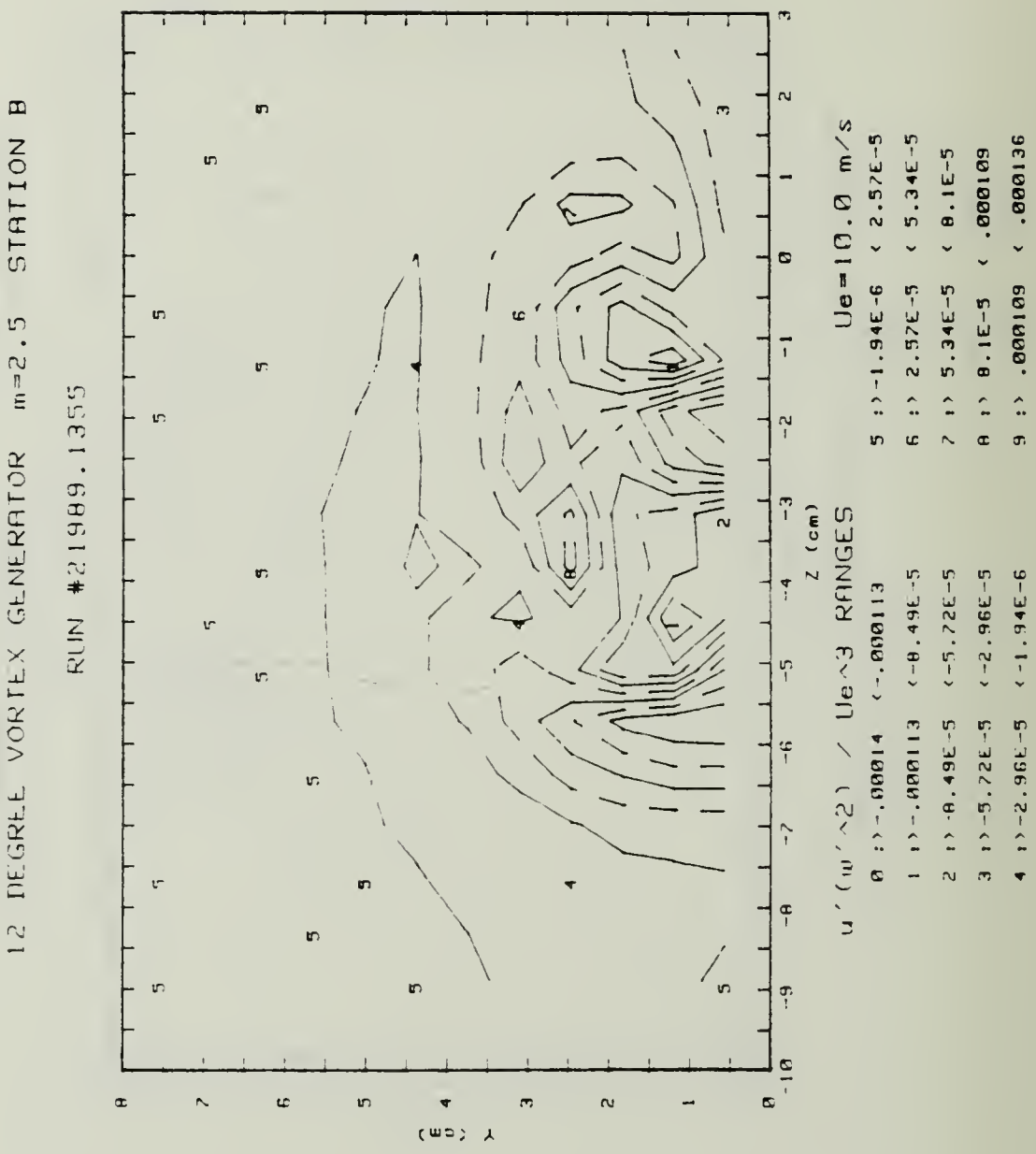

Figure 175. $\overline{u'w'^2}$ (boundary layer / vortex / wall jet, station B, $\Delta = 0.25$ inches, $m = 2.5$)

LIST OF REFERENCES

1. Von Karman Institute for Fluid Dynamics Project Report 1981-19, *Heat Transfer on Endwalls of a Turbine Cascade With Film Cooling*, by A. Ongoren, June 1981.

2. Ligrani, P. M., Joseph, S. L., Ortiz, A., and Evans, D. L., "Heat Transfer in Film-Cooled Turbulent Boundary Layers at Different Blowing Ratios as Affected by Longitudinal Vortices," *Experimental Thermal and Fluid Science*, Vol. 1, pp. 347-362, 1988.

3. Ligrani, P. M., Ortiz, A., Joseph, S. L., and Evans, D. L., "Effects of Embedded Vortices on Film-Cooled Boundary Layers," *ASME Transactions-Journal of Turbomachinery*, Vol. 111, Number 1, pp. 71-77, 1989.

4. Ligrani, P. M., and Williams, W. W., "Effects of an Embedded Vortex on Injectant from a Single Film-Cooling Hole in a Turbulent Boundary Layer," to appear in *ASME Transactions-Journal of Turbomachinery*, 1989.

5. Shabaka, I. M. M. A., Mehta, R. D., and Bradshaw, P., "Longitudinal Vortices Embedded in Turbulent Boundary Layers. Part I. Single Vortex,"*Journal of Fluid Mechanics*, Vol.155, pp.37-57, 1985.

6. Stanford University Thermosciences Division Report MD-48, *An Experimental Investigation of the Heat Transfer Effects of a Longitudinal Vortex Embedded in a Turbulent Boundary Layer*, by P. A. Eibeck and J. K. Eaton, 1985.

7. Cutler, A. D., and Bradshaw, P., "The Interaction Between a Strong Longitudinal Vortex and a Turbulent Boundary Layer," AIAA paper No. AIAA-86-1071, 1986.

8. Mehta, R. D., and Bradshaw, P., "Longitudinal Vortices Embedded in Turbulent Boundary Layers. Part 2. Vortex Pair with 'Common Flow' Upwards," *Journal of Fluid Mechanics*, Vol. 188, pp. 529-546, 1988.

9. NASA Technical Memorandum 88361, *Interaction Between a Vortex and a Turbulent Boundary Layer, Part I: Mean Flow Evolution and Turbulence Properties*, by R. V. Westphal, W. R. Pauley, and J. K. Eaton, 1987.

10. Von Karman Institute Special Course on Aerodynamic Characteristics of Controls Report No. 711, *Control of the Forebody Vortex Orientation by Asymmetric Air Injection: (Part A) Application to Enhance Departure/Spin Recovery of Fighter Aircraft and (Part B) Details of the Flow Structure*, by A. M. Skow, and D. J. Peake, March 1983.

11. Heffernan, K. G., *Trailing Vortex Attenuation Devices*, Master's Thesis, Naval Postgraduate School, Monterey, California, June 1985.

12. Schwartz, G. E., *Control of Embedded Vortices Using Wall Jets*, Master's Thesis, Naval Postgraduate School, Monterey, California, September 1988.

13. Iwanski, K., Ng, T., and Nelson, R., "An Experimental Investigation of Delta Wing Vortex Flow With and Without External Jet Blowing," paper presented at the 27th Aerospace Sciences Meeting, Reno, Nevada, 9-12 January, 1989.

14. Visser, K., Nelson, R., and Ng, T., "A Flow Visualization and Aerodynamic Force Data Evaluation of Spanwise Blowing on Full and Half Span Delta Wings," paper presented at 27th Aerospace Sciences Meeting, Reno, Nevada, 9-12 January, 1989.

15. Ligrani, P. M., and Schwartz, G. E., "Control of Embedded Vortices Using Wall Jets," in preparation for *Physics of Fluids*, 1989.

16. Bradshaw, P., *Turbulence*, Springer-Verlag, 1978.

17. Joseph, S. L., *The Effects of an Embedded Vortex on a Film Cooled Turbulent Boundary Layer*, Master's Thesis, Naval Postgraduate School, Monterey, California, December 1986.

18. Craig, D. W., *Effect of Vortex Circulation on Injectant From a Single Film-Cooling Hole and a Row of Film-Cooling Holes in a Turbulent Boundary Layer, Part I: In-*

jection Beneath the Vortex Downwash, Masters Thesis, Naval Postgraduate School, Monterey, California, June 1989.

19. Lomas, C. G., *Fundamentals of Hot Wire Anemometry*, Cambridge University Press, 1986.

20. Collis, D. C., and Williams, M.J., "Two-Dimensional Convection from Heated Wires at Low Reynolds Numbers," *Journal of Fluid Mechanics*, Vol. 6, pp. 357-370, 1959.

21. NASA Technical Memorandum 85871, *Crossed Hot-Wire Data Acquisition and Reduction System*, by R. V. Westphal, pp. 12-29, 1985.

22. NACA Report 1247, *Characteristics of Turbulence in a Boundary Layer with Zero Pressure Gradient*, by P. S. Klebanoff, 1955.

23. Stanford University Thermosciences Division Report HMT-17, *Turbulent Transport of Heat and Momentum in a Boundary Layer Subject to Deceleration, Suction and Variable Wall Temperature*, by A. F. Orlando, R. J. Moffat and W. M. Kays, 1974.

24. Wang, T., Simon, T. W. and Buddhavarapu, J., "Heat Transfer and Fluid Mechanics Measurements in Transitional Boundary Layer Flows," paper presented at the 30th International Gas Turbine Conference and Exhibit, Houston, Texas, 18-21 March, 1985.

BIBLIOGRAPHY

Bradshaw, P., *An Introduction to Turbulence and Its Measurement*, Pergaman Press, Inc., 1971.

Cebeci, T., and Smith, A. M. O., *Analysis of Turbulent Boundary Layers*, Academic Press, 1974.

Emrich, R. J., *Methods of Experimental Physics, Vol. 18, Part A, Fluid Dynamics*, Academic Press, 1981.

Goldstein, R. J., *Fluid Mechanics Measurements*, Hemisphere Publishing Corp., 1983.

Hinze, J. O., *Turbulence*, 2nd Edition, McGraw-Hill, 1975.

Perry, A. E., *Hot-Wire Anemometry*, Oxford University Press, 1982.

Richards, B. E., *Measurement of Unsteady Fluid Dynamic Phenomena*, Hemisphere Publishing Corp., 1977.

Schlichting, H., *Boundary-Layer Theory*, 7th Edition, McGraw-Hill, 1979.

INITIAL DISTRIBUTION LIST

		No. Copies
1.	Defense Technical Information Center Cameron Station Alexandria, VA 22304-6145	2
2.	Library, Code 0142 Naval Postgraduate School Monterey, CA 93943-5002	2
3.	Department Chairman, Code 69 Department of Mechanical Engineering Naval Postgraduate School Monterey, CA 93943-5000	1
4.	Professor Phillip M. Ligrani, Code 69Li Department of Mechanical Engineering Naval Postgraduate School Monterey, CA 93943-5000	8
5.	Professor Chelakara S. Subramanian, Code 69Su Department of Mechanical Engineering Naval Postgraduate School Monterey, CA 93943-5000	5
6.	LT James G. Green, USN 2324 Spruce Place White Bear Lake, MN 55110	2

Thesis
G7259
c.1

Green
Turbulence structure resulting from interaction between an embedded vortex and wall jet.

Thesis
G7259
c.1

Green
Turbulence structure resulting from interaction between an embedded vortex and wall jet.

AMERICAN BINDERY
TOPEKA KANSAS

thesG7259
Turbulence structure resulting from inte
3 2768 000 86773 3
DUDLEY KNOX LIBRARY